(NASA-TT-F-784) INTERPLANETARY MEDIUM AND PHYSICS OF THE MAGNETOSPHERE (Scripta Publishing Corp., Washington, D.C.)
[illegible] p HC $8.75 CSCL 03B

N75-13707
THRU
N75-13723
Unclas
H1/90 04836

1. Report No. NASA TT F-784	2. Government Accession No.	3. Recipient's Catalog No.
4. Title and Subtitle INTERPLANETARY MEDIUM AND PHYSICS OF THE MAGNETOSPHERE		5. Report Date November 1974 6. Performing Organization Code
7. Author(s) G. A. Skuridin et al., Editors		8. Performing Orgsnization Report No. 10. Work Unit No.
9. Performing Organization Name and Address Scripta Publishing Corp. Washington, D.C. 20005		11. Contract or Grant No. NASw-2484
12. Sponsoring Agency Name and Address National Aeronautics and Space Administration Washington, D.C. 20546		13. Type of Report and Period Covered Translation 14. Sponsoring Agency Code

15. Supplementary Notes

Translation of "Mezhplanetnaya Sreda i Fizika Atmosfery", Moscow, "Nauka" Press, 1972, pp 1-210

16. Abstract

This collection presents papers on various aspects of solar-terrestrial physics. Along with articles in which theoretical problems are treated, there are others that describe the results of experiments on spacecraft.

An abstract precedes each article.

17. Key Words (Suggested by Author(s))	18. Distribution Statement Unclassified - unlimited STAR Category 30		
19. Security Classif. (of this report) Unclassified	20. Security Classif. (of this page) Unclassified	21. No. of Pages 293	22. Price* $6.75

*For sale by the National Technical Information Service, Springfield, Virginia 22151

TABLE OF CONTENTS

	Page
Certain Problems in the Physics of the Magnetosphere A.I. Yershkovich, G.A. Skuridin, and V.P. Shalimov	1
Hydromagnetic Waves Guided by the Geomagnetic Field. L.L. Van'yan, L.A. Abramov, M.B. Gokhberg, and V.L. Yudovich	34
Magnetic Measurements in Model Experiments E.M. Dubinin, G.G. Managadze, and I.M. Podgornyy	45
Dissipation of Energy in Model Experiments I.M. Podgornyy	59
Analysis of Methods of Measuring Electric-Field Strength in the Magnetosphere. S.I. Klimov	68
High-Frequency Turbulence in the Cosmic Plasma V.A. Gudkova and V.A. Liperovskiy	83
Structural Formations in the Interplanetary Medium A.V. Bogdanov	103
The Internal Structure of the Convective Envelope of the Sun I.M. Yavorskaya	124
An Investigation of the Cosmic Radiation in the Vicinity of the Moon on the Luna 10, 11, and 12 Artificial Lunar Satellites. N.L. Grigorov, V.G. Kurt, V.N. Dutsenko, V.L. Maduyev, N.F. Pisarenko, and I.A. Savenko	151
Low-Energy Protons of Solar Origin and Investigation of the Interplanetary Medium. V.N. Lutsenko and N.F. Pisarenko	174
Thermal Instability and Energy Relations in the Convective Envelopes of Slowly Rotating Stars I.M. Yavorskaya	203
Calculation of the Shape of the Boundary of the Magnetosphere. S.A. Mart'yanov	224
Transport of Charged Particles in the Earth's Magnetosphere. V.P. Shalimov	247
Vibrations of the Earth's Magnetic Tail. A.I. Yershkovich and A.A. Nusinov	266
Short-Range Repulsive Forces Between Atoms and Molecules of Atomspheric Gases. A.P. Kalinin, V.B. Leonas, and A.V. Sermyagin	274
Apparatus for Calibration of On-Board Instruments and Laboratory Modelling of Rarefied Plasma Flows Past Models. Ye.N. Yevlanov, V.B. Leonas, and S.V. Umanskiy	282

PRECEDING PAGE BLANK NOT FILMED

N75 13708

CERTAIN PROBLEMS IN THE PHYSICS OF THE MAGNETOSPHERE

(Translation of "Nekotoryye problemy fiziki magnitosfery.")

A. I. Yershkovich, G. A. Skuridin, and V. P. Shalimov

ABSTRACT

A review of experimental and theoretical studies devoted to analysis of physical processes in the magnetosphere is presented. Attention is focused on the interrelationships among the most important geophysical phenomena in the magnetosphere: magnetic storms, auroras, the radiation belts, and processes in the geomagnetic tail. Recommendations are submitted for future experiments that are needed for development of a theory of magnetospheric phenomena. With 1 table, 8 illustrations, and 158 source citations.

CERTAIN PROBLEMS IN THE PHYSICS OF THE MAGNETOSPHERE* /3#

A.I. Yershkovich, G.A. Skuridin, and V.P. Shalimov

The idea that the sun emits clouds of quasineutral plasma from time to time suggested to Chapman and Ferraro [1] that a cavity enclosing the earth's magnetic field is formed inside the plasma stream. After Parker's hypothesis [2-3] of the more or less constant solar wind found experimental confirmation in [4], it became clear that this cavity, which was named the magetosphere (the term was introduced by Gold [5]), also has a permanent existence. Figure 1, which is borrowed from O'Brien's paper [6], shows the general pattern of the earth's magnetosphere.[1]

The solar plasma produces various geophysical phenomena in the earth's magnetosphere. A number of discoveries have been made during recent years with the aid of rockets and satellites: the radiation belts (S.N. Vernov et al. [7], Van Allen et al. [8]), the plasmopause (K.I. Gringauz [9-10], Carpenter [11]), the ring current (Sh.Sh. Dolginov et al. [12], Cahill [13], Frank [14-15]), and the magnetic tail (Ness et al. [16]). Study of the interaction of the solar wind with the magnetic field of the earth and the whole complex of interrelated geophysical phenomena that arise as a result is the task of magnetospheric physics – a new field of geophysics whose inception became possible chiefly as a result of /4 progress made in space and plasma-pnysics research.

Many survey papers devoted to various problems of magnetospheric phvsics have recently been published [17-21]. Below we

---

*Paper presented at the Assembly of the Interunion Commission on Solar-Terrestrial Relationships. London, 1969 (see Space Sci. Rev., 1969, Vol. 10, 262).

[1]Below we shall use O'Brien's classification [6] of the magnetospheric regions that are populated by high-energy particles, even though it is not generally accepted. In accordance with this terminology, particles belonging to the trapped radiation region (McIlwain parameter $L \lesssim 6$-8) are capable of completing at least a few drift revolutions around the earth. Charged particles within the magnetosphere that are unable for one reason or another to complete a drift revolution around the earth belong to the auroral-radiation region. Thus, this region includes the particles situated between the capture zone and the boundary of the magnetosphere (the magnetopause) on the sunlit side and the radiation in the plasma layer of the magnetic tail and cusp at the transition to the neutral layer, regardless of whether these particles can oscillate in latitude on quasitrapped orbits at great distances from the earth or are spilled into the atmosphere, where they cause auroras and the associated phenomena.

#Numbers in the margin indicate pagination in the foreign text.

shall dwell only on a few specific problems: Section 1 is concerned with various statements of the problem of flow of the solar plasma around the earth and theoretical models of the magnetosphere; Section 2 is devoted to the problem of the ring current and the behavior of charged particles during magnetic storms; Section 3 discusses the energetics of the most important geophysical phenomena and certain ways in which solar-wind energy is transferred into the magnetosphere; in the conclusion, a number of possible space experiments are examined.

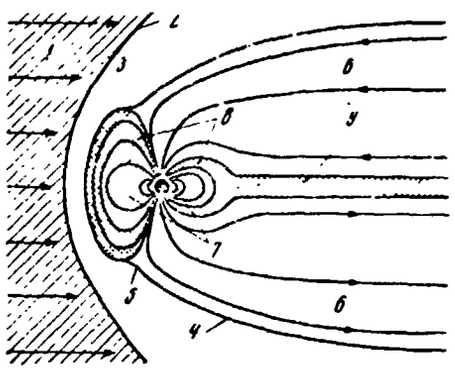

Figure 1. General Pattern of the Magnetosphere According to [6], Illustrating the Terminology Used in this Review. 1) Region of solar wind; 2) front of collisionless shock wave; 3) transitional region; 4) magnetopause; 5) neutral point; 6) magnetosphere; 7) trapped radiation zone; 8) auroral radiation zone; 9) plasma layer.

1. Flow of the Solar Wind Past the Magnetosphere, and Theoretical Models of the Magnetosphere

The development of a quantitative theory that gives a satisfactory description of the solar-terrestrial relationships requires solution of the problem of flow of the solar plasma past the geomagnetic field. Here it is necessary to take account of collisionless dissipation, which determines the nature of the interaction between the plasma and the magnetic field. This problem is essentially nonlinear and very probably will not be solved in its complete form in the immediate future. However, even the analysis of greatly simplified models in which many interesting phenomena are excluded in advance contributes substantially to better understanding of the problem of the solar-terrestrial relations. Thus, even the solution of the two-dimensional problem (in which plasma impinges on a plane magnetic dipole), which does not consider either the magnetic field frozen into the plasma or the thermal motion of the plasma particles [22], has brought out many characteristic features of the flow around the geomagnetic field and suggested the possible existence of the earth's magnetic tail, which was later discovered by Ness et al. [16].

Most of the papers devoted to determination of the shape of the magnetosphere's boundary do not leave the framework of the following formulation of the problem: a) there is no plasma inside the magnetosphere (pressure is created solely by the magnetic field, $P = B^2/8\pi$) and the magnetic field has a specified singularity at the location of the magnetic dipole; b) there is no magnetic field outside of the magnetosphere, and the particles of the free-molecule flux participate both in a directional motion

along the sun-earth line (a dynamic pressure P_d corresponds to this motion) and in a thermal motion (related to the isotropic pressure P_0); in particular cases, either $P_0 = 0$ or $P_d = 0$; c) the transitional layer between the plasma and the magnetic field is assumed infinitesimally thin, and reflection of particles from the boundary is assumed to be specular. Then the boundary condition at the unknown interface can be written

$$P_0 + P_d \cos^2 \theta = B^2/8\pi \quad \text{for } \frac{\pi}{2} \leqslant \theta \leqslant \pi, \text{ (daytime side)}$$

$$P_0 = B^2/8\pi \quad \text{for } 0 \leqslant \theta \leqslant \pi/2 \text{ (night side)}$$

(here θ is the angle between the directional velocity of the stream and the outer normal to the surface of the magnetosphere). This problem is, of course, nonlinear, since the magnetic field created by currents on the unknown boundary appears in the boundary condition. A solution of the two-dimensional problem can be obtained in analytic form in the case $P_d \neq 0$, $P_0 = 0$ (using a conformal-mapping method [22]) and in the case $P_d = 0$, $P_0 \neq 0$ (dipole immersed in an equilibrium plasma [23]). A solution of a more general two-dimensional problem with $P_d \neq 0$ and $P_0 \neq 0$ was /5 obtained in [24] with certain hypotheses regarding the nature of the directional particle motion.

There are several approximate methods for determining the shape of the magnetosphere's boundary in the three-dimensional case in the formulation considered above: the method of moments [25-26], the method of the free surface [27-28], and the self-consistent-field method [29-31] (see also the review [32], in which these methods are discussed). Although they yield approximately the same shape for the boundary of the magnetosphere on the daytime side, the shape of the earth's magnetic tail cannot be obtained in natural fashion in the above formulation of the problem, and it is necessary to add a current layer artificially on the night side to obtain agreement with magnetic-field measurements made in the tail [33].

Consideration of the interplanetary magnetic field [34] is an important advance, since a relation is observed in experiments between variations in the direction of the solar-wind magnetic field and the occurrence of various geophysical phenomena (for example, the transition from the initial phase of a storm to the principal phase [35-36]). However, most papers that take account of the magnetic field frozen into the solar-wind plasma are of hypothetical nature, e.g., [37-39]. Attempts to take the interplanetary magnetic field into account consistently were made in [40], where the system of quasihydrodynamic equations is solved by

successive approximations, and in [41-42], which were devoted to aerodynamic calculation of the flow around a magnetosphere of specified shape.

Together with experimental research in space and the solution (chiefly with the aid of modern computers) of flow problems that reflect actual conditions more and more completely, there is one more approach with which significant progress in the physics of the magnetosphere can be made: laboratory modelling.

Here, however, it is necessary to preserve similarity criteria. The system of dimensionless parameters on which the solution of a flow problem may depend was investigated in [43, 43a]. Accurate modelling with respect to all dimensionless parameters was found to be impossible in principle, although it is admissible to model the flow around the magnetosphere with respect to certain determining parameters, leaving the modelling approximate for the other dimensionless parameters (which are small in space and on which, therefore, the solution does not depend strongly).

Although there have already been rather many experimental studies in which the flow of the solar wind around the earth's magnetosphere has been modelled in the laboratory, it appears that the necessary similarity relations corresponding to the conditions of collisionless flow were adhered to only in the experiments of I.M. Podgornyy et al. [44-46]. These experiments were performed with a two-dimensional magnetic dipole, and the plasma stream was characterized by the following parameters: concentration $n \sim 10^{13}$ cm^{-3}, electron temperature $T_e \sim 15$ eV, velocity of stream $v \sim$ $\sim 3 \cdot 10^7$ cm/sec, magnetic field frozen into the plasma at $B \sim 30$ Oe. The following requirements are then satisfied: a) the magnetic Reynolds number in the experiment $Re_m \sim 10^3 >> 1$ (in space $Re_m \sim 10^{12}$), i.e., the conditions for formation of the magnetic cavity in the stream are satisfied; b) directional velocity of stream 7-8 (in space, 8-10) times the velocity of ion sound and 8 times (as in space) the velocity of magnetic sound; c) free path 10 times the characteristic dimension of the system (in space, $\sim 10^3$); d) the radius of curvature in the plasma-magnetic-field boundary layer is much smaller than the dimensions of the layer for electrons and of the same order as these dimensions for ions.

The experiment established the formation of the magnetic cavity in the plasma stream (the intensity of the magnetic field at the cavity boundary was 300-500 Oe), the existence of a detached collisionless shock wave and a transitional region between the plasma stream and the dipole magnetic field, and the formation of the magnetic tail (the field intensity changes sign on passage across the neutral layer, passing through zero), with the plasma concentration in the neutral layer of the tail at $5 \cdot 10^{12}$ cm^{-3}, which is only half the free-stream concentration. /6

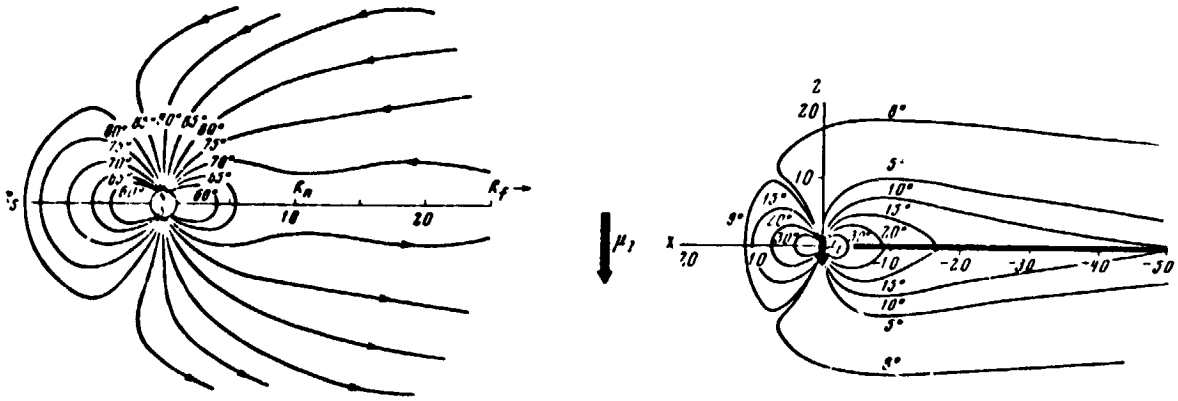

Figure 2. Meridional Section Through the Magnetosphere along the Earth-Sun Line in the Mead-Williams Model [33] (Distances Indicated in Earth Radii). R_S is the geocentric distance to the subsolar point on the magnetopause and R_n and R_f are the distances to the boundaries of the current layer in the tail of the magnetosphere (magnetic-field intensity in the tail B_T - 15 γ); also indicated are the latitudes at which the lines of force of the magnetic field cross the surface of the earth.

Figure 3. Meridional Section Through the Magnetosphere along the Earth-Sun Line in the Hones-Taylor Model [49] (Distances Indicated in Earth Radii). μ_E is the magnetic moment of the terrestrial dipole and μ_I is the magnetic moment of the imaginary (image) dipole; the heavy line in the tail of the magnetosphere corresponds to the current layer; the latitudes at which lines of force of the magnetic field cross the surface of the earth are indicated.

Let us now consider theoretical models of the geomagnetic field that are composed of a field of internal terrestrial sources (which is often assumed to be a simple dipole field) and the field of the currents that arise when the solar wind flows around the magnetosphere.

Confining ourselves to consideration only of the currents flowing along the boundary of the magnetosphere, and using the magnetopause shape found in [29-30], Mead [47] determined the coefficients in the series expansion of the surface-current magnetic field in spherical harmonics from the condition that the resultant magnetic field **vanishes** outside the magnetosphere. However, in order to describe the shape of the magnetic tail, it was necessary to introduce an additional field of a certain homogeneous current [33] flowing in the equatorial plane on the night side (perpendicular to the plane of the midnight meridian) beginning at geocentric distances of 8-10 earth radii. Figure 2 shows the /7

geomagnetic-field force lines calculated from the Mead-Williams model [33] in the plane of the day-night meridian. There are four parameters in this model: R_S, the geocentric distance to the subsolar point on the boundary of the magnetosphere; R_n and R_f, the minimum and maximum distances to the current layer in the tail; B_T, the intensity of the magnetic field in the current layer. If R_f is made sufficiently large (for example, $R_f = 200 \cdot R_E$; R_E is the earth's radius), there remain only three parameters, and we can assign them (in accordance with experimental values) to obtain the distribution of the magnetic field in the magnetosphere at a given time. Variation of the parameters in the Mead-Williams model showed that the best agreement is obtained between the distribution of the magnetic field in this model and synchronous-satellite magnetic measurements ($\sim 6.6\ R_E$) at $R_S = 10.7\ R_E$, $R_n = 10\ R_E$, $B_T = 10.5\ \gamma$.

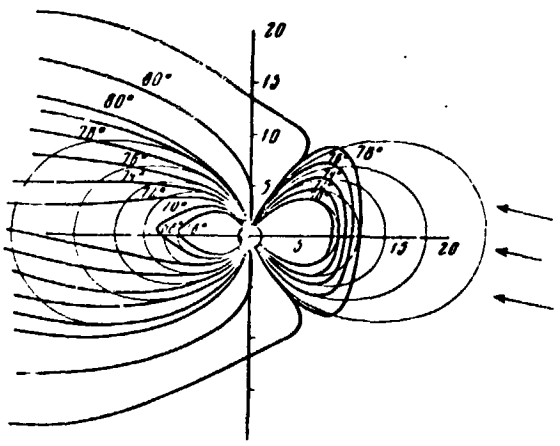

Figure 4. Force Lines of Geomagnetic Field in the Plane of the Day-Night Meridian According to Measurements on the IMP-1, 2, and 3 Satellites [52] (Distances Indicated in Earth Radii). The numerals indicate the latitudes at which they cut the surface of the earth; the light closed lines correspond to lines of force of the undisturbed dipole field.

The Hones-Taylor model [48-50] is often used (see also [51]). In this model (Fig. 3), the boundary-current effect is simulated with the aid of an imaginary magnetic dipole placed between the sun and the earth. The parameters of this model are the ratio of the magnetic moments of the imaginary and terrestrial dipoles ($\sim$30-40) and the distance between the dipoles ($\sim 40\ R_E$). A current layer $0.5 R_E$ thick is added to describe the field in the tail [49].

The Mead-Williams and Hones-Taylor models are discussed in detail by Roederer [51]. Both models describe satisfactorily the general distribution of the magnetic field in the magnetosphere, the compression of lines of force on the daytime side, their elongation on the night side, and the appearance of the neutral points. For comparison, Fig. 4 shows the pattern constructed by Fairfield [52] for the magnetospheric lines of force on the basis of IMP-1, 2, and 3 satellite magnetic-field measurements. Although the agreement between direct measurements of the fields in the magnetosphere and predictions based on the theoretical models is in

general satisfactory, there are also certain discrepancies. Thus, the points of intersection of the lines of force with the plane of the equator are found to be farther from the earth than according to the Mead-Williams model (the agreement is good to distances of $6-7R_E$, but deteriorates with increasing distance). The latitude at which force lines passing near a neutral point cut the surface of the earth is found to be lower ($\sim 78°$, see Fig. 4) than in the Mead-Williams ($\sim 82°$) and Hones-Taylor ($81°$) models. If the boundary of the magnetosphere is quite close to the earth, the Mead-Williams model is evidently invalid [51]. Thus, for example, with $R_S = 6.6R_E$ and $B_T = 35\gamma$[2], this model gives 210 γ for B at the subsolar point, a value much larger than that measured by a synchronous satellite [52] as it crossed the magnetopause.

The basic deficiency of these models is the artificial addition of a current layer in the tail with a sharp inner edge that produces the fictitious neutral line on the night side. Mead [47] calculated the surface currents in the magnetopause without consideration of the tail current. Addition of this current disturbed the original self-consistent pattern in the calculation of the boundary of the magnetosphere and the geomagnetic field and caused deterioration of the agreement with the real distribution of the fields on the daytime side. Further, neither model takes account of the ring-current field, and they assume that the earth's magnetic moment is perpendicular to the plane of the ecliptic (which precludes study of the diurnal and seasonal variations of the fields). It is very difficult to take account of this inclination in the Mead-Williams model. This is much simpler in the Hones-Taylor model [54-55], but in this case there is little physical justification for the model itself.

Needless to say, a model of the magnetosphere that is free of /8 these deficiencies must still contain a limited number of time-dependent measurand parameters if it is to be useful. The development of such a model is an urgent problem of magnetospheric physics. It is needed for adequate description of many geophysical phenomena: trapped and auroral radiation, convective motion of the plasma, propagation of hydromagnetic waves, etc. (for details see [51]). It is known that McIlwain's coordinate system [56] becomes inapplicable for $L \gtrsim 7$ because of wide departures of the real magnetic field from the dipole field. The influence which distortions of the magnetosphere caused by a symmetrical ring current and the presence of the boundary on the daytime side have on the (L, B) coordinate system was taken into account in [57] (the field in the tail was not, so that these results are inapplicable on the night side). It was found that certain effects that were observed by Explorer 12 and interpreted in the usual (L, B) system as a manifestation of radial diffusion across the magnetic field ("diffusion waves")

[2]It was assumed in the calculation of [51] that $R_n/R_E = 10-0.06$ ($B_T = 10$); $R_f = 200R_E$.

vanished in a modified coordinate system that takes account of magnetosphere distortion. What was apparently observed in this case was motion of particles together with the lines of force, rather than their transport across the lines of force.

Thus, an adequate model of the magnetic field is of extreme importance for differentiation of adiabatic from nonadiabatic effects of particle motion. If the field inside the magnetosphere is known with sufficient accuracy, a new coordinate system suitable for study of charged particles far from the earth can be constructed. Such a system was proposed by Roederer (see [51]). The invariant coordinates are $K = I^2 B_m$ and $L = -2\pi M/\Phi$ (here B_m is the field intensity at the reflection point at a particular point in time and $I = \int \left(1 - \frac{B(S)}{B_m}\right)^{1/2} dS$ is proportional to the second invariant; M is the magnetic moment of the earth, and Φ is the magnetic flux across the drift surface of the particle). The values of the real magnetic field are used in calculating K and L. Thus, as soon as a convenient theoretical model of the magnetosphere is created, it will be possible to describe the time variations of the particles at large distances from the earth, just as this became possible in the inner regions of the magnetosphere on introduction of the McIlwain coordinate system [56]. Perhaps it would be advantageous to represent the magnetic field in such a model with the aid of Euler potentials [58-60], since this would greatly simplify the procedure of determining the drift velocities, drift shells, etc.

Electric fields with intensities $\varepsilon \gtrsim 10^{-5}$ V/cm strongly influence the motion of particles with energies $\lesssim 2$ keV [51], since $v_E \gtrsim v_M$ for such particles (v_E is the electrical drift velocity and v_M is the drift velocity in an inhomogeneous magnetic field). It appears that even particles with energies of a few tens of kiloelectron-volts (and less) are affected by electric fields in the magnetosphere [62]. Until recently, there had been no direct measurements of the electric fields in the earth's magnetosphere. However, such fields may arise as a result of convective plasma motions [63] or from other effects (see, for example, [64]). For this reason, various models of electric fields in the earth's magnetosphere were discussed in [65-67], and the drift trajectories of charged particles with various energies in the presence of an electric field were found in [49-50, 68].

If the plasma is ideally conductive $\left(\mathcal{E} + \frac{1}{c} v \times B = 0\right)$, the lines of force of the magnetic field and the lines of flux lie on equipotential surfaces $\left(\frac{1}{c} v \times B = -\mathcal{E} = \operatorname{grad} \varphi\right)$. If, therefore, it somehow becomes possible to construct the system of convective plasma motions in the magnetosphere, it will be possible to find the /9

distribution of electrical potential. Axford and Hines [63] constructed a convective-motion system based on a quasiviscous-interaction mechanism between the stream of solar plasma and the plasma in the magnetosphere, and extended it along the magnetic lines of force (which are lines of ϕ = const) into the ionosphere.

It was established experimentally in [69] that the plasma in the transitional region flows almost tangentially to the boundary; hence it also follows from continuity of the mass flux density j across the interface that the normal components of plasma velocity vanish on either side of the boundary; $v_{1n} = v_{2n} = 0$. If we assume that the normal component B_n of the magnetic field at the boundary of the magnetosphere is nonvanishing, it follows from continuity of the energy and momentum fluxes (see [70]) that the tangential components of velocity ($v_{t1} = v_{t2}$) and the magnetic field ($B_{t1} = B_{t2}$) are discontinuous; in magnetohydrodynamics, such discontinuities are called contact discontinuities. However, the presence of the magnetic-field discontinuity at the boundary of the magnetosphere ($B_{t1} - B_{t2} = (4\pi/c)I_s$, where I_s is the density of the surface current) must be regarded as a firmly established fact, at least on the daytime side [71], so that B_n must obviously vanish at the boundary of the magnetosphere in the stationary state (provided that these phenomena can be described with the aid of magnetohydrodynamics). At the interface, therefore, we have $j = 0$, $B_n = 0$; in this case, it follows from the magnetohydrodynamic equations that, generally speaking, $B_{t1} - B_{t2} = 0$; $v_{t1} - v_{t2} = 0$ (see [70]). Such a discontinuity is said to be tangential. Hence it follows that the direction of the plasma convective motions assumed by Axford and Hines [63] is a possibility. References to experimental observations of convection of this type will be found in [72-74] (in [74], measurements of the >50 eV ion flux showed that the direction of this flux is practically the same on either side of the daytime boundary). A convection system similar to that of [63] can be obtained from a model in which the lines of force of the terrestrial and interplanetary magnetic fields merge[3] (Dungey [37]).

Transport of the system of currents from the ionosphere along the lines of force B also makes it possible to sketch out the pattern of the convective motions in the magnetosphere [49, 156], but the uncertainty in the assumed conductivity values precludes determination of the potential ϕ with sufficient accuracy. Another method based on measurements of the plasma-plasmapause density jump (which was discovered by K.I. Gringauz et al. [4, 9]; see also [10], and Carpenter [11] and is situated at $L \sim 3$-6),

[3]This model requires $B_n \neq 0$ on the boundary of the magnetosphere and evidently cannot be described by the magnetohydrodynamic equations if $j = 0$.

was proposed by Brice [66].

It is known [61] that the motion of low-energy charged particles in the equatorial plane of the magnetic dipole in the presence of a homogeneous interplanetary magnetic field and a homogeneous electric field (parallel to the plane of the equator) is accompanied by formation of a forbidden region into which particles arriving from infinity cannot penetrate. Nishida [65] proposed that the separatrix bounding the forbidden region for thermal particles might be identified with the plasmapause.[4] Figure 5 shows the convection scheme obtained by Brice [66] with consideration of the fields induced by the earth's rotation. The last closed equipotential line corresponds to the position of the plasmapause according to [75]. This convection system is evidently in satisfactory agreement with ground observations (for example, observations of the motion of auroral arcs) and with direct satellite measurements of low-energy particles [74, 76]. It also enables us to explain certain features of the motion of high-energy particles. Thus, the morning-evening asymmetry of the fast-electron flux can be explained as due to coincidence of their magnetic drift with the direction of the electric field on the daytime side and their anticoincidence on the night side. As a result, the highest electron fluxes will occur on the morning side. For protons, on the other hand, the highest fluxes should be observed on the evening side, in approximate agreement with the measurements of [77].

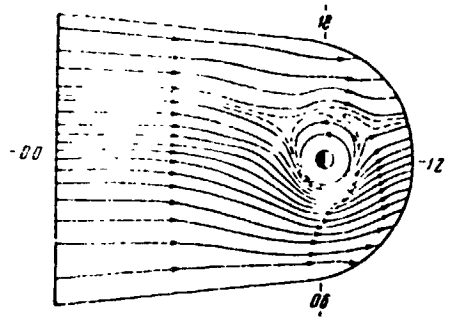

Fig. 5. Lines of Plasma Flux in the Equatorial Plane of the Magnetosphere as Obtained in [66]. The potential difference between solid lines is 3 kV, and that between dashed lines is 1 kV. The last closed dashed line corresponds to the position of the plasmapause according to the measurements of [75]; the numerals indicate local time.

/10

The dense plasma ($\sim 10^2$-10^3 cm^{-3}) within the plasmapause may be of ionospheric origin, while in more remote regions of the magnetosphere (densities 1-10 cm^{-3}), plasma may penetrate directly from the tail and, in the final analysis, from the solar wind [66, 68]. As a result of the polar wind, plasma from the ionosphere should also find its way onto the open lines of force that run out into the tail of the magnetosphere (Banks and Holzer [78]).

---

[4]Recent measurements of the electric fields in the magnetosphere (see [156]) failed to confirm this hypothesis, and this problem therefore requires detailed study.

Brice [66] showed that the position of the plasmapause should be sensitive to variations in the electrical-potential distribution, and that accurate measurements of its configuration (with the aid of satellites or based on the propagation of atmospheric whistlers) could become an effective method for study of the large-scale electric fields in the magnetosphere.

2. High-Energy Charged Particles in the Earth's Magnetosphere, and the Problem of the Ring Current

O'Brien's proposal [6] that the regions of the magnetosphere populated by high-energy charged particles be divided into zones of trapped and auroral (or, according to [79], unstable) radiation (see Fig. 1) appears highly useful. According to O'Brien [6], the auroral plasma may have a kinetic-energy density $\rho v^2/2$ (where ρ is the density and v is the average particle velocity) on the order[5] of the magnetic-energy density $B^2/8\pi$.

This concept is somewhat broader than the notion of quasi-trapped radiation that was introduced by Roederer [80] for particles that are not capable of completing a drift revolution around the earth because of splitting of the drift shells in the outer magnetosphere (Fig. 6). However, the impossibility of prolonged drift in longitude remains the basic characteristic of the auroral particles. It appeared at one time that the essential feature of the auroral radiation should be a pitch-angle distribution different from that characteristic for the trapped-particle zone. However, this applies only for spilled particles. And the auroral radiation is also conceived of as including particles of the plasma layer of the tail and the outermost radiation belt [4, 81-82], which has a sharp inner boundary at practically all longitudes [83-84]. In addition, particles with pitch angles $\sim 90°$, which drift in the peripheral regions of the magnetosphere along lines of equal intensity B that do not close around the earth, may also /11 be included in the auroral radiation.

The basic problems in study of the auroral radiation are its origin, the mechanisms of particle acceleration, and the role of the auroral particles in the excitation of auroras and were discussed in detail in O'Brien's review [6]. It is appropriate to dwell on the possible magnetic effects.

It has been observed that augmented charged-particle fluxes in the auroral-radiation zone are accompanied by magnetic-field disturbances. Thus, "islands" [85], "bursts" [86], and fluxes of spilled particles become more intense on local decreases in the magnetic field in the tail of the magnetosphere [87]. With the development of a magnetic bay, the flux of spilled electrons increases with the disturbance and decreases as it decays. The

[5] For the trapped radiation, $\rho v^2/2 \ll B^2/8\pi$, and in interplanetary space $\rho v^2/2 \gg B^2/8\pi$.

plasma fluxes in the tail vary in the opposite direction [88]. During magnetic disturbances, the auroral zone expands and its southern boundary is shifted equatorward [89, 90]. Simultaneously with the development of magnetic disturbances, the boundary of the plasma (and neutral) layer in the tail of the magnetosphere moves closer to the earth. In a number of papers (see, for example, [91] and its bibliography), it has been suggested that a current flows in the region of the auroral radiation near the boundary of the trapped-particle zone and is responsible for the main phase of the magnetic storm. There is as yet no experimental verification of this hypothesis. There are, however, indications (see, for example, [92]) of the existence of two different ring currents. Two parts are distinguished in the field of the ring current DR (on the basis of the rise and fall rates of the main phase): a fast part DR-1 and a slow part DR-2, with the amplitude of DR-1 much greater than that of DR-2 for strong storms. In Obayashi's interpretation [93], the currents that cause the variations of DR-1 and DR-2 should be situated near the earth (at a distance of a few earth radii) and in the outer magnetosphere (and perhaps also in the tail), respectively.

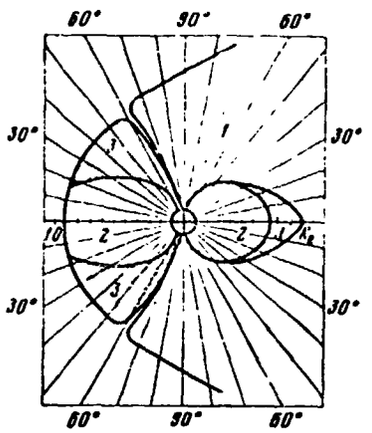

Figure 6. Position of Quasitrapped-Particle Zone in the Mead-Williams Model According to [80]. 1) Region of non-closed lines of force; 2) trapped-radiation zone; 3) quasitrapping zone; particles having reflection points within this region do not complete a full drift revolution around the earth; geocentric distances in earth radii and geomagnetic latitudes are indicated.

The ring current in the trapped-radiation zone, whose existence had been suggested many years previously, was detected in Frank's experiments [14, 15]. At the same time, attention is drawn to the close relation between the development of DR currents and polar substorms [94]. It is shown in [95] that there are pulsewise injections of energy into the ring current that exhibit a time dependence similar to the course of a DP substorm but lagging slightly behind it. This suggests that the high-energy particles responsible for DR-1 and DR-2 have a single common source[6] and appear suddenly. It was accordingly proposed in [96] that the sudden onset of the main phase of the DR-1 storm is determined by the current of the auroral particles that caused the DP substorm. Then, under the influence of the electric fields induced by this current, particles are injected at high latitudes into the trapping /12

[6]According to the concepts advanced in [95], the source of these particles is the plasma layer in the tail of the magnetosphere, and the cusp in particular.

zone, with the resulting development of the DR-2 ring current, which makes a substantial contribution to the DR field, becoming symmetrical during the recovery phase of the storm and dropping off much more slowly than DR-1.

Recent observations tend increasingly to confirm that polar storms are the key factor [97] in the development of magnetic storms. It is concluded in [98] that a symmetrical ring current develops during a severe storm out of a sequence of currents that arise in the evening-to-night sector of the magnetosphere as a result of polar storms.

The problem of the ring current as the factor responsible for the main phase of the magnetic storm has recently come under experimental and theoretical study (see, for example, [99]). The possible existence of this current was indicated by measurements from the spacecraft Luna 1 and Luna 2 [12], Explorer 6 [100], Electron 2 and Electron 4 [101], and Explorer 12 [13]. However, pending direct measurements of the fluxes of electrons and protons with energies from 200 eV to 50 keV on $L \sim 3$-8 (Frank [14, 15]), it was not possible to explain the decrease in the magnetic field that is observed during the main phase of a storm (see, for example, [102]).

Definite progress has now been made in self-consistent calculations of the ring-current magnetic field for various particle pitch-angle distributions (see [92, 102]). However, the magnetic effect of the ring current at the earth's surface does not depend on this distribution. Thus, it was shown in Sckopke's paper [103] that Dessler and Parker's relation [104]

$$\frac{\Delta B_{e0}}{B_{e0}} = -\frac{2}{3}\frac{u}{u_T}$$

(B_{e0} is the equatorial magnetic-field intensity at the earth's surface, B_{e0} is the decrease in the field at the equator, u_T is the total energy of the undisturbed magnetic field outside of the earth's surface, and u is the total particle kinetic energy) is valid for an arbitrary particle pitch-angle distribution. The derivation of this relation with the virial theorem and a further generalization will be found in [105]. Thus, there exists a simple relation between the total particle kinetic energy in the ring current and the decrease in the magnetic-field horizontal component at the equator on the earth's surface:[7] ΔB_{e0} (in gammas) = $2.5 \cdot 10^{-21} u$ (in ergs).

[7] The particle energy density required to lower the horizontal field component at the surface of the earth $\Delta B_{e0} \geq 100\gamma$ may, in a certain region of space, be found comparable to the geomagnetic-field energy density $B^2/8\pi$. In this case, self-consistent calculations are necessary (see [102]).

At the same time, such problems as particle injection and (or) transfer of energy into the ring current during the main phase of the storm, the decay of the current and its dissipation during the recovery phase, and the relation of the DR current to processes in the auroral radiation zone and to various other geophysical phenomena require further study.

Analysis of the effects of magnetic-storm-type disturbances on high-energy particles in the trap zone is important both for solution of these problems and for clarification of the questions that remain open as to the origin of the trapped radiation and the mechanisms of the acceleration and loss of particles. One of the first mechanisms to be studied was that in which the trapped radiation originates as a result of beta decay of albedo neutrons (S.N. Vernov [106], Singer [107], and Kellogg [108]). Further research indicated (see, for example, [109]) that only the formation of high-energy ($E_p \geq 50$ MeV) protons at small L near the plane of the equator can be explained in this way. The attention /13 of investigators was then drawn to a diffusion mechanism — the transport of trapped particles across geomagnetic-field drift shells as a result of violation of the third adiabatic invariant (the invariant of the flux Φ), accompanied by betatron acceleration of the particles [110-113]. "Sudden impulses" of the geomagnetic field that occur on solar-wind pressure changes are now regarded as the basic cause of this transport (see [20]). Study of particle diffusion under the action of various types of electromagnetic impulses by numerical methods [114-116] and comparison with experimental data on protons with energies of $\sim$100 keV and more have shown that this transport mechanism is apparently not effective enough to create an external proton belt.[8] As for the electrons, the velocity of their transport as calculated from the diffusion theory is usually 1-2 orders below that obtained empirically from analysis of experimental data (see, for example, [117]). Consideration of the electrostatic fields associated with convective plasma motions in the magnetosphere makes it possible to obtain a transport velocity an order higher than that for the magnetic disturbances [118]. The motion of the charged particles may also be influenced strongly by electric fields directed along magnetic lines of force (which arise when the finite conductivity of the plasma is taken into account).

Thus, the problem of the origin of the trapped radiation, including identification of the particle-acceleration mechanism, remains unsolved. Transport of charged particles in the trapping

---

[8]We should note, however, that this conclusion is based on a comparatively small amount of experimental material, so that a final judgment as to the effectiveness of this transport mechanism must await simultaneous measurements of the intensity of particles with constant magnetic moment on various L shells near the plane of the geomagnetic equator.

zone during the recovery phase of a storm was examined in [91] with conservation of all three adiabatic invariants. The transport velocity was found to be much higher than that predicted by the theory of diffusion under the influence of sudden impulses. Such transport of electrons with E_e > 160 keV was recorded during the recovery phase of a magnetic storm in IMP-1 measurements [119]. An increase in the flux of these electrons, which was especially strong on the night side of the magnetosphere, was recorded over the entire trapping region all the way to the auroral-radiation zone, and reached a maximum toward the end of the storm.

For lower-energy electrons (E_e > 40-50 keV), the long-established distinct correlation with magnetic activity is characteristic: their fluxes seldom decrease during the principal phase of a storm, and increase during the recovery phase [82, 120]. During magnetically quiet periods, the intensity of electrons with E_e > > 40 keV reaches a maximum near the night boundary of the trapping region [121].

In the aggregate, the experimental data suggest that the origin of these particles is closely related to the auroral zone and that their acceleration is most effective during magnetic storms.[9] On the other hand, note should be taken of an increase in the electron fluxes (E_e > 230 keV) during the recovery phase of a storm on shells with L ∿ 3 and their subsequent transport into the regions of small and large L [123]. It appears that the source of these electrons is situated in the ionosphere or in the plasmapause.[10]

The behavior of trapped protons during magnetic disturbances /14 has also been studied extensively [15, 97, 120, 125, 126].

Significant experimental material has now been accumulated in favor of the operation of several particle-accelerating mechanisms in the magnetosphere. The most thoroughly studied mechanism is acceleration with conservation of the adiabatic invariants of the motion of the charged particle in the magnetic field (see, for example, [127]). In a number of studies [97, 122, 126, 128], however, reference is made to the existence and importance of

---

[9]A new concept, that of the magnetospheric substorm, is discussed in [122]. This is a large-scale, quasiperiodic (with a period of 2-3 hours) increase in the fluxes of high-energy trapped and spilled electrons, accompanied by polar substorms, auroras, and disturbances in the magnetic tail. The magnetic storms and magnetospheric substorms are apparently of common origin [98], although the latter are not related to the formation of a closed ring current.

[10]The possibility of acceleration of trapped electrons during variations of the ionospheric currents was treated in [124].

nonadiabatic effects, which must be among the subjects of future research.

3. Mechanisms of Transfer of Solar-Wind Energy into the Magnetosphere

The expenditure of energy on the geophysical phenomena associated with flow of the solar wind over the earth's magnetosphere is usually $\sim 10^{18}$-10^{19} erg/sec (see, for example, [6, 93]). This energy is expended on auroras[11] ($\sim 10^{18}$ erg/sec), on Joulean and viscous dissipation in the ionosphere ($\lesssim 2 \cdot 10^{18}$ erg/sec) [130], and on formation of the ring current during the magnetic storm[12] ($\sim 10^{19}$ erg/sec). The total kinetic energy of the trapped radiation is $\sim 10^{22}$ ergs (see [6]), so that the latter cannot be responsible for these phenomena and is itself developed as a result of the processes associated with flow of the solar plasma past the magnetosphere. It can hardly be doubted that the main source of the energy of these geophysical phenomena is the solar wind. Its energy flux density is usually on the order of 10^{-1} erg/cm^{2}sec (concentration $n \sim 5$ cm^{-3}, velocity $v \sim 300$ km/sec), and may reach a maximum of 10 erg/cm^{2}sec (at $n \sim 10$ cm^{-3} and $v \sim 1000$ km/sec). Consequently, the total influx of energy to the entire surface of the magnetosphere (with radius $\sim 30 R_E$) is $\sim 10^{20}$-10^{22} erg/sec. Although the mechanism of quasiviscous interaction between the solar wind and the magnetosphere, which is supposed to give rise to convective motions, remains unclear, the upper limit of the power transferred into the magnetosphere[13] can be estimated from the velocity of convection in the magnetosphere at 10^{20} erg/sec [130] or $\sim 1\%$ of the maximum power carried by the solar wind). This exceeds the usual expenditure of energy in auroras and magnetic

---

[11] Very strong auroras may require a much larger influx of energy. According to an estimate [129] for the aurora of 11 February 1958, the luminous energy in the red oxygen line at 6300 Å was $5 \cdot 10^{23}$ ergs only at low and middle latitudes (between -60° and +60° of geomagnetic latitude) on the night side, or 5 times the total energy of the average geomagnetic storm.

[12] The particle energy required to lower the horizontal magnetic-field component by 200 γ is on the order of 10^{23} ergs; formation of the ring current takes place within a few hours, i.e., the energy expenditure may reach $\sim 10^{19}$ erg/sec.

[13] It appears that the relation of the solar wind flowing around the magnetosphere to the convective motions of the plasma within the latter (which occurs as a result of momentum transfer across the magnetopause) is more direct than the relation to the auroras and the ring current, so that estimation of the transferred power from the convection velocity in the magnetosphere appears reasonable (see also [42]). We might also propose, following Axford and Hines [63], that the convective motions may ultimately lead to the appearance of the auroras and the ring current.

storms, so that the solar wind can be regarded as the main source of energy for the most important geophysical phenomena.

But how is energy transferred within the magnetosphere? Direct exchange of charged particles is, of course, difficult, unless account is taken of an interplanetary magnetic field frozen into the solar-wind plasma. But even in this case there are a number of possibilities. B.A. Tverskoy [131] showed that the drift trajectories of particles in the equatorial plane, coinciding with lines of equal intensity B = const, energe at $B < B_S$ into a thin boundary layer between the geomagnetic field and the solar wind (B_S corresponds to the field intensity on the separatrix that bounds the drift trajectories that are closed within the magnetosphere). Figure 7 shows B = const contours according to IMP-1, 2, and 3 satellite measurements [52]. Along contours with $B < B_S$, transitional-region particles drift onto the night side all the way out to $L \sim 7$, from which they may be spilled into the auroral zone if for some reason their pitch angles are reduced.[14] /15

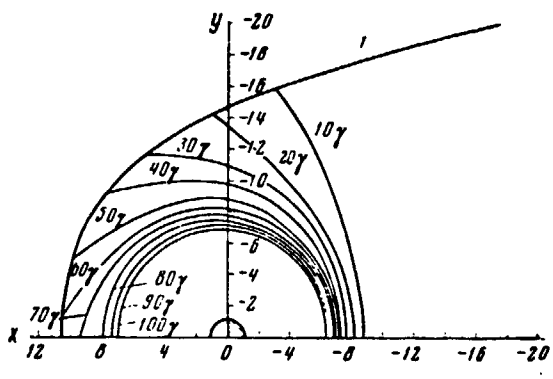

Figure 7. Lines of Constant Geomagnetic-Field Intensity in the Equatorial Plane Constructed According to IMP-1, 2, and 3 Measurements [52]. Geocentric distances in earth radii and values of |B| in gammas are indicated; 1) magnetopause.

Another possibility involves transfer of energy and momentum by various types of waves. Axford [133] believes that magnetoacoustic waves penetrating across the magnetopause transfer the momentum necessary to create convection in the magnetosphere; the power that they transfer may reach $\sim 10^{19}$ erg/sec. Reference [134] considers waves with frequencies on the order of the proton cyclotron frequency generated as a result of instability at the boundary of the magnetosphere. Resonance interactions with these waves result in rapid diffusion of particles across the magnetic field and a large momentum transfer. The effective viscosity is found approximately equal to that necessary to sustain convection [63]. Energy transfer in a collisionless plasma by scattering of particles

[14] Numerical calculations of particle trajectories in [132] showed that particles can penetrate into the magnetosphere if there is a tangential component of the gradient of B on its boundary (such calculations are needed because the conditions for applicability of the drift theory are violated on the boundary).

on magnetic inhomogeneities was studied in a one-dimensional model in [135]. It was found that the effective velocity of diffusion across the magnetic field may exceed the classical value by a factor of 10^6.

The presence of the interplanetary magnetic field enables particles to penetrate into the magnetosphere as a result of adiabatic drift [61] or along lines of the interplanetary field that merge with the geomagnetic field (Dungey [37]).[15] The very possibility of such merging in a collisionless plasma would evidently involve a decrease in the effective conductivity of the plasma as a result of turbulence. Merging of lines of force is a mechanism with a whole series of interesting consequences. As a result of the earth's rotation, some of the lines of force of the geomagnetic field are drawn out into the tail, so that solar-wind energy is accumulated in the form of magnetic energy in the tail [38].[16] Dissipation of this energy may occur by linking of lines of force /16 across the neutral layer of the tail, i.e., by annihilation of the magnetic field, which should result in heating of the plasma (at an intensity of $\sim$1 γ, the magnetic-field energy density $B^2/8\pi$ is 2.5 eV/cm ; If the density is $\sim$0.1 cm^{-3} and $B \approx 5\ \gamma$, the plasma will be heated to an energy on the order of 1 keV). The merging mechanism is capable of supporting the momentum transfer into the magnetosphere that is necessary to sustain convection; the power transmitted into the magnetosphere in the process is $\sim 10^{18}$-10^{19} erg/sec (see, for example, [66, 93]).

Finally, solar-wind energy can be transferred into the magnetosphere by direct transfer of solar-wind electric fields $\mathcal{E} = -(1/c)v \times B$ (in a frame of reference bound to the earth) [64]: since there is doubt as to the existence of surface charges on the boundary of the magnetosphere, the electric field should be

---

[15]Certain indications of experimental confirmation of this merging of fields will be found in [52]: the total magnetic flux across the equatorial plane and across the tail was found to be somewhat smaller than the flux crossing the surface of the earth, and this can be interpreted as a result of merging of some of the lines of force with the interplanetary magnetic field. However, such estimates are burdened with a rather large uncertainty.

[16]Reference [128] reports a lag of $\sim$12 hours between variations of the solar-wind parameters and variations in the flux of electrons with energies $\geq$300 keV on $L \approx 5$. This fact, together with the 1-1.5-hour lag in the development of the magnetic bay and its associated auroral-intensity maximum on the night side behind the daytime-aurora maximum [136] can be interpreted as a result of energy accumulation in the tail and subsequent transfer of energy into the magnetosphere. This process might also explain the development and periodicity of magnetospheric substorms.

continuous.[17] Obviously, this mechanism could explain the close relation between changes in the direction of the interplanetary magnetic field B and certain phenomena in the magnetosphere: a change in the direction of B from north to south is accompanied by the appearance of polar storms [35], and by formation of the ring current responsible for the main phase of magnetic storms [36]. Such phenomena may be associated with changes in the direction of the electric field ε in the magnetosphere.

A change in the direction of the external magnetic field may serve as the "triggering mechanism" that releases magnetic energy accumulated in the tail, with the resulting auroras, magnetospheric substorms, etc. The need for such a mechanism, which was noted by O'Brien [6], results from the sharp contrast between the very large amplitudes of the auroral and magnetic-storm time variations and the insignificant variations of the solar-wind parameters. Thus, fluxes of electrons with energies $\gtrsim 40$ keV spilled into the atmosphere on $L \sim 6$ may vary through six orders and increase by a factor of approximately 5 for each unit of increase in the K_p index [6], while the velocity of the solar wind increases by only 20% at the same time [137]. The intensity of the interplanetary magnetic field and the density of the plasma also undergo comparatively small changes [137].[18]

The "triggering mechanism" may also be an increase in the dynamic pressure of the solar wind on the boundary of the magnetosphere, with the result that lines of force on the daytime side are thrown back into the tail. The increase in the magnetic field in the tail contributes to annihilation of the field and heating of the plasma. Exchange of lines of force between the tail and the daytime side of the magnetosphere should also result in exchange of particles between the tail and the inner regions of the magnetosphere, i.e., it might be one of the mechanisms by which the radiation belts and ring current are replenished. Numerous experimental data appear to be consistent with the hypothesis that the night-side auroras are produced by intrusion of particles from the plasma layer of the tail. Thus, electron-energy spectra measured by Chase [138] on rockets launched into auroras were found to be similar to the spectra of electrons in the plasma layer of the tail. The position of the auroral oval constructed by O.V. /17

[17] On a tangential discontinuity (such as the magnetopause), the normal velocity and magnetic-field components vanish; consequently, the tangential electric-field component is always continuous ($\varepsilon_t = -1/c\,[v \times B]_t = 0$ on either side of the interface).

[18] Frank [158] recently detected geoeffective solar-wind protons with energies $\sim$5-50 keV, whose energy flux is sufficient to give rise to various geophysical phenomena. With this discovery, the question as to the accumulation of energy and the triggering mechanism will perhaps require review.

Khorosheva [139] and Ya.I. Fel'dshteyn [140] (see also [141]) is such that the lines of force connect it to the magnetopause on the daytime side, while on the night side of the oval they come from inner regions of the magnetosphere [52] and possibly from the plasma layer of the tail. The approach of the edge of the neutral layer to the earth on an increase in the K_p index also corresponds to an equatorward shift of the auroral zone. Apparently, the auroras on the daytime side arise as a result of direct intrusion of transition-region particles near the subsolar neutral points (see, for example, [142-143]), while the night-side auroras are due to incursion of particles from the tail. This is also suggested by the aforementioned [136] time variation of the auroras: the intensity maximum of daytime auroras is 1-1.5 hours earlier than the beginning of the magnetic bay and the auroras on the night side of the oval that are associated with it.

It is interesting that the ratio of the fluxes of 200-keV alpha particles to the flux of 100-keV protons in the aurora immediately after the decay of forms with ray structure is approximately the same as that in the solar wind ($\sim$2%) [144], or two orders above the upper limit of this ratio in the inner magnetosphere. Unfortunately, simultaneous measurements were not made in the tail. It appears probable that transitional-region particles can penetrate freely into the tail of the magnetosphere,[19] from which, accelerated as a result of action of a "triggering mechanism" (associated with an increased dynamic pressure of the solar wind on the boundary of the magnetosphere or with a change in the direction of the interplanetary magnetic field), they invade the upper atmosphere, causing auroras. For experimental verification of these conceptions, it would be helpful to make simultaneous measurements of the alpha-particle/proton flux ratio in the transitional region, in the magnetic tail, in the aururas, and in the inner magnetosphere.

The solar wind, which is capable of transferring up to 10^{20} erg/sec into the magnetosphere, is no doubt the principal source of energy supply to the major geophysical phenomena. With the aid of a "triggering mechanism," however, it is capable of releasing energy (possibly accumulated in the tail) that has the rotation of the earth as its source.

---

[19]The measurements of [157] indicated that the magnetopause is apparently unstable beginning at distances of $\geq 11R_E$ near the plane of the geomagnetic equator on the morning and evening sides, so that solar-wind plasma may penetrate into the tail of the magnetosphere across its lateral surface. In [158], the strengthening of the "ring current" on the night side of the magnetosphere is associated with the penetration of 5-50-keV protons from the solar wind across the magnetopause. Laboratory experiments [44-46] also indicate rapid penetration of solar-wind particles into the tail.

Electric fields induced by the rotation of the earth give rise to convective motions in the magnetosphere and are taken into account in construction of convective systems (see, for example, [66, 67]). The phenomenon of unipolar induction has also been advanced as a possible mechanism of charged-particle acceleration (Ya.L. Terletskiy [145], Davis [146], Jones and Bergeson [147]). If a magnetic dipole rotates in a vacuum, large electric fields arise along magnetic lines of force and accelerate particles into the tens of kiloelectron-volts; but if the dipole is surrounded by a plasma fully capable of cancelling the longitudinal electric-field component ($\varepsilon_\parallel = 0$), the particles are not accelerated [147, 148]. The solution obtained by Cunningham and Northrop for this problem in [148] is as follows: if there were no magnetic fields near the earth other than an external dipole field rigidly bound to the rotating earth, particles would experience practically no acceleration when $\varepsilon_\parallel = 0$. However, the presence of an $\varepsilon_\parallel \neq 0$[20] and consideration of external magnetic-field sources (ring current, currents in the magnetopause and in the tail) that are not rigidly bound to the rotating earth results in a substantial change in particle energies. /18

The following question arises: if some part of the earth's rotational energy is used to accelerate particles and to generate convective motions and is perhaps accumulated in the tail of the magnetosphere as a result of sweeping of lines of force into the tail under the action of solar-wind pressure, could not the observed nonuniformity of the earth's rotation prove to be related to the appearance of auroras, magnetic storms, and other effects?[21]

Let q be the power expended on excitation of various geophysical phenomena due to the earth's rotation. An elementary calculation shows that the increase in the length of the day $\Delta\tau = q\tau^2/2W$ (where τ is the length of the day, $W = I\omega^2/2 = 2.15 \cdot 10^{30}$ ergs is the kinetic energy of the earth's rotation, and $\omega = 2\pi/\tau$; $I = 8.1 \cdot 10^{44}$ g·cm^2 is the earth's moment of inertia [149]). The table gives values of $\Delta\tau$ for various q. We note for comparison that the action of tidal forces ($q \sim 10^{19}$ erg/sec) gives $\Delta\tau \approx 2 \cdot 10^{-8}$ sec [149]. The decelerating moment of the forces can be transferred to the earth only via the magnetic field. As we know [150], the volume density of the ponderomotive forces can be expressed in the stationary case in terms of the Maxwellian stress tensor:

$$f_i = \sum_{k=1}^{3} \frac{\partial T_{ik}}{\partial x_k}.$$

---

[20] It is reported in [61] that one of the reasons for the appearance of an $\varepsilon_\parallel$ in a collisionless plasma may consist in different pitch-angle distributions of the electrons and protons.

[21] The authors are indebted to O.L. Vaysberg for a discussion of this problem.

According to the Gauss theorem, the resultant of all forces acting on a certain volume V bounded by a closed surface S reduces to the forces applied to this surface from the outside:

q, erg/sec	Δτ sec	L'
10^{18}	$1.7\cdot10^{-5}$	9,9
10^{19}	$1.7\cdot10^{-6}$	4,6
10^{20}	$1.7\cdot10^{-7}$	2,1
10^{21}	$1.7\cdot10^{-8}$	1,0

$$F_i = \int_V f_i\,dV = \int_V \sum_{k=1}^{3} \frac{\partial T_{ik}}{\partial X_k}\,dV = \oint_S T_{in}\,d\sigma,$$

where n is the outer normal to the surface element dS. For estimates, we shall examine a sphere of radius LR_E and set $T_{ik} = B^2/8\pi$. The accelerating force applied to the surface S of a sphere is

$$F = \frac{I\frac{d\omega}{dt}}{LR_E} = \frac{q}{\omega LR_E}.$$

Equating $F/S = B'^2/8\pi$, we obtain the magnetic-field intensity B' necessary to transfer the decelerating moment to the surface S:

$$B' = \left(\frac{2q}{\omega L^3 R_E^3}\right)^{1/2} \sim L^{-3/2},$$

while the dipole magnetic field in the equatorial plane $B = 0.32L^{-3}$. Consequently, there is a certain critical value L = L' such that B' > B when L > L' and, consequently, the decelerating moment cannot be transmitted to the surface S from more remote regions by the pull of the magnetic field. Values of

$$L' = \left(\frac{0.32^2 R_E^3 \omega}{2q}\right)^{1/3} = 9.9\cdot10^6\cdot q^{-1/3}$$

also appear in the table. It is assumed here that the sphere S is rigidly bound to the rotating earth and that the force F is tangential to the surface of the sphere. The expenditure of $\sim10^{18}$ erg/sec of energy is an order smaller than the tidal expenditure, so that it cannot have a substantial effect on the deceleration of the earth. Consequently, the rotation of the earth is a practically inexhaustible energy source for average geophysical phenomena, which require $\sim10^{18}$ erg/sec. Obviously, a power $\gtrsim10^{21}$ erg/sec ($\Delta\tau \gtrsim 2\cdot10^{-6}$ sec) cannot be transmitted by pulling of geomagnetic-field lines of force even to a phenomenon that takes place near the earth (for example, the auroras). It had been reported previously (Danjon [151]) that following the solar flares of 23 February 1956 and 15 July 1959, the day became 9.7 and 850 μsec longer, respectively. Such large values of Δτ appear doubtful because the corresponding decelerating moment cannot be transmitted

/19

to the earth via its magnetic field.

CONCLUSION

One of the most important problems of magnetospheric physics is study of ways in which solar-wind energy penetrates into the magnetosphere. The solution of such problems as the origin of the radiation belts and the nature of magnetic storms and auroras is related to it. Magnetic measurements on the OGO-A satellite [157] and the results of [158] appear to indicate the possibility of intrusion of transitional-region particles into the tail. Laboratory modelling of the flow of solar wind past the magnetosphere [44-46] also indicates comparatively rapid penetration of particles of the impinging plasma stream into the tail. On the other hand, the position of the auroral oval [139-141] and the similarity between the electron spectra in the auroras and in the tail of the magnetosphere according to [138] suggest that the auroras on the night side of the earth are due to incursion of particles from the plasma layer of the tail. Evidently, the auroras on the daytime side may arise as a result of direct incursion of solar-wind particles (which have been thermalized in the transitional region) in the neighborhood of the neutral points, since the lines of force of the geomagnetic field passing through this region cross the earth's surface in the auroral zone. Coordinated study of these regions with the aid of a special system of satellites would be appropriate. Possible experiments for a satellite passing near a neutral point and the requirements made of the instrument package are discussed in detail in [152]. Figure 8 shows satellite orbits passing through

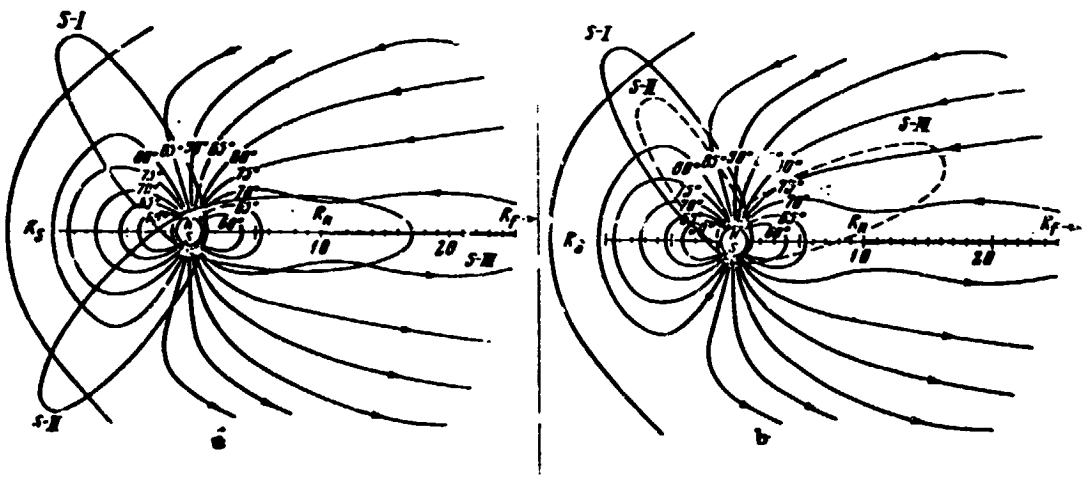

Figure 8. Approximate Orbits of Satellite System for Coordinated Experiments in High-Latitude Regions and in the Tail of the Magnetosphere.

the region of the daytime neutral points and the neutral plane of the tail. Orbits with apogees of $\sim 30R_E$ would make it possible to

compare various characteristics of the geomagnetic field and trapped and auroral radiation within the magnetosphere with the parameters of the solar wind (such as the direction of the frozen magnetic field, particle temperature and concentration, etc.) and the transitional region. However, it is a technically difficult problem to pass a satellite near the south point. Moreover, if the satellite spends a long time outside the magnetosphere, we lose some of the measurements inside the magnetosphere. Instead of orbit SII (Fig. 8a), therefore, it would be advantageous to launch the satellite into the region of the north neutral point, /20 but with a lower apogee, $\sim 15R_E$ (see orbit SII in Fig. 8b). The three-satellite system shown in Fig. 8b (which is more advantageous from an engineering standpoint than that in Fig. 8a) would permit various measurements simultaneously in the solar wind, the transitional region, near the neutral point, in the plasma layer of the tail (including the neutral plane), and in the zones of auroral and trapped radiation.

Such a satellite system could be used, for example, to compare the simultaneous particle compositions in the above regions of near-earth space. This is necessary for solution of many problems in magnetospheric physics, e.g., the mystery of the auroras. There are references [144] to the effect that the ratio of the alpha-particle and proton fluxes (I_α/I_p) in the aurora is approximately the same as in the solar wind, although it is unknown how these particles penetrate into the auroral region; there have been no simultaneous measurements of the ratio I_α/I_p in the tail.

Measurements of particle composition are also of interest in study of various mechanisms of particle transport into the magnetosphere. For example, experiments [153-154] indicate that the ratio I_α/I_p is approximately two orders smaller in the inner magnetosphere than in the solar wind and an order higher than predicted by the theory of particle diffusion as an effect of sudden impulses.

Let us now list other experimental problems related to those discussed above.[22]

1. Determination of the shape of the magnetopause in the polar regions and the shape of the magnetic tail at large distances from the earth.

---

[22]We have not dealt in this survey with such important problems of magnetospheric physics as the formation of the detached collisionless shock wave, processes in the transitional region, the appearance of various kinds of instabilities in the plasma, propagation of various waves in the magnetosphere, and their interaction with the particles.

2. Investigation of the asymmetry of the magnetosphere in the north-south direction that was indicated by experiments on Explorer 12 [155] (such asymmetry is not explained by existing theories).

3. Continuous magnetic measurements on a synchronous satellite ($L \sim 6.6$) would make it possible to reconstruct the most important parameters of the magnetosphere if a satisfactory theoretical model were available (for details, see [51]).

4. Detailed study of the distribution of the magnetic field on and near the boundary of the magnetosphere. /21

In the Hones-Taylor model, lines of force near the sunward side of the magnetopause have, according to [55], high-latitude minima of the intensity B that are topologically related to equatorial minima of B on the night side. As a result, particles that were equatorial on the night side may, as they drift to the daytime side, reach higher latitudes. There is no analogous topological relation in the Mead-Williams model. Thus, these magnetic-field measurements will make it possible to choose among the various theoretical models and, along with direct particle measurements, will make it possible to determine the boundaries of the regions of trapped and quasitrapped radiation. Further, detailed study of the position of the magnetopause may resolve the question as to whether the boundary of the magnetosphere is in fact the envelope of a family of magnetic lines of force (i.e., whether the normal magnetic-field component vanishes at the interface), a matter of interest for the problem of solar-wind flow around the magnetosphere.

5. Detailed measurement of the magnetic field intensity vector in various regions of the magnetosphere are important for evaluation of theoretical models and would yield the distribution of the current density $j = (c/4\pi)$ curl B; in particular, interest attaches to experimental verification of the two-ring-current hypothesis [92].

6. Construction of a model of the electric field in the magnetosphere is of great importance for study of the behavior of particles with energies of a few tens of kiloelectron volts and less. In addition to direct electric-field measurements, this could evidently be done by using Brice's method [66] to reconstruct the pattern of the large-scale electric field from the position and shape of the plasmapause. The "escape" of plasma along non-closed lines of force (polar wind, [78]) should result in distortion of the plasmapause on these lines of force. Experimental verification of this effect, i.e., measurements of the boundary of the plasmasphere at various latitudes, is necessary.

7. Certain convection models (see, for example, [65]) assume that the plasma near the magnetopause should flow in opposite

directions in the magnetosphere and in the transitional region. This conclusion is not inconsistent with the conditions on a tangential discontinuity: $v_{n1} = v_{n2} = 0$, $t_{t1} \neq v_{t2}$.

It would be interesting to find out whether such plasma flows actually occur, since this knowledge is needed for construction of an adequate picture of the electric field.

In conclusion, we enumerate once again the most important problems facing the physics of the magnetosphere.

1. How is the boundary of the magnetosphere (including the polar regions and the magnetic tail) formed as a result of interaction of the solar wind with the geomagnetic field? To what degree is magnetohydrodynamics applicable to description of these phenomena?

2. How does solar-wind energy (or particles) penetrate into the magnetosphere? How is momentum transferred to convective plasma motions in the magnetosphere? Do solar-wind particles invade any region of the magnetosphere directly? Are energy and momentum transferred into the magnetosphere at a constant rate or periodically?

3. Does energy accumulate in the magnetic tail and, if so, how? What is the "triggering mechanism" that suddenly liberates the accumulated energy? What changes in the solar wind cause the transition from quiet to disturbed conditions? What is the mechanism by which magnetospheric substorms arise, and how are they related to the accumulation of energy in the tail and to its release?

4. Is the tail plasma layer a source of the particles that cause auroras? How are these particles accelerated to the necessary energies? (Measurements in the "horns" of the plasma layer, which project into the upper atmosphere in the auroral zone, are especially important.) /22

5. What are the sources of the radiation belts and the mechanisms by which they lose particles? How are particles transported across drift shells of the geomagnetic field? What is the nature of the ring current?

6. To what instabilities is the plasma subject in the magnetosphere, and what is their role in particle acceleration? To what degree are they responsible for the transport of particles across the magnetic field and for particle losses?

REFERENCES

1. S. Chapman and V.C.A. Ferraro, Terr. Magn. Atmos. Electr., 1931, Vol. 36, 77, 171, 186; 1932, Vol. 37, 147, 421; 1933, Vol. 38, 79.

2. E.N. Parker. Astrophys. J., 195-, Vol. 128, 664.
3. E.N. Parker. Interplanetary Dynamic Processes. Russ. ed., Mir, Moscow, 1970.
4. K.I. Gringauz, V.V. Bezrukikh, V.D. Ozerov, and R.Ye. Rybchinskiy. Dokl. Akad. Nauk SSSR, 1960, Vol. 131, 1301.
5. T. Gold. J. Geophys. Res., 1959, Vol. 64, 1219.
6. B.J. O'Brien. Paper Presented at Intern. Symp. on the Solar-Terrestrial Physics, Belgrade, 1966.
7. S.N. Vernov, N.L. Grigorov, and Yu.I. Logachev. Dokl. Akad. Nauk SSSR, 1958, Vol. 120, 123.
8. J.A. Van Allen, G.H. Ludwig, E.C. Ray, and C.E. McIlwain. Jet Propulsion, 1958, Vol. 28, 588.
9. K.I. Gringauz, V.G. Kurt, V.I. Moroz, and I.S. Shklovskiy. Dokl. Akad. Nauk SSSR, 1960, Vol. 132, 1062.
10. K.I. Gringauz. Space Res., 1962, Vol. 1, 539; Planet. Space Sci., 1963, Vol. 11, 281.
11. D.L. Carpenter. Paper presented at the Fourteenth General Assembly of URSI (Tokyo), 1963.
12. Sh.Sh. Dolginov, Ye.G. Yeroshenko, L.N. Zhuzgov, N.V. Pushkov, and L.O. Tyurmina. Iskusstvennyye sputniki Zemli (Artificial Earth Satellites), Izd-vo Akad. Nauk SSSR, 1960, No. 5, 16.
13. L.J. Cahill. J. Geophys. Res., 1966, Vol. 71, 4505.
14. L.A. Frank. J. Geophys. Res., 1967, Vol. 72, 1905.
15. L.A. Frank. J. Geophys. Res., 1967, Vol. 72, 3753.
16. N.F. Ness, C.S. Scearce, and J.B. Seek. Initial Results of the IMP-1 Magnetic Field Experiment. J. Geophys. Res., 1964, Vol. 69, 3531.
17. Geofizika. Okolozemnoye kosmicheskoye prostranstvo (Geophysics. Near-Earth Cosmic Space), Moscow, "Mir," 1964.
18. Kosmicheskaya fizika (Space Physics), Moscow, "Mir," 1966.
19. Solnechno-zemnaya fizika (Solar-Terrestrial Physics), Moscow, "Mir," 1968.
20. B.A. Tverskoy. Dinamika radiatsionnykh poyasov Zemli (The Dynamics of the Earth's Radiation Belts), Moscow, "Nauka," 1968.
21. V.P. Shabansky. Magnetospherical Processes and Related Geophysical Phenomena. Space Sci. Rev., 1968, Vol. 8, 366.
22. V.N. Zhigulev and Ye.A. Romishevskiy. Dokl. Akad. Nauk SSSR, 1959, Vol. 127, 1001.
23. J.D. Coll and J.H. Huth. Phys. Fluids, 1959, Vol. 2, 624.
24. Yu.S. Sigov. Space Res., 1966, Vol. VII, 550.
25. J. Midgley and L. Davis. J. Geophys. Res., 1962, Vol. 67, 409.
26. J. Midgley and L. Davis. J. Geophys. Res., 1963, Vol. 68, 5111.
27. R.J. Slutz. J. Geophys. Res., 1962, Vol. 67, 505.
28. R.J. Slutz and J.R. Winkelman. J. Geophys. Res., 1964, Vol. 69, 4933.
29. D.B. Beard. Rev. Geophys., 1964, Vol. 2, 335.
30. G.D. Mead and D.B. Beard. J. Geophys. Res., 1964, Vol. 69, 1169.
31. I.R. Spreiter and B.R. Briggs. J. Geophys. Res., 1962, Vol. 67, 37.

32. L.S. Chesalin. Trudy Pyatoy Vsesoyuznoy yezhegodnoy zimney shkoly po kosmofizike (mart 21 - aprel' 5, 1968) (Transactions of Fifth Annual Winter School for Space Physics) (March 21-April 5, 1968). Kola Division of the USSR Academy of Sciences. "Apatity," 1968, p. 223.
33. D.I. Williams and G.D. Mead. J. Geophys. Res., 1965, Vol. 70, 3017.
34. J.R. Spreiter and W.P. Jones. J. Geophys. Res., 1963, Vol. 68, 3555.
35. D.H. Fairfield and L.J. Cahill. J. Geophys., 1966, Vol. 71, 155.
36. J. Hirshberg and D.S. Colburn. A Detailed Comparison of an Interplanetary Magnetic Storm and its Corresponding Geomagnetic Storm. Paper Presented at the Intern. Symp. on the Physics of the Magnetosphere, Washington, Sept. 3-13, 1968.
37. J.W. Dungey. Phys. Rev. Letters, 1961, Vol. 6, 47.
38. W.I. Axford, H.E. Petschek, and G.L. Siscoe. J. Geophys. Res., 1965, Vol. 70, 1231.
39. A.J. Dessler and R.D. Juday. Planet. Space Sci., 1965, Vol. 13, 63.
40. M.V. Samokhin. Magnitnaya gidrodinamika, 1966, Vol. 4, 19. /23
41. J.R. Spreiter, A.L. Summers, and A.Y. Alksne. Planet. Space Sci., 1966, Vol. 14, 223.
42. M. Dryer and G.R. Heckman. Planet. Space Sci., 1967, Vol. 15, 515.
43. V.B. Baranov. "Kosmicheskiye issledovaniya," 1969, Vol. 7, 109.
43a. K. Schindler. Rev. Geophys., 1969, Vol. 7, No. 1-2.
44. G.G. Managadze, I.M. Podgornyy, and V.D. Rusanov. Geomagnetizm i aeronomiya, 1968, Vol. 8, 545.
45. G.G. Managadze and I.M. Podgornyy. Geomagnetizm i aeronomiya, 1968, Vol. 8, 618.
46. G.G. Managadze and I.M. Podgornyy. Dokl. Akad. Nauk SSSR, 1968, Vol. 180, 1333.
47. G.D. Mead. J. Geophys. Res., 1964, Vol. 69, 1181.
48. E.W. Hones. J. Geophys. Res., 1963, Vol. 68, 1209.
49. H.E. Taylor and E.W. Hones. J. Geophys. Res., 1965, Vol. 70, 3605.
50. H.E. Taylor. J. Geophys. Res., 1966, Vol. 71, 5135.
51. J.G. Roederer. Quantitative Models of the Magnetosphere. Review Paper Presented at the Intern. Symp. on the Physics of the Magnetosphere. Washington, Sept. 3-13, 1968.
52. D.H. Fairfield. The Average Magnetic Field Configuration of the Outer Magnetosphere. Paper Presented at the Intern. Symp. on the Physics of the Magnetosphere. Washington, Sept. 3-13, 1968.
53. W.D. Cummings and P.I. Coleman. J. Geophys. Res., 1968, Vol. 73, 5699.
54. W.P. Olson. The Determination of the Shape of the Magnetopause for Various Orientations of the Geomagnetic Dipole with Respect to the Solar Wind. Paper Presented at the Intern. Symp. on the Physics of the Magnetosphere. Washington, Sept. 3-13, 1968.

55. A.Ye. Antonova and V.P. Shabanskiy. Geomagnetizm i aeronomiya, 1968, Vol. 8, 801.
56. C.E. McIlwain. J. Geophys. Res., 1961, Vol. 66, 3681.
57. L.D. Kavanagh. J. Geophys. Res., 1968, Vol. 73, 185.
58. T. Northrop and E. Teller. Phys. Rev., 1960, Vol. 117, 215.
59. D.P. Stern. J. Geophys. Res., 1967, Vol. 72, 3995.
60. D.P. Stern. J. Geophys. Res., 1968, Vol. 73, 1373.
61. H. Alfven and C.-G. Faelthammer. Cosmical Electrodynamics. Russ. ed., Mir, Moscow, 1967.
62. V.I. Krasovskiy. Issledovaniya kosmicheskogo prostranstva (Investigations of Cosmic Space), Moscow, "Nauka," 1965, p. 11.
63. W.I. Axford and C.O. Hines. Can. J. Phys., 1961, Vol. 39, 1433.
64. H. Alfven. J. Geophys. Res., 1968, Vol. 73, 4379.
65. A. Nishida. J. Geophys. Res., 1966, Vol. 71, 5669.
66. N.M. Brice. J. Geophys. Res., 1967, Vol. 72, 5193.
67. T. Obayashi and A. Nishida. Space Sci. Rev., 1968, Vol. 8, 3.
68. L.D. Kavanagh, J.W. Freeman, and A.J. Chen. J. Geophys. Res., 1968, Vol. 73, 5511.
69. A.J. Hundhausen, J.R. Asbridge, S.J. Bame, H.E. Gillbert, and I.B. Strong. Observations of Plasma Flow in the Earth's Magnetosheath. Paper Presented at the Intern. Symp. on the Physics of the Magnetosphere. Washington, Sept. 3-13, 1968.
70. L.D. Landau and Ye.M. Lifshits. Elektrodinamika sploshnykh sred (The Electrodynamics of Continuous Media), Moscow, GITTL, 1956, Chapter VIII.
71. L.J. Cahill and P.G. Amazeen. J. Geophys. Res., 1963, Vol. 68, 1835.
72. J.W. Freeman, L.D. Kavanagh, and C.S. Warren. Plasma Flow in the Magnetosphere. Paper Presented at the Intern. Symp. on the Physics of the Magnetosphere. Washington, Sept. 3-13, 1968.
73. L.A. Frank. Several Comments Concerning the Distributions of Low-Energy Charged Particles in the Earth's Magnetosphere. Paper Presented at the Intern. Symp. on the Physics of the Magnetosphere. Washington, Sept. 3-13, 1968.
74. J.W. Freeman, C.S. Warren, and J.J. Maguire. J. Geophys. Res., 1968, Vol. 73, 5719.
75. D.L. Carpenter. J. Geophys. Res., 1966, Vol. 71, 693.
76. J.W. Freeman. J. Geophys. Res., 1968, Vol. 73, 4151.
77. R.D. Sharp, R.G. Johnson, M.F. Shea, and G.B. Shock. J. Geophys. Res., 1967, Vol. 72, 227.
78. P.M. Banks and T.E. Holzer. The Polar Wind. Paper Presented at the Intern. Symp. on the Physics of the Magnetosphere. Washington, Sept. 3-13, 1968; see also:J.Geophys.Res. 1968, 73, 6846.
79. S.N. Vernov, P.V. Vakulov, S.N. Kuznetsov, Yu.I. Logachev, Ye. I. Sosnovets, and V.L. Stolpovskiy. Geomagnetizm i aeronomiya, 1967, Vol. 7, 417.
80. J.G. Roederer. J. Geophys. Res., 1967, Vol. 72, 981.
81. K.I. Gringauz. J. Geophys. Res., 1964, Vol. 69, 1007.
82. J.W. Freeman. J. Geophys. Res., 1964, Vol. 69, 1691.
83. V.M. Freeman. J. Geophys. Res., 1968, Vol. 73, 2839.

84. V.M. Vasyliunas. A Survey of Low Energy Electrons on the Day Side of the Magnetosphere with OGO-3. Paper Presented at the Intern. Symp. on the Physics of the Magnetosphere. Washington, Sept. 3-13, 1968.
85. K.A. Anderson, H.K. Harris, and R.J. Paoli. J. Geophys. Res., /24 1965, Vol. 70, 1039.
86. I.B. McDiarmid and I.R. Burrows. J. Geophys. Res., 1965, Vol. 70, 3031.
87. K.W. Behannon and N.F. Ness. J. Geophys. Res., 1966, Vol. 71, 2327.
88. E.W. Hones, S.J. Bame, S.E. Singer, and R.R. Brawn. J. Geophys. Res., 1968, Vol. 73, 6189.
89. G.V. Starkov and Ya.I. Fel'dshteyn. Geomagnetizm i aeronomiya, 1967, Vol. 7, 62.
90. S.I. Belyakova, S.A. Zaytseva, and M.I. Pudovkin. Geomagnetizm i aeronomiya, 1968, Vol. 8, 712.
91. V.D. Pletnev and. V.P. Shalimov. Paper Presented at the International Symposium on the Physics of the Magnetosphere. Washington, USA, September 3-13, 1968.
92. S.-I. Akasofu. Space Sci. Rev., 1963, Vol. 2, 91.
93. T. Obayashi. Paper Presented at the Intern. Symp on the Solar-Terrestrial Physics, Belgrade, 1966.
94. S.A. Zaytseva, M.I. Pudovkin, and O.I. Shumilov. Geomagnetizm i aeronomiya, 1968, Vol. 8, 905.
95. T.N. Davis and R. Pathasarathy. J. Geophys. Res., 1967, Vol. 72, 5825.
96. V.P. Shalimov. Kosmicheskiye issledovaniya, 1968, Vol. 6, 941.
97. W.L. Brown, L.J. Cahill, L.R. Davis, C.E. McIlwain, and C.S. Roberts. J. Geophys. Res., 1968, Vol. 73, 153.
98. P.J. Coleman and W.D. Cummings. Storm-Time Variations in the Magnetic Field of Synchronous Distances. Paper Presented at the Intern. Symp. on the Physics of the Magnetosphere. Washington, Sept. 1968.
99. S. Chapman. In: "Geophysics. The Earth's Environment," 1963, p. 373.
100. E.J. Smith, P.J. Coleman, D.L. Judge, and C.P. Sonett. J. Geophys. Res., 1960, Vol. 65, 1858.
101. Sh.Sh. Dolginov, Ye.G. Yeroshenko, and L.N. Zhuzgov. Issledovaniya kosmicheskogo prostranstva (Investigations of Cosmic Space), Moscow, "Nauka," 1965, p. 342.
102. R.A. Hoffman and P.A. Bracken. J. Geophys. Res., 1965, Vol. 70, 3541; J. Geophys. Res., 1967, Vol. 72, 6039.
103. N. Sckopke. J Geophys. Res., 1966, Vol. 71, 3125.
104. A.J. Dessler and E.N. Parker. J. Geophys. Res., 1959, Vol. 64, 2239.
105. S. Olbert, G L. Siscoe, and V.M. Vasyliunas. J. Geophys. Res., 1968, Vol. 73, 1115.
106. S.N. Vernov. Special Lecture at the Fifth IGY General Assembly, Moscow, 1958.
107. S.F. Singer. Phys. Rev. Letters, 1958, Vol. 1, 171, 181.
108. P.J. Kellogg. Nuovo Cimento, Ser. X, 1959, Vol. 11, 48.
109. W.N. Hess. Radiation Trapped in the Earth's Magnetic Field, ed. by B.M. McCormac, 1966, p. 187.

110. P.J. Kellogg. Nature, 1959, Vol. 183, 1295.
111. E.N. Parker. J. Geophys. Res., 1960. Vol. 65, 3117.
112. L. Davis and D.B. Chang. J. Geophys. Res., 1962, Vol. 67, 2 69.
113. B.A. Tverskoy. Geomagnetizm i aeronomiya, 1964, Vol. 4, 436.
114. A.I. Yershkovich, G.A. Skuridin, L.S. Chesalin, and V.P. Shalimov. "Kosmicheskiye issledovaniya," 1967, Vol. 5, 792.
115. L.S. Chesalin, A.I. Ershkowich, and G.A. Skuridin. Space Res., VIII, Amsterdam, 1968.
116. A.I. Yershkovich and L.S. Chesalin. Trudy V Vsesoyuznoy yezhegodnoy zimney shkoly po kosmofizike (Mart 21-Aprel' 5, 1968) (Transactions of Fifth Annual All-Union Winter School for Space Physics) (March 21-April 5, 1968), Kola Division of the USSR Academy of Sciences. "Apatity," 1968, p. 231.
117. L.D. Kavanagh. J. Geophys. Res., 1968, Vol. 73, 2959.
118. T.J. Birmingham and F.C. Jones. Two Problems Dealing with the Radial Difiusion of Trapped Particles. Paper Presented at the Intern. Symp. on the Physics of the Magnetosphere. Washington, Sept. 3-13, 1968.
119. T. Muryama and T. Hirose. Variation of Electron Intensities in the Magnetic Tail and in the Outer Radiation Belt with Geomagnetic Disturbances. Paper Presented at the Intern. Symp. on the Physics of the Magnetosphere. Washington, Sept. 3-13, 1968.
120. J.A. Van Allen, L.A. Frank, and H.K. Hills. J. Geophys. Res., 1964, Vol. 69, 2171.
121. G.K. Parks, T.W. Lezniak, and J.R. Winckler. The Magnetospheric Substorm: A Fundamental Mode of Production of Energetic Electrons in the Van Allen Belt. Paper Presented at the Intern. Symp. on the Physics of the Magnetosphere. Washington, Sept. 3-13, 1968.
122. L.A. Frank. J. Geophys. Res., 1965, Vol. 70, 1593.
123. D.J. Williams, J.E. Arens, and L.J. Lanzerotti. J. Geophys. Res., 1968, Vol. 73, 5673.
124. I.B. Cladis. J. Geophys. Res., 1966, Vol. 71, 5019.
125. I.A. Savenko, M.V. Tel'tsov, and P.I. Shavrin. Geomagnetizm i aeronomiya, 1968, Vol. 6, 298.
126. A. Konradi. J. Geophys. Res., 1968, Vol. 73, 3449.
127. R.W. Fillius and C.E. McIlwain. J. Geophys. Res., 1967, Vol. 72, 4011.
128. L.J. Lanzerotti. J. Geophys. Res., 1968, Vol. 73, 438. /25
129. Yu.L. Truttse. Planet. Space Sci., 1968, Vol. 16, 981.
130. E. Walbridge, J. Geophys. Res., 1967, Vol. 72, 5213.
131. B.A. Tverskoy. Geomagnetizm i aeronomiya, 1964, Vol. 4, 224.
132. T.E. Stevenson and C. Comstock. J. Geophys. Res., 1968, Vol. 73, 175.
133. W.I. Axford. Planet. Space Sci., 1964, Vol. 12, 45.
134. A. Eviatar and R.A. Wolf. J. Geophys. Res., 1968, Vol. 73, 5561.
135. T. Obayashi and T. Tsuda. Energy Transfer Across the Magnetospheric Boundary, 1966 (Preprint).
136. G.V. Starkov and Ya.I. Fel'dshteyn. Geomagnetizm i aeronomiya, 1967, Vol. 7, 367.

137. C.W. Snyder, M. Neugebauer, and U.R. Rao. J. Geophys. Res., 1963, Vol. 68, 6361.
138. L.M. Chase. Energy Spectra of Auroral Zone Particles. Paper Presented at the Intern. Symp. on the Physics of the Magnetosphere. Washington, Sept. 3-13, 1968.
139. O.V. Khorosheva. Geomagnetizm i aeronomiya, 1961, Vol. 1, 696; 1962, Vol. 2, 839; 1963, Vol. 3, 363.
140. Ya.I. Fel'dshteyn. Geomagnetizm i aeronomiya, 1963, Vol. 3, 183.
141. Ya.I. Feldstein and G.V. Starkov. Planet. Space. Sci., 1968, Vol. 16, 129.
142. A.I. Yershkovich, V.D. Pletnev, and G.A. Skuridin. Kosmicheskiye issledovaniya, 1966, Vol. 4, 378.
143. A.I. Ershkowich, V.D.Pletnev, and G.A. Skuridin. J. Atmos. Ter. Phys., 1967, Vol. 29, 367.
144. D.R. Reasoner, R.H. Eather, and B.J. O'Brien. J. Geophys. Res., 1968, Vol. 73, 4185.
145. Ya.P. Terletskiy. Dokl. Akad. Nauk SSSR, 1945, Vol. 47, 104; ZhETF, 1949, Vol. 19, 1059.
146. L. Davis. Phys. Rev., 1947, Vol. 72, 632; 1948, Vol. 73, 536.
147. E.W. Hones and J.E. Bergeson. J. Geophys. Res., 1965, Vol. 70, 4951.
148. T.J. Birmingham and T.G. Northrop. J. Geophys. Res., 1968, Vol. 73, 83.
149. C.W. Allen. Astrophysical Quantities. Russ. ed., IL, Moscow, 1960, p. 132.
150. I.Ye. Tamm. Osnovy teorii elektrichestva (Fundamentals of the Theory of Electricity), Moscow, GITTL, 1956.
151. M.A. Danjon. Comptes Rendus, Vol. 247, 2061, 1958; 1960, Vol. 250, 1399.
152. B.J. O'Brien. Space Sci. Rev., 1967, Vol. 7, 293.
153. S.M. Krimigis and J.A. Van Allen. J. Geophys. Res., 1967, Vol. 72, 5779.
154. G.A. Paulikas and J.B.Blake. Trapped Alpha-Particles in the Radiation Belt. Paper Presented at the Intern. Symp. on the Physics of the Magnetosphere. Washington, Sept. 3-13, 1968.
155. G.D. Mead and L.J. Cahill. J. Geophys. Res., 1967, Vol. 72, 2737.
156. J.P. Heppner. Magnetospheric Convection Patterns Inferred from High Latitude Activity. August, 1968 (Preprint).
157. J.P. Heppner, M. Sugiura, T.L. Skillman, B.G. Ledley, and M. Campbell. J. Geophys. Res., 1967, Vol. 72, 5417.
158. L.A. Frank. Further Comments Concerning Low-Energy Charged Particle Distributions within the Earth's Magnetosphere and its Environs. U. of Iowa. Res. Rep. 69-42, July, 1969.

N75 13709

HYDROMAGNETIC WAVES GUIDED BY THE GEOMAGNETIC FIELD

(Translation of "Gidromagnitnyye volny, napravlyavemyye geomagnitnym polem.")

L. L. Van'yan, L. A. Abramov, M. B. Gokhberg, and V. L. Yudovich

ABSTRACT

Properties of hydromagnetic waves propagating in the magnetosphere from a source of limited dimensions are considered. It is shown that they are closely related to electric currents flowing along geomagnetic lines of force. The notions developed form a theoretical basis for interpretation of fluctuations and polar bays. With 4 source citations.

HYDROMAGNETIC WAVES GUIDED BY THE GEOMAGNETIC FIELD

/26

L.L. Van'yan, L.A. Abramov, M.B. Gokhberg,
and V.L. Yudovich

Geomagnetic disturbances localized on comparatively small areas in the hundreds or few thousands of kilometers are often observed at the earth's surface, especially in high latitudes. The intensities of these disturbances drop off more or less sharply with increasing distance from this region.

Pulsations with periods in the tens and hundreds of seconds and baylike disturbances lasting about an hour are among the variations of this type. In the attempt to comprehend the nature of such geomagnetic variations, the investigator first inquires as to the location of the disturbance source giving rise to the localized electric currents in the lower ionosphere. The posing of this question results from the fact that local disturbances in an isotropic medium can be produced only by a nearby source, while the electromagnetic field of a distant source is characterized by small spatial gradients and covers a large area. It is clear that for a source located in the magnetosphere, the laws of disturbance transport undergo radical changes. It becomes possible for the electromagnetic field to be transported along geomagnetic lines of force with no appreciable dissipation.

Let us examine this question in greater detail. We begin with the choice of model for the source. Obviously, the plane wave usually used to study the behavior of propagating waves in a plasma is not valid in this case: it does not enable us to investigate the geometrical dissipation of disturbance energy with increasing distance from the source. We are therefore obliged to consider a source of limited dimensions. The limiting case is the point source, which may be either of two types.

The first type of source is a small region of the plasma in which charge separation takes place. We shall not touch upon the numerous hypotheses as to the causes of charge separation in the magnetosphere, being interested only in the result, which reduces to equivalence of the small region under consideration to an electric dipole with a time-dependent moment.

The second type of source is a closed current of small dimension that is equivalent to a magnetic dipole. Such a source might arise, for example, on expansion of a small volume of plasma in a magnetic field. The currents induced on the boundary of this volume are equivalent to a magnetic dipole whose moment is parallel to the external field. In concluding our discussion of these two types of idealized sources, we note that we shall be concerned with disturbances whose intensities are small by comparison with

the geomagnetic field B.

Let us place the above sources in the magnetospheric plasma. Because of the high intensity of the geomagnetic field, the cold-plasma approximation is often used, without consideration of the magnetospheric regions in which this idealization may be violated. Propagation of disturbances in the plasma is possible only as a result of an inseparable combination of mechanical and electromagnetic processes. In our case of small (compared to the geomagnetic field) disturbances, the magnetized plasma may be likened to a dielectric with a complex dielectric tensor ε' [1]. If we neglect the curvature of the geomagnetic lines of force and direct B along the Z axis, the tensor takes the form /27

$$\hat{\varepsilon}' = \begin{vmatrix} \varepsilon_{xx} & \varepsilon_{xy} & 0 \\ \varepsilon_{yx} & \varepsilon_{yy} & 0 \\ 0 & 0 & \varepsilon'_{zz} \end{vmatrix}.$$

Three characteristic frequencies determine the relations among the components of the tensor: the frequency of collisions of charged particles with one another and with neutral molecules, the frequency of rotation of the ions around geomagnetic lines of force (the ion gyrofrequency ω_i), and, finally, the frequency of the geomagnetic variation.

In most of the magnetosphere, the collision frequencies are so low that they can be neglected by comparison with the ion gyrofrequency. We recall that the latter satisfies the inequality $\omega_i > 1\text{-}10$ even on the periphery of the magnetosphere. The magnetospheric plasma is usually regarded as collisionless for practical purposes beyond the first few hundred kilometers. In this case, as we know [1],

$$\frac{\varepsilon_{xy}}{\varepsilon_{xx}} = \frac{\omega\omega_e}{\omega_i\omega_e - \omega^2},$$

where ω_e is the electron gyrofrequency, which exceeds ω_i by a factor of 1840. It is easily seen that a property of the geomagnetic-disturbance frequency range of interest to us consists in validity of the inequality $\varepsilon_{xy} \ll \varepsilon_{xx}$. In fact, for a variation with period longer than 100 sec,

$$\frac{\varepsilon_{xy}}{\varepsilon_{xx}} \approx \frac{\omega}{\omega_i} \leqslant {}^1/_{20}.$$

In most of the magnetosphere, therefore, the dielectric tensor becomes diagonal:

$$\varepsilon_{xx} = \varepsilon_{yy} = \frac{\omega_0^2}{\omega_e \omega_i} \varepsilon_0; \qquad \varepsilon_{xy} = 0; \qquad \varepsilon'_{zz} = \frac{-\omega_0^2 \varepsilon_0}{\omega(\omega + i\nu_{ei})}.$$

The tensor components transverse to the magnetic field are real in a collisionless plasma, while the longitudinal component is complex. It is much greater than ε_{xx} in absolute magnitude. For example, when

$$\omega = 10^{-2}, \text{ we have } \frac{|\varepsilon_{zz}|}{\varepsilon_{xx}} > 10^4.$$

At heights in the first few hundred kilometers, the tensor components become imaginary because of the sharp increase in the number of collisions with neutral molecules. Here it is more convenient to use the tensor $\hat{\sigma}$

$$\hat{\sigma} = \begin{vmatrix} \sigma_1 & \sigma_2 & 0 \\ -\sigma_2 & \sigma_1 & 0 \\ 0 & 0 & \sigma_0 \end{vmatrix},$$

where σ_0 is the conductivity along the geomagnetic field, σ_1 is the conductivity across the geomagnetic field but along the applied electric field (Pedersen conductivity), and σ_2 is the conductivity across both the geomagnetic and applied electric fields (Hall conductivity).

On the whole, we may state that the collisionless magnetospheric plasma with diagonal tensor $\hat{\varepsilon}$ is limited near the earth to a comparatively thin film with tensor conductivity (the ionosphere). The ionosphere is separated from the conducting earth by a layer of nonconductive atmosphere approximately 80 km thick.

The most important property of the magnetospheric plasma consists in the fact that it is pierced by curvilinear geomagnetic lines of force. The direction along which the complex dielectric constant is large in absolute value (ε_{zz}) varies, following the geomagnetic-field vector. This gives rise to serious mathematical difficulties in solving the problem of disturbance propagation in the magnetosphere. However, a number of characteristic features of the process that interests us can be investigated on a much simpler model. Let us neglect the curvature of the lines of force and assume that, like the plasma density, the geomagnetic field is everywhere homogeneous. The result is the problem of a harmonic dipole in a medium with a diagonal dielectric tensor. The electric E and magnetic b fields of the disturbance must satisfy Maxwell's equations, which take the following form in the SI system:

/28

$$\operatorname{rot} \boldsymbol{b} = -i\omega\mu_0 \hat{\varepsilon}' \boldsymbol{E},$$

$$\operatorname{rot} \boldsymbol{E} = i\omega \boldsymbol{b}.$$

If a magnetic dipole is placed in the plasma with its moment along the geomagnetic field, recourse is usually taken to the vector potential A^*, which is introduced with the aid of the equalities

$$b = \varepsilon_{xx}\mu_0\omega^2 A^* + \text{grad div } A^*,$$

$$E = i\omega\varepsilon_{xx}\hat{\varepsilon}^{-1}\,\text{rot}\,A^*,$$

where

$$\hat{\varepsilon}^{-1} = \begin{vmatrix} \frac{1}{\varepsilon_{xx}} & 0 & 0 \\ 0 & \frac{1}{\varepsilon_{xx}} & 0 \\ 0 & 0 & \frac{1}{\varepsilon_{zz}} \end{vmatrix}.$$

(see [3]). In virtue of the axial symmetry of the problem, it is found possible to put $A_x^* = A_y^* = 0$. We find an equation for the single nonzero vector-potential component by substituting the expressions for b and E into the second Maxwell equation:

$$\text{rot}\,\varepsilon_{xx}\hat{\varepsilon}^{-1}\,\text{rot}\,A^* = \varepsilon_{xx}\mu_0\omega^2 A^* + \text{grad div } A^*,$$

from which

$$\frac{\partial^2 A_z^*}{\partial x^2} + \frac{\partial^2 A_z^*}{\partial y^2} + \frac{\partial^2 A_z^*}{\partial z^2} + K_1^2 A_z^* = 0.$$

where

$$k_\perp = \omega\sqrt{\varepsilon_{xx}\mu_0}.$$

The solution of the above equation for a source in the form of a magnetic dipole is

$$A_z^* = \frac{M\mu_0}{4\pi}\,\frac{e^{ik_\perp R}}{R},$$

where

$$R = \sqrt{x^2 + y^2 + z^2}.$$

The basic characteristic feature of this solution is spherical symmetry, which suggests isotropic propagation of the geomagnetic wave in all directions from the magnetic dipole. We see from the formula for A_z^* that this process is accompanied by a decrease in the intensity of the wave. We are struck by the absence of directional propagation of the disturbance along geomagnetic lines of /29

force. This property should be recognized as the most important property of eddy-current-type sources, one that distinguishes them from sources of the electric-dipole type, to which we shall now turn our attention.

In this case, the field components are expressed in terms of the vector potential A, and the symmetry of the solution permits setting $A_y = 0$ [3] (the dipole is directed along the X axis):

$$E = i\omega A - \operatorname{grad} u,$$

$$b = \operatorname{rot} A, \quad i\omega\varepsilon_{xx}\mu_0 u = \operatorname{div} A.$$

Substituting these expressions into the first Maxwell equation, we find

$$\frac{\partial^2 A_x}{\partial x^2} + \frac{\partial^2 A_x}{\partial y^2} + \frac{\partial^2 A_x}{\partial z^2} + k_\perp^2 A_x = 0,$$

$$\frac{\partial^2 A_z}{\partial^2 A_z} + \frac{\partial^2 A_z}{\partial^2 y^2} + \frac{\varepsilon_{xx}}{\varepsilon_{xx}}\frac{\partial^2 A_z}{\partial z^2} + k_\parallel^2 A_z =$$

$$= \left(1 - \frac{\varepsilon_{zz}}{\varepsilon_{xx}}\right)\frac{\partial^2 A_x}{\partial x\, dz}, \text{ where } k_\parallel = \omega\sqrt{\varepsilon_{zz}\mu_0}.$$

It is easily seen that the vector-potential component A_x, which is parallel to the current in the source, is defined by the expression

$$A_x = \frac{I\mu_0}{4\pi}\frac{e^{ik_\perp R}}{R},$$

where I is the dipole moment. The properties of the part of the disturbance that is related to the component A_x are the same as in the field of a magnetic dipole. This part of the field is dissipated isotropically, its intensity diminishing with increasing distance from the source. Sharp anisotropy of the electrical properties of the plasma has no influence on the horizontal component of the vector potential.

To determine A_x, we present it in the form of a Hankel integral transform:

$$A_z = \frac{I\mu_0}{4\pi}\frac{\partial}{\partial x}\int_0^\infty zJ_0(mr)\,dm,$$

using a similar representation for A_x:

$$A_x = \frac{I\mu_0}{4\pi}\int_0^\infty XJ_0(mr)\,dm.$$

It follows from the formula for the Sommerfeld integral that

$$X = \frac{m}{n_\perp} e^{-n_\perp |z|}, \text{ where } n_\perp^2 = m^2 - k_\perp^2.$$

Using the equation for A_Z, we find

$$\frac{d^2Z}{d^2z^2} - (\Lambda n_\parallel)^2 Z = (\Lambda^2 - 1) X',$$

where

$$\Lambda = \frac{k_\perp}{k_\parallel}.$$

Solving the equation, we find for z > 0 /30

$$Z = \frac{e^{-\Lambda n_\parallel z} - e^{-n_\perp z}}{m}.$$

Finally,

$$A_z = -\frac{I\mu_0 z}{4\pi r} \int_0^\infty (e^{-n_\perp z} - e^{-\Lambda n_\parallel z}) J_1'(mr)\, dm,$$

with the integral evaluated in the form

$$A_z = \frac{I\mu_0}{4\pi} \frac{zz}{r^2} \left(\frac{e^{ik_\perp R}}{R} - \Lambda \frac{e^{ik_\parallel \bar{R}}}{\bar{R}} \right),$$

where $\bar{R}^2 = r^2 + (\Lambda z)^2$.

Let us consider the component A_Z near the geomagnetic tube of force on which the source is located, i.e., at r << z. We construct the cone in accordance with the equation r = Λz. Since Λ ∼ ∼ 10^{-2}-10^{-4}, the vertex angle of our cone is reckoned in minutes of arc. In this region, where z >> r >> Λz:

$$A_z = \frac{I\mu_0}{4\pi} \frac{zz}{r^3} \left(\frac{e^{ik_\perp z}}{z} - \Lambda \frac{e^{ik_\parallel r}}{r} \right) =$$

$$= \frac{I\mu_0}{4\pi} \frac{z}{r^3} e^{ik_\perp z} \left(1 - \frac{\Lambda r}{r} \frac{e^{ik_\parallel r}}{e^{ik_\perp z}} \right) \approx \frac{I\mu_0}{4\pi} \frac{z}{r^3} e^{ik_\perp z}.$$

The resulting expression is interesting primarily because the component A does not decrease along the Z axis in the region outside

the cone (but near the tube of force on which the source is situated). Consequently, it becomes possible for the disturbance to be transported along the geomagnetic field with practically no damping. With the approach to the Z axis, $|A_z|$ increases in accordance with the decrease in r. Its maximum value as $r \to 0$ can be found by examining the region inside the cone.

We represent A_z for $r \ll \Lambda z \ll z$ in the form

$$A_z \approx \frac{I\mu_0}{4\pi}\frac{x}{r^2}\left[e^{ik_\perp z}\frac{1}{\sqrt{1+\left(\frac{r}{\Lambda z}\right)^2}}e^{ik_\perp z}\sqrt{1+\left(\frac{r}{\Lambda z}\right)^2}\right] \approx$$
$$\approx \frac{I\mu_0}{4\pi}\frac{x}{r^2}e^{ik_\perp z}\left\{1-\left[1-\frac{1}{2}\left(\frac{r}{\Lambda z}\right)^2\right]e^{ik_\perp z}\frac{1}{2}\left(\frac{r}{\Lambda z}\right)^2\right\} \approx$$
$$\approx \frac{I\mu_0}{4\pi}\frac{x}{r^2}e^{ik_\perp z}\left\{1-\left[1+\frac{1}{2}\left(\frac{r}{\Lambda z}\right)^2(ik_\perp z-1)\right]\right\} =$$
$$= \frac{-I\mu_0}{8\pi}\frac{x}{z^2}e^{ik_\perp z}\frac{\varepsilon_{zz}}{\varepsilon_{xx}}(ik_\perp z-1).$$

In accordance with the formula obtained above, the highest intensity $|A_z|$ decreases with increasing distance from the source, first as $1/z^2$ and then, at larger $k_\perp z$, as $1/z$. Thus, dissipation of the hydromagnetic wave is observed within the cone $r = \Lambda z$. But in this case the inequality $|A_z| >> |A_x|$ is preserved because of the coefficient $\varepsilon_{zz}/\varepsilon_{xx}$, whose absolute value is, as we have noted, 10^4-10^8. The laws of dissipation of hydromagnetic energy emitted by a point dipole also enable us to form a qualitative conception for a source of nonzero dimensions. If the width of the dissipation cone at a given z is a small fraction of the source dimensions ($\Lambda z \ll a$), we may neglect dissipation and assume that the disturbance is transported along geomagnetic lines of force at constant intensity. If, on the other hand, the source size is comparable to the dissipation-cone width at a certain distance z_0, strong damping should be observed at $z > z_0$. /31

The second most important property of the radiation of an electric dipole in a plasma is the excitation of two phase-opposed waves of electric current along geomagnetic lines of force. The results of calculation of the current density j_z in the vertical plane passed through the source indicate that this density changes sign on passage across a line of force from the source and tends rapidly to zero outside the dissipation cone. Thus, the current flows out of one pole of the dipole and into the other. The existence of a pair of phase-opposed currents can also be established from the nature of the component A_z of the vector potential outside the dissipation cone. Indeed,

$$A_z = \frac{I\mu_0}{4\pi}\frac{x}{r^2}e^{ik_\perp z} = \frac{J\Delta l\mu_0}{4\pi}\frac{x}{r^2}e^{ik_\perp z}$$

is nothing other than the vector potential of a two-conductor line. The distance between wires is Δl, the current in one wire is $Ie^{ik_\perp z}$, and that in the other is $-(-Ie^{ik_\perp z})$. Thus, two antiphase current waves propagate along geomagnetic lines of force with a phase velocity $V = \omega/k_\perp = \sqrt{\varepsilon_{xx}\mu_0}$. It is easily seen that V is the Alfven velocity $V_A = B/\sqrt{\rho\mu_0}$, where ρ is the plasma density.

Thus, a hydromagnetic wave that is described by the longitudinal vector-potential component, is damped slowly with increasing distance, and is accompanied by two phase-opposed current waves propagates at the Alfven velocity along the geomagnetic tube of force on which the source is situated. This wave is characterized by a small longitudinal electric field (because of the large value of $\varepsilon_{zz}/\varepsilon_{xx}$) and by a small longitudinal magnetic field $b_z = -dZ_x/dy$, because $|A_x|$ diminishes rapidly with increasing distance from the source. For practical purposes, therefore, the wave is a pure transverse wave. It is analogous to waves in two-conductor lines and may be referred to as a guided hydromagnetic wave. However, this analogy should not be abused. The two-conductor line is a pair of linear conductors in an isotropic dielectric. To the contrary, the plasma in which the guided hydromagnetic wave propagates is fully homogeneous. The tubes through which the current flows are defined only by the positions of the charge-separation regions. A displacement of these regions also results in a displacement of the current tubes.

In the light of the above, we may conceive of the role of geomagnetic-field-guided hydromagnetic waves as follows. Suppose that charge separation has occurred in a certain volume of the peripheral region of the magnetosphere near the equatorial plane. As a result, a disturbance begins to propagate along tubes of force joining the volume under consideration to the Northern and Southern Hemispheres. This process can be described either in the language of hydromagnetic waves or in the language of longitudinal currents [4]. As it approaches the lower ionosphere, the hydromagnetic wave will excite electric currents in it. We note that the length of a line of force in the outer magnetosphere will be on the order of 10^5 km, while the average Alfven velocity is around 10^3 km. Consequently, the travel time of the wave is measured in the hundreds of seconds. It is therefore convenient to divide all geomagnetic disturbances into two groups. In the first group we shall include variations whose duration is of the same order as the travel time between the ends of the tube of force. The second group is composed of disturbances of much longer duration. In the former case, the guided wave is subject to multiple reflection from the ends of the tube of force, since a sharp change in the propagation characteristics occurs here. Standing waves appear, their periods determined by the travel time between conjugate points. Longitudinal currents, oscillating with the period of the /32
standing waves, form a current system in the lower ionosphere. The resultant effect of oscillating longitudinal and ionospheric currents is registered at the surface of the earth.

In estimating the magnetic field of the ionospheric currents, it is necessary to remember that the electromagnetic induction effect in the ionosphere is negligibly small in the very-low-frequency range considered. As we know, this effect is evaluated in thin layers in terms of the dimensionless parameter $\omega\mu_0\Sigma r$, where Σ is the integral conductivity of the layer $\left(\Sigma = \int \sigma_1 dz\right)$ and r is the distance from the source. At $\omega = 0.05$ (periods around 120 sec) and the value $\Sigma \approx 1$ mho that is typical for the quiet ionosphere, $\omega\mu_0\Sigma r \sim 0.1$ out to distances of $2 \cdot 10^3$ km. With a small parameter $\omega\mu_0\Sigma r$, the spread of the current over the anisotropic ionosphere is described by the Laplace equation. In this case, the electric field is the field of a two-dimensional dipole, and the surface current can be presented as a sum of current systems: a "Pedersen" system $(i_1 = \sigma_1 E)$ and a "Hall" system $\left(i_2 = \sigma_2 \frac{[EB]}{B}\right.$, where B is the field magnetizing the ionosphere). Here the "Pedersen" current system is the result of spreading of the longitudinal magnetospheric currents, and the "Hall" system is fully closed in the lower ionosphere. Estimates indicate that longitudinal currents make the basic contribution to the magnetic field at the earth's surface up to heights around $2 \cdot 10^3$ km. Since the geomagnetic inclination is near 90° in high latitudes, we substitute vertical straight lines for the curved lines of force. It is easily shown that in this idealized model, the magnetic field of the longitudinal currents is fully compensated below the ionosphere by the magnetic field of the "Pedersen" current system. For the proof, we present the "two-conductor line" along which current flows into the lower ionosphere as the sum of the currents flowing in and out [4]. Each of them spreads out radially in the ionosphere. Since the ionosphere is separated from the earth's surface by a nonconductive atmosphere, the circulation of the magnetic field along a horizontal contour coaxial with the incoming current vanishes: $\oint H_\varphi dl = 0$. We select a contour in the form of a circle of radius L. In virtue of the axial symmetry, $\oint H_\varphi db = H_\varphi \cdot 2\pi L = 0$, from which $H_\varphi = 0$. At the surface of the earth, therefore, we shall register only the magnetic field created by the "Hall" current system. From the standpoint of an observer on the earth, the equivalent current system in this case consists of two horizontal eddies that are fully closed in the ionosphere.

The properties of geomagnetic-field-guided hydromagnetic waves that have been discussed above should be manifested in the generation mechanism of geomagnetic fluctuations, in the appearance of longitudinal currents as a result of ring-current asymmetry – i.e., in processes accompanied by charge separation.

REFERENCES

1. V.L. Ginzburg. Rasprostraneniye elektromagnitnykh voln v plazme (Propagation of Electromagnetic Waves in Plasma), Moscow, Fizmatgiz, 1960.
2. L.L. Van'yan and V.I. Dmitriyev. Geomagnetizm i aeronomiya, 1967, Vol. 5, 887.
3. D.N. Chetayev. Zhurnal tekhnicheskoy fiziki, 1962, Vol. 32, 11, 1342.
4. L.L. Van'yan and M.B. Gokhberg. Geomagnetizm i aeronomiya, 1968, Vol. 3, 516.

N75 13710

MAGNETIC MEASUREMENTS IN MODEL EXPERIMENTS

(Translation of "Magnitnyye izmereniya v model'nykh eksperimentakh.")

E. M. Dubinin, G. G. Managadze, and I. M. Podgornyy

ABSTRACT

Plasma parameters for modeling of the interaction between the solar wind and the earth's magnetic field are selected on the limited-modeling principle (plasma velocity $3 \cdot 10^7$ cm/sec, density 10^{13}cm^{-3}, electron temperature ~15 eV). Measurements were made with magnetic probes capable of developing all 3 components inside the magnetic field. The resulting magnetic-field charts indicate that a neutral layer forms on the night side in the model experiments. A magnetosphere free of plasma streams is established on the daytime side. A shock wave forms on the boundary of the magnetosphere, its width c/Ω_0 in accordance with theory, where Ω_0 is the total Langmuir width. With one table, 11 illustrations, and 23 source citations.

MAGNETIC MEASUREMENTS IN MODEL EXPERIMENTS /33

E.M. Dubinin, G.G. Managadze, and I.M. Podgornyy

1. Introduction

Although exact modelling of the interaction between the solar wind and the earth's magnetic field is not practically feasible, it is possible to design a laboratory experiment for limited modelling, i.e., to reproduce the most interesting phenomena under laboratory conditions [1-3]. It has been shown in earlier studies that selection of the experimental conditions can be based on the dimensionless parameters responsible for the evolution of the phenomena chosen for modelling. Thus, laboratory reproduction of the magnetosphere requires that the magnetic Reynolds number $\mathrm{Re}_m = \frac{4\pi\sigma L\bar{v}}{c^2}$ be quite large compared to unity. Unfortunately, treatment of the magnetic Reynolds number always involves an uncertainty in calculation of the plasma conductivity σ. This is because collective processes in the plasma result in an effective conductivity σ_{ef} whose value may differ strongly from the classical conductivity as calculated from Coulomb collisions. Since it is impossible to predict the value of σ_{ef}, the skin-layer thickness $\delta = \frac{c^2}{4\pi\sigma_{ef}\bar{v}}$ can be determined only experimentally. As a result of this situation, it is necessary to have a margin of two or three orders in Re_m. In the present experiment, Re_m exceeds 10^3. The possibility of the existence of a collisionless shock wave and its structure are determined by the following basic dimensionless parameters: the Mach number M, the ratio β of the gas-kinetic plasma pressure to the magnetic-field pressure, the ratio λ/L of the free path to the front width of the shock wave, the ratio α of the magnetic-field energy density to the relativistic electron energy, and the ratio T_i/T_e of the ion and electron temperatures.

The table gives the values of the dimensionless parameters selected for modelling of the magnetosphere and of the shock wave formed on interaction of the solar wind with the earth's magnetic field. The dimensionless parameters of the interplanetary plasma are included for comparison.

The dimensionless parameters listed here correspond to the following experimental conditions: directional velocity of hydrogen plasma $v = 3 \cdot 10^7$ cm/sec, electron temperature $T_e \sim 15$-20 eV, ion temperature $T_i \sim 3$-5 eV, plasma concentration $n \sim 10^{13}$ cm^{-3}, frozen magnetic field in plasma $H \sim 30$ Oe.

REPRODUCIBILITY OF THE ORIGINAL PAGE IS POOR.

Dimensionless quantity	Laboratory experiment	Interplanetary plasma
Mach number $M = \frac{\bar{v}}{\sqrt{v_A^2 + \left(\gamma \frac{p}{\rho}\right)^2}}$	8—10	8—10
Magnetic Reynolds number $Re_m = \frac{4\pi\sigma v L}{c^2}$	$>10^3$	$\sim 10^{12}$
Ratio of free path to dimension of magnetosphere, λ/L	10	10^8
Ratio of gaskinetic pressure to magnetic-field pressure $\beta = nkT \Big/ \frac{H^2}{\gamma\pi}$	~ 4	$\geqslant 1$
Ratio of magnetic-field energy density to electron relativistic energy $\alpha = \frac{H^2/8\pi}{nmc^2} = \left(\frac{\omega_H}{\omega_0}\right)^2$	$\sim 10^{-4}$	$\sim 10^{-5}$

A basis for modelling of the tail of the magnetosphere with the neutral layer was found in the results of experiments in the plasma filling of traps with sharp-ended configuration [4]. In these experiments, the plasma penetrated into the magnetic-field region as a result of anomalous resistance, pulling out the lines of force along the directional-velocity vector.

Earlier papers [3, 5] reported on modelling of the magnetosphere with the tail on the night side and on observation of phenomena accompanying the shock wave. Here we shall consider data from magnetic measurements on the front of the shock wave, including studies of microfluctuations, and report more detailed data on the configuration of the night-side field. All measurements were made on a two-dimensional dipole formed by two parallel conductors in which currents flowed in opposite directions. The distance between the centers of the conductors was 2 cm. The plasma-velocity vector was perpendicular to the axes of the conductors and in their plane. /34

2. The Shock Wave

The most significant departure of the present study from earlier ones [6-11] consists in the large value of the Alfven Mach number compared to the critical value and the possibility of dissipation on ion-accoustic oscillations in virtue of satisfaction of the conditions $T_e >> T_i$ and $\beta \gtrsim 1$. The large value of the parameter β also makes possible the development of anisotropic hydromagnetic-wave instabilities, including firehose instability. Any appreciable contribution of Coulomb collisions to energy

dissipation is fully excluded, since the particle free path in the plasma exceeds the width of the plasma-field transitional region by two orders of magnitude.

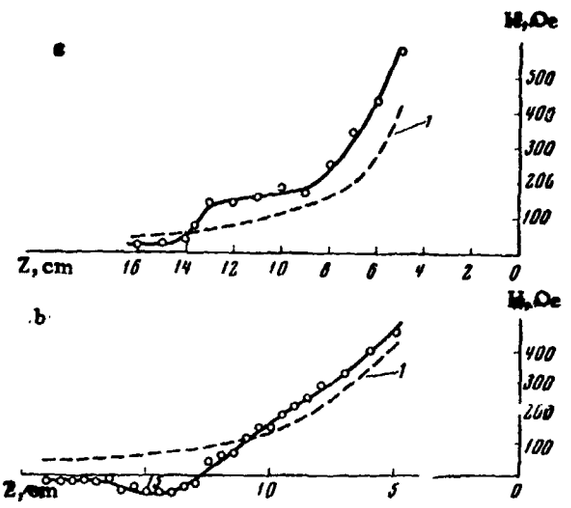

Figure 1. Contours of Magnetic Field (Vertical Component) on the Daytime Side as Obtained in Various Experiments. 1) Field of undisturbed dipole.

The main object of interest in the experiment was the shock wave near its vertex, and for this reason many of the measurements were concerned with the variations of the magnetic field along the axis parallel to the plasma-velocity vector and intersecting the symmetry axis of the two-dimensional dipole (the z axis). Figure 1a shows the intensity of the magnetic field as a function of distance to the dipole axis. It is seen from the curve that a rather sharp increase in the magnetic field is observed on the free-stream boundary, followed by a small plateau, after which the magnetic field again increases to form the magnetosphere. Working from the theory of shock waves formed in supersonic flow past obstacles, it is natural to explain this magnetic-field profile in terms of the formation of a shock wave detached from the magnetosphere. From purely external attributes and the analogy with the field profile obtained in space experiments, the first intensity rise can be identified with the shock-wave front. The segment on which the variation of the magnetic-field intensity is weak is analogous to the plasma flow behind the /35
front of a shock wave or to the so-called turbulent-plasma region. The curve in Fig. 1a was obtained by averaging over a large number of measurements, so that no field fluctuations are evident here. Finally, the second intensity rise corresponds to the magnetopause in the geomagnetic field or to a magnetic system exciting the detached shock wave [12]. Figure 1b shows the magnetic-field intensity as a function of distance to the dipole in the case in which the frozen magnetic field is antiparallel to the dipole field.

A remark is in order concerning the experimentally obtained curve of the vertical magnetic-field component $H_y(z)$ in Fig. 1a. After passage through the front, the intensity of the magnetic field increases, as a rule, by a factor of five and sometimes even six over the intensity of the field frozen into the undisturbed plasma stream. This increase in the field cannot be explained

within the framework of shock-wave theory, since the concentration and the field frozen into the plasma should increase in accordance with the Hugoniot relation

$$\frac{H_1}{H_0} = \frac{n_1}{n_0} = \frac{(\gamma+1)M^2}{(\gamma-1)M^2+2}.$$

With the adiabatic exponent $\gamma = 5/3$ and large Mach numbers, the concentration and the magnetic field increase by no more than a factor of four.

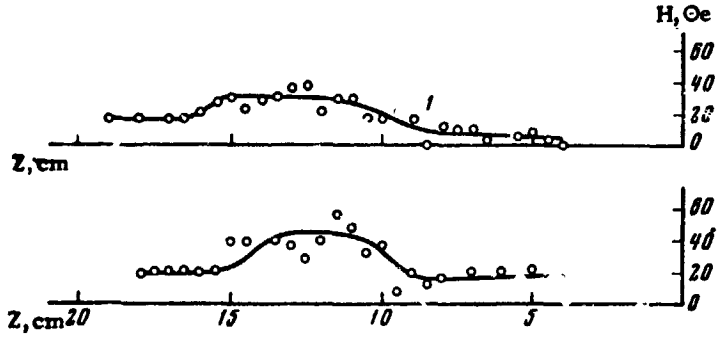

Figure 2. Plot of Horizontal Magnetic-Field Intensity Component (H_x) Against Distance to Dipole Axis on Daytime Side.

To obtain additional information on the width of the shock front and to establish the causes of the anomalously large increase in intensity behind the shock-wave front, we investigated the behavior of the horizontal component H_x (the z axis is directed along the velocity vector). These measurements are distinguished by the absence of the component h_x in the field of the two-dimensional dipole, so that vanishing of H_x means that the probe is inside the magnetosphere. Control measurements showed that the presence of a weak component H_x registered by the probe within the magnetosphere is due entirely to errors in the adjustment of the dipole and the measuring equipment.

Figure 2 presents typical results of two successive measurements of $H_x(z)$ on the axis of the setup ($y = 0$). For curve 1, the component $H_x^{(0)}$ in the undisturbed plasma stream equals 16 Oe. Simultaneous measurements of the vertical component yielded $H_y^{(0)} = 20$-21 Oe, i.e., in the plane of the wave front, the intensity vector forms an angle $\alpha \approx 38°$ with the vertical and has an absolute magnitude $H^{(0)} = 27$ Oe. Measurements made behind the front of the

wave showed that the component H_x^s increased by a factor of about two, becoming equal to 30 Oe. However, the component $H_y^{(s)}$ increased by a factor of approximately five to 105 Oe. The resultant vector H^s behind the front equals 110 Oe, i.e., we find that the intensity has increased by four times, which corresponds to the Hugoniot adiabat with $\gamma = 5/3$. The orientation of the field vector changed during the flow process, and the angle between this vector and the vertical decreased to 16°.

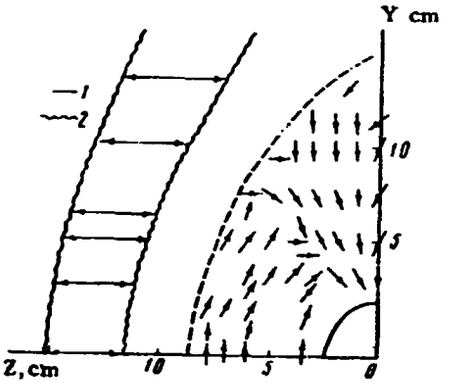

Figure 3. Vector Diagram of Magnetic Field on Daytime Side. 1) Boundaries of magnetosphere; 2) boundaries of shock wave.

Using the measured results for H_x at various distances from the midplane of the dipole, it is possible to construct the contours of the magnetosphere and of the shock-wave front. As the width of the front we took the distance from the first point at which the frozen field increased above the background level to the point at which the curve turned horizontal. The processed data appear in Fig. 3 together with the field vectors within the magnetosphere. It is clear from the vector diagram that the lines of force are curved against the flow in the region of the pole, as follows from theoretical considerations [13, 14].

The relative freedom in the definition of front width leads to an error of several tens of percent. Nevertheless, the data obtained indicate, in the aggregate, the existence of a shock wave that stands off from the boundary of the magnetosphere. Everywhere inside this region, we observe strong fluctuations of the magnetic field at a frequency in the megahertz range. It will be recalled that the ion cyclotron frequency here is $\Omega_H \sim$ $\sim$ 1 MHz. /37

The fluctuations of the magnetic field in the boundary region between the undisturbed plasma and the magnetic field are clearly evident in the stage of magnetosphere formation in the model experiments. The field surges are found to be especially large when the frontal part of a plasma bunch carries a substantial frozen magnetic field. A sharp magnetic-field spike several times the average level of the field frozen into the undisturbed plasma is then observed in the transitional region during formation of the magnetosphere. The position of this spike and its magnitude reproduced poorly from one time to the next. Figure 4 presents the results of magnetic measuremerts made in the stage of magnetosphere formation. The position of the spike and its absolute magnitude are represented by a single point on the

diagram. The abscissa of this point corresponds to the average position of the spike, and the ordinate to its average amplitude. The latter varies through a factor of two or three from one experiment to the next, and the position of its maximum drifts in a range of ±1 cm from the average position. The strong fluctuations and poor reproducibility preclude accurate construction of the contours of this surge, and for this reason the diagram indicates only the average value.

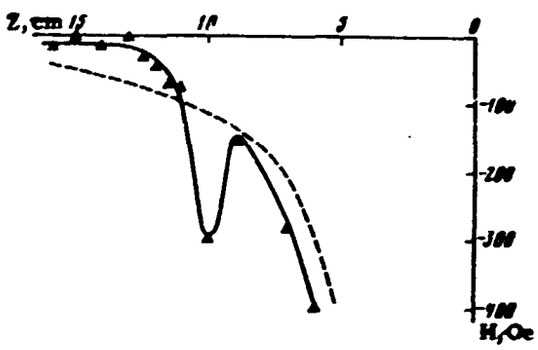

Figure 4. Contour of Magnetic Field on Daytime Side in Stage of Stationary-Wave Formation.

The appearance of the magnetic-field spike in the initial stage of interaction of the plasma bunch with the dipole field is ascribed naturally to flattening of the magnetic field frozen into the frontal part of the bunch. If the magnetic-field distribution curve is steeper in the frontal part of the bunch than the concentration distribution, the ratio of the magnetic-field intensity to the density of the plasma, H/n, is much larger in this region than in the rest of the plasma. An increase in concentration at the front of the shock wave also causes an increase in the field frozen into the plasma. As a result of compression by the main stream of the plasma, the region of the bunch with relatively low plasma concentration in the frontal part is compressed more strongly. With a sufficiently steep field contour, this increase may result in a cumulative burst of the field to a value several times the average on the shock front.

The magnetic-measurement data indicate that the nature of the observed fluctuations may be related to nonuniformity of the field frozen into the plasma bunch. On the other hand, it is known that discontinuities with equal total pressures on either side exist in the solar wind:

$$\frac{H^2}{8\pi} + nk(T_e + T_i) = \text{const}.$$

For certain types of discontinuities, e.g., for those in which the sum $T_e + T_i$ undergoes a stepwise change, the ratio H/n also changes stepwise. This means that conditions similar to those examined in the present experiment are developed in the solar-wind plasma, i.e., the magnetic-field fluctuations in the solar wind should increase as the plasma stream crosses the shock wave. It appears that the interaction of the solar wind with the earth's magnetic field is accompanied by enhancement of such fluctuations, which are also observed behind the shock-wave front in the so-called

turbulent-plasma zone.

An independent confirmation of shock-wave formation in experiments with supersonic flow past a magnetic dipole is also found in the results of direct measurements of plasma concentration along the z axis in [4].

The formation of a shock wave at a concentration $\sim 10^{13}$ cm^{-3} and a temperature of $\sim$15 eV cannot be explained as due to dissipation by Coulomb collisions, since the free path is considerably longer than the characteristic dimension of the interaction region. The existence of a collisionless shock wave is also indicated by the width of the transitional layer between the magnetosphere and the free stream, which is near c/Ω_0, where $\Omega_0 = \sqrt{\frac{4\pi e^2 n}{M}}$ is the ion Langmuir frequency. A front width $c/\Omega_0 \sim \rho_i$ is obtained in shock-wave theory [15], agreeing quite closely with data from measurements on space vehicles [16]. /38

In the aggregate, therefore, the existing experimental and theoretical data permit the statement that a collisionless shock wave whose front lies at a certain distance from the boundary of the magnetosphere is observed under the conditions of the present model experiment. Since there are a number of various physical processes that might be responsible, either separately or simultaneously, for the formation of the shock-wave front, special interest attaches to investigation of the nature of the microfluctuations on the front. Ion-acoustic instability is often cited to explain dissipation in a collisionless plasma. The characteristic wavelength of the ion-acoustic instability is on the order of several Debye lengths, i.e., $\sim 10^{-3}$ cm for the present experiment, and the high-frequency end point of the spectrum is $\sim\Omega_0$, i.e., $\sim 10^9$ Hz. A report on the development of ion-acoustic instability under somewhat different conditions within the shock-wave front will be found in [17].

Under the conditions of this study ($\beta > 1$), there is every reason to expect microfluctuations related to the instability of the hydrodynamic waves due to pressure anisotropy.

Yu.A. Berezin and R.Z. Sagdeyev recently investigated Alfven instability arising at $P_\parallel > P_\perp + H^2/4\pi$. Magnetoacoustic turbulence is excited in the converse case with $P_\perp > P_\parallel$. It was shown in [18] that an anisotropy of $\sim$5 results in a fluctuation amplitude on the order of the field frozen into the plasma. The characteristic frequencies should lie in the range of the ion Larmor frequency, i.e., near 1 MHz, and the wavelengths should be $\sim\rho_i$, i.e., $\sim$5 cm.

The microfluctuations were measured with two magnetic probes having a loop diameter of 2 mm. The signal from the probes was

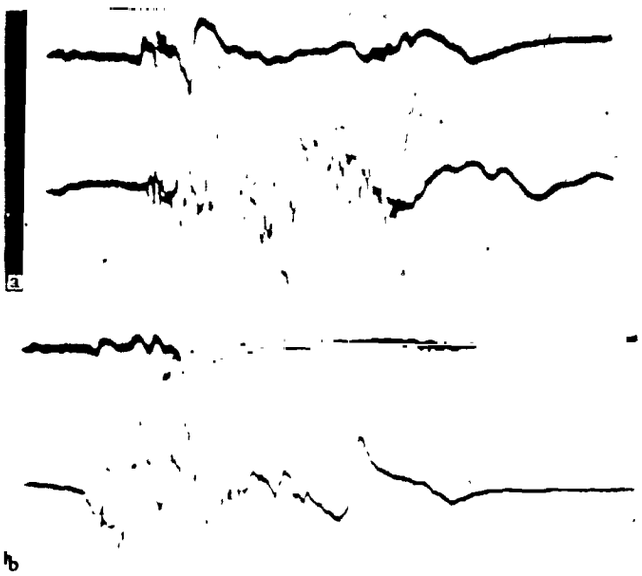

Figure 5. Magnetic-Field Fluctuations (Scanning Time 20 μsec). a) In free plasma stream and within shock-wave front; b) in magnetosphere and within front.

applied to an oscillograph, i.e., the time derivative of the magnetic field was registered directly. When the probe was introduced into the frontal region of the shock wave, its signal level increased by more than 1 order. The characteristic frequency of the fluctuations was around 1 MHz. Strong fluctuations with amplitudes $\sim H_0$ were observed near the front and over the entire distance from the shock wave to the boundary of the magnetosphere.

Placed inside the magnetosphere, the probe registered weak oscillations of approximately the same magnitude as those in the free plasma stream. Figure 5b presents oscillograms from the probes, one of which was in the magnetosphere, while the other was inside the shock-wave front. Figure 5a shows fluctuations typical for the undisturbed artificial solar wind. The upper beam recorded the signal from a probe in the free plasma stream, and the lower beam that of a probe inside the shock-wave front.

Figure 6 presents oscillograms obtained with both probes in the region of strong fluctuations. They were recorded with the two probes less than ~ 3 cm apart, and indicate a rather high correlation of the signals, indicating a wavelength considerably greater than the Debye length and on the order of the ion Larmor radius. When the probes are separated by approximately four or more centimeters, the correlation becomes weak, apparently indicating strong absorption of the waves by the plasma.

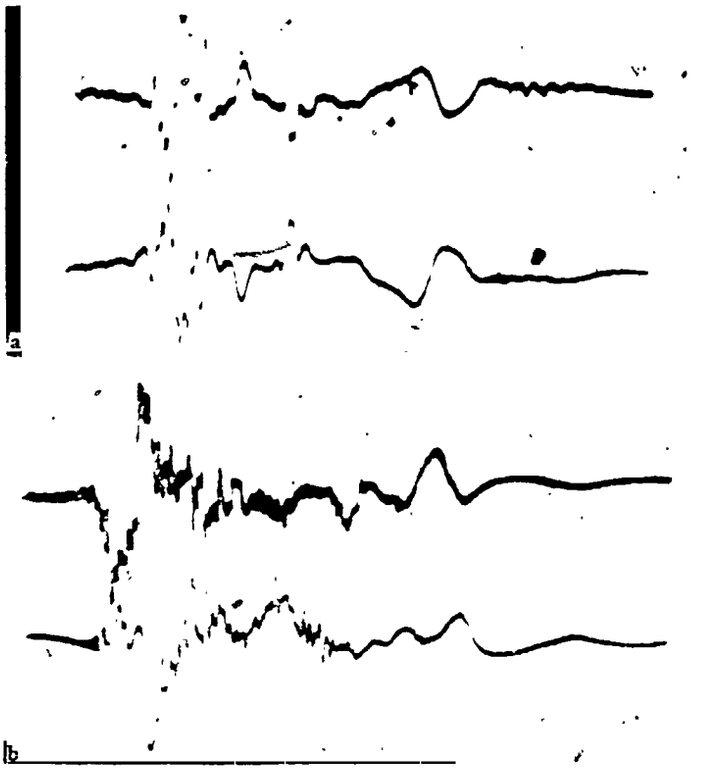

Figure 6. Field-Fluctuation Measurements with Two Probes at Different Distances from One Another. a) l = 1 cm; b) l = 2 cm.

Patrick and Pugh recorded fluctuations with frequencies of ~1 MHz at Mach numbers around 2. It is possible that disspiation was also related to hydromagnetic-wave instability in that case. /40 Precise comparison of the results of [19] with experimental data is impossible, because Patrick and Pugh did not make correlation measurements.

3. The Neutral Layer

It was assumed in designing the experiments to model the shape of the geomagnetic field on the night side that the plasma stream penetrates across the boundary of the magnetosphere. Most probably, the penetration takes place either through the neutral points, which degenerate into neutral lines in the two-dimensional case, or by way of instability of the plasma/magnetic-field boundary.

Penetrating the magnetic cavity, the plasma stream should pull lines of force to the night side, thereby giving rise to the neutral layer that has recently been detected by satellites. The field intensity in the neutral layer is zero. Near the median

REPRODUCIBILITY OF THE ORIGINAL PAGE IS POOR.

plane, the lines of force are parallel to the neutral layer and take opposite directions in the north and south half-spaces. Actually, it appears that the magnetic field in the median plane does not vanish exactly, although it is small enough to permit use of this approximation [20, 21]. It is in this sense that the current term "neutral layer" should be understood.

Figure 7 shows the shape of the lines of force in the plane passing through the magnetic axis and the earth-sun line according to satellite data. For comparison, the same figure shows the configuration of the undisturbed magnetic-dipole field. We see on comparison of the configurations that when a neutral layer is formed, the vertical component H_y of the magnetic field should vanish at a certain distance from the center of the dipole.

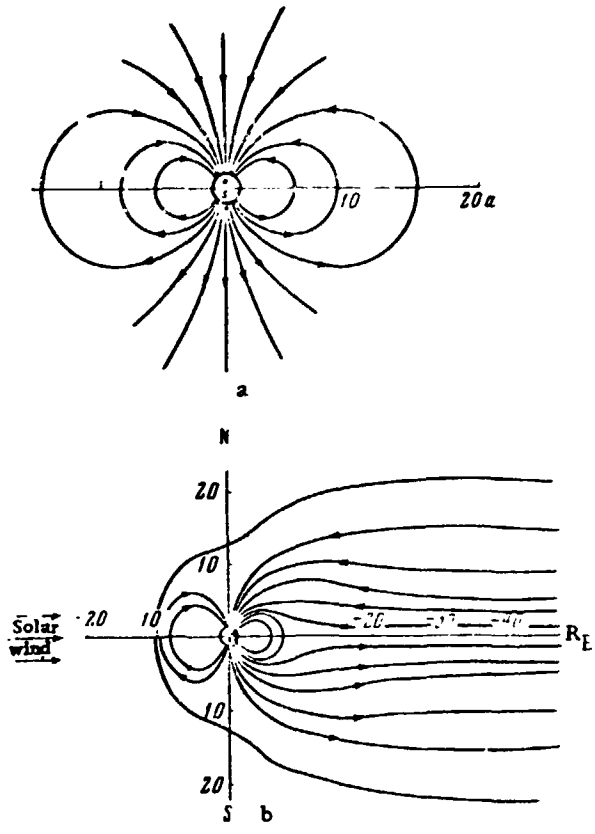

Figure 7. Shape of the Earth's Magnetic Field According to Artificial-Satellite Data, and the Field of the Undisturbed Dipole. a) Undisturbed magnetic dipole; b) magnetic dipole disturbed by solar wind.

Let us now consider how the shape of the magnetic field changes on the night side in the flow around the magnetic dipole in the present experiment. The measurement was made with a magnetic probe having two coils 6 mm in diameter, which were positioned in such a way that the probe could measure two magnetic-field intensity components simultaneously: H_y and H_z. Figure 8 shows experimental distribution curves of the vertical component for two cases: the undisturbed-dipole field (curve 1) and the field when a plasma stream is directed at the two-dimensional dipole (Fig. 2). It is evident from comparison of the curves that the interaction of the plasma with the dipole magnetic field causes the vertical field-intensity component to vanish beginning at a distance of 15 cm from the center of the dipole. However, the good agreement of this experimental curve with what occurs on formation of the neutral layer does not constitute irrefutable proof of its formation. This is because vanishing of the component along the axis does not mean an increase in the

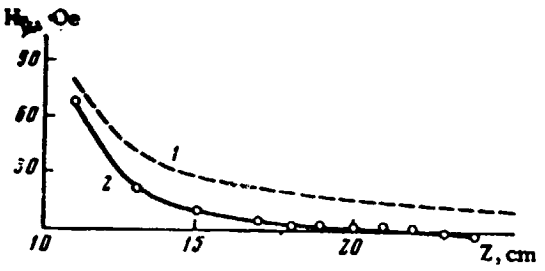

Figure 8. Vertical Intensity Component (H_y) on Night Side.

horizontal components H_z, which have different directions above and below the hypothetical neutral layer.

An experiment in which both magnetic-field intensity components are measured simultaneously near the central plane yields much more information. Such measurements were undertaken at several fixed values of the z coordinate. In each series of measurements, the magnetic probe was moved in the vertical direction, crossing the equatorial plane, and the components H_y and H_z were measured simultaneously at each point. The results of the measurements can be used not only to determine the direction and magnitude of the field-intensity vector, but also to follow the progressive transition from the configuration of the weakly disturbed field near the center of the dipole to the configuration of the neutral layer at greater distances.

The complete directional pattern of the intensity vector in /42
the model experiment appears in Fig. 9. We observe a rather long segment on which the lines of force near the equatorial plane are parallel to the stream velocity on one side of it and antiparallel on the other, i.e., exactly the configuration that corresponds to the neutral layer detected by satellites. The lines of force diverge at greater distances. It is difficult to state at the present time whether this divergence is a consequence of the development of instability or cross-connection of lines of force. Estimates indicate that the time to development of the instability [22, 23] exceeds the time of the experiment, and, on the other hand, decomposition of the plasma on the side walls of the vacuum chamber should lower the external plasma pressure on the magnetic

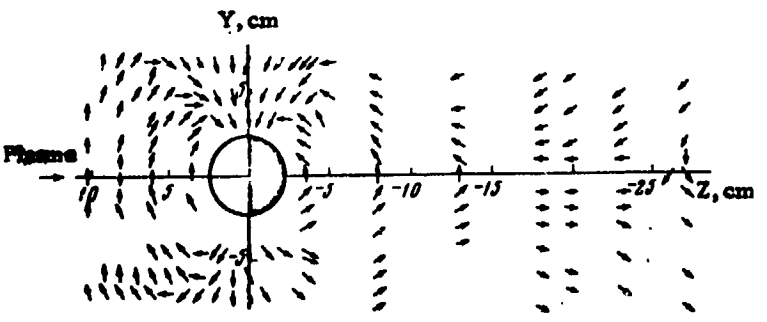

Figure 9. Vector Diagram of Magnetic Field in Model Experiment.

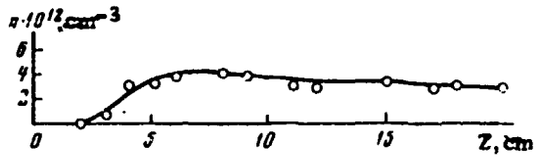

Figure 10. Distribution of Plasma Concentration Along the Neutral Layer.

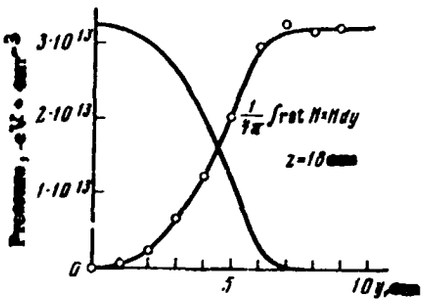

Figure 11. Curves of Magnetic and Gas-Kinetic Pressure Distributions in the Direction Perpendicular to the Plane of the Neutral Layer.

tail with increasing distance from the dipole.

To confirm the hypothesis of tail formation as a result of extension of lines of force, it is important to investigate the concentration distribution in the region of the layer of vanishing magnetic field. Such data can be obtained by two independent methods:

a) obtaining the distribution curve of the plasma gas-kinetic pressure nkT from the pressure balance:

$$\frac{1}{c} j \times H = \nabla P, \text{ where } j = \frac{c}{4\pi} \operatorname{rot} H;$$

b) direct measurement of the plasma concentration and electron temperature with a double electric probe.

Figures 10 and 11 show the plasma-pressure distribution in the direction perpendicular to the neutral layer and the concentration distribution along the plane of symmetry. Data obtained by both methods are in agreement, indicating that the average energy and average concentration of the plasma in the neutral layer are of the same order of magnitude as in the plasma stream.

Formation of the tail of the magnetosphere in experiments with a two-dimensional terrella is difficult to explain in terms of leakage of plasma into the tail through the neutral points on the daytime side, and the pulling of lines of force by a stream penetrating into the magnetosphere as a result of plasma anomalous resistance agrees most closely with experiment.

REFERENCES

1. G.G. Managadze and I.M. Podgornyy. Geomagnetizm i aeronomiya, 1968, Vol. 8, 612.
2. I.M. Podgornyy and G.G. Managadze. Vestnik Akad. Nauk SSSR, 1968, Vol. 7, 38.
3. G.G. Managadze and I.M. Podgornyy. Dokl. Akad. Nauk SSSR, 1968, Vol. 180, 1333.
4. I.M. Podgornyy and V.N. Sumarokov. Nucl. Fusion Suppl., 1962, Vol. 1, 87.
5. G.G. Managadze, I.M. Podgornyy, and V.D. Rusanov. Geomagnetizm i aeronomiya, 1968, Vol. 8, 545.
6. K. Schindler. ESRO, Paper Presented at Conference on the Magnetosphere, New York, September, 1968.
7. W.H. Bostick, H. Byfield, and A. Jarmakian, Phys. Fluids, 1966, Vol. 9, 2287.
8. J.B. Cladis, T.D. Miller, and J.B. Baskett. J. Geophys. Res., 1964, Vol. 69, 2257.
9. M.P. Bashynsky and B.W. Gibbs. Phys. Fluids, 1966, Vol. 9, 523.
10. L. Danielsson and L. Lindberg. Phys. Fluids, 1964, Vol. 7, 1878.
11. N. Kawashima and S. Mori. Phys. Fluids, 1965, Vol. 8, 378.
12. J.H. Spreiter, A.L. Summers, and A.Y. Alksne. Planet. Space Sci., 1966, Vol. 14, 223.
13. V.N. Zhigulev and Ye.A. Ramishevskiy. Dokl. Akad. Nauk SSSR, 1959, Vol. 127, 1001
14. S. Chapman. In collection entitled: "Geofizika. Okolozemnoye kosmicheskoye prostranstvo" (Geophysics. Near-Earth Cosmic Space), Moscow, "Mir," 1964, p. 243.
15. R.Z. Sagdeyev. In collection entitled: "Voprosy fiziki plazmy" (Problems of Plasma Physics), Vol. 4, Moscow, Atomizdat, 1964, p. 20.
16. R.L. Kaufman. J. Geophys. Res., 1967, Vol. 72, 2323.
17. S.G. Alikhanov et al. Paper Presented at International Conference on Thermonuclear Reactions. Novosibirsk, 1968.
18. Yu.A. Berezin and R.Z. Sagdeyev. Dokl. Akad. Nauk SSSR, 1969, Vol. 184, 570.
19. E. Pugh and R. Patrick. Phys. Fluids, 1967, Vol. 10, 2579.
20. W.H. Hess. Radiation Belts, N.Y., 1968.
21. N.F. Ness. J. Geophys. Res., 1965, Vol. 70, 2989.
22. B. Coppi, G. Lawal, and R. Pellant. Phys. Rev. Lett., 1966, Vol. 16, 1207.
23. H.P. Furth. Advanced Plasma Theory, N.Y., 1964.

N75 13711

DISSIPATION OF ENERGY IN MODEL EXPERIMENTS

(Translation of "Dissipatsiya energii v model'nykh eksperimentakh.")

I. M. Podgornyy

ABSTRACT

Studies of the interaction of a plasma stream with a magnetic dipole have shown that the thickness of the plasma/ field interlayer is considerably greater than the characteristic plasma dimension c/ω_0. Broadening of the layer is due to the formation of a collisionless shock wave. To demonstrate collisionless dissipation, the Joulean losses were calculated using the conductivity value obtained from the skin-layer thickness. Analysis of the various physical processes showed that the hypothesis of collisionless dissipation of the directional plasma flow is justified. With 1 illustration and 17 source citations.

DISSIPATION OF ENERGY IN MODEL EXPERIMENTS

I.M. Podgornyy

A collisionless shock wave is observed in experiments to model the interaction of the solar wind with the earth's magnetic field when they are carried out under conditions that satisfy the limited-modelling principle [1-3]. Since the width of the shock wave and its distance from the boundary of the magnetosphere are comparable, it is not possible to make an accurate comparison of the experimental magnetic-field contour shape with those obtained theoretically under various assumptions. Under these conditions, it is important to have an independent proof of dissipation of the energy of the directional plasma motion, since it is possible to advance an alternative explanation of the magnetic measurements that states that the broadening of the transitional layer from the undisturbed plasma to the magnetic field of the magnetosphere in the model experiment is not associated with appreciable dissipation of energy, i.e., the shock wave is not formed. Although this last assumption is inconsistent with the aggregate of available experimental data, the best way to refute it is to find a direct proof of strong energy dissipation in the transitional layer.

The width of the plasma/magnetic-field transitional layer depends on the stream-energy dissipation mechanism and is found to be different for different initial conditions. In the interaction of a magnetic field with an ideally conductive plasma, when the plasma pressure on the boundary is offset by the field pressure, the transitional-layer width is c/ω_0[1]. This quantity, which is derived from the Chapman-Ferraro theory, corresponds to the case in which collective processes, which further broaden the layer, are absent. Analysis of a fluid of finite conductivity bounded by a magnetic wall leads to a layer width determined by the magnetic viscosity $c^2/4\pi\sigma$, where $\sigma = e^2 n\bar{\tau}/m_e$ is the conductivity of the plasma due to Coulomb collisions. For plasma flow past the magnetic-field region, the transitional-layer width is then found to be

$$\delta_{\text{skin}} = c^2/4\pi\sigma\bar{v}, \qquad (1)$$

where v is the velocity of the plasma stream.

Leaving aside consideration of the specific phenomena that accompany the interaction of a supersonic plasma stream with a magnetic field, we may assume that a certain transitional layer

---

[1]Here c is the velocity of light and $\omega_0 = \sqrt{\frac{4\pi e^2 n}{m}}$ is the plasma frequency.

3-5 cm thick, or two orders thicker than the inductive (or collisionless) skin layer c/ω_0 or the skin layer determined by Joulean heat losses in (1) exists between the magnetic field and the undisturbed plasma.

If we generalize expression (1) to the case of particle-wave interaction and use the experimentally determined value of the layer width, we obtain an electron-collision frequency hundreds of times higher than the frequency of Coulomb collisions in a plasma with the parameters selected. Consequently, the broadening of the plasma/field transitional layer yields a direct indication of the presence of collective interactions, which may be responsible for dissipation of the energy of the directional motion and for the formation of the shock wave. /45

Plasma theory considers several mechanisms of charged-particle-energy dissipation in the time interval between two Coulomb collisions. These include Landau damping [4], scattering of waves by particles [5], and mixing of particle orbits in the magnetic field [6]. The first of these mechanisms provides for transfer of energy from the wave to the particle if the phase velocity of the wave is near the velocity of the particle. Landau damping results in direct transfer of energy from the wave to the particle and is apparently one of the basic thermalization mechanisms of the turbulent wave spectra. At a high enough turbulence level, the effective free path $\lambda_{turb} \sim 1/\tilde{E}^2$ ($\tilde{E}$ is the amplitude of the turbulent field) may be much smaller than the free path for Coulomb collisions. Thus, the part played by collisionless processes depends on the turbulence level of the plasma, which, in turn, depends on which instabilities are excited under the particular experimental conditions. A typical example of the appearance of collisionless dissipation of directional plasma motion is found in shock waves in a strongly rarefied plasma.

The possibility of formation of a shock wave in a collisionless plasma propagating perpendicular to the lines of force of a magnetic field was examined by R.Z. Sagdeyev [7, 8]. If the Langmuir frequency $\omega_0 = \sqrt{\frac{4\pi e^2 n}{m}}$ exceeds the Larmor frequency $\omega_H = eH/mc$, we have, for waves longer than c/ω_0, a complete analogy with ocean waves on a shore with a gently sloping bottom profile. The motion of waves in shallow water is described by the one-dimensional equations

$$\frac{\partial v}{\partial t} + v\frac{\partial v}{\partial x} = -g\frac{\partial h}{\partial x},$$

$$\frac{\partial h}{\partial t} + \frac{\partial}{\partial x}(hv) = 0. \qquad (2)$$

Here g is the acceleration of gravity.

A wave of arbitrary form becomes steeper as a result of deceleration against the bottom. The upper layers of water run ahead of the lower layers, forming a crest. The lead is limited by gravity, the action of which causes water to fall from the crest. The wave "overflows across itself."

Equation (2) agrees exactly with the equations of motion of a plasma with small $\beta=\frac{nkT}{H^2/8\pi}$ across a magnetic field when the wavelength exceeds the characteristic dimension c/ω_0. The magnetic field plays the part of channel depth for such waves. Indeed, the propagation velocity $v_A=\frac{H}{\sqrt{4\pi\rho}}$ of the disturbance is highest for the apex, and the profile of a wave of arbitrary shape should become steeper.

Steepening of the wave front should be observed not only for low-frequency disturbances propagating at the Alfven velocity, but also for higher-frequency disturbances. The necessity of steepening follows from the dispersion relation. For frequencies below the hybrid frequency $\omega_h=\frac{eH}{c\sqrt{mM}}$ and a sufficiently dense plasma, when the Langmuir frequency exceeds both cyclotron frequencies (under the conditions of the present experiment, $\omega_0 > 10^{11}$ sec^{-1} and $\omega_H \sim 5 \cdot 10^9$ sec^{-1}), the dispersion relation takes the form /46

$$k^2c^2=\frac{\omega_0^2}{\frac{\omega_H\Omega_H}{\omega^2}-1}. \qquad (3)$$

It follows from this relation that as the disturbance wavelength $1/k$ increases, so does its phase velocity ω/k; long waves tend to overtake short waves, and the front becomes steeper. Otherwise, the oscillation front would be drawn out, since short waves would run out ahead. Rapid steepening continues until the front width reaches a value $\sim c/\omega_0$, at which the phase velocity becomes independent of disturbance wavelength. At sufficiently large Mach numbers ($M > 3$), the ordered structure is disturbed and it becomes impossible to construct a nonlinear flow in which the stream velocity has a unique value at each point. Breaking occurs in much the same way as in the propagation of an ocean wave at a gently inclined shoreline, and the velocity on the front becomes many-valued. It has three values at one point. On breaking, the width of the front in a liquid is established by the falling of water from the crest under the influence of gravity. It was shown in [7] that the magnetic field takes the part of gravity in the breaking of a shock wave in a plasma, and that the width of the transitional region is approximately equal to the radius of curvature of the ion trajectory in the transitional layer:

$$\delta = \frac{Mv_{\perp}c}{eH}.$$

Since the magnetic pressure on the boundary is offset by the stream pressure,

$$\frac{H^2}{8\pi} = Mnv^2, \qquad (4)$$

the width of the transitional layer is

$$\delta = c/\Omega_0; \qquad \Omega_0 = \sqrt{\frac{4\pi e^2 n}{M}}. \qquad (5)$$

The countercurrent that forms on breaking of the wave front at a velocity difference larger than $\sqrt{kT/M}$ is accompanied by buildup of ion-acoustic oscillations. B.B. Kadomtsev [9] showed that for two opposed beams with velocities v_0 and $-v_0$, the characteristic instability wavelength at $v_0 < H/\sqrt{4\pi Mn}$ is c/ω_0. For a hot enough plasma with $nT \gtrsim H^2/8\pi$, when $v_{Ti} \sim H/\sqrt{4\pi Mn}$, the wavelength corresponding to maximum increment equals c/Ω_0. Analysis of the ion-acoustic instability and the firehose instability of Alfven waves also leads to the same length scale [10]. The characteristic frequency of development of such instabilities, $\Omega H = eH/Mc$, and their development requires that $\beta \gtrsim 1$, i.e., that conditions corresponding to the experiment under consideration be satisfied. The Alfven and magneto coustic instabilities arise in the presence of a plasma-pressure anisotropy and develop at $P_{\parallel} > H^2/8\pi + P_{\perp}$ and $P_{\perp} > P_{\parallel}$, respectively. Here $P_{\parallel}$ and $P_{\perp}$ are the plasma pressures along and across the lines of force.

Thus, the width of the transitional layer cannot be smaller than c/ω_0 and is apparently near c/Ω_0. Under the conditions of the present experiment [1-3], these quantities are equal to 0.2 and 7 cm, respectively. The value obtained by experiment is ~5-6 cm (from which it is necessary to subtract the standoff distance of the shock wave from the obstacle, ~2 cm), i.e., it falls in the range indicated.

The satisfactory agreement between the experimental value of /47
the layer width and the theoretical estimate for breaking of a wave propagating across the magnetic field still cannot be regarded as a definite proof of dissipation by this mechanism. However, there is no doubt that the considerable width of the transitional region as compared to c/ω_0 indicates the presence of dissipative processes unrelated to Coulomb collisions.

The distribution curve of magnetic-field intensity at the plasma/field boundary can be used to estimate the fraction of

directional-motion energy that is transformed into heat, i.e., to establish whether the conditions for formation of a shock wave are at hand in the present experiment. The energy dissipated in the form of heat per cubic centimeter of transitional layer per second can be written

$$W = jE. \tag{6}$$

Let us examine the area of the plasma in the neighborhood of the frontal point. Since the stream pressure is offset by the force $\frac{1}{c} j \times H$, the direction of the current is perpendicular to the directional-motion vector of the plasma stream and to the lines of force of the magnetic field. Then the relation between j and E can be obtained from the generalized Ohm's law:

$$\frac{dj}{dt} = \frac{ne^2}{m} E - \frac{e}{mc} j \times H + \frac{e}{m} \nabla p - \frac{j}{\tau}. \tag{7}$$

Placing the x axis parallel to j, we obtain the projection onto this axis.

$$E = \frac{1}{\sigma} j. \tag{8}$$

As already noted, the conductivity of the plasma under the conditions of our experiment is determined not only by Coulomb collisions, but also by specific collisionless processes, so that determination of the dissipation requires knowledge of the effective conductivity value σ_{ef}. The effective conductivity is related to the transitional-layer width δ by

$$\sigma_{ef} = \frac{c^2}{4\pi\delta v}. \tag{9}$$

Using Maxwell's equation for the current density, we obtain an expression for the power dissipated in the form of heat in a column of plasma with a cross section of 1 cm^2:

$$\int W dz = \frac{\delta v}{4\pi} \int (\mathrm{rot}\, H)^2 dz. \tag{10}$$

We note in passing that the existence of a single current component, j_x, follows from the two-dimensional statement of the problem, and that the remaining components of the curl are equal to zero; consequently, curl $H = \frac{\partial H_y}{\partial z} - \frac{\partial H_z}{\partial y}$. Since the second term is an order smaller than the first for the frontal point, the following formula can be used for rough estimates:

$$\int W\,dz \approx \frac{\delta v}{4\pi}\int\left(\frac{\partial H}{\partial z}\right)^2 dz. \qquad (11)$$

Using experimental data for the distributions of H_y and H_z and comparing the value calculated for the energy that has been converted into heat with the energy transferred by the stream, we obtain a figure near 50% for the percentage of energy dissipated in the form of heat. It is difficult to make a more accurate estimate on the basis of available data. However, the large dissipation coefficient obtained in this way provides additional support /48 for the statement that a collisionless shock wave does exist in the present experiment.

The existence of dissipative processes under supersonic-flow conditions should result in formation of a shock wave with a front width equal to the dissipation length; in the transitional-layer region, therefore, we should observe a concentration jump, such as occurs in experiments with θ-pinch shock waves. The figure presents typical results of such an experiment as obtained by J. Staemper at the University of Maryland. The shock wave in these experiments was excited by a magnetic-field pulse with lines of force antiparallel to the field frozen into the plasma. The configuration of the magnetic field outside the plasma (magnetic "piston") is not indicated in the figure.

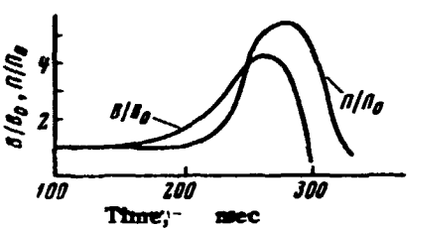

Magnetic-Field and Concentration Contours on Front of Collisionless Shock Wave. The Field Direction in the Piston is Antiparallel to the Field Frozen into the Plasma.

Experiments on the concentration distribution in the region of the plasma-field transitional layer offer an independent proof of the formation of a shock wave in interaction of a stream of collisionless plasma with a magnetic dipole. Such an experiment was also performed in [1], so that one more proof of the existence of the shock wave exists. According to the available data, the shock wave set up in supersonic flow past a body stands off from the obstacle, so that a subsonic flow of plasma that has been heated on passage through the shock front exists in the space between the body and the shock front. (The term "sonic velocity" is used here in its generalized sense, i.e., it refers to the propagation velocity of the waves responsible for formation of the shock wave.) The most characteristic propagation velocities of disturbances in plasma are the ion-acoustic velocity $\sqrt{T_e/M}$ and the Alfven velocity. Ion-acoustic oscillations build up when $T_e > T_i$.

Then the width of the plasma/field transitional region is composed of two parts: the shock-wave front and the region of heated plasma behind it.

If we use Spreiter's numerical calculations of the standoff distance of the shock wave from the magnetopause [11], it must be assumed that approximately half of the transitional-layer width (~2.5 cm) is determined by the standoff distance of the shock wave from the obstacle, while an equal amount is due to the shock front.

Distribution curves of the vertical magnetic-field component do not clearly separate the region behind the shock-wave front from the magnetosphere. Measurements of the horizontal component perpendicular to the velocity vector are much more indicative in this respect. Since this component vanishes in the magnetosphere, the position of the magnetopause is easily determined here, so that an inference can be drawn regarding the standoff of the shock wave from the magnetic piston.

The shock wave is observed to stand off from the obstacle in space when the solar wind interacts with the earth's field. Many independent measurements indicate that the shock-wave front stands off from the magnetosphere at a distance of $\sim 10^9$ cm, which agrees within the limits of measurement error with the calculated data of [11]. The entire space between the magnetosphere and the shock front is filled with hot turbulent plasma, in which the magnetic-field intensity vector fluctuates strongly, both in magnitude and in direction. These fluctuations are clearly evident on plots of magnetic measurements made on the IMP-1 and IMP-2 satellites [12, 13]. A similar picture is obtained, according to [14, 15], for the interaction of the solar wind with Venus. The concentration jump and the magnetic-field fluctuation front that occur at a distance of 15 000 km from Venus are interpreted as the front of a shock wave that stands off from the surface of the obstacle in the flow. Throughout this region, the plasma concentration and the average magnetic-field intensity are several times larger than the corresponding values for the undisturbed solar wind. The occurrence of magnetic-field microfluctuations on the shock-wave front favors the hypothesis that the present experiment is characterized by precisely this picture. /49

The question as to the specific mechanism of stream-energy dissipation on the shock-wave front has not yet been finally resolved. Measurements of the magnetic-field fluctuations in the model experiment considered here [16] indicated the existence, within the front of oscillations at a frequency $\sim\Omega_H = eH/Mc$ and wavelength $\sim\rho_i = Mvc/eH$. These results indicate instability of the magnetohydrodynamic waves that arise when plasma pressure is anisotropic. This mechanism may not be the only one, since the possibility of buildup of ion-acoustic instability at $\beta \gtrsim 1$ and $T_e > T_i$ cannot be excluded.

It appears that the instability of the two-stream ion motion that results from reflection from potential humps plays an important role in the stage of formation of the shock-wave front [17].

REFERENCES

1. G.G. Managadze and I.M. Podgornyy. Dokl. Akad. Nauk SSSR, 1968, Vol. 180, 1333.
2. G.G. Managadze, I.M. Podgornyy, and V.D. Rusanov. Geomagnetizm i aeronomiya, 1968, Vol. 8, 545.
3. E.M. Dubinin, G.G. Managadze, and I.M. Podgornyy. Magnetic Measurements in Terrella Experiments. This collection, p. 46.
4. L.D. Landau, J. Phys. USSR, 1946, Vol. 10, 25.
5. A.A. Vedenov. In collection entitled: "Voprosy teorii plazmy" (Problems of Plasma Theory), Vol. 3, Moscow, Atomizdat, 1963, p. 203.
6. C.S. Gardner, H. Goertzel, H. Grad, C.S. Morawetz, M.H. Rose, and H. Rubin. Progr. Nucl. Energy, 1959, Vol. 11, 232.
7. R.Z. Sagdeyev. ZhTF, 1961, Vol. 31, 1955.
8. R.Z. Sagdeyev. In collection entitled: "Voprosy teorii plasmy" (Problems of Plasma Theory), No. 4, Moscow, Atomizdat, 1964, p. 200.
9. B.B. Kadomtsev. In collection entitled: "Fizika plazmy i problemy upravlyayemykh termoyadernykh reaktsiy" (Plasma Physics and Problems of Controlled Thermonuclear Reactions), Vol. 4, Moscow, Izd-vo Akad. Nauk SSSR, 1958, p. 54.
10. Yu.A. Berezin and R.Z. Sagdeyev. Dokl. Akad. Nauk SSSR, 1969, Vol. 184, 570; C.F. Kennel and R.Z. Sagdeev. J. Geophys. Res., 1967, Vol. 72, 3303.
11. J.H. Spreiter, A.L. Summers, and A.Y. Alksne. Planet. and Space Sci., 1966, Vol. 14, 223.
12. N. Ness. J. Geophys. Res., 1965, Vol. 70, 2989.
13. R.L. Kaufman. J. Geophys. Res., 1967, Vol. 72, 2323.
14. K.I. Gringauz, V.V. Bezrukikh, L.S. Musanov, and T.K. Breus. Kosmicheskiye issledovaniya, 1969, Vol. 6, 411.
15. Sh.M. Dolginov, Ye.G. Yeroshenko, and L.N. Zhuzgov. Kosmicheskiye issledovaniya, 1968, Vol. 6, 561.
16. E.M. Dubinin, G.G. Managadze, and I.M. Podgornyy. Trudy Mezhdunarodnogo seminara po fizike mezhplanetnogo prostranstva (Transactions of International Seminar on the Physics of Interplanetary Space), Leningrad, 1969, p. 244.
17. I.M. Podgornyy, E.M. Dubinin, and Yu.V. Andriyanov. Paper Presented at Fifteenth COSPAR Session, Madrid, 1972.

N75 13712

ANALYSIS OF METHODS OF MEASURING ELECTRIC-FIELD STRENGTH IN THE MAGNETOSPHERE

(Translation of "Analiz metodov izmereniy napryazhennosti elektricheskogo polya v magnetosfere.")

S. I. Klimov

ABSTRACT

Various methods of electric field strength measurements are examined and evaluated as to accuracy, and the requirements made of instrumentation for satellite measurements of electric field strength in the magnetosphere are indicated. With 4 tables, 3 illustrations, and 25 source citations.

ANALYSIS OF METHODS OF MEASURING ELECTRIC-FIELD STRENGTH IN THE MAGNETOSPHERE

/50

S.I. Klimov

The motions of the magnetospheric plasma as a single entity and a number of processes that take place in it are determined by the electromagnetic tensor of the interplanetary medium. The magnetic component of this tensor has now been adequately studied, thanks to measurements made from satellites.

Theoretical calculations indicate that electric fields may be generated in wind motions at the ionospheric level, on the interaction of the solar wind with the earth's magnetosphere, and in drift motions, and influence processes taking place in auroras, in the trapped-radiation zone, at the boundary of the magnetosphere, etc. Determination of the electric component of the tensor is difficult because very few direct measurements of the electric field have as yet been made [1-8]. This has been due both to the low strength of the field and to the presence of interference of various types. Thus far, no reliable and accurate method has been found for measurement of small electric fields, under either space or laboratory conditions [9, 10].

The present paper defines the requirements to be met by known methods of measuring electric-field strength, compares measurement accuracies, and discusses the possibilities for use of the methods for measurements in various parts of the magnetosphere.

1. Determination of Measurement Range and Accuracy

In all methods of electric-field measurement except that of the artificial ionized cloud, the measuring instrument moves together with the satellite in the magnetospheric plasma. The electric field E, measured in fixed earth axes, is defined by the equation

$$E = E' - E_{VH} - E_s, \tag{1}$$

where E' is the electric field measured by the instrument in the coordinate frame of the moving satellite, $E_{VH} = \mu [V \times H]$ is the induced electric field, V is the velocity of the satellite's motion relative to the earth, H is the intensity of the geomagnetic field, and E_s is the electric field created by the charge on the satellite.

Let us evaluate the contribution made by each of the terms. E_s is related to the potential ϕ_s of an area of the satellite's surface with respect to the neutral plasma by

$$E_s\delta = \varphi_s, \tag{2}$$

where δ is the thickness of the space-charge layer surrounding the satellite.

The potential of a conducting body in a plasma is found from the condition of zero total current to the body [11]:

$$I_e + I_{re} = I_i + I_{ri} + I_p + I_s, \tag{3}$$

where I_e is the current of thermal-plasma electrons, I_{re} is the current of radiation-belt electrons, I_i is the current of plasma ions, I_{ri} is the current of "radiation" protons, I_p is the photoelectric current, and I_s is the secondary-electron current.

In the ionosphere, where the electron and ion concentrations are high ($n_e = n_i \approx 10^4$-10^6 particles/cm^3), the photocurrent and radiation-particle current can usually be disregarded, determining the potential of the body from the condition $I_e = I_i$, which can be used to find an expression for the potential of the satellite surface [12]: /51

$$\varphi_s = \frac{kT_e}{e} \ln \frac{S_e V_e}{2S_+ V_s}, \tag{4}$$

where k is Boltzmann's constant, T_e is the electron temperature, e is the electronic charge, S_e is an area approximately equal to the area of the projection of the satellite onto the plane normal to the magnetic line of force, S_+ is the area of the projection of the satellite onto the plane normal to the velocity vector, V_e is the average thermal velocity of the electrons, and V_s is the velocity of the satellite. For a satellite 1 meter in diameter the surface potential of the satellite is approximately 0.3 V at $T_e \approx 1000°K$. As a satellite with a conductive surface moves in the geomagnetic field, a potential difference of about 0.4 V (at a 1-meter satellite diameter) may arise between two diametrically opposite points on the surface. In this case, the surface of the satellite is no longer equipotential.

In the ionosphere, the satellite's surface potential is for the most part negative at about 1 volt. At $\delta \approx 1 \cdot 10^{-2}$ meters, $E_s = 10^2$ V/m. The electric field measured experimentally in [7] at the surface of a satellite was $(1.5\text{-}1.6) \cdot 10^2$ V/m. In some cases [13, 14], higher negative potentials ($\sim$20 V) and positive potentials have been observed on the surface of the body. Negative potentials on the order of 1 kV are possible in the outer

TABLE 1*

Height, km	Experimental conditions	V, m/sec	λ_{De}, m	E, V/m	E_{VH}, V/m	ΔE_{VH}, V/m	ΔV, m/sec	ΔH, γ	$\Delta\theta$, deg	$\frac{\Delta E'}{E'}$
300	Night	$8\cdot10^{3}$	$4\cdot10^{-3}$	$3\cdot10^{-2}$	$4\cdot10^{-1}$	$3\cdot10^{-3}$	45	250	0,24	$8\cdot10^{-6}$
300	»	$8\cdot10^{3}$	$3\cdot10^{-3}$	$3\cdot10^{-2}$	$4\cdot10^{-1}$	$3\cdot10^{-3}$	45	250	0,24	$8\cdot10^{-6}$
3000	»	$7\cdot10^{3}$	$5\cdot10^{-2}$	$1\cdot10^{-2}$	$1\cdot10^{-1}$	10^{-4}	50	110	0,3	$8\cdot10^{-6}$
20000	»	$5\cdot10^{3}$	0,7	$1\cdot10^{-3}$	$4\cdot10^{-2}$	10^{-4}	85	12	0,7	$2\cdot10^{-3}$
50000	»	$3\cdot10^{3}$	40	$1\cdot10^{-4}$	$2\cdot10^{-4}$	10^{-4}	110	2,5	1,4	$3\cdot10^{-3}$

*Commas indicate decimal points.

Note: λ_{De} is the Debye length for the electron and $\Delta E'/E'$ is the relative error of measurement of E'.

radiation belt [11], since the concentration of "radiation" electrons is high and the plasma-electron concentration is $\sim10^2$ particles/cm^3. In this case, E_s may be quite large.

The space charge that forms around the satellite screens the satellite's electric field. At a distance on the order of the Debye length λ_{De} (see Table 1), this field drops by a factor of e. At heights below 5000 km, therefore, E_s can be disregarded if the measuring instrument is at least 1 meter away from the surface of the satellite. In the outer magnetosphere, the Debye length is about 40 m. Consequently, the measuring instrument must be deployed at a distance on the order of 100 m.

Let us evaluate the contribution of E_{VH}. Table 1 lists data from experiments to measure electric-field strengths on satellites [15]. The maximum relative error of measurements of E_{VH}, assuming that its contribution permits measurement of E with errors no greater than 10%, should not exceed the value determined from the relation /52

$$\frac{\Delta E_{VH}}{E_{VH}} = 10^{-1}\frac{E}{E_{VH}}.$$

Values of the absolute error E_{VH} appear in Table 1. The field E_{VH} can be calculated from knowledge of |V|, |H| and the angle between these vectors in the satellite frame [16] or the components V and H in this frame. Proceeding from the requirement

$$\left(\frac{\Delta V}{V}\right)^2+\left(\frac{\Delta H}{H}\right)^2=\left(\frac{\Delta E_{VH}}{E_{VH}}\right)^2, \quad (5)$$

we obtain the largest admissible values of the absolute error ΔV and ΔH, which are given in Table 1.

The value of |V| can be obtained by computing the trajectory of the satellite in the orbital coordinate frame. The absolute error ΔV with which a velocity component is determined depends on the accuracy of determination of the orientation Δθ of the satellite frame with respect to the orbital frame, and can be calculated with the conversion matrix linking the two frames [16]. To determine the velocity with the required accuracy, it is necessary that the orientation be determined with an error no greater than 0°.25 in the ionosphere or 1°.5 in the upper magnetosphere.

Let us consider whether the required measurement accuracy ΔH can be obtained. The intensity of the geomagnetic field is defined in our coordinate frame by the expression

$$H = H' + \varepsilon |V \times E|. \quad (6)$$

Even at the largest value of E (see Table 1), the contribution of the term $\varepsilon |V \times E|$ is negligibly small, and it can be assumed that H = H'. The accuracy of determination of the magnetic-field intensity depends on the error of the magnetometer and, unless measurements are made simultaneously in all three components, on the rate of change dH/dt of the magnetic field and the rate of change of the direction of the vector H. All of these errors should, taken together, yield a figure smaller than that determined from Eq. (5).

A three-component magnetometer with a measurement range of 50-50 000 γ and an error of ±50 γ is required in the ionosphere. Since the largest value of dH/dt = 1000 γ/sec, the telemetry interrogation frequency must be such that the field can change by no more than 50 γ during interrogation of all three components. Rotation of the instrument also imposes requirements on interrogation frequency. The position of the instrument may not change by more than 0.3° during interrogation of all components.

As we see from Table 1, $E_{VH} > E$. If it is required that the error of measurement of E be no greater than 10%, the error of measurement of E' will be determined by the following expression with consideration of the possible disturbing factors:

$$\frac{\Delta E'}{E'} = 10^{-3}\frac{E}{E+E_{VH}}.$$

Values of $\Delta E'/E'$ for certain experiments appear in Table 1.

Thus, the measuring instrument must have a range of $5 \cdot 10^{-5}$-$4 \cdot 10^{-1}$ V/m and be accurate to $\pm 3 \cdot 10^{-4}$ V/m. It is expedient to have an instrument with a range of $5 \cdot 10^{-3}$-$4 \cdot 10^{-1}$ V/m and an error of $\pm 3 \cdot 10^{-4}$ V/m for measurements in the ionosphere, and one with a range of $5 \cdot 10^{-5}$-10^{-3} V/m and an error of $\pm 10^{-6}$ V/m for the upper magnetosphere.

2. Methods of Measurement

/53

Methods of measuring electric-field strength can be classified in accordance with the scheme in Table 2. The classification is based on the nature of the instrument-plasma interaction.

TABLE 2. CLASSIFICATION OF METHODS OF ELECTRIC-FIELD MEASUREMENT*

Method	Sensor type
Probe method	Floating-potential probes: static, rotating or translational motion Probes at plasma potential
Electrostatic induction method	Electrostatic Fluxmeter

*The artificial ionized cloud method is also used to measure electric fields [6, 7]. Since the motion of the cloud is observed from the ground, this method may be classed as a ground observation method; it is not considered in this paper.

PROBE METHOD

The Langmuir-probe method is widely used in plasma diagnostics for electric-field measurements. Let us examine the possibility of using this method for satellite electric-field measurements [17]. Figure 1 shows a typical current-voltage characteristic of a double floating probe. If the plasma is in an external electric field, the characteristic is not symmetrical about the coordinate origin. In this case, the characteristic is, for identical probes and a homogeneous plasma, symmetrical about the point at which the current vanishes (see Fig. 2), but this point U_d is shifted by the amount of the potential difference between the zones of the plasma in which the probes are situated. Knowing the distance between the probes, we can determine the strength of the electric field.

Probes at Floating Potential

If a voltmeter is connected between the probes, they will be at a floating potential determined by the current balance as given

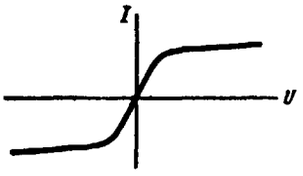

Figure 1. Typical Current-Voltage Characteristic of Double Probe.

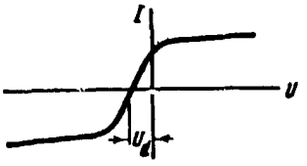

Figure 2. Current-Voltage Characteristic of Double Probe in External Electric Field.

by Eq. (3). In certain cases, this equation can be simplified to

$$I_e + I_i + I_p = I, \tag{7}$$

where I is the current flowing through the voltmeter.

The expression for the probe potential can be used [15] to estimate the errors incurred in probe measurements. With consideration of all currents appearing in Eq. (7) and the motion of the probe in the plasma, the floating potential ϕ of the probe is determined by the expression /54

$$\varphi = -\frac{kT_e}{e} \ln \frac{\sqrt{\frac{kT_e}{2\pi m_e}}}{\sqrt{\frac{kT_i}{2\pi m_i} + \frac{V^2}{16} + \frac{I_{p_r}}{4\pi\varepsilon} + \frac{I}{4\pi r^2 ne}}}, \tag{8}$$

where r is the radius of the probe.

For measurement of the minute potential difference between the probes, it is very important that the probes be made of identical material and have identical sizes and shapes, preferably spherical. Nonspherical probes must be oriented in exactly the same way, since the magnetospheric plasma is anisotropic.

Static probes

The potential difference U measured with the voltmeter is defined as

$$U = dE_d' - 2\Delta U,$$

where d is the distance between probes, E_d' is the electric-field component along d in the satellite frame, $\Delta U \simeq \left| I \frac{d\varphi}{dI} \right|$ is the change in probe potential as a result of the current through the voltmeter, and $d\varphi/dI$ is determined from Eq. (8):

TABLE 3*

Height, km	Experimental conditions	$(Rr^2)_{min}$, ohm-m^2	$(r^2/d^3)_{max}$, m^{-1}	$(R/d^3)_{max}$, ohm-m^{-2}	d_{min}, m	r_{opt}, m	R_{opt}, ohm	v_{max}, m/sec
300	Night	$1,6\cdot10^5$	$1,4\cdot10^{-2}$	$4\cdot10^8$	0,5	$4\cdot10^{-2}$	$9\cdot10^7$	30
300	»	$9\cdot10^4$	$7\cdot10^{-3}$	$4\cdot10^8$	0,5	$3\cdot10^{-2}$	$1\cdot10^8$	17
3000	»	$1,9\cdot10^6$	$1,6\cdot10^{-3}$	$4\cdot10^7$	2,0	0,11	$1,6\cdot10^8$	60
20 000	»	$6\cdot10^6$	$4\cdot10^{-5}$	$4\cdot10^5$	14	0,3	$7\cdot10^7$	—
50 000	»	$6\cdot10^8$	$4\cdot10^{-6}$	$4\cdot10^3$	140	3	$7\cdot10^7$	—

*Commas indicate decimal points.

$$\frac{\partial\varphi}{\partial I} = -\frac{\sqrt{2\pi m_e kT_e}}{4\pi r^2 ne^2}\exp\left(\frac{e\varphi}{kT_e}\right).$$

For the measurement error to be small, it is necessary that

$$2\Delta U \leqslant d\cdot\Delta E'_d \approx \Delta E'/E'\cdot R|I|,$$

where R is the resistance of the voltmeter. From this requirement, we obtain

$$Rr^2 \geqslant (Rr^2)_{min} = \frac{1}{\Delta E'/E' ne^2}\sqrt{\frac{nekT_e}{2\pi}}\exp\left(\frac{e\varphi}{kT_e}\right). \qquad (9)$$

Values of $(Rr^2)_{min}$ for $\Delta E'/E'$ (see Table 1) appear in Table 3.

Recognizing that the accuracy of measurement of E is an order higher than the accuracy of measurement of E', and that a potential difference $\Delta U_p \approx \frac{kT_e}{e}\frac{r^3}{4d^3}$ may arise between the probes as a result of shadowing of one by the other [15], we obtain a requirement necessary for estimation of the distance d:

$$\Delta U_p < d\cdot\Delta E' = 10^{-3}d\cdot E,$$

from which

$$\frac{r^3}{d^3} \leqslant \left(\frac{r^3}{d^3}\right)_{max} = 4\cdot10^{-3}\frac{eE}{kT_e}. \qquad (10)$$

These values are also included in Table 3.

Any resistance, including the voltmeter resistance R, is a generator of thermal noise. With a large enough distance between probes, the potential difference should be greater than the

thermal-noise voltage, i.e., /55

$$d \cdot \Delta E' > \sqrt{4kTAR},$$

where I is the temperature of the resistance and A is the amplifier bandwidth (10^3-10^4 Hz). We have the condition

$$\frac{R}{d^2} \leqslant \left(\frac{R}{d^2}\right)_{\max} = \frac{(\Delta E')^2}{4kTA} = \frac{10^{-4}E^2}{4kTA}. \quad (11)$$

Values of $(R/d^2)_{max}$ are given in Table 3.

An expression for the smallest possible probe system can be obtained from Eqs. (9)-(11):

$$d > d_{\min} = \left(\frac{10^8 k^2 T_e T A}{\Delta E'/E' n e^2 E^2}\right)^{1/6} \left(\frac{m_e k T_e}{2\pi}\right)^{1/6} \exp\left(-\frac{e\varphi_0}{5kT_e}\right), \quad (12)$$

$$l = r_{opt} = 0.2\sqrt{\frac{eE}{kT_e} d_{\min}^3}, \quad (13)$$

$$R = R_{opt} = \frac{10^{-4}E^2}{4kTA} d_{\min}^2. \quad (14)$$

Values of d_{min}, r_{opt}, and R_{opt} are given in Table 3.

On the basis of the requirements as to the error $\Delta E'/E'$ (see Table 1), we find that the error of determination $\Delta d/d$ of the distance between probes in the ionosphere may be no greater than $\pm 8 \cdot 10^{-4}$ or $\pm 2 \cdot 10^{-3}$ in the upper magnetosphere. Bending deflections of the booms may also contribute to the error Δd. The maximum angular deflection of one of the probes may not exceed 2° in the ionosphere or 3° in the upper magnetosphere.

Rotating probes

Difficulties arise in instruments with static probe systems because of the appearance of a contact potential difference and zero-point drift of the dc amplifier. These difficulties can be eliminated by using a rotating probe system and making alternating-current measurements. This increases the sensitivity of the voltmeter by an order or more. But this method gives rise to its own difficulties, which are associated with the higher probability, as compared with static probes, that the probes will enter shaded zones. They may also have different velocities with respect to the plasma. The maximum velocity difference equals $2\omega d$, where ω is the angular velocity of the probe system ($\omega d \ll V$). The potential difference ΔU_{ro} that arises between the probes as a result of rotation must satisfy the condition

$$\Delta U_{vo} < \omega d \frac{\partial \varphi}{\partial V},$$

where, from Eq. (8), /56

$$\frac{\partial \varphi}{\partial V} = \frac{V}{16\varepsilon}(2\pi m_e k T_e)^{1/2}\left(\frac{kT_i}{2\pi m_i} + \frac{V^2}{16}\right)^{-1/2} \exp\left(-\frac{e\varphi}{kT_e}\right).$$

The voltage measured with the voltmeter is defined as

$$U = d \cdot E'_d \cos \omega t - \Delta U_{vo}.$$

The condition

$$\Delta U_{vo} \leqslant d\Delta E' = 10^{-2} dE$$

requires that

$$\omega < \omega_{max} = 4 \cdot 10^{-2} eE \left(1 + \frac{8kT_i}{\pi m_i v^2}\right)^{1/2} (2\pi m_e k T_e)^{-1/2} \exp\left(\frac{e\varphi}{kT_e}\right). \qquad (15)$$

Values of ω_{max} appear in Table 3. The calculation of the basic probe parameters is the same as for the static method.

Oscillating probes

Use of a system of probes that describe oscillatory motions with respect to one another also permits alternating-current measurements and preserves the advantages of the rotating probe system. Probe-shading effects can also be eliminated with this method. The probes also move at different velocities with respect to the plasma, and the oscillation frequency must be determined with Eq. (15). The sensitivity of this method is lower than that of the rotating-probe method, but of the same order as (or even higher than) that of the static method.

Probes at Plasma Potential

The probe potential is usually negative, and the ion current to the probe makes a large contribution. The ion current can be minimized if the probe potential is near the plasma potential. To hold one of the electrodes of a double probe at plasma potential, it is necessary that its surface area stand in a certain relation to the surface area of the sign to this electrode, so that the current of charges of one sign onto this electrode can be compensated, regardless of its potential, by the current of charges of the opposite sign to the other electrode.

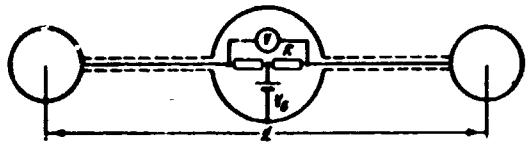

Figure 3. Probes at Floating Potential.

If there are two electrodes, both at the plasma potential, the electric-field strength components can be determined by measuring the potential difference between them. This system can be used with three probes (Fig. 3). The voltage measured by the voltmeter is defined as

$$U = dE' + \varphi_1 - \varphi_2$$

and

$$\varphi_b - \varphi_s = \frac{1}{2} RI_1 + \varphi_1 + \frac{1}{2} dE' = \frac{1}{2} RI_2 + \varphi_2 - \frac{1}{2} dE',$$

where ϕ_b is the bias-battery voltage, ϕ_s is the potential of the central electrode, ϕ_1 and ϕ_2 are the potentials of probes 1 and 2, respectively, and I_1 and I_2 are the currents to probes 1 and 2, respectively. /57

TABLE 4*

Height, km	Experimental conditions	$(\varphi_b)_{min}$, V	P_{min}, W	d_{min}, m	r_{opt}, m	P_{opt}, ohm	$R_{s\,opt}$, m
300	Night	110	$1,4 \cdot 10^{-4}$	1	$5 \cdot 10^{-3}$	$4 \cdot 10^{6}$	0,06
300	»	200	$5 \cdot 10^{-4}$	1	$3 \cdot 10^{-3}$	$4 \cdot 10^{6}$	0,04
3000	»	500	$6 \cdot 10^{-4}$	4	$4 \cdot 10^{-2}$	$5 \cdot 10^{6}$	0,13
20 000	»	190	$5 \cdot 10^{-4}$	30	0,14	$3 \cdot 10^{6}$	0,5
50 000	»	130	$4 \cdot 10^{-4}$	200	0,2	$1,5 \cdot 10^{6}$	4,0

*Commas indicate decimal points.

If ϕ_b is so selected that $\phi_2 = 0$, we obtain, in analogy to Eq. (9),

$$Rr^3 > (Rr^3)\min = \frac{1}{\Delta E'/E' n e^2} \sqrt{\frac{m_e k T_e}{2\pi}}. \qquad (16)$$

It can be found from the definitions of the currents to the probes that

$$\frac{r^2}{r_s^2}=\frac{1}{2}\frac{\exp\left(\frac{e\varphi_0}{kT_e}\right)-\exp\left(\frac{e\varphi_s}{kT_e}\right)}{1-\exp\left(\frac{e\varphi_0}{kT_e}\right)}. \tag{17}$$

If the area of the central probe is much larger than that of probe 1 or 2, ϕ_s can be neglected by comparison with ϕ_b, and then

$$\varphi_b\simeq\sqrt{\pi}Rr^2ne\sqrt{\frac{2kT_e}{m_e}}>\frac{kT_e}{(\Delta E'/E')e}. \tag{18}$$

The power P necessary to support the plasma potential in the probes is

$$P\approx\frac{1}{2}R(I_1^2+I_2^2)\approx\frac{4\varphi_b^2}{R}>\frac{4}{R}\left(\frac{kTe}{(\Delta E'E')e}\right)^2. \tag{19}$$

Values of ϕ_b and P are given in Table 4. In an analogy to (12)-(14), we can obtain the parameters of the smallest probe system with a central electrode:

$$d>d_{\min}=2\left[\frac{10^6k^2T_e^2TA}{(\Delta E'/E')ne^2E^2}\left\{\exp\left(-\frac{e\varphi_0}{kT_e}\right)-1\right\}\right]^{1/6}\left(\frac{m_ekT_e}{2\pi}\right)^{1/12}, \tag{20}$$

$$r=r_{opt}=5\cdot10^{-2}\sqrt{\frac{eE}{kT_e}d_{\min}^3}\left\{\exp\left(-\frac{e\varphi_0}{kT_e}\right)-1\right\}^{-1/6}, \tag{21}$$

$$R=R_{opt}=\frac{10^{-6}E^2}{4kTA}d_{\min}^2, \tag{22}$$

$$r_c=r_{copt}=0.1\sqrt{\frac{eE}{kT_e}d_{\min}^3}. \tag{23}$$

These values are given in Table 4.

For a rotating (or oscillating) probe system, the maximum permissible angular velocity can be found on the assumption that $\phi = 0$ [see Eq. (15)]. Values of ω_{max} appear in Table 4.

Since ϕ_b depends on T_e [see Eq. (18)], which also varies, it would be desirable to use an automatic device capable of holding the probes at plasma potential. This device might, for example, be based on a second-harmonic meter for the current through the voltmeter with an extremely small oscillating field superimposed on ϕ_b [18]. The first derivative of the probe current with respect to the potential is also sensitive to plasma potential. The potential at which the first derivative is largest is taken as the

/58

plasma potential [19]. The second potential derivative of probe current, which changes sign at a probe potential near the plasma potential, is even more sensitive [20, 21]. We should also note that the value of the current I_p at the plasma potential can be used to determine the electron concentration n_0 in the undisturbed plasma:

$$n_0 = \frac{4I_p}{e\bar{v}_e S}, \tag{24}$$

where $\bar{v}_e$ is the average electron velocity and S is the area of the probe.

Electrostatic-Induction Method

Some of the first measurements of electric-field strength were made using electrostatic fluxmeters [1-3]. In a method proposed by I.M. Imyanitov [22, 23], two electrostatic fluxmeters are placed at diametrically opposite points on the surface of a satellite and measure the electric-field strength E' at the surface of the satellite. On the assumption that the dimensions of the satellite greatly exceed the thickness of the space charge, the electric field directed along the line joining the fluxmeters is determined by the relation

$$E = \frac{E'_1\delta_1 - E'_2\delta_2}{2a}, \tag{25}$$

where δ is the thickness of the space-charge layer, a is the diameter of the satellite, and the subscripts 1 and 2 identify the parameters at points 1 and 2.

If it is assumed that $\delta_1 = \delta_2 = \delta$ and δ is known with high accuracy, we have

$$\frac{\Delta E}{E} = \frac{\delta}{2a}\frac{2\Delta E_{1,2}}{E'_1 - E'_2},$$

where $\Delta E_{1,2}$ is the sensitivity of either fluxmeter.

Usually, a is on the order of 1 meter. The difference ($E'_1 - E'_2$) that inevitably appears in motion in the geomagnetic field has a maximum in the ionosphere at 0.4 V/m, and is $\sim 2 \cdot 10^{-4}$ V/m in the upper magnetosphere. To determine E with accuracy no poorer than 10%, it is necessary that the instrument have a sensitivity no poorer than 10 V/m in the ionosphere (where $\delta \approx 5 \cdot 10^{-3}$ m) and no poorer than $5 \cdot 10^{-7}$ V/m in the upper magnetosphere (where $\delta \approx$ $\approx$ 50 m). On the other hand, the fluxmeters used to date have had

REPRODUCIBILITY OF THE ORIGINAL PAGE IS POOR.

sensitivities around 5 V/m [24], the limit imposed by the contact potential difference that arises between their plates. An instrument in which this effect was minimized is described in [25]: it has a sensitivity of 1 V/m. Consequently, fluxmeters can be used only for measurements in the ionosphere.

It must also be noted that a minimum of four fluxmeters is necessary to measure the vector E. In this case, the two fluxmeter pairs will not be operating under the same conditions. It is necessary to determine many correction factors, and this greatly lowers the accuracy of determination of E.

CONCLUSION

/59

Our review of various methods for electric-field measurement has indicated that the probe method can be used with all types of sensors listed in Table 2. For measurements in the ionosphere, it is advantageous to use a rotating or oscillating system, since these systems have the highest sensitivities and make it possible to tune out contact effects. Use of rotating probes in the upper magnetosphere gives rise to major design difficulties, which arise out of the fact that the system has large geometrical dimensions. Use of oscillating-system detectors is therefore advantageous in this region.

In the probe method, special attention must be given to cleanliness of the probe surfaces. This requires thorough cleaning of surfaces on the ground and maintenance of this cleanliness on injection into orbit. Metallized inflated probes must be used in the upper magnetosphere. The development of such probes is an independent problem.

To permit fuller interpretation of the measurements, it would be desirable to measure particle concentrations and temperatures, as well as the distribution of the space charge around the satellite, concurrently with the electric-field measurements. Electrostatic fluxmeters, which are capable of giving additional information concerning the charge on the satellite, could be used in this combination.

To obtain complete data on the distribution of the electric fields in the magnetosphere, it will be necessary to make measurements regularly and at various heights. Such experiments would make it possible to improve the accuracy of the measurements and might possibly lead to new measurement methods.

REFERENCES

1. G.L. Gdalevich. Iskusstvennyye sputniki Zemli, 1963, Vol. 17, 42-58.
2. I.M. Imyanitov and Ya.M. Shvarts. Iskusstvennyye sputniki Zemli, 1963, Vol. 17, 59-65.

REPRODUCIBILITY OF THE ORIGINAL PAGE IS POOR.

3. I.M. Imyanitov, G.L. Gdalevich, and Ya.M. Shvarts. Iskusstvennyye sputniki Zemli, 1963, Vol. 17, 66-81.
4. F.S. Mozer. Preprint, Space Sci. Lab., 1968.
5. F.S. Mozer and P. Bruston. J. Geophys. Res., 1967, Vol. 72, 3, 1109-1114.
6. G. Haerendel, R. Lust, and E. Rieger. Planet. and Space Sci., 1967, Vol. 15, 1, 1-18.
7. H. Föppl. Planet. and Space Sci., 1967, Vol. 15, 2, 357-372.
8. S.B. Mende. J. Geophys. Res., 1968, Vol. 73, 3, 991-997.
9. V.A. Kurilov, V.V. Veselov, A.F. Yelkin, V.V. Apinyan, and N.I. Vasilevskaya. "Elektronnaya tekhnika", Series 10, 1968, No. 3, 114-130.
10. V.A. Pryanishnikov. In book entitled: "Metody i sredstva zashchity organizma cheloveka ot staticheskogo elektrichestva" (Ways and Means to Protect the Human Organism from Static Electricity), Material of seminar. Moscow, 1968.
11. V.G. Kurt and V.I. Moroz. Iskusstvennyye sputniki Zemli, 1961, Vol. 7, 78-88.
12. K.I. Gringauz and M.Kh. Zelikman. UFN, 1957, Vol. 63, 15, 239-252.
13. C.I. Johnson and E.B. Meadows. J. Geophys. Res., 1955, Vol. 60, 2, 193.
14. C.I. Johnson and I.P. Heppuer. J. Geophys. Res., 1956, Vol. 67, 575.
15. U. Fahleson. Space Science Rev., 1967, Vol. 7, 2/3, 238-262.
16. Problemy orientatsii iskusstvennykh sputnikov Zemli (Problems of Orientation of Artificial Earth Satellites), Moscow, "Nauka," 1966.
17. H. Dolezalek. Z. Geophys., 1966, Vol. 32, 5-6, 318-329.
18. R.L.F. Boyd and A.P. Willmorf. Space Res., 1963, 111, 1168.
19. Yu.M. Kulakov and A.A. Zaychev. Vestnik MGU, 1949, Vol. 3, 101.
20. R.L.F. Boyd and J. Thompson. Proc. Roy. Soc. 1959, Vol. 250, 53.
21. I.A. Vorob'yeva, Yu.M. Kogan, and V.M. Meleshin. PETF, 1963, No. 15, 1-18.
22. I.M. Imyanitov. Pribory i metody dlya izucheniya elektrichestva atmosfery (Instruments and Methods for the Study of Atmospheric Electricity), Moscow, 1957.
23. I.M. Imyanitov. Usp. Fiz. Nauk, 1957, Vol. 63, 16, 267-282.
24. I.M. Imyanitov and Ya.M. Shvarts. Iskusstvennyye sputniki Zemli, 1959, Vol. 3, 77-83.
25. K. Knot. In collection entitled: "Pribory dlya nauchnykh issledovaniy (Instruments for Scientific Research), 1967, Vol. 5, 25-27.

N75 13713

HIGH-FREQUENCY TURBULENCE IN THE COSMIC PLASMA

(Translation of "Vysokochastotnaya turbulentnost' v kosmicheskoy plasme.")

V. A. Gudkova and V. A. Liperovskiy

ABSTRACT

The problem of quasistationary high-frequency Langmuir turbulence, which is one of the types of turbulence encountered in the cosmic plasma, is examined theoretically. With 5 illustrations and 18 source citations.

HIGH-FREQUENCY TURBULENCE IN THE COSMIC PLASMA /60

V.A. Gudkova and V.A. Liperovskiy

1. An enormous amount of experimental material on the physical processes that take place in space has been accumulated as a result of the space research of recent years. However, there remain many problems whose theoretical aspects have been neglected. In explaining many cosmic phenomena, it has been found helpful and promising to treat outer space as a rarefied plasma with developed collective processes. The development of plasma theory over the last few decades in the attempt to solve the problem of thermonuclear fusion has led to a conception in which the plasma is almost always unstable, and our picture of the plasma instabilities has accordingly been filled in quite completely.

Moreover, vigorous development of turbulent-plasma research began when it developed that the stable plasma is an extreme rarity. Here we mean by "turbulent plasma" a plasma in which strong disordered fluctuations of wave nature have developed as a result of instabilities and interact with one another and with plasma particles.

To understand the properties of the turbulent plasma, it is necessary to treat it as a mixture of gases: particles (electrons, ions) and quasiparticles (photons and plasmons of various species) with consideration of Cerenkov radiation, induced scattering, and decays involving three and four quasiparticles in the kinetic equations for the particles and quasiparticles. As a result of developed turbulence, both cosmic and laboratory plasmas exhibit a number of peculiar properties. As a result of the development of instability, the plasma contains regions of elevated particle density with which single particles "collide" under the conditions of a practically collisionless (in the sense of pair collisions) plasma. The "collective collisions," which are often many orders more intense than pair collisions, result in such macroscopic processes as anomalous diffusion of particles across lines of force of the magnetic field and anomalous resistance. A plasma with developed turbulence may be a source of high-frequency electromagnetic radiation with a frequency $\omega >> \omega_{0e}$; a mechanism of statistical particle acceleration operates in such a plasma, leading to the appearance of a small number of very fast particles (subcosmic and cosmic rays).

Plasma turbulence is therefore a highly important factor in a number of cosmic phenomena. Thus, in the interaction of the solar wind with the earth's magnetosphere, the basic transfer of energy takes place through a turbulent layer on the boundary of the magnetosphere, where intense collective collisions develop. They cause anomalous diffusion of particles across the lines of

force of the geomagnetic field.

The processes of particle breakthrough in the vicinity of the neutral points and processes of auroral-electron acceleration along magnetic tubes of force, which lead to the appearance of auroras, may be related to plasma turbulence. Satisfactory agreement has not been attained either among investigators or between theory and experiment in theoretical solution of these problems. Hence follows the need for further development of plasma-turbulence theory for application to these and other cosmic phenomena. In these investigations of cosmic plasma turbulence, study of slowly-varying "quasistationary" states is particularly important, since these states are obviously those most frequently encountered in space. /61

Waves of various types may be generated as a result of instabilities in plasmas: Langmuir, electron-cyclotron, ion-acoustic, whistler, Alfven, magnetoacoustic, and other waves. All of these wave types interact with one another in a turbulent plasma. Since there are very many wave types and possible "elementary" interactions among them, solution of the problem of the turbulent quasistationary states is not feasible in the general case.

Since the investigation of turbulent quasistationary states has become a necessary and pressing task of modern space physics, it appears reasonable to begin this study with the simplest cases, which are now within the reach of theory. In the future, solution of these simple quasistationary-turbulence problems will make it possible to go on to the solution of more complex problems involving many types of waves, an electric field, etc.

In the present article, we shall dwell on one of the problems of this sort that have been solved in recent years: the problem of quasistationary high-frequency Langmuir turbulence.

2. Let Langmuir turbulence be excited in a plasma, with the waves (plasmons) having frequencies corresponding to the dispersion laws of the linear theory:

$$\omega_k = \omega_{0e} + \frac{3}{2}\frac{v_e^2 k^2}{\omega_{0e}}, \qquad \omega_{0e} = \sqrt{\frac{4\pi e^2 n_0}{m_e}}, \qquad v_e = \sqrt{\frac{T_e}{m_e}}. \tag{2.1}$$

Thus, we shall henceforth be considering only weak turbulence, in which the energy density W^l of the waves is much smaller than the thermal-energy density nT_e. As we know [1], it is necessary in the problem of the evolution of Langmuir turbulence to consider nonlinear processes of induced scattering of Langmuir plasmons on electrons, induced scattering on ions, four-plasmon decay, in which two Langmuir plasmons decay into two Langmuir plasmons with different wave numbers ($l + l' \to l'' + l'''$), and the decay of Langmuir waves into ion-acoustic waves at $T_e \gg T_i$ ($l \to l + s$). The transmis on

range of Langmuir waves is limited by the inequality $\lambda_e k \ll 1$, where $\lambda_e = v_e/\omega_{0e}$.

In analysis of all of these processes, the transmission range is broken up into a number of subranges, in each of which one or another of the processes enumerated above will dominate, depending also on the turbulent energy W^l.

The four-plasmon interaction has been examined in a number of papers [1-5]. However, the expressions obtained for the probability of this interaction were valid, strictly speaking, only for small wave numbers $k\lambda_e \ll {}^1/_3 v_i/v_e$. For large $k\lambda_e > {}^1/_3\ v_i/v_e$ (but $k\lambda_e \ll 1$) the results were either inaccurate, or were of the nature of estimates, or did not take the ions into account consistently. It therefore became necessary for correct comparison of all possible nonlinear processes to find a complete expression for the probability of the four-plasmon interaction for any $k\lambda_e$. The mathematical complexity of the calculations for determination of this probability was found to be considerably greater for $k\lambda_e > v_i/3v_e$ than for $k\lambda_e \ll v_i/3v_e$ [5], because of the strong compensation effects in calculation of the nonlinear current. It was therefore necessary to make the calculations accurate to the fourth order of the small parameter to obtain the first nonvanishing term. We present the derivation of the probability of the four-plasmon decay $l + l' \to l'' + l'''$.

The kinetic equation for Langmuir plasmons, which takes account only of four-plasmon processes of the type $l + l' \to l'' + l'''$, takes the form [1] /62

$$\frac{\partial N(k)}{\partial t} = \int \frac{dk_1 dk_2 dk_3}{(2\pi)^9} w_{ll}^{ll}(k_1, k_2 | k_3, k)\{N(k)N(k_1)(N(k_2) - N(k_3)) + N(k_2)N(k_3)(N(k_1) - N(k))\}, \quad (2.2)$$

where N(k) is the numerical density of Langmuir plasmons in k-space, referred to 1 cm^3 of plasma:

$$N(k) = 2\pi^3 |E_{k_1}|^2 \left| \frac{\partial \varepsilon^l(\omega, k)}{\partial \omega} \right|_{\omega=\omega(k)}. \quad (2.3)$$

The relations used in averaging over the ensemble of random-wave fields are

$$\langle E_{k_i} E_{k_j}^* \rangle = \frac{k_i k_j}{k^2} \delta(k - k') \delta(\omega - \omega') |E_k|^2, \quad (2.4)$$

$$|E_k|^2 = |E_k|^2 \delta(\omega - \omega(k)) + |E_{-k}| \delta(\omega + \omega(k)), \quad (2.5)$$

REPRODUCIBILITY OF THE ORIGINAL PAGE IS POOR.

where

$$E_{k_i} = \frac{1}{(2\pi)^4} \int E_i(r, t)\, e^{-i(kr-\omega t)}\, dr\, dt \qquad (2.6)$$

is the Fourier component of the total field and $w_{ll}^{ll}(k_1, k_2 \mid k_3, k)$ is the four-plasmon decay probability.

In the limit as $N(k) \to 0$, the rate of change of the Langmuir-wave energy due to the nonlinear interaction (2.2) equals

$$Q^l = \int \frac{\omega_l dk}{(2\pi)^3} \frac{\partial N(k)}{\partial t} = \int \frac{\omega dk}{(2\pi)^3} N(k_1) N(k_2) \times \\ \times N(k_3) w_{ll}^{ll}(k_1, k_2 \mid k_3, k) \times \frac{dk_1 dk_2 dk_3}{(2\pi)^9}. \qquad (2.7)$$

On the other hand, this same energy change is the radiant intensity of the nonlinear "extrinsic current" $j^{(3)}(k)$, which is proportional to E^3, i.e.,

$$j^{(3)}(k) = \int \Sigma_{ilmn}(k, k_1, k_2, k_3)\, E_{k_1 l} E_{k_2 m} E_{k_3 n}\, d\lambda_{123},$$

where $d\lambda_{123}^0 = dk_1 dk_2 dk_3 d\omega_1 d\omega_2 d\omega_3 \delta(k - k_1 - k_2 - k_3)\delta(\omega - \omega_1 - \omega_2 - \omega_3)$, and $\Sigma_{ilmn}(k, k_1, k_2, k_3)$ is the nonlinear conductivity tensor of the electronic component of the plasma, which corresponds to E^3 and is symmetrical with respect to the permutation $k_1 \rightleftarrows k_2 \rightleftarrows k_3$.

The radiant intensity of the current $j^{(3)}(k)$ is

$$Q^l = -\lim_{\substack{T\to\infty \\ V\to\infty}} \int \frac{(2\pi)^4}{TV} dk\, d\omega \langle j_i^{*(3)}(k)\, \Pi_{ij}^{(l)}(k) j_j^{(3)}(k) \rangle = \\ = \lim_{V,T\to\infty} \frac{(2\pi)^6}{2VT} \int \left\langle \left| \frac{k j^{(3)}}{k} \right|^2 \right\rangle dk\, d\omega\, \delta(\omega - \omega(k)) = \\ = \frac{9}{\pi^2} \int \omega(k)\, dk N(k_1) N(k_2) N(k_3) \delta(k - k_1 - k_2 - k_3) \delta(\omega(k) - \\ - \omega(k_1) - \omega(k_2) - \omega(k_3))\, \omega_1^2 \omega_2^2 \omega_3^2 |\Sigma(k, k_1, k_2 - k_3)|^2 \times \\ \times \left\{ \left| \frac{\partial}{\partial\omega} \omega^2 \varepsilon^l \right|_{\omega=\omega(k)} \left| \frac{\partial}{\partial\omega} \omega^2 \varepsilon^l \right|_{\omega=\omega(k_1)} \left| \frac{\partial}{\partial\omega} \omega^2 \varepsilon^l \right|_{\omega=\omega(k_2)} \left| \frac{\partial}{\partial\omega} \omega^2 \varepsilon^l \right|_{\omega=\omega(k_3)} \right\}^{-1} \qquad (2.8)$$

Here

$$\Pi_{ij}^l(\omega, k) = -\frac{4\pi i\omega}{k^2} \frac{k_i k_j}{\omega^2 \varepsilon^l(k, \omega)}$$

is the longitudinal term of the inverse Maxwell operator (see /63

REPRODUCIBILITY OF THE ORIGINAL PAGE IS POOR

for example, [1]) (we shall neglect the transverse term).

The formulas used in integration were

$$\delta^2(k) \to \delta(k)\frac{TV}{16\pi^4},$$
$$\frac{1}{\varepsilon^l(\omega, k)} \to P\frac{1}{\varepsilon^l(\omega, k)} - i\pi\delta(\varepsilon^l(k, \omega)).$$

On averaging over the ensemble $\left\langle \left| j^{(3)}\frac{k}{k} \right|^2 \right\rangle$ we had

$$\left\langle \left| j^{(3)}\frac{k}{k} \right|^2 \right\rangle = 6\int dk_1 dk_2 dk_3 |\Sigma(k, k_1, k_2, k_3)|^2 \delta^2(k-k_1-k_2-k_3) \times \times |E_{k_1}|^2 |E_{k_2}|^2 |E_{k_3}|^2. \quad (2.9)$$

where

$$\Sigma(k, k_1, k_2, k_3) = \Sigma_{ilmn}(k, k_1, k_2, k_3)\frac{k_i e_{1l} k_{2m} k_{3n}}{k k_1 k_2 k_3},$$

with the following substitutions made in the last expression in recognition of (2.6): $\omega \to \omega(k)$, $k_3 \to -k_3$, $\omega_3 \to -\omega_3$, i.e., with the conversion to $\Sigma(k, k_1, k_2 - k_3)$.

The expression for $\Sigma_{ilmn}(k, k_1, k_2, k_3)$ is obtained on solving the kinetic equation for the electrons accurate to terms $\sim E^3$.

Much as was done, for example, in [2], we shall proceed from the kinetic equation for the electrons:

$$\frac{\partial f}{\partial t} + v\frac{\partial f}{\partial r} + \frac{e}{m}E\frac{\partial f}{\partial v} = 0. \quad (2.10)$$

Let us assume that $f = f_0 + f_1 + f_2 + f_3$, where f_0 is the Maxwellian distribution function and f_1, f_2, and f_3 are the corrections to it corresponding to the first, second, and third powers of the total field E. We write these corrections in the form of Fourier integrals and obtain from the equations for the corrections

$$f_{1k} = \frac{1}{\omega - kv}\frac{e}{im}E_k\frac{\partial f_0}{\partial v} \quad (2.11)$$

$$f_{2k} = \frac{1}{\omega - kv}\left(\frac{e}{im}\right)^2\int E_{k_1}\frac{\partial}{dv}\frac{1}{\omega_2 - k_2 v}E_{k_2}\frac{\partial f_0}{\partial v}d\lambda^0_{12}, \quad (2.12)$$

$$f_{3k} = \frac{1}{\omega - kv}\left(\frac{e}{im}\right)^3\int E_{k_1}\frac{\partial}{\partial v}\frac{1}{\omega_1 + \omega_2 - (k_1 + k_2)v} \times \times E_{k_2}\frac{\partial}{\partial v}\frac{1}{\omega_3 - k_3 v}E_{k_3}\frac{\partial f_0}{\partial v}d\lambda^0_{123}, \quad (2.13)$$

$$d\lambda^{\circ}_{12} = \delta(k_1 + k_2 - k)\,\delta(\omega_1 + \omega_2 - \omega)\,dk_1 dk_2 d\omega_1 d\omega_2,$$

$$d\lambda^{\circ}_{123} = \delta(k_1 + k_2 + k_3 - k)\,\delta(\omega_1 + \omega_2 + \omega_3 - \omega)\,dk_1 dk_2 dk_3 d\omega_1 d\omega_2 d\omega_3.$$

The nonlinear current of plasma electrons, which we shall henceforth regard as extrinsic, can be written

$$j_{\text{нел}(k)} = e\int(f_{2k} + f_{3k})\,v\,dv = \int S_{ilm}(k_1 k_1, k_2)\,E_{k_1 l}E_{k_2 m}d\lambda^{\circ}_{12} + \\ + \int \Sigma^{I}_{ilmn}(k, k_1, k_2, k_3)\,E_{k_1 l}E_{k_2 m}E_{k_3 n}d\lambda^{\circ}_{123}. \tag{2.14}$$

Here

$$S_{ilr}(k, k_1, k_2) = \frac{1}{2}\,[S'_{ilm}(k, k_1, k_2) + S'_{iml}(k, k_2, k_1)], \tag{2.15}$$

$$S'_{ilm}(k, k_1, k_2) = \frac{n_0 e^2}{m_e^2 v_e^2}\int \frac{v_l dv}{\omega - kv}\,\frac{\partial}{\partial v_l}\,\frac{v_m f_0}{\omega_2 - k_2 v}\,; \tag{2.16}$$

$$\Sigma^{I}_{ilmn}(k, k_1, k_2, k_3) = \frac{1}{6}\,\{\Sigma^{I'}_{ilmn}(k, k_1, k_2, k_3) + \Sigma^{I'}_{ilnm}(k, k_1, k_3, k_2) + \\ + \Sigma^{I'}_{imln}(k, k_2, k_1, k_3) + \Sigma^{I'}_{imnl}(k, k_2, k_3, k_1) + \Sigma^{I'}_{inlm}(k, k_3, k_1, k_2) + \\ + \Sigma^{I'}_{inml}(k, k_3, k_2, k_1)\}, \tag{2.17}$$

/64

$$\Sigma^{I'}_{ilmn}(k, k_1, k_2, k_3) = \\ = -\frac{ie^4 n_0}{m_e^3 v_e^2}\int\left(\frac{\partial}{\partial v_l}\,\frac{v_l}{\omega - kv}\right)\frac{dv}{\omega_2 + \omega_3 - (k_2 + k_3)\,v}\,\frac{\partial}{\partial v_m}\,\frac{v_n f_0}{\omega_3 - k_3 v}\,. \tag{2.18}$$

We shall assume further that the total field $E = E^{(1)} + E^{(2)} + \ldots$, where $E^{(2)}$ is the part of the total field associated with nonlinear effects $\sim E^2$, and is expressed in terms of the second-order nonlinear current by the formula

$$E^{(2)}_l(k) = \Pi^{I}_{ij}(k)\,j^{(2)}_j(k). \tag{2.19}$$

We then find that we can also separate the part of the total current that is proportional to E^3 from the first term of (2.14):

$$\int S_{ilm}(k, k_1, k_2)\,(E^{(1)}_{k_1 l}E^{(2)}_{k_2 m} + E^{(2)}_{k_1 l}E^{(1)}_{k_2 m})\,d\lambda^{\circ}_{12} = \\ = 2\int S_{ill}(k, k_1, k_2 + k_3)\,\Pi^{I}_{lq}(k_2 + k_3)\,S_{qmn}(k_2 + k_3, k_2, k_3)\,E^{(1)}_{k_1 l}E^{(1)}_{k_2 m} \times \\ \times E^{(1)}_{k_3 n}d\lambda^{\circ}_{123} = \int \Sigma^{II'}_{ilmn}(k, k_1, k_2, k_3)\,E_{k_1 l}E_{k_2 m}E_{k_3 n}d\lambda^{\circ}_{123} = \\ = \int \Sigma^{II}_{ilmn}(k, k_1, k_2, k_3)E_{k_1 l}E_{k_2 m}E_{k_3 n}d\lambda^{\circ}_{123}. \tag{2.20}$$

In the last equation, we have converted to a kernel that is symmetrical with respect to 1l, 2m, and 3n. We stress that

although the integrals are equal, the kernels (symmetrical and not symmetrical) are unequal.

In (2.20)

$$\Sigma^{II'}_{illmn}(k, k_1, k_2, k_3) = (S'_{ill}(k, k_1, k_2 + k_3) + S'_{ill}(k, k_2 + k_3, k_1) \times \times \Pi_{lg}(k_2 + k_3) S'_{gmn}(k_2 + k_3, k_2, k_3), \quad (2.21)$$

$$\Sigma^{II}_{ilmn}(k, k_1, k_2, k_3) = \frac{1}{6}\{\Sigma^{II'}_{illmn}(k, k_1, k_2, k_3) + \Sigma^{II'}_{illnm}(k, k_1, k_3, k_2) + + \Sigma^{II'}_{imln}(k, k_2, k_1, k_3) + \Sigma^{II'}_{imnl}(k, k_2, k_3, k_1) + \Sigma^{II'}_{inml}(k, k_3, k_2, k_1) + + \Sigma^{II'}_{inlm}(k, k_3, k_1, k_2)\}. \quad (2.22)$$

Collecting terms proportional to E^3 in the expression for the nonlinear current, we find that $\Sigma_{ilmn}(k, k_1, k_2, k_3)$ consists of the two terms

$$\Sigma_{ilmn}(k, k_1, k_2, k_3) = \Sigma^{I}_{illmn}(k, k_1, k_2, k_3) + \Sigma^{II}_{illmn}(k, k_1, k_3, k_2). \quad (2.23)$$

Further, collecting (2.22), (2.21), (2.16), (2.17), and (2.18) we obtain a specific expression for the nonlinear conductivity $\Sigma(k, k_1, k_2 - k_3)$. Carrying the expansion in kv/ω_0 up to and including the fourth power in the resulting formula and substituting the result into (2.8), we obtain the unknown probability $w^{II}_{ll}(k_1, k_2 | k_3, k)$ from comparison with (2.7) after rather cumbersome calculations:

$$w^{II}_{ll}(k_1, k_2 | k_3, k) = \frac{(2\pi)^9 e^4}{2m_e^2 v_e^4 (4\pi)^3} \delta(k_1 + k_2 - k_3 - k)\delta(\omega(k_1) + + \omega(k_2) - \omega(k_3) - \omega(k))(k^2 k_1^2 k_2^2 k_3^2)^{-1} \left\{ \frac{\varepsilon'_l(k_2 - k_3)}{\varepsilon^l(k_2 - k_3)} k k_1 k_2 k_3 + + \frac{\varepsilon'_l(k_1 - k_3)}{\varepsilon^l(k_1 - k_3)} k k_3 k_1 k_2 - \lambda_e^2 [k k_1 k_2 k_3 (k_3 - k_2)^2 + k_3 k_1 k k_2 (k_1 - k_3)^2] + \right. \quad /65$$

$$+ \lambda_e^2 \left[\frac{4}{3} \frac{k_1^2 k_2^2 - (k_1 k_2)^2}{k_+^2} (k_1 k_3 k_+^2 - k k_+ k_3 k_+) + k_+^2 (k_1 k_3) + k_2^2 k k_1 k_3 k_1 + \right.$$

$$+ k_1^2 k k_2 k_3 k_2 - k_1 k_2 (k_1^2 k_2 k_+ + k_2^2 k_1 k_+ + k_3 k_1 k k_1 + k_3 k_2 k k_2) +$$

$$\left. \left. + k k_1 k_3 k_2 \frac{(k - k_1)^2 + (k_2 - k_3)^2}{2} + k k_2 k_3 k_1 \frac{(k_1 - k_3)^2 + (k - k_2)^2}{2} \right] \right\}, \quad (2.24)$$

$$k_+ = k_1 + k_2$$

In accordance with the probability found above, and considering the probability of induced scattering on ions and electrons [1], we write the complete kinetic equation for Langmuir plasmons at $T_e \gtrsim T_i$, when the decay $l \to l' + s$ is forbidden:

$$\frac{\partial N(k)}{\partial t} = \int \frac{dk_1 dk_2 dk_3}{(2\pi)^9} \{N(k) N(k_1)(N(k_2) - N(k_3)) + N(k_2) N(k_3)(N(k) - N(k_1))\} w_{ll}^{ll}(k_1 k_2 | k_3, k) + N(k) \int w^{il}(p, k, k') h(k - k') \frac{\partial f^i}{\partial p} N(k') \frac{dp dk'}{(2\pi)^4} + N(k) \int w^{el}(p, k, k') h(k - k') \frac{\partial f^e}{\partial p} N(k') \frac{dp dk'}{(2\pi)^4}, \quad (2.25)$$

where

$$w^{(e)} = \frac{4(2\pi)^3 e^4 (kk')^2 \delta(\omega_k - \omega_{k'} - (k - k') v)}{m^2 \omega_k^4 k^2 k'^2 \frac{\partial \varepsilon^l}{\partial \omega}\Big|_{\omega=\omega_k} \frac{\partial \varepsilon^l}{\partial \omega}\Big|_{\omega=\omega_{k'}}} \left| \frac{2vk'}{\omega_{k'}} + \frac{\varepsilon_i^l(\omega_k - \omega_{k'}, k - k')}{\varepsilon^l(\omega_k - \omega_{k'}, k - k')} \right|^2 \quad (2.26)$$

and where

$$w^{(i)} = \frac{4(2\pi)^3 e^4 (kk')^2 \delta(\omega_k - \omega_{k'} - (k - k') v)}{m^2 \omega_k^4 \frac{\partial \varepsilon^l}{\partial \omega}\Big|_{\omega=\omega_k} \frac{\partial \varepsilon^l}{\partial \omega}\Big|_{\omega=\omega_{k'}} k^2 k'^2} \left| \frac{\varepsilon_e^l(\omega_k - \omega_{k'}, k - k') - 1}{\varepsilon^l(\omega_k - \omega_{k'}, k - k')} \right|^2. \quad (2.27)$$

Different terms dominate on different intervals of $k\lambda_e$ in the expressions for the probability w_{ll}^{ll}, $w^{(e)}$, $w^{(i)}$. The equation of the nonlinear interaction must therefore be analyzed separately on the various intervals of $k\lambda_e$.

3. Let us consider the case of isotropic turbulence on the interval $k\lambda_e > v_i/3v_e$. The nomenclature

$$N(k) = N(k) = W^l(k)(2\pi)^3/4\pi k^2 \omega_{0e} h, \qquad \int W^l(k)\, dk = W_0^l,$$

where W_0^l is the total energy of the Langmuir turbulence per unit volume, is convenient for the isotropic case.

For a sufficiently smooth spectrum, the four-plasmon interaction (2.2) can be described for $k\lambda_e > v/3v_e$ (but $k\lambda_e < (m_e/3m_i)^{1/4}$) by a formula corresponding to a "relay" multiple-decay process with small absolute changes in k:

$$\frac{\partial N(k)}{\partial t} = -\int \frac{dk_1 dk_2 dk_3}{(2\pi)^9} w_{ll}^{ll}(k_1, k_2 | k_3, k) \{N(k) N(k_1) N(k_3) + N(k) N(k_2) N(k_3) - N(k) N(k_1) N(k_2) - N(k_1) N(k_2) N(k_3)\} = D \int \left\{ F_1(k_1, k_2) (N^2(k) \frac{\partial N(k_2)}{\partial (k_2^2)} - N^2(k_2) \frac{\partial N(k)}{\partial (k^2)} + F_2(k, k_2)(N(k) - N(k_2)) \frac{\partial N(k)}{\partial (k^2)} \frac{\partial N(k_2)}{\partial (k_2^2)} \right\} dk_2^2, \quad (3.1)$$

where

$$D = \frac{\pi\omega_0^5}{3v_e^3(4\pi)^5(m_e n_i v_e^2)^2}\left\{\frac{4}{3\lambda_e}\sqrt{\frac{m_e}{m_i}}\right\}^3\int_0^\infty y^2 f^2(y)\,dy\Big\} \qquad (3.2)$$

(consult, for example, [18] for an expression for $J_+(y)$) and

$$F_1 \simeq k \text{ for } k_2 \simeq k,\ F_2 \simeq k^3 \text{ for } k_2 \sim k. \qquad (3.3)$$ /66

Detailed expressions for F_1 and F_2 and a more detailed conversion to (3.1) are given in [11].

When $k\lambda_e > (m_e/9m_i)^{1/4}$ (but $k\lambda_e \ll 1$), the terms without (e_i^l/e^l) become more important in the expression for the probability $w_{ll}^{ll}(k_1, k_2|k_3, k)$ i.e., the "nonrelay" process predominates.

Suppose, for example, $N(k) = N(k \neq 0)$ in a spherical layer of k-space with radius k_0 and thickness $\Delta k \lesssim k_0$; then

$$N(k) = W^l(2\pi)^3/4\pi k_0^2 \Delta k\,\omega_{0e}.$$

Formulas (3.1), (3.2), and (3.3) can be used to obtain estimates of the four-plasmon scattering increment in the range

$$v_i/3v_e \ll k\lambda_e < (m_e/9m_i)^{1/4},$$
$$\gamma_{\text{relay}}^{(4)} \simeq \omega_{0e}U^2\left(\frac{m_e}{m_i}\right)^{1/2}\left(\frac{k}{\Delta k}\right)^3\frac{1}{4}(3k\lambda_e)^{-8}, \qquad (3.4)$$
$$U = \frac{W^l}{nT_e}.$$

On the other hand, the term corresponding to "relay" induced scattering on ions can also be reduced to differential form when $v_i/3v_e \ll k\lambda_e \ll 1$ [10-13]:

$$\frac{\partial W(k)}{\partial t} = W(k)\frac{\partial W(k)}{\partial k}\frac{\pi\omega_{0e}^3}{4\cdot 27 m_i n_0 v_e^4(1+T_e/T_i)^3}. \qquad (3.5)$$

The increment of the process is easily obtained from (3.5) (for an isothermal plasma $v_i/v_e = \sqrt{m_e/m_i}$)

$$\gamma_{\text{ind. relay}}^{(4)} \approx \frac{\omega_{0e}}{4}U\left(\frac{k}{\Delta k}\right)^3\left(\frac{\sqrt{m_e/9m_i}}{k\lambda_e}\right)^3, \qquad (3.6)$$

where Δk is the "width" of the spectrum in k-space.

The condition for dominance of induced scattering on ions over four-plasmon processes takes the form

$$U < (k\lambda_e)^3 \left(\frac{m_i}{m_e}\right)^{1/6} 36\pi \frac{\Delta k}{k}. \qquad (3.7)$$

This condition is almost always satisfied for weak turbulence ($U \ll 1$ always) owing to the large coefficient in the right-hand side of (3.7). Hence the term corresponding to four-plasmon processes in the complete kinetic equation should be taken into account only as a correcting term when the energy transfer due to scattering on ions vanishes (for example, if $\frac{d(k^2 N(k))}{dk} \to 0$).

On comparison of (3.6) with the increment for nonlinear scattering on electrons [8, 9] ($0 < k\lambda_e \ll 1$)

$$\gamma^e_{\text{ind. scat}} \approx \omega_{0e} U (k\lambda_e)^2 \qquad (3.8)$$

it will be seen that this last process is always immaterial on the interval $k\lambda_e < (m_e/9m_i)^{1/4}$ under consideration.

In the range of $k\lambda_e > (m_e/9m_i)^{1/4}$, the main process is nonlinear scattering on electrons (3.8), which proceeds with an increment $\gamma^e_{\text{ind.scat.}}$ More precisely, we find from the condition $\gamma^e_{\text{ind.scat}} > \gamma^i_{\text{relay}}$ ($\Delta k \sim k$) that the criterion for predominance is $k\lambda_e > (m_e/9m_i)^{1/4}$ ($k\lambda_e > 1/6$ for hydrogen). /67

A determination of the Langmuir-wave spectrum in the quasi-stationary case with consideration only of scattering on electrons in the range $k\lambda_e > (m_e/9m_i)^{1/4}$ was made in [10] (for hydrogen $k\lambda_e > 1/11$). However, the range in which induced scattering on electrons predominates is very narrow for light plasmas, since Landau damping is very strong when $k\lambda_e > 0.3$.

Four-plasmon scattering with $k\lambda_e > (m_e/9m_i)^{1/4}$ takes place for the most part on large $\Delta k \sim k$ (with an absolute change in k on the order of k_0). This is the "nonrelay" process. For this case, the four-plasmon interaction increment can be obtained from (2.2) and (2.24):

$$\gamma^{(4)} \approx \frac{1}{16} \omega_{0e} U^2 \frac{k}{\Delta k} (k\lambda_e)^2. \qquad (3.9)$$

For sufficiently large U, four-plasmon scattering may sometimes be of the same order as nonlinear scattering on electrons

(3.8) on this interval of $k\lambda_e$.

4. A study of the competing processes of four-plasmon interaction and induced scattering on ions was made in [5-7] in the range of $k\lambda_e \ll r_i 3r_e$ for the isotropic case. The four-plasmon scattering increment with broadening of the spectrum by Δk is expressed by the formula

$$\gamma_1^{(4)} \approx \frac{1}{16}\omega_{0e}U^2\left(\frac{T_e}{T_e + T_i}\right)^2 \frac{k}{\Delta k}\frac{1}{(k\lambda_e)^2}. \qquad (4.1)$$

The competing process, nonlinear scattering on ions, has the increment

$$\gamma^{(i)} \approx \omega_0 \frac{(T_e/T_i)^{3/2}}{(1+T_e/T_i)}(k\lambda_e)\left(\frac{m_i}{m_e}\right)^{1/2} U\frac{\Delta k}{k}. \qquad (4.2)$$

The dominance condition $j^{(4)} > j^{(i)}$ gives

$$U > 16\left(\frac{T_i}{T_e}\right)^{1/2}(k\lambda_e)^3\left(\frac{m_i}{m_e}\right)^{1/2}\left(\frac{\Delta k}{k}\right)^2 = U_1. \qquad (4.3)$$

On the other hand, it will be recalled that the random-phase approximation is valid for $\gamma^{(4)} \ll \Delta\omega = 3\lambda_e k a\,\omega_0$, i.e.,

$$U \ll \frac{\sqrt{3}}{2}\frac{\Delta k}{k}(k\lambda_e)^2\frac{T_e + T_i}{2T_e}. \qquad (4.4)$$

For the existence of a range of U that satisfies (4.3) and (4.4) simultaneously, it is necessary that

$$\Delta k\lambda_e \ll \frac{\sqrt{3}}{32}\frac{T_e + T_i}{2T_e}\left(\frac{T_e}{T_i}\right)^{1/2}\left(\frac{m_e}{m_i}\right)^{1/2}, \qquad (4.5)$$

which is obviously usually the case because $\Delta k\lambda_e \leqslant k\lambda_e \leqslant {}^1/_3 v_i/v_e$.

To illustrate this analysis of the importance of the various nonlinear processes on various intervals of k, we present diagrams showing the variation of the corresponding increments $\gamma(k)$ for a particular case. Figure 1 shows the nonlinear interaction increments in the isotropic case as function of $k\lambda_e$. Figure 2 shows the region I in which four-plasmon processes predominate, region II, in which the determining processes are those of nonlinear scattering on ions, and region III, where nonlinear scattering on plasma electrons predominates.

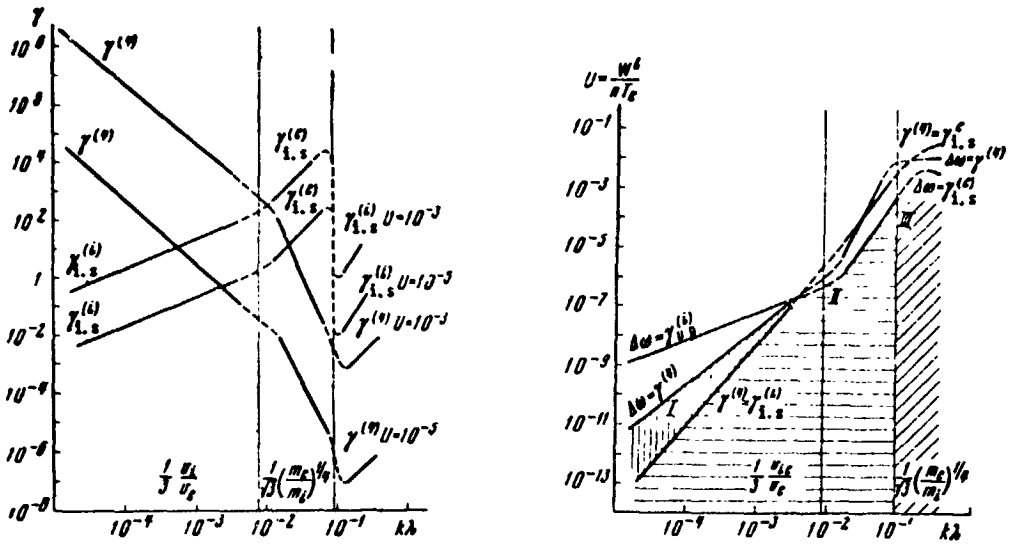

Figure 1. Increments of Nonlinear Processes of Four-Plasmon Scattering, $\gamma^{(4)}(k)$, and Scattering on Plasma Ions $[\gamma^{(i)}_{i.s}(k)]$ and Electrons $[\gamma^{(e)}_{i.s}(k)]$ Leading to Spectral Evolution of Isotropic Langmuir-Wave Spectra for the Particular Case $\Delta k/k \sim 1$, $T_e = 4 \cdot 10^{-13}$ erg, $h = 3 \cdot 10^{12}$ cm^{-3}, $T_e \sim T_i$, $\omega_{0e} = 10^6$ sec^{-1}.

Figure 2. Dominance Regions of Four-Plasmon Scattering (I) and Nonlinear Scattering on Plasma Particles (II) in Spectral Evolution of Isotropic Langmuir-Wave Spectra in the Particular Case $h = 3 \cdot 10^2$ cm^{-3}, $T_e \sim T_i$, $\omega_{0e} = 10^6$ sec^{-1}, $\Delta k \sim k$, $T_e = 4 \cdot 10^{-13}$ erg.

A quasistationary Langmuir-wave spectrum was found on the basis of the investigations made to ascertain the parts played by the various nonlinear processes [7, 10, 14]. It was established as a result that the fluctuations usually excited at large k are transformed into the range of small k until the transformation rate, which decreases with decreasing k, becomes equal to the dissipation rate in the neighborhood of the main turbulence scale k_0. /68

There are three possible fluctuation energy dissipation mechanisms in a plasma: paired collisions, radiation of fast particles (subcosmic and cosmic rays), and, in an inhomogeneous plasma, radiation of electromagnetic waves. The dissipation due to radiation is significant only in an inhomogeneous plasma. Radiation at high frequencies by accelerated particles occurs in such a way that the radiant energy is taken for the most part from fast particles [6, 7], and the resulting turbulence-energy dissipation is found to be small compared to the dissipation due to paired collsions. Dissipation in cosmic and subcosmic rays is found to be substantial

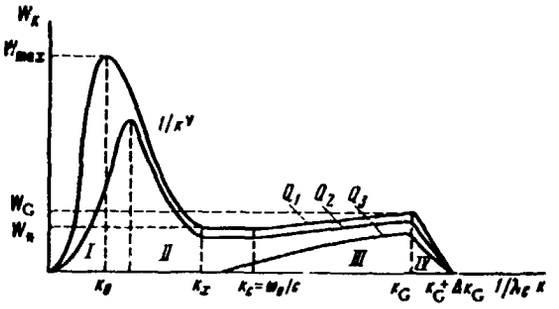

Figure 3. Turbulence Spectra of "Hot" Plasma $k_c > k_x$ for Source Powers $Q_1 > Q_2 > Q_3$.
$k_0 = 2\pi/L$;
$k_x = (1/3\lambda_{Oe})\ (v_i/v_e)$;
$k_c = \omega_0/c$.

only for a fluctuation with $v_\Phi = \omega_0/k < c$. Allowance for the dissipation due to paired collisions in finding the quasistationary Langmuir-wave spectrum made it possible to find the basic turbulence scale k_0 at which the turbulent-energy spectral density has its maximum. Here it was assumed in accordance with data available on the cosmic plasma [13] that the appearance of stationary turbulence in the plasma requires the existence of a region in which oscillations are generated at large $k\lambda_e >> 1/3v_i/v_e$, a region of spectral turbulent-energy transfer in the direction of small $k\lambda$, and a region of absorption around k_0.

A typical spectrum appears in Fig. 3, where I is the generation region, II is the region of spectral transfer with induced scattering on ions, III is the transfer region with four-plasmon processes, and IV is the absorption region. The main turbulence scale k_0 depends on the turbulent-energy generating power Q as /69

$$k_0 = \text{const}\ Q^{-\frac{1}{2(\nu-1)}}. \qquad (4.6)$$

where ν is the exponent in the turbulence spectrum for $k_0 \ll k \ll k_m$, which, depending on Q and the presence of fast particles (subcosmic rays), may assume values from $\nu = 2.84$ to $\nu = 4$ [7]. The established spectrum makes it possible to explain the shape of the subcosmic-ray spectrum in a broad range of cosmic-plasma parameters. For example, with a sufficiently high turbulence level, the fast-particle spectrum should have the form $f(\varepsilon) \sim \sqrt{\varepsilon}$.

In turn, the presence of fast particles strongly influences the shape of the Langmuir-wave spectrum, lowering the height of the maximum of the spectral-energy density W_k at k_0 and then causing it to vanish when there are sufficient numbers of subcosmic rays and the generating power is small (curve c in Fig. 3).

5. In the context of the problem of finding quasistationary Langmuir-turbulence spectra, let us discuss the problem of the transition to the isotropic quasistationary turbulent state

described under the preceding heading [11]. In the cosmic plasma, it appears that the basic sources of strong plasma turbulence are regions behind the fronts of shock waves. Obviously, the turbulence is anisotropic and nonstationary in these regions immediately after passage of the shock wave. There is then a rapid transition to the quasistationary isotropic states. The evolution of "pencils" of Langmuir waves that are defined at an initial point in time is a kind of simple "element" of this complex process. By "pencil," we mean here a distribution of plasmons in k-space such that all plasmons have wave vectors near k_0 in the neighborhood of dimension a, where $a \ll k_0$. We shall first examine the interval $^1/_3 r_i/r_e \ll k\lambda_e \ll 1$. It is this interval that is of particular importance to us, since wave generation is most probable at wave phase velocities on the order of a few times v_e.

On the interval in question, the basic nonlinear process in evolution of the pencil is induced scattering on ions.

It follows from analysis of the equation for scattering on ions, which is obtained from (2.25)-(2.27) for a Maxwellian distribution function,

$$\frac{\partial N(k)}{\partial t} = N(k)\frac{3}{8}\frac{\omega_0 (T_e/T_i)}{n_e h_0 r_i}\int \frac{hN(k')\,dk'}{(2\pi)^3}\frac{(kk')}{k^2 k'^2}\frac{k'^2-k^2}{|k'-k|}\exp\left\{-\frac{\omega_-^2}{2k_-^2 r_i^2}\right\},$$
$$\omega_- = {}^3/_2\, v_e^2(k'^2-k^2)/\omega_{0e}, \qquad k_- = k-k', \qquad v_i = \sqrt{T_i/m_i} \tag{5.1}$$

that scattering is maximal at $|\omega_-| \lesssim k_- v_i$, which we can rewrite in the form /70

$$|k'-k| \lesssim \frac{2}{\lambda_e}\frac{r_i}{3v_e}\frac{|k'-k|}{(k'+k)} \tag{5.2}$$

[(5.2) is a necessary condition for the maximum increment].

It must be stressed that the evolution of the Langmuir-wave pencil in k-space depends on "seeding" in the k-space, i.e., for induced scattering to begin in an element dk of k-space around k, it is necessary that a "seeding" plasmon level exist there.

Under real conditions, it is obvious that the seeding numerical plasmon density exists in all directions of k. With this in mind, we may conclude from (5.2) that, since $\frac{|k'-k|}{k'+k} \sim 1$,

$$|k'-k_0| \lesssim \frac{v_i}{3v_e}\frac{2}{\lambda_e} \equiv \Delta k_{\max} \ll k_0 \tag{5.3}$$

is always valid.

Thus we find that a pencil of Langmuir waves defined at time zero will quickly be scattered (isotropized) more or less uniformly in all directions.

If the initial spectrum has a small enough radial dimension $a < \Delta k_{max}$, energy will be transferred to our point k with maximum increment from the entire region of k-space occupied by the initial spectrum, since any point k' of the initial spectrum will satisfy the condition $|k - k'| \lesssim \Delta k_{max}$. In this case, the process increment is easily obtained from (5.1):

$$\gamma^{I}_{ind.\ scat} \approx \omega_{0e} U. \tag{5.4}$$

Spectral transfer toward smaller k is much slower than isotropization, as can be seen on comparing (5.4) with (3.6).

If the initial spectrum has a radial dimension $a > \Delta k_{max}$, the increment is smaller than (5.4):

$$\gamma^{II}_{ind.\ scat} \approx U\omega_{0e}\frac{\Delta k_{max}}{a}. \tag{5.5}$$

The increment (5.5) differs from (5.4) by a factor $\Delta k_{max}/a = 2v_i/3v_e\lambda_e a$, since not all of the spectrum N(k') participates in energy transfer to the given point k, but only the part of it corresponding to a spherical layer of thickness Δk_{max}. Compared to (5.5), induced scattering on electrons is always of little importance.

For decays leading to isotropization, when the wave-vector modulus of each plasmon in the process changes insignificantly, the four-plasmon decay increment on the same interval $k\lambda_e >> v_i/3v_e$ is estimated as

$$\gamma_0^{(4)} \approx \frac{\pi}{128}\left(\frac{k}{a}\right)^3 U^2 \frac{1}{(k\lambda_e)^2}\omega_{0e}. \tag{5.6}$$

The spreading of the spectrum over the moduli is much slower. The condition for dominance of four-plasmon processes over induced scattering on electrons, $\gamma_0^{(4)} >> \gamma^{l}_{i.s}$, yields

$$U \gg \frac{128}{\pi} a\lambda_e \frac{v_i}{3v_e}. \tag{5.7}$$

As the spectrum broadens, a/k increases. Thus, the four-plasmon processes predominate only for rather narrow pencils and large energies U. In view of the condition for applicability of the /71

random-phase approximation, $\gamma^{(4)} \ll \Delta\omega = 3\lambda_e^2 ak\omega_{0e}$, we obtain a limitation on U:

$$U \ll 4(k\lambda_e)^2\left(\frac{2a}{k}\right)^{4/3}. \qquad (5.8)$$

We see from (5.7) and (5.8) that the existence of a region in wh[illegible] four-plasmon processes predominate for waves with random phase [illegible]quires that $a\lambda_e \gg v_i/v_e$, which is a rather stringent condition, so that nonlinear scattering on ions is the basic process for all practical purposes.

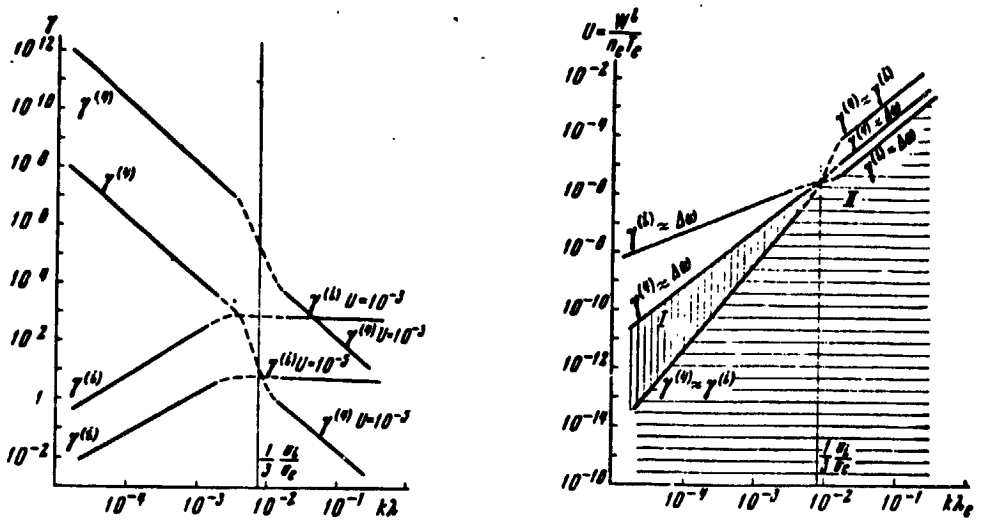

Figure 4. Increments of Nonlinear Processes of Four-Plasmon Scattering $\gamma^{(4)}(k)$ and Scattering on Plasma Ions $[\gamma^{(i)}_{i.s}(k)]$ and Electrons $[\gamma^{(e)}_{i.s}(k)]$ Leading to Spectral Evolution of Langmuir-Wave Pencils for the Particular Case $T_e = 4 \cdot 10^{-13}$ erg, $h = 3 \cdot 10^2$ cm^{-3}, $T_e/T_i = 10$, $\Delta k/k = 0.1$, $\omega_{0e} = 10^6$ sec^{-1}.

Figure 5. Dominance Regions of Four-Plasmon Scattering (I) and Nonlinear Scattering on Plasma Electrons and Ions (II) in Spectral Evolution of Langmuir-Wave Pencils in the Particular Case $h_e \approx 3 \cdot 10^2$ cm^{-3}, $\omega_{0e} = 10^6$ sec^{-1}, $T_e/T_i \sim 1$, $\Delta k/k \sim 10^{-1}$.

In the range of small $k\lambda_e \ll v_i/3v_e$, the maximum increment $\gamma^{(4)}$ of four-plasmon scattering for broadening of the spectrum in k-space by an amount on the order of its initial width is determined by the expression

$$\gamma^{(4)} \approx \frac{\pi}{8}\left(\frac{T_e}{T_e+T_i}\right)^2 \frac{k^2}{4a^2} U^2 \frac{1}{(k\lambda_e)^2}\omega_0. \qquad (5.9)$$

It was recognized here in evaluation of the increment that when $k\lambda_e < 1/3v_i/v_e$, the ratio that appears in the probability expression

$$\varepsilon_i'(k_-)/\varepsilon'(k_-) \approx T_e/(T_e+T_i),$$

and it was assumed that $N(k) = 6\pi^2 W^l/a^3\omega_0 \neq 0$ in a small spherical region of k-space with a radius of about k_0 ($k_0 \gg a$). The increment for scattering of Langmuir waves on ions for transfer in k-space by an amount on the order of the initial width of the spectrum will be given by

$$\gamma^{(1)}_{\text{ind. scat}} \approx \omega_0 \frac{2(T_e/T_i)^{3/2}}{(1+T_e/T_i)^2}(k\lambda_e)\left(\frac{m_i}{m_e}\right)^{1/2} U. \qquad (5.10)$$

The condition for dominance of four-plasmon scattering, $\gamma^{(4)} >> >> \gamma^{(1)}_{i.s}$, becomes

$$U \gg U_1 = \left(\frac{2a}{k}\right)^2 \frac{16}{\pi}\left(\frac{T_i}{T_e}\right)^{1/2}\left(\frac{m_i}{m_e}\right)^{1/2}(k\lambda_e)^2. \qquad (5.11)$$

Let us now take account of the condition for applicability of the random-phase approximation, $\gamma^{(4)} \ll \Delta\omega = 3\lambda_e^2 \cdot 2ak\omega_0$, i.e.,

$$U \ll U_2 = \left(\frac{2a}{k}\right)^{1/2}\sqrt{\frac{96}{\pi}}(k\lambda_e)^2\frac{T_e+T_i}{2T_e}. \qquad (5.12)$$

The condition for insignificance of Coulomb collisions $\gamma^{(4)} \gg \gamma_{ei} = \omega_0/n\lambda_e^3$, i.e.,

$$U \gg U_3 = \sqrt{\frac{32}{\pi}}\frac{2a}{k}k\lambda_e \frac{1}{\sqrt{n\lambda_e^3}}\frac{T_e+T_i}{2T_e} \qquad (5.13)$$

is usually always satisfied. Conditions (5.11) and (5.12) define the region in which four-plasmon interactions of waves of random phase predominate over other processes when $U_1 < U < U_2$.

The range of values of U permitted by (5.11) and (5.12) exists for $(2a/k) \ll (m_e/m_i)(k\lambda_e)^{-2}(T_e+T_i)^2/4T_e^2$, i.e., practically always for $k\lambda_e \ll 1/3 v_i/v_e$ and $2a \lesssim k$. Let us take, for example, a hydrogen plasma with $T_e \approx T_i$, $2a = 0.1k_0$ and $k\lambda_e = 0.1(m_e/m_i)^{1/2}$. In this case, dominance of four-plasmon processes over nonlinear scattering on ions (and, at

the same time, applicability of the random-phase approximation) requires that the wave energy density U be in the range $2{,}5\cdot10^{-8} \ll U \ll 10^{-4}$. We note that, in virtue of (5.12) and $k\lambda_e \ll 1/3\, v_i/v_e$, the theory is applicable if the wave energy density has the upper bound $U \ll m_e/m_i$. If $U < U_1$, induced scattering on ions predominates. /72

We note that there is a qualitative difference in the spectral evolution of the Langmuir-wave pencil in k-space in the interval $1/3\, v_i/v_e \ll k\lambda_e \ll 1$ as compared to $k\lambda_e \ll 1/3\, v_i/v_e$. In the latter case, the initial spectrum corresponding to the pencil of Langmuir waves is shifted toward smaller k in k-space as a result of induced scattering on ions and becomes somewhat narrower in modulus simultaneously with isotropization (see [5]), which is not the dominant process in this case. To illustrate this section of the article, we present a plot of the nonlinear-interaction increments γ against $k\lambda_e$ for wave pencils defined at time zero and several values of U (Fig. 4; see also Fig. 5, which shows the dominance regions of the various processes that determine the evolution of anisotropic turbulence).

In concluding this paper, we stress that the investigation of quasistationary plasma turbulence with quasiparticles of one species must be regarded primarily as one of the first steps in study of the complex picture of plasma turbulence, in which turbulent fluctuations of various types are inseparably related.

REFERENCES

1. V.N. Tsytovich. Nelineynyye effekty v plazme (Nonlinear Effects in Plasmas), Moscow, "Nauka," 1967.
2. V.A. Liperovskiy and V.N. Tsytovich. Izv. Vuzov. Radiofizika, 1965, Vol. 9, 469.
3. V.Ye. Zakharov. Zh. Eksp. Teor. Fiz., 1966, Vol. 51, 689.
4. A.A. Vedenov, A.V. Gordeev, and L.I. Rudakov. Plasma Physics, 1967, Vol. 9, 719.
5. L.M. Kovrizhnykh. Zh. Eksp. Teor. Fiz., 1965, Vol. 49, 237; L.M. Kovrizhnykh, Zh. Eksp. Teor. Fiz., 1965, Vol. 49, 1376.
6. V.A. Liperovskiy and V.N. Tsytovich. Izv. Vuzov. Radiofizika, 1969, Vol. 12, 823.
7. S.B. Pikel'ner and V.N. Tsytovich. Zh. Eksp. Teor. Fiz., 1968, Vol. 55, 977.
8. L.M. Gorbunov and V.P. Silin. Zh. Eksp. Teor. Fiz., 1967, Vol. 47, 200. /73
9. A.K. Gaylitis and V.N. Tsytovich. Izv. Vuzov. Radiofizika, 1964, Vol. 7, 1190.
10. V.A. Liperovskiy and V.N. Tsytovich. Zh. Eksp. Teor. Fiz., 1969, Vol. 57, 1252.
11. V.A. Gudkova and V.A. Liperovskiy. Prikl. Mat. Tekh. Fiz., 1970, No. 3.
12. A.A. Galeyev, V.I. Karpman, and R.Z. Sagdeyev. Dokl. Akad. Nauk SSSR, 1964, Vol. 157, 108.

13. A.A. Galeyev, V.I. Karpman, and R.Z. Sagdeyev. Yadernyy sintez, 1965, Vol. 5, 20.
14. Ye.N. Zhiakov, V.A. Liperovskiy, V.G. Makhan'kov, S.B. Pikel'ner, Che-Zey-Khen, and V.N. Tsytovich. Spectra of Quasistationary Langmuir Plasma Turbulence. Paper at Ninth International Conference on Phenomena in Ionized Gases. Bucharest, 1969 (Contr. Papers Conf. Bucharest, 1969, p. 585).
15. S.B. Pikel'ner and V.N. Tsytovich. Astr. zh., 1969, No. 1.
16. V.N. Tsytovich. Usp. Fiz. Nauk, 1966, Vol. 89, 89.
17. V.A. Liperovskiy and V.N. Tsytovich. Prikl. Mat. Tekh. Fiz., 1965, No. 5, 15.
18. V.P. Silin and A.A. Rukhadze. Elektromagnitnyye svoystva plazmy i plazmopodobnykh sred (Electromagnetic Properties of Plasma and Plasma-Like Media), Moscow, Gosatomizdat, 1961.

N75 13714

STRUCTURAL FORMATIONS IN THE INTERPLANETARY MEDIUM

(Translation of "Strukturnyye obrazovaniya v mezhplanetnoy Srede.")

A. V. Bogdanov

ABSTRACT

The results of research on the fine structure of the interplanetary medium are reviewed. The characteristics of shock waves, filaments, and contact surfaces according to space-probe measurements are discussed. With 7 illustrations and 50 source citations.

STRUCTURAL FORMATIONS IN THE INTERPLANETARY MEDIUM /74

A.V. Bogdanov

During recent years, the use of greatly improved instruments, computer data-processing methods, and numerous space vehicles in the investigation of interplanetary space has made possible a considerable broadening of our conceptions as to the properties of the interplanetary medium.

Simultaneously with the accumulation of experimental data, theoretical reduction of the results obtained has improved. Theoretical methods that had been used previously in research on controlled thermonuclear fusion and in magnetohydrodynamics, stability analysis, the solution of problems in nonlinear plasma oscillations, the theory of collisionless shock waves and their dissipation, and turbulent plasma heating came into extensive use along with the generally accepted astrophysical methods of investigating outer space.

Theory and experiment are in rather good agreement, at least in the region between Venus and Mars, where direct measurements of the parameters of the interplanetary plasma have been made.

These studies nave shown that the interplanetary medium is not an isotropic and homogeneous formation having spherical symmetry, and that, further, its parameters may vary over rather broad ranges with variations in solar activity.

To explain the origin of geomagnetic storms, Chapman and Ferraro [1] suggested back in the 1930's that from time to time, the sun expels streams of plasma at high velocity, and that these streams, impinging upon the earth, disturb its magnetic field and thus cause magnetic storms. This hypothesis was subsequently widely developed [2, 4-6].

Bierman [3] published certain results of observations of type 1 cometary tails, indicating that: a) the pressure of the sunlight is clearly inadequate to explain the observed repulsion of the tails from the sun, and b) the observed degrees of ionization and excitation in cometary tails cannot be accounted for by the photoeffect alone.

It was concluded from this that a stream of particles with quite high energies, directed radially outward from the sun, exists at all times in interplanetary space. Parker explained the origin of this stream in his theory of the expanding solar corona and the large-scale structure of the interplanetary magnetic field. The basic results of Parker's theory are as follows:

1. A steady stream of fully ionized plasma (the solar wind) flows outward from the solar corona.

2. Under certain conditions in the corona, this stream is accelerated to a certain asymptotic velocity v_∞. The acceleration is purely gasdynamic in nature, like the outflow of gas into a vacuum through a Laval nozzle with a transition from subsonic to supersonic flow.

3. Since $\beta = P_{gas}/B^2_{8\pi} \simeq 1$ for the plasma in the corona, and the magnetic Reynolds number [7] is very large (10^{13}– 10^{15}), the magnetic field is also involved in the acceleration. As a result of freezing-in, it is pulled out of the corona by the solar wind and determines in many respects the processes that unfold in solar wind.

/75

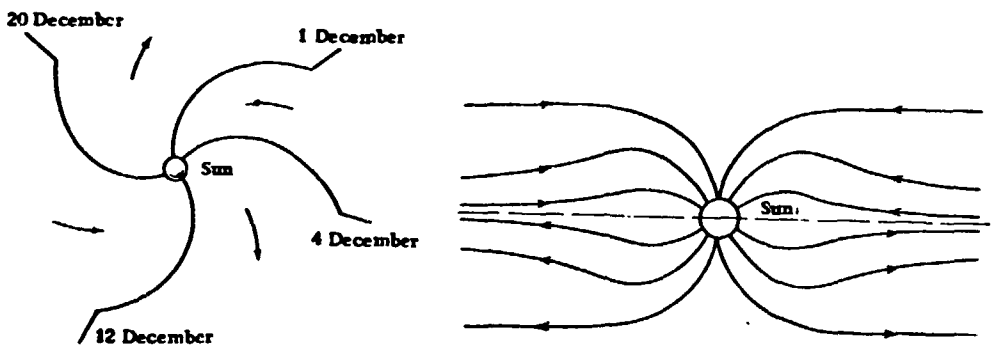

Figure 1. Sector Structure of Interplanetary Magnetic Field in the Plane of the Solar Equator.

Figure 2. Patterns of Magnetic-Field Lines of Force (Seen in Meridional Section).

4. Because of the rotation of the sun, the magnetic lines of force assume the form of Archimedean spirals (the so-called corotation effect).

5. Shock waves are generated during disturbances on the sun and propagated through the solar wind to cause geomagnetic storms. A stream of particles, which are called solar cosmic rays, is generated simultaneously with the shock wave and can be registered on the earth. The cosmic rays may be registered far in advance of the geomagnetic disturbances. Sometimes they appear immediately, only a few minutes after a registered chromospheric flare.

Let us now consider the corotation effect in greater detail. Since the magnetic Reynolds number $Re_m \gg 1$ on the scale of the

solar system R ∿ 10 a.u., the magnetic field is set in rotation by the sun with a period T = 27 days, and is simultaneously distended by the outflow of the solar wind. As a result of simultaneous involvement of the magnetic field in rotation with the sun and in motion in the radial direction with the solar wind, the lines of force assume the form of Archimedean spirals and lie preferentially in the plane of the solar equator (Figs. 1 and 2).

1. Macrostructure

The spherically symmetrical model of the solar corona is actually somewhat different from what is observed in experiments.

Thus, numerous individual filaments in which the particle temperatures and densities may differ substantially (by several times) have been detected in the corona. As a result, the true picture of the solar wind differs somewhat from that obtained according to the Parker model. The first experiment with direct observation of the solar-wind parameters over an extended period was carried out in 1962 during the flight of the Mariner 2 spaceprobe.

It was observed that four sectors in which the polarities of the magnetic field alternated existed throughout the duration of the flight [8, 9]. The angular dimensions of these sectors remained practically constant through several solar rotations. The velocity of the solar wind was lowest at the boundaries of the sectors and increased inside them. The thickness of the transitional layer between sectors varied over a considerable range, the average velocity gradient of the solar-wind flux was found to be 14 km/sec according to [10] and the maximum gradient 86 km/sec; the /76 Mariner 2 data were compared with ground cosmic-ray observations and the planetary geomagnetic activity index K_p. This comparison showed a correlation of the measured results with ∿27-day periodicity.

Regular solar-wind measurements were made subsequently with the high-orbit IMP and Vela earth satellites and interplanetary spaceprobes. These measurements have been made in different years with different levels of solar activity.

In general, 1963-1964 observations of the interplanetary medium with the IMP-1 satellite confirmed the picture observed on Mariner-2. A strictly ordered sector structure persisted throughout the entire period of the observations. There were two pairs of sectors with different magnetic-field polarities. Three of the sectors were of about the same duration, approximately twice as long as the fourth.

Ground observations of the K_p index during this period also correlated well with the observed sector structure of the plasma velocities. All of these results were obtained at a solar activity minimum.

As solar activity increases, the organization of the interplanetary field and its sector structure become sharper and more distinct, and the general pattern of the field less stationary. This conclusion was drawn from measurements of the magnetic field and plasma in 1964 and 1966 [11, 14, 19]. At these times, the variations of field direction were observed to be more frequent than those observed on Mariner 2. The velocity of the solar wind was also subject to equally frequent fluctuations.

Study of the solar cosmic rays, which consist basically of protons with energies from hundreds of kiloelectron volts to tens of megaelectron volts, is of special interest for understanding of the structure of the interplanetary medium.

The high-energy particles that compose the solar cosmic rays are generated as pulses during chromospheric flares of various intensities, and also at times at which no pronounced active processes are observed on the sun. In the latter case, high-energy-particle streams may persist for rather long times. Sometimes these streams can be traced through several rotations of the sun.

Solar cosmic rays propagate along lines of force, simultaneously executing Larmor rotation around the lines of force. The motion of charged particles in slowly varying magnetic fields was examined in detail in [12]. There it was shown that if the field varies slowly in time and space as compared with the Larmor rotation of the particle, the adiabatic invariant $\mu_\perp = mv_\perp^2/2B$ is preserved in a collisionless plasma, such as the solar wind out to 1 a.u.; in addition, the total energy of the particle

$$\varepsilon = \frac{mv_\perp^2}{2} + \frac{mv_\parallel^2}{2} \qquad (1)$$

should be conserved under these conditions.

The decrease in the magnetic field with increasing distance from the sun should result in the following. With decreasing magnetic field, $\varepsilon_\perp = mv_\perp^2/2$ will decrease, while $\varepsilon_\parallel = mv^2/2$ increases. In other words, this means that the particles will have a velocity directed preferentially along the magnetic field, i.e., the fast particle stream will be collimated in the direction of the magnetic-field vector with increasing distance from the sun. The registered fast-particle flux should be strongly anisotropic. The degree of the anisotropy may be lowered as a result of violation of adiabaticity conditions during rapid variations of the magnetic field in time and in space. Fast particles are scattered and isotropized on rapid variations or large gradients of the field. /77

Experiments conducted to observe solar cosmic rays have confirmed this theoretical picture. Substantial anisotropy in the angular distribution of cosmic rays from the sun has been detected [13, 20].

Solar cosmic rays may be formed in flares on any part of the solar disk, although the weaker fluxes in the region of the earth have a tendency to arise more frequently from flares on the western limb. These particles usually appear slightly in advance of a geomagnetic disturbance. Another group of fast particles is trapped by the shock wave and registered on the earth simultaneously with the geomagnetic disturbance. Observations of solar cosmic rays have made it possible to identify not only large-scale structures in the solar wind and the interplanteary field, but also smaller-scale formations [16] such as the sector boundaries. Thus, certain streams of solar cosmic rays have been identified with passage across a sector boundary. These cosmic rays had a 27-day periodicity and appear to have been emitted from a small active region on the sun.

Simultaneous measurements of the magnetic field from two and three vehicles have produced an important confirmation of the rotation of the sector structure of the magnetic field as a whole. Such measurements were made on IMP-3 and Pioneer 6 [17] and on Mariner 4 and OGO-1 [18, 47].

The recurrence of stationary solar cosmic ray fluxes confirms the rotation of the magnetic structure as a whole together with the sun. Streams of fast protons are drawn into synchronous rotation by the solar-wind magnetic field.

Let us now turn to the most important measured results for the interplanetary magnetic field, which were obtained by Ness and Burlaga with Pioneer 6 [15]. The magnetic field has a tendency to align itself in the plane of the ecliptic. Figures 1 and 2 show two projections of the heliosphere. The lines of force of the field resemble spirals. The field was observed to be directed toward the sun in 4% of cases and away from it in 41%. The directions did not coincide with spirals in the remaining 10% of cases.

An interesting phenomenon was detected in the Pioneer 6 measurements. Magnetic-field variations with a cycle of approximately 29 days were observed. Correction for the motion of the satellite made it possible to adjust this period with respect to the earth. It was found that it was slightly more than 28 days. This indicates that the field might have originated at high solar latitudes, which rotate somewhat more slowly than equatorial latitudes.

The measured magnetic-field gradient agreed with the theoretical calculation by the Parker model, and it was found that $B_\phi \sim 1/r$ and $B_r \sim 1/r^2$ for the azimuthal and radial fields, respectively, at distances of 0.8-0.98 a.u.

A shock wave should exist in the region in which the kinetic pressure of the solar wind is offset by the pressure of the interstellar gas, bounding the region within which a supersonic solar wind is observed (the heliosphere). In the region of the shock wave, the convective energy of the solar wind will be dissipated into thermal energy of individual particles.

The velocity distribution of the solar-wind particles beyond the shock-wave boundary should probably be nearly isotropic. This would mean that a layer of hot plasma should exist behind the shock wave and separate the solar-wind region from the undisturbed interstellar medium. There would be reciprocal diffusion of hot protons into the interstellar medium and cold neutral atoms into the layer of hot plasma. Charge exchange between fast protons /78
and cold neutral atoms would be possible, and would result in the formation of certain fractions of fast neutral atoms and cold protons. Fast neutral atoms from the boundary of the heliosphere could have velocities directed against the solar wind and could be registered at the earth's orbit. By measuring the energy spectrum of the neutral-atom flux from the boundary, if this flux exists, it would be possible to obtain data on the boundary without dispatching an instrument directly into the shock-wave region. Hundhausen [50] studied the possible concentration of charge-exchanging neutral atoms as a function of heliocentric distance. No direct measurements of the energy spectra of interplanetary neutral hydrogen have as yet been made. Tentative data on the neutral-hydrogen concentration have been obtained by spectroscopic methods from study of the skyglow [49]. According to this source, the heliosphere might have a boundary situated at a distance of >20 a.u.

2. Mesostructure and Contact Discontinuities in the Solar Wind

In Sec. 1, we examined the characteristics of the solar wind on the average over a long time interval. On the basis of these data, we formed a large-scale picture of the solar wind. We shall now consider smaller time scales — smaller than one hour — and discuss processes that take place at short range.

A detailed analysis of the rapidly varying properties of the solar-wind plasma has shown that a broad spectrum of disorganized oscillations of various scales exists in it [23]. Occasional orderly variations of field, velocity, density, etc. can be discerned against the background of these oscillations. Such variations usually occur over rather short time intervals. They can be identified with discontinuities [21]. This source also gave a classification of the discontinuities that may persist for extensive periods in a plasma with a frozen magnetic field.

These discontinuities may take the form of shock waves, contact discontinuities, and combinations of the two. Each of these discontinuity types has its distinctive features. In ordinary

gasdynamics, for example, the shock wave is a stable formation and the contact tangential discontinuity is unstable with respect to disturbances such as rippling of the contact surface. Such disturbances lead to turbulence and displacement and, eventually, to disintegration of the discontinuity. Quite long-lived discontinuities are possible in magnetohydrodynamics. Let us estimate the lifetime of a discontinuity in which the direction of the magnetic-field vector varies, while the remaining parameters remain constant during passage across the discontinuity.

In this case, a stepwise change in the magnetic field by an amount $|\Delta B| \simeq |B|$ is caused by currents flowing in a comparatively narrow layer. Experiments indicate that such current sheets have thicknesses of 10^2-10^3 km [25].

The currents flowing in current sheets can be estimated from the Maxwell equation

$$\mathrm{rot}\,\mathbf{B} = \frac{4\pi}{c}\mathbf{j}.$$

For order-of-magnitude estimates, we write the equation in the form

$$\frac{|\Delta B|}{l} \simeq \frac{4\pi}{c}|j|,$$

from which

/79

$$j \sim \frac{c}{4\pi}\frac{\Delta B}{l};$$

here l is the thickness of the current sheet and $|\Delta B|$ is the height of the step change in the magnetic field.

In the case of the interplanetary magnetic fields, where $l = 10^8$ m and $\Delta B \simeq 5 \cdot 10^{-5}$ G,

$$|j| \simeq 10^{-17}\ \mathrm{A/m^2}.$$

In order of magnitude, the energy stored on the discontinuity will be

$$\varepsilon_{magn} \simeq 10^{-11}\ \mathrm{J/m^3}.$$

The time for total dissipation of the discontinuity energy will be $\varepsilon_{magn}/(l^2/\sigma)$. Taking a conductivity $\sigma \approx 1$ for the

interplanetary plasma, we obtain $\tau \sim 10^{10}$ sec.

This result indicates that the lifeitme of such a discontinuity is much greater than its propagation time in the heliosphere, $\tau \approx (10^6-10^7)$ sec.

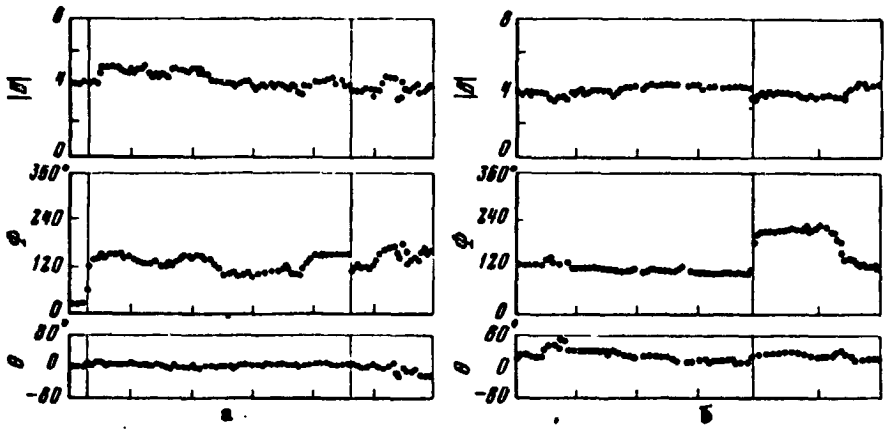

Figure 3. Experimental Data from Magnetic-Field Observations. The dots represent 30-second average values; note the quiet periods and (contact) discontinuities.

The present rough calculation indicates that the discontinuities of magnetic-field direction can be regarded as constant in time, and that all changes that take place in them are purely drift effects.

The existence of contact discontinuities has been detected experimentally in observed geomagnetic disturbances during a time in which there were no noteworthy flares on the sun. Contact discontinuities were observed directly in 1964 on Mariner 4 and in 1966 on Pioneer 6 [21-23]. Observations of magnetic-field variations represent a highly important method of identifying contact discontinuities. This method has an advantage over the plasma method in that it usually has higher time resolution, about an order higher than that of the plasma methods. About 1.0 second was required for transmission of a value of the total magnetic-field vector to the ground by telemetry, while the time to record the complete ion spectrum ranged up to a minute or more.

Two types of contact discontinuity can be distinguished on the basis of measured magnetic-field data. The first type is a discontinuity that accompanies a change in the magnitude of the magnetic field, and the second is a discontinuity accompanied only by a rotation of the field and no change in its value [26, 27].

During quiet periods, during which no noteworthy disturbances /80
were observed on the sun, the observed magnetic-field pattern was

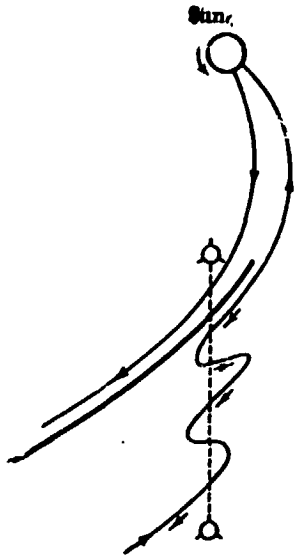

Figure 4. Possible Pattern of Magnetic Lines of Force Near a Sector Boundary.

usually as follows (Fig. 3). For about an hour, there were no changes in the field within the 10-15% limits of error. Sharp changes in the direction and magnitude of the field were sometimes observed against a relatively steady field background. The observed variations $|\Delta B| \simeq |B|$ during these abrupt changes. The thickness of the region in which the field change was observed was $\sim 10^5$ km. On certain occasions, several successive abrupt field changes were observed.

In [24, 28, 29], anisotropy of the solar cosmic-ray flux was observed simultaneously with a change in the field. The flux anisotropy amounted to 50%. The measurements indicated that the direction of anisotropy changed simultaneously with the change in field direction, and in such a way that the flux maximum was always directed along the line of force. There were times at which the field and flux-anisotropy directions were nearly reversed. In occasional cases, there were several synchronous changes of this kind (as many as three). These changes were explained as the result of bending of the force lines in a certain region (Fig. 4).

Another proof of the interrelation between the magnetic field and the plasma is found in the relationship between magnetic field and temperature anisotropy [37].

This temperature anisotropy may be caused by preservation of the adiabatic invariance of $\mu_\perp$ and ε_{tot} for the plasma particles and the cosmic rays. Let us again consider the motion of a single particle as it propagates away from the sun with the solar-wind flux. In this case, the relation between $\varepsilon_\perp$ and $\varepsilon_\parallel$ will change with the magnetic field:

$$\varepsilon_\perp = \mu_\perp B, \tag{2}$$

$$\varepsilon_\parallel = \varepsilon_{tot} - \mu_\perp B. \tag{3}$$

Let f(v) be the particle distribution function in the plasma. Let us now take the second moments of the distribution function. We shall assume that the distribution remains Maxwellian for the components along and across the field:

$$P_\parallel = \int m v_\parallel^2 f(\mathbf{v})\, d^3v, \tag{4}$$

$$P_{\perp} = \int \frac{mv_{\perp}^2}{2} f(v) d^3v. \quad (5)$$

The quantities $P_{\parallel}$ and $P_{\perp}$ might be called the longitudinal and parallel components of the pressure tensor P_{ij}:

$$P_{ij} = \int m v_i v_j f(v) d^3v, \quad (6)$$

and we might also introduce the temperature tensor, defined as

$$T_{ij} = P_{ij}/n.$$

We see from comparison of expressions (2)-(5) that $P_{\parallel}$ and $P_{\perp}$ and, accordingly, also $T_{\parallel}$ and $T_{\perp}$, will vary with variation of the magnetic field.

The possibility of thermal anisotropy was predicted theoretic- /81
ally by Parker on the basis of reasoning similar to that set forth above. An experimental confirmation of the existence of thermal anisotropy was found by Hundhausen [39] and Wolf [48]. The degree of the thermal anisotropy $K = T_{\parallel}/T_{\perp}$ was found to be 2-5.

Observations of the thermal anisotropy that were made simultaneously with magnetic-field observations indicated that a change in the direction of the anisotropy occurs simultaneously with the field change on passage across the discontinuity. The direction of the anisotropy correlates well with that of the field. The dynamics of the anisotropy change on passage across the discontinuity has not yet been established because such observations cannot be made at the time resolutions of available plasma detectors.

Combined measurements of the magnetic field, cosmic rays, and plasma have made it possible to form the following picture of the interplanetary plasma. The lines of force of the magnetic field are probably grouped into individual filaments that originate in the corona.

Solar cosmic rays propagate along the filaments, undergoing collimation along lines of force as they move. A single particle can emerge from a filament only after scattering on field inhomogeneities. This scattering produces the background solar cosmic rays. This background is also anisotropic, but this anisotropy does not depend on field direction and is rather weak (20-30%) (the so-called "equilibrium" anisotropy [29]). Cosmic-ray observations represent an important method for identification of single filaments, bends, and loops of the magnetic field.

Data on the thermal anisotropy, whose direction changes on passage from one filament to another, can be used for the same purpose. Individual filaments may be bent and kinked on discontinuities, but there is usually no mixing between individual filaments.

Stepwise changes in the direction or magnitude of the magnetic field, and sometimes in both simultaneously, occur at a contact discontinuity. Discontinuities with a change in the direction of the magnetic field are observed most frequently, in up to 79% of cases on the average.

In [15], a discontinuity was defined as a case in which the angle of rotation of the magnetic-field vector was at least 30° after 30 sec. This corresponded to $|\Delta B| = |B| 2$. The structures of individual discontinuities can sometimes be observed on these time scales; most discontinuities do not exhibit such structure. A current sheet is a region in which there flows a current that causes a field change at a discontinuity. The field variations and current sheets are interrelated, and we may therefore state that they determine the same structure. An analysis of current sheets [25] has shown that they behave like ordinary magnetohydrodynamic tangential discontinuities.

Let $P(\tau)$ be the probability that a current sheet begins and ends entirely within the interval τ, and let $F(\tau)$ be the probability that the current sheet has a total duration smaller than τ. $F(\tau)$ is nothing other than the integral duration distribution function of the current sheets. In this case, the relation between $P(\tau)$ and $F(\tau)$ is expressed by

$$P(\tau) = \lambda \int_0^\tau F(\tau - \zeta) d\zeta, \tag{7}$$

where λ is the reciprocal of the average duration of the discontinuities. Taking it equal to unity, we obtain

$$F(\tau) = dP/d\tau. \tag{8}$$

A second differentiation yields the differential duration distribution function of the discontinuities, $f(\tau)$: /82

$$f(\tau) = d^2P/d\tau^2. \tag{9}$$

This method was used in [25].

Another, more lucid method was used in Burlaga's previously cited paper [23]. In this paper, a discontinuity was defined by satisfaction of the condition $|\Delta B| \approx |B|/2$ or a time interval of 30 sec.

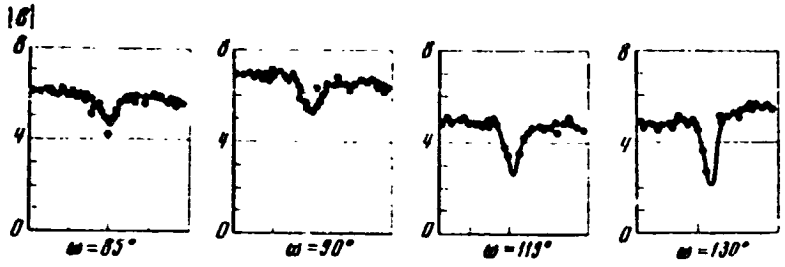

Figure 5. Examples of D Sheets.

The following types of discontinuities were detected:

1) single - a single field change during 30 sec;

2) double - the field rotates successively at two points;

3) triple and multiple - three or more successive rotations;

4) the field reverts to its original direction after a certain number of reading points.

Discontinuities of the first type are encountered in 70% of cases, those of the second type in 20%, and the other types still less often. Discontinuity regions were then examined in greater detail, with 1.5-second resolution. The results agreed with the discontinuity distribution obtained in [25], which was described above. Half of the discontinuities have durations shorter than 14 sec, and 10% are shorter than 2 sec. By the duration of a discontinuity, we mean the time for the magnetic field to rotate all the way from the old direction to the new one.

Analysis of the discontinuity distribution as a function of field rotation angle at the discontinuity yielded the empirical formula

$$f(\omega) = Ae^{-\left(\frac{\omega}{75^\circ}\right)^2}. \qquad (10)$$

Here ω is the rotation angle and A is a normalizing constant.

Another type of contact discontinuity is the so-called D sheet (see Fig. 5). In discontinuities of this type, we observe a decrease in the magnitude of the field within the discontinuity. The field remains unchanged on either side of the discontinuity. The field decrease in the discontinuity is probably to be explained by annihilation of oppositely directed field components at the discontinuity [15]. The theory indicates that the following condition must be satisfied in this case if the fields before and after the discontinuity are equal:

$$\frac{|B_{min}|}{|B|} \approx \cos\frac{\omega}{2}. \qquad (11)$$

Experiment confirms this relation. The thicknesses of the discontinuities are found to be about 10^3-10^4 km, which corresponds to a few seconds in the time scale.

It can be assumed on the basis of magnetic measurements that /83
the basic form of the magnetic fields in interplanetary space is that of individual filaments [51]. The magnitude and direction of the magnetic field vary little within each separate filament. The boundary of the particular filament is obviously situated where there is an abrupt change in the direction of the magnetic field. Basically, the cross sections of individual filaments may be elliptical or circular [25]. In regions where the field direction changes significantly, up to 90°, a decrease in the field is observed (sometimes almost to 0.5 γ). Heating of the plasma by currents that lower or totally annihilate the magnetic field might possibly occur in the same regions.

The propagation of cosmic rays and the direction of thermal anisotropy are related to individual filaments of magnetic lines of force. The filamentary structure of the magnetic field is easily explained by the theory of the continuously expanding solar corona and in terms of discrete magnetic-field sources.

Simultaneous measurements of the plasma and the magnetic field have made it possible to compare the magnetic-field and plasma-velocity discontinuities for coplanarity. The direction of the normal to the plane of the magnetic-field discontinuity was determined from the vector product of the fields on either side of the discontinuity. The directions of the normals to the plasma-velocity discontinuity planes were determined from the jumps in the radial and tangential field components. Comparison of these data indicate that the discontinuities are coplanar within the limits of experimental error. The existence of contact discontinuities is related to the frozen property of the magnetic field. Displacement of one filament or stream with respect to another gives rise to an electrodynamic-force reaction, leading to formation of current sheets and, in some cases, to annihilation of the magnetic field. Such displacement of individual filaments may result from an inhomogeneity in the solar-wind flux. Highly interesting data were given in [48].

The density, velocity, and temperature of the plasma were recorded simultaneously in order to distinguish shock waves from tangential discontinuities. Increases and decreases in each of these quantities were denoted by plus signs, minus signs, or zeros, respectively.

Thus, on a discontinuity denoted by (+, -, 0) there is an increase in density, a decrease in velocity, and no change in temperature. This is therefore a tangential discontinuity. In a

shock wave, there are usually simultaneous increases in all parameters, so that the notation is (+, +, +).

The percentage contents of doubly ionized helium in the solar wind were measured simultaneously. In quiet periods, $n_{He}^{++}/n_{H} \simeq 0.045$.

On the average, the percentage helium content increased during passage of shock waves, and substantial variations of this quantity were recorded simultaneously.

3. Shock Waves in the Solar Wind

The processes that occur in the solar wind cannot be investigated without study of the shock waves. They are important because they may make an additional contribution to the thermal budget of the solar wind, to turbulence, to the formation of the true structure of the interplanetary magnetic field, etc. Before the advent of direct measurements of the solar wind with spaceprobes, the existence of shock waves had been surmised indirectly from observations of geomagnetic disturbances associated with active processes on the sun [42].

Direct measurements of shock waves were first carried out in 1969 during the flight of Mariner 2 [22].

In later experiments, an increase in the total pressure $P_{gas} + B^2/8\pi$ behind the shock wave and increases in plasma temperature and velocity were detected by means of magnetic and plasma measurements. Simultaneous ground observations of the index K_p indicated a correlation with the Mariner 2 measurements [34, 35, 41]. /84

Let us briefly examine the theory of shock waves in which the shock front is at an angle to the velocity vector. To simplify the calculations, we shall assume that the magnetic pressure is small. We write the equations of conservation of the mass, momentum, and energy fluxes across the shock front:

$$\rho_1(\mu_1 n) = \rho_2(\mu_2 n_2), \tag{11'}$$

$$\rho_1(\mu_1 n)^2 + P_1 = \rho_2(\mu_2 n)^2 + P_2, \tag{12}$$

$$h_1 + \frac{\mu_1^2}{2} = h_2 + \frac{\mu_2^2}{2}. \tag{13}$$

In these equations, μ is the velocity of the gas at the given point in the flow, n is the normal to the shock-wave front, h is the enthalpy of the gas, P is its pressure, and ρ is its density.

If the waves propagate relative to a solar wind at rest, we obtain

$$T_2 = \frac{\rho_1}{\rho_2} T_1 + \frac{m}{2}\left[\frac{\rho_2}{\rho_1}(\mu_1 n)^2 - (\mu_2 n)^2\right], \quad (14)$$

$$T_2 = T_1 + \frac{\gamma - 1}{\gamma}\frac{m}{2}(\mu_1^2 - \mu_2^2). \quad (15)$$

In deriving these relations, we used

$$P\rho^{\gamma} = \text{const.}$$

Equations (14) and (15) are analogous to the conventional Hugoniot adiabat, which describes shock waves in an ideal gas [36]. The Hugoniot adiabat defines the relation between the values of the variables on either side of the shock wave. The characteristic distance on which these states are established can be obtained in ordinary gasdynamics by taking the viscosity and thermal conductivity of the gas into account. This characteristic distance (front thickness) is found to be approximately equal to the free path of an atom in the gas. In the case of a collisionless plasma, the free path is infinite, implying at first glance that shock waves cannot exist in such a plasma. In fact, experiment has shown that such waves do exist. They exhibit many properties of ordinary gasdynamic shock waves, although there are also many differences. Their chief distinctive property is a different set of dissipation mechanisms. In the ordinary shock wave, viscosity and thermal conductivity, which are determined basically by paired collisions, are these dissipative mechanisms. In collisionless shock waves, on the other hand, dissipation occurs as a result of collective effects that arise as a result of plasma instability. R.Z.Sagdeyev [37] was the first to draw attention to this. He showed that in the case of a rarefied plasma placed in a magnetic field, in which case the free path is much larger than the ion Larmor radius, the formal gasdynamic description (for motion across lines of force) also remains valid in the absence of collisions. For this it is only necessary that all parameters of the plasma change little on a distance on the order of the ion Larmor radius.

We shall examine as concisely as possible the mechanism of dissipation in collisionless shock waves, referring basically to [38, 39]. All processes will be treated rather qualitatively.

As we noted earlier, an anisotropy of temperatures parallel and perpendicular to the magnetic field, $T_{\parallel}/T_{\perp} = 3$, exists in the solar-wind plasma. The existence of this anisotropy may be the condition determining the dissipation mechanism. /85

In the case of a thermal anisotropy that satisfies the condition

$$n(T_{\parallel} - T_{\perp}) > B^2/8\pi$$

the plasma becomes unstable with respect to buildup of Alfven waves (the so-called firehose instability [30-33]. Alfven waves built up by firehose instability become damping waves in the range in which the wavelength comes to be of the order of the Larmor radius. Thus, the instability increment has a distinct maximum as a function of wavelength. The oscillations will build up most rapidly in the range of wavelengths around the increment maximum.

As the amplitude of the Alfven waves increases, the instability increment decreases, tending to zero at a certain limiting amplitude. This phenomenon is known as quasilinear stabilization of the instability [38, 44]. A stable wave spectrum is established in the plasma, together with a certain nonMaxwellian particle velocity distribution.

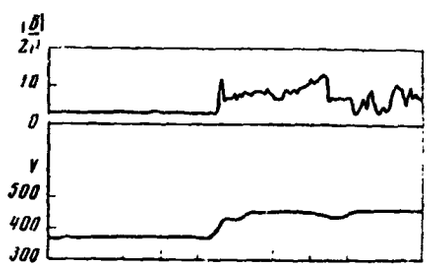

Figure 6. Variations of Magnetic Field and Plasma Velocity on Passage of Shock Wave.

As the equilibrium spectrum of the oscillations is established, the so-called decay processes begin to play a substantial role; these are processes in which one wave may decay into two and, conversely, a third wave may be formed from two waves. Conservation of wave total energy $\omega_3 = \omega_1 + \omega$ and total momentum $k_3 = k_1 + k_2$ is a condition for these processes. The latter may give rise to rapidly damping waves, e.g., ion-acoustic waves. In principle, the damping may result in dissipation of wave kinetic energy and heating of the plasma by collective processes, even in the absence of collisions. The possible dissipation mechanism presented here is not the only one possible.

A more detailed quantitative theory of collective dissipation was developed in [44, 40]. The front thickness determined in this way for the collisionless shock wave is $\sim R_+/M^2 - 1$, where R_+ is the Larmor radius of the ions and M is the Mach number. The heating of the plasma behind the shock wave is also described by the Hugoniot relations in this case.

Let us now consider experimental data on shock waves in the solar wind in greater detail. Several shock waves were detected during the flight of Mariner 2. Thus, one of them was the event of 7 October 1962, which is definitely identifiable with a shock wave (Fig. 6). Here an increase in the magnetic field was registered. A considerable increase in the amplitude of the magnetic-field variations was observed simultaneously, and a plasma probe registered increases in plasma velocity and in the density and temperature of the ions. The parameter variations before and after the discontinuity satisfied the Hugoniot relations. On this

basis, the observed jump was definitely identified as a shock wave. Later measurements made on the Vela 3 satellite with plasma detectors confirmed the correctness of the ordinary Hugoniot relations for the solar-wind parameters. The measured shock-wave velocities were described quite accurately by formulas (14) and (15), which were derived without consideration of the magnetic field. The observed shock waves had small Mach numbers and, accordingly, small discontinuities in all quantities. The thickness of the front could not be determined because of the poor time resolution of the instruments. As many as two minutes were required to record one spectrum, while the front thickness on the time scale should have been on the order of a few seconds. Magnetic measurements made to date have indicated the following properties for the shock /86
waves. At the time of passage across the shock-wave front, the magnetic field undergoes a step change simultaneously with all other plasma parameters. A broad spectrum of magnetic-field oscillations was observed in the transitional region behind the shock-wave front. These oscillations may confirm the firehose instability of Alfven waves. The characteristic times of these fluctuations range from a few seconds to a minute. Alfven turbulence is especially conspicuous in observations of the shock wave that arises in the flow around the earth's magnetosphere.

The energy distribution across the front of the shock wave is a highly interesting question. Study of geomagnetic disturbances resulting from flares at various points on the solar disk has shown that the strongest geomagnetic disturbances are observed when the flare occurs at the center. Flares arising at the limb of the solar disk generally produce considerably weaker geomagnetic disturbances. We may conclude from this that the largest portion of energy propagates in a comparatively narrow range of angles. A similar picture is also observed in the shock wave at the earth. The intensity is highest at the vertex of the shock wave and drops off quite rapidly with increasing distance from it.

Double shock waves are a highly interesting formation that has been observed in the solar wind. They have been investigated theoretically and experimentally [45, 46]. The double shock wave is composed of two successive shock waves separated by a contact discontinuity. The first wave is called the fast wave and the second the slow wave. The distance between them increases as /87
they propagate. In a system at rest relative to the solar wind, they may be traveling waves moving in opposite directions. In a reference frame bound to the observer, the two waves are carried away by the solar wind, which flows at supersonic velocity.

CONCLUSION

The structures discussed in this paper are closely related to one another. Thus, shock waves might, for example, strongly distort the large-scale interplanetary magnetic field with simultaneous heating of the solar-wind plasma. Contact discontinuities

sometimes separate two shock waves, etc. Nevertheless, it is highly convenient to classify all of the observed formations on four space-time scales (Fig. 7).

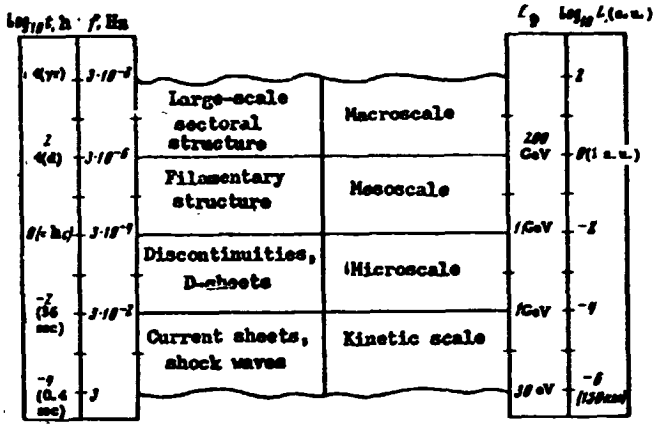

Figure 7. Four Structure Scales in the Interplanetary Plasma. The energy of a proton having a Larmor radius on the order of the length scale is used on the energy scale.

By the characteristic scale energy we mean the energy of a proton whose Larmor radius is of the order of the spatial scale. There is still some uncertainty in regard to the processes on various scales and in the structure of the interplanetary medium much above and below the plane of the ecliptic. Thus far, we have only indirect experimental data on these regions, data obtained from radio observations and observations of the tails of comets.

REFERENCES

1. S. Chapman and V.S.A. Ferraro. Terrest. Magnetism and Atmospheric Electr., 1931, Vol. 36, 77; 1932, Vol. 37, 147.
2. S. Chapman and H. Zizin. Smithsonian Contributions to Astrophysics, 1957, Vol. 2, 1, 1.
3. L.S. Bierman. Astrophys. J., 1951, Vol. 29, 274.
4. E.N. Parker. Astrophys. J., 1958,Vol. 128, 664.
5. E.N. Parker. Interplanetary Dynamic Processes. Russ. Ed., Moscow, "Mir," 1965.
6. E.N. Parker. In collection entitled: "Solnechno-zemnaya fizika"(Solar-Terrestrial Physics), Moscow, "Mir," 1968.
7. A. Alfven. Cosmical Electrodynamics. Clarendon, Oxford, 1950.
8. P.H. Coleman et al., J. Geophys., 1966, Vol. 71, 2831.
9. R. Lust. In collection entitled: "Solnechno-zemnaya fizika" (Solar-Terrestrial Physics), Moscow, "Mir," 1968.
10. P.J. Coleman, P.J. Davis, L.J. Smith and E.P. Sonnet. Science, 1962, Vol. 138, 1099.
11. N.F. Ness and J.M. Wilcox. Astrophys. J., 1964, Vol. 143, 23.
12. D.V. Sivukhin. In collection entitled: "Voprosy teorii plazmy" (Problems of Plasma Theory), No. 1, Moscow, Atomizdat, 1963.
13. K.G. McCracken and N.F. Ness. J. Geophys. Res., 1966, Vol. 71, 3315.
14. N.F. Ness. J. Geophys. Res., 1966, Vol. 71, 3309.
15. L.F. Burlaga and N.F. Ness. Preprint. NASA-G.S.F.C. NX-612-67-278, 1967.

16. K.G. McCracken. J. Geophys. Res., 1962, Vol. 67, 423.
17. E.J. Smith et al. Comparison of Simultaneous Measurements of Interplanetary Magnetic Field. Presented at Inter-Union Symposium on Solar-Terrestrial Physics, Belgrade, 1966.
18. J.J. O'Galenger and J.A. Simpson. Phys. Rev. Letters, 1966, Vol. 16, 1212.
19. N.F.Ness. In collection entitled: "Solnechnyy veter" (The Solar Wind), Moscow, "Mir," 1968.
20. H.R. Anderson. In collection entitled: "Solnechnyy veter" (The Solar Wind), Moscow, "Mir," 1968.
21. D.S. Colburn and C.P. Sonett. Space Sci. Rev., 1966, Vol. 5, 439.
22. C.P. Sonett, D.S. Colburn, L.J. Davis, E.J. Smith, and P.J. Coleman. Phys. Rev. Lett. 1964, Vol. 13, 153.
23. L.F. Burlaga. Preprint. G.SFCX-616-68-224, 1968.
24. W.C.R.P. Buhata et al. J. Geophys. Res., 1966, Vol. 71, 3297.
25. G.L. Siscoe et al. J. Geophys. Res., 1968, Vol. 73, 61.
26. L.D. Landau and Ye.M. Lifshits. Elektrodinamika sploshnykh sred (Electrodynamics of Continuous Media), Moscow, Gostekhizdat, 1957.
27. T. Cowling. Magnitnaya gidrodinamika (Magnetohydrodynamics), Russ. Ed., Moscow, IL, 1958.
28. C.Y. Fan, J.F. Lamport, J.A. Simpson, and O.R.J. Smith. J. Geophys. Res., 1966, Vol. 71, 3289.
29. K.G. McCracken. Preprint G.SFC X-612-67-584, 1967.
30. J.F.L. Scarf et al., J. Geophys. Res., 1967, Vol. 72, 993.
31. F. Hundhausen et al., J. Geophys. Res., 1967, Vol. 72, 81.
32. M.D. Montgomery, S.J. Bame, and A.J. Hundhausen. J. Geophys. Res., 1968, Vol. 73, 15.
33. J.H. Wolf et al. J. Geophys. Res., 1966, Vol. 71, 3329.
34. J.M. Wilcox. Irish Astron. Soc., 1965, Vol. 7, 82.
35. J.M. Wilcox and N.F. Ness. Solar Phys., 1967, Vol. 1, 437.
36. L.D. Landau and Ye.M. Lifshits. Mekhanika sploshnykh sred (Mechanics of Continuous Media), Moscow, Gostekhizdat, 1948. /88
37. R.Z. Sagdeyev. In collection entitled: "Voprosy teorii plazmy" (Problems of Plasma Theory), No. 4, Moscow, "Mir," 1964.
38. A.A. Vedenov. In collection entitled: "Voprosy teorii plasmy" (Problems of Plasma Theory), No. 3, Moscow, Atomizdat, 1963.
39. C.F. Cannel and R.Z. Sagdeev. J. Geophys., 1967, Vol. 72, 3303.
40. R.Z. Sagdeev and A.A. Caleev. Preprint Int. Center for Theoretical Phys., No. 66/64, 1966.
41. J.T. Gosling et al., J. Geophys. Res., 1967, Vol. 72, 3251.
42. Cold Gas Dynamics of Cosmic Cloud. North Holland Publ. Co., Amsterdam, 1955, p. 103.
43. J.T. Gosling et al. J. Geophys. Res., 1968, Vol. 73, 43.
44. A.A. Vedenov, Ye.P. Velikhov, and R.Z. Sagdeyev. In collection entitled: "Yadernyy sintez" (Nuclear Fusion), No. 4, 1962, 465-475.
45. R. Zelner et al. J. Geophys. Res., 1967, Vol. 72, 3374.
46. W.R. Cummings and W.G. Schubert. J. Geophys. Res., 1967, Vol. 72, 2275.

47. C.Y. Fan et al., J. Geophys. Res., 1966, Vol. 71, 1837.
48. K.W. Ogilvie, L.F. Burlaga, and T.D. Wilkerson. J. Geophys. Res., 1968, Vol. 73, 6809.
49. G.L. Siscoe, J.M. Turner and A.J. Lassarus. Solar Phys., 1969, Vol. 73, 6809.
50. A.T. Hundhausen. Planetary and Space Sci., 1968, Vol. 16, 783.

N75 13715

THE INTERNAL STRUCTURE OF THE CONVECTIVE ENVELOPE OF THE SUN

(Translation of "K voprosy o vnutrennem stroyenii konvektivnoy obolochki solntsa.")

I. M. Yavorskaya

ABSTRACT

An axisymmetric hydrodynamic model of the sun consisting of a core at radiant equilibrium and a convective envelope is studied with consideration of gravitational forces, rotation, turbulence effects, and electromagnetic forces. The dimensionless parameters that control the equations of plasma motion within the sun and the boundary conditions are investigated; estimates are given for these parameters on the basis of experimental data and the existing theoretical models. Stability conditions are derived for convective equilibrium, developed cellular convection, and developed turbulent convection with consideration of rotation and turbulent Reynolds stresses. These conditions characterize the possible physical state of the matter in the convective envelope. Using estimates of the dimensionless parameters and models of some of them, a method of successive approximations is proposed for solution of the problem as a whole. Differential equation systems with boundary conditions are obtained for the first 4 approximations. The results of certain preliminary calculations are presented. With 39 source citations.

THE INTERNAL STRUCTURE OF THE CONVECTIVE ENVELOPE OF THE SUN

/89

I.M. Yavorskaya

The theory of the internal structure of the stars and of the sun in particular has undergone particularly rapid development during the last decade as a result of removal of the basic theoretical difficulties associated with the opacity of the matter of the stars and with the question as to the stellar-energy sources. Many papers devoted to calculations of the internal structure of various stellar models have been published [1].

However, most of these studies have been concerned with hydrostatic spherically symmetrical models in which rotation, magnetic forces, and turbulent-viscosity forces are neglected. Hydrostatic models of the sun, while they give accurate determinations of the radial pressure, density, temperature, and radiant-flux distributions, are not suitable for study of more subtle phenomena, such as the meridional circulation, differential rotation, and the generation and maintenance of magnetic fields. In recent years, a number of authors have attempted to construct stellar models with consideration of rotation [2-5] and magnetic forces [6-8] and to compute models of stellar convective envelopes [9-12]. However, considerable mathematical difficulties arise in the construction of stellar models in which fine structure is taken into account.

In the present paper, an attempt is made to formulate the magnetohydrodynamic problem of internal stellar structure for the lower Main Sequence stars (chiefly the sun) on the assumption that the problem is axisymmetric. For this purpose, the magnetohydrodynamic equations are written with consideration of the physical conditions under which matter exists in the core and convective envelope; the general nature of gas turbulence in the envelope is studied in detail; possible mechanisms of the origin and mainteannce of magnetic fields by axisymmetric motions are examined. The boundary conditions of the problem are formulated at the center of the star, at the interface between the core and the envelope, and on the surface of the star. On the basis of observational data, physical hypotheses, and existing hydrostatic models, the operating forces in the core and convective zone are evaluated comparatively with a view to introducing a number of possible simplifications into the equation system in accordance with the values of determining dimensionless parameters. The estimates obtained make it possible to introduce simplified models and propose methods for their calculation.

1. Certain Observational Data

A brief remark is in order concerning observational data with a bearing on the phenomena that should, from our standpoint, be determined by the sun's hydrodynamic convective envelope. Observations of sunspots and other long-lived formations on the sun have yielded the following empirical formulas for its angular velocity of rotation:

$$\Omega = 14^\circ.38 - 2^\circ.77 \sin^2 \varphi$$

or

/90

$$\Omega = 14^\circ.42 - 1^\circ.40 \sin^2 \varphi - 1^\circ.33 \sin^4 \varphi,$$

where ϕ is the heliographic latitude, i.e., the sun does not rotate as a rigid body, and its equator has an angular velocity approximately 20% higher than that at the poles. Another no less interesting phenomenon is associated with the magnetic field of the sun and the succession of solar-activity cycles [13]. It is known that the solar cycle spans a period of about 11 years. At the beginning of a cycle, active regions appear at latitudes of approximately ±30°. Each active region may exist for up to a year, and various solar phenomena are concentrated in it: sunspots, faculae, flocculi, and prominences. However, the principal characteristic of an active region is its magnetic field. The active regions migrate toward the equator as their intensity rises. While the total magnetic field of the sun is very weak, on the order of 1 G, and is of approximately dipolar nature, the local fields of the active regions, and of the spots and bipolar regions in particular, may reach values in the hundreds and even thousands of gauss and come to be oriented approximately along parallels. During one cycle, all of the eastern parts of bipolar regions and spots in one hemisphere have one polarity, while the western parts have the other. The polarities are reversed in the other hemisphere. Every 11 years there is a reversal of active-region polarities. And there is yet another peculiarity: the weaker the local field of a bipolar region, the larger, on the average, are its dimensions,i.e., it appears that the regions have magnetic fluxes of approximately the same order. All of this provides some justification for concurring with a modified Bjerknes hypothesis of the formation of toroidal magnetic-field belts in the interior of the convective zone as a result of anisotropic turbulent convection and differential rotation. Here it appears that fragments of the field may be carried out to the surface of the sun owing to the development of kinetic instabilities of various types.

2. Fundamental Equations of Motion

Let us turn to mathematical formulation of the internal-structure problem, regarding the sun as a stationary axisymmetric gaseous configuration consisting of a core at radiant equilibrium

and a convective envelope. It is known from spectroscopic observations that the sun consists basically of hydrogen and helium. Taking account of available temperature estimates for the interior of the sun, we shall assume that our model consists of a fully ionized plasma with the equation of state

$$P = \frac{kpT}{\mu m_x}, \tag{2.1}$$

where P, ρ, and T are the plasma pressure, density, and temperature, m_x is the mass of the proton, μ is the average molecular weight expressed in units of the proton mass,

$$\frac{1}{\mu} = 2X + \frac{3}{4}Y + \frac{1}{2}Z.$$

X, Y, and Z characterize the chemical composition (i.e., the fractions of the mass accounted for by hydrogen, helium, and all other heavier elements, respectively). Thus, we have X ≈ 0.73, Y ≈ 0.25, and Z ≈ 0.02 for the surface layers of the sun. Equation (2.1) is quite legitimate under the conditions of total ionization and the high interior temperatures of the star [1] and is not satisfied only in the outermost layers. As was shown in [1], the radiation pressure can be neglected for the sun and most stars.

Within the axisymmetric configuration, the motion of the gas under the action of gravitational, Lorenz electromagnetic, and turbulent-viscosity forces will be described by the equation of motion /91

$$\frac{1}{2}\nabla V^2 - V \times \operatorname{rot} V + \frac{1}{\rho}\nabla P + \nabla\Phi - \frac{1}{\rho c} j \times H - \frac{1}{\rho}\nabla\tau = 0, \tag{2.2}$$

where V is the velocity of the gas, c is the velocity of light, H and j are the magnetic-field intensity and current density, Φ is the gravitational potential determined by the Poisson equation

$$\nabla^2\Phi = -4\pi\rho, \tag{2.3}$$

$(1/\rho c) j \times H$ is the Lorenz electromagnetic force, and $\tau = \{\tau_{ik}\}$ is the Reynolds turbulent stress tensor, which is nonvanishing only in the convective envelope and is written in the form of the continuity equation

$$\operatorname{div}(\rho V) = 0. \tag{2.4}$$

To determine the field intensity H and the current density j, it is necessary to attach Maxwell's equations

$$j=\frac{c}{4\pi}\operatorname{rot} H; \qquad \operatorname{div} H=0;$$
$$\operatorname{rot} E=\frac{\partial H}{\partial t}; \qquad \operatorname{div} E=4\pi\rho_e \tag{2.5}$$

and the generalized Ohm's law [15]

$$j=\sigma\left[E^x+\frac{1}{n_e e}\nabla P_e-\frac{j\times H}{n_e ec}+\frac{XY(w\times H)}{2(X+{}^1/_2Y)c}+\frac{1}{2}\frac{en_e}{\sigma}\frac{XY}{X+{}^1/_2Y}w\right], \tag{2.6}$$

to the system (2.1)-(2.4), the latter derived for simplicity on the assumption that the plasma is a hydrogen-helium plasma (Z = 0) and, as usual, neglecting electron diffusion and substituting Vd/dt for dv_x/dt and dv_y/dt. In (2.6), e is the electronic charge, n_e is the number of electrons per cubic centimeter

$$n_e=\frac{\rho}{m_x}\left(X_i+\frac{1}{2}Y\right);$$

σ is the conductivity of the medium, which is, in the general case, an assigned function of temperature, $E^x=E+1/cV\times H$ is the electric-field strength in a coordinate frame moving with the plasma as a whole, $w=v_x-v_y$ is the relative velocity of the hydrogen and helium ions, determined from the equation

$$\frac{Y+{}^1/_2X}{X+{}^1/_2Y}\frac{1}{c}(w\times H)-\frac{1}{X+{}^1/_2Y}\left(\frac{{}^4/_3m_x}{m_e}\right)^{1/2}\frac{n_e e}{\sigma}w_i=$$
$$=\frac{\nabla P_x}{n_e eX}-\frac{\nabla P_y}{n_e eY}-\frac{E^x}{2(X+{}^1/_2Y)};$$

and P_e, P_x, and P_y denote the partial pressures of electrons, protons, and helium ions:

$$P_e=\frac{X+{}^1/_2Y}{2X+{}^3/_4Y}P; \qquad P_x=\frac{X}{2X+{}^3/_4Y}P; \qquad P_y=\frac{{}^1/_4Y}{2X+{}^3/_4Y}P.$$

3. Possible Mechanisms of Generation and Maintenance of Magnetic Fields /92

Since our model of the sun is axisymmetric, the question arises as to the possibility of generation and support of a magnetic field in it. As we know, Cowling's theorem demonstrates the impossibility of maintenance of a magnetic field by axisymmetric motions of a fluid (see, for example, the most general method of proof for Cowling's theorem in [15]). However, there are at least two mechanisms capable of supporting a magnetic field in models

that are axisymmetric in the mean. If the averaged motion is axisymmetric, there is nothing to prevent nonaxisymmetric turbulent or small-scale vortical motions from supporting a magnetic field [16, 17]. It was shown in Parker's classical paper [16] how the action of a Coriolis force on convective motions of the medium in the sun's envelope creates the conditions necessary for the work of a hydromagnetic dynamo. Steenbeck and Krause [17] proposed a mechanism by which a magnetic field is sustained by anisotropic turbulent fluctuations of a medium in axisymmetric averaged motion. Here an additional term curl $\overline{(V' \times H)}$, which represents the electromotive force due to the correlation of the turbulent velocity and magnetic-field fluctuations V' and H', appears in the induction equation. Since the field is created by turbulent velocity fluctuations V', this correlation exists, and the average value of $V' \times H'$ may differ from zero.

A formula for the correlation is obtained with certain additional hypotheses as to the nature of the turbulent fluctuations:

$$\overline{V' \times H'} = -\frac{\sigma\lambda^2}{18}\{\overline{(V')^2}\operatorname{rot}\bar{H} + \overline{V' \cdot \operatorname{rot} V' H}\},$$

where λ is the correlation length. The first term indicates the decrease in the effective plasma conductivity due to the turbulence and has no relation whatever to the possibility of generation of a field. Interest attaches to the second term, which determines the appearance of the turbulence emf if the turbulence is such that

$$\overline{V' \operatorname{rot} V'} \neq 0.$$

It was shown by the authors that the turbulence arising under the action of Coriolis forces in the case of a rotating gaseous body can satisfy this condition, so that it becomes possible for turbulent fluctuations of the gas to support an averaged organized magnetic field.

There is also a mechanism by which magnetic fields are formed due to the mechanical electromotive force described in the generalized Ohm's law by the term $E_{mech} = \frac{1}{n_e e}\nabla P_e$ (which is usually omitted in the derivation of Cowling's theorem). This mechanism, which was first indicated by Bierman [17], goes into action if

$$\operatorname{rot} E_{mech} = \operatorname{rot}\left(\frac{1}{n_e e}\nabla P_e\right) \neq 0. \qquad (3.1)$$

The expression for the mechanical electromotive force can be obtained from the equations of motion, and it is therefore possible to determine the conditions to be imposed on the motion and the forces acting on the plasma to make the generation of a magnetic field a possibility. It is shown in [18] that a magnetic field

can be generated in axisymmetric models under the following conditions:

1. In vortical motions of the plasma, when the Helmholtz theorem of the conservation of vortex lines and the intensity of vortex tubes becomes invalid. This condition is satisfied everywhere /93 inside the sun as a result of its differential rotation with the angular velocity $\Omega = \Omega(r, \vartheta)$.

2. When nonpotential forces act on the plasma. For example, in the convective envelope of the sun, where a meridional circulation arises with velocity $V_p \sim 10^2 \sim 10^3$ cm/sec, a Coriolis force F_e operates:

$$\mathrm{rot}\, F_e = 2\,\mathrm{rot}(\Omega \times V_p) \neq 0,$$

thus making it possible for substantial magnetic fields to appear.

3. In regions where plasma molecular viscosity is substantial and curl curl curl $V \neq 0$.

4. In regions where the motion is essentially turbulent and curl $(1/\rho \nabla\tau) \neq 0$. It is obvious that this last condition can be satisfied within the sun's conductive envelope.

5. As a result of inhomogeneities of plasma chemical composition with $\nabla P \times \nabla X \neq 0$, i.e., if the chemical composition of the plasma is not constant on isobaric surfaces. Recognizing the thermonuclear reactions that take place in the interior, the theory of stellar evolution predicts the following relation for the chemical composition of star cores in the lower Main Sequence:

$$X = X_0 - AX^2\rho T^{4.5}$$

(X_0 is the initial chemical composition and A is a factor that takes evolutionary time into account). Considering the differential rotation of the stars, it can be assumed with confidence that the condition $\nabla P \times \nabla X \neq 0$ is satisfied rather often within the cores of stars.

Thus, available information on the internal structure of stars permits the conclusion that the conditions necessary for generation of magnetic fields exist in the interior of the sun.

The induction equation with consideration of the mechanical emf takes the form

$$\frac{\partial H}{\partial t} = \nu_m \nabla^2 H + \mathrm{rot}(V \times H) + c\,\mathrm{rot}\, E_{\mathrm{mech}} - \frac{1}{n_e e}\mathrm{rot}(j \times H), \qquad (3.2)$$

where $\nu_m = c^2/4\pi\sigma$ is the magnetic viscosity. If there is no field in

the plasma at time zero, Eq. (2.3) indicates that a toroidal magnetic field will begin to grow due to curl E_{mech}. Because of the finite conductivity, this process will be accompanied by dissipation. A stationary state will be reached, in which the field increase due to the mechanical emf will be offset by Joule heat losses Equation (3.2) can be used for an order-of-magnitude estimate of the stationary-field intensity and the time needed to reach the stationary state:

$$H \sim \frac{4\pi\sigma}{c} E_{mech} L, \qquad \tau \sim \frac{4\pi\sigma}{c} L^2$$

(L is the characteristic linear scale of the problem).

4. Energy Equations and Conditions for Convective Instability

The equation system (2.1)-(2.6) is not complete, and must be supplemented by an energy equation or heat-flux equation, together with determination of the Reynolds stresses that appear in Eq. (2.2). For this, it is first necessary to understand the physical processes that take place in the core and the convective envelope. We shall assume in accordance with the conventional view that in the central regions of the star, where $T \gtrsim 10^7$ °K, energy is released /94 by the proton-proton reaction that takes place there in accordance with the law [1]

$$\varepsilon = 2.8 \cdot 10^{-33} X^2 \rho T^{4.5} = \varepsilon_0 \rho T^{4.5}, \tag{4.1}$$

where ε is the energy released by one gram of matter in one second. This energy must be transferred by some transfer mechanism from the central regions to the surface, where it must be radiated into space in the form of the star's luminosity L_0. It is known that of the three known transfer mechanisms – heat conduction, convection, and radiation – the mechanism most effective for the cores of lower Main Sequence stars is radiation. The radiation field in stellar interiors is very nearly isotropic owing to the high density of the gas and the short free path. The radiant flux can therefore be calculated with the aid of the radiant heat-conduction approximation [1]:

$$F = -\frac{4ac}{3} \frac{T^3}{\varkappa\rho} \nabla T. \tag{4.2}$$

A heat-flux equation in the following form is then valid for a central region at radiant equilibrium with consideration of the proton-proton reaction:

$$\nabla F = \varepsilon\rho + E^* j + \frac{P}{\rho}(V_p \nabla \rho) - \frac{1}{\gamma - 1} \frac{P}{T}(V_p \nabla T), \tag{4.3}$$

where V_p is the velocity of meridional circulation of the gas and κ is the absorption index of the matter.

The opacity of the matter is determined basically by the following atomic processes: photoionization or bound-free transitions of an atom that absorbs a photon and releases a previously bound electron; free-free transitions, as a result of which an electron absorbs a photon and jumps from one free orbit to another with higher energy; Thompson scattering on free electrons. This last absorption process is important at low densities and high temperatures, at which the first two processes become rather insignificant. Comprehensive tables are available for various chemical compositions and wide density and temperature ranges.

However, approximate formulas that have been averaged over the frequencies and give a rough description of the opacity of the matter — the Cramers opacity laws — are usually used for the absorption indices. We know that the first two processes are effective for the sun, and that a modified Cramers law is used to obtain the best possible description of the tabular absorption-index values in the hypothetical temperature and density range:

$$\varkappa = \frac{4.34 \cdot 10^{25}}{\left(\frac{t}{g}\right)_0} Z(1+X)^{1-\alpha} \frac{\rho^{1-\alpha}}{T^{3.5}} \equiv \varkappa_0 \frac{\rho^{1-\alpha}}{T^{3.5}} \tag{4.4}$$

($\alpha = 0.25$ and $\ln(t/g)_0 = 0.82$ for the sun).

Thus, the motion of the plasma in the central regions of the sun will be described by a system of differential and algebraic equations, (2.1)-(2.6) and (4.1)-(4.4). In the outer regions of the sun, however, the radiative-equilibrium condition will be violated due to the appearance of convective instability. The condition for the onset of convective instability is formulated for spherically symmetrical hydrostatic models as the condition under which the absolute value of the true lapse rate exceeds the adiabatic value [1]:

$$\Delta\nabla T \equiv -\nabla T - \left(-\frac{\gamma-1}{\gamma}\frac{T}{P}\nabla P\right) = \frac{\gamma-1}{\gamma P}\frac{T}{P}\nabla P - \nabla T > 0. \tag{4.5}$$

Condition (4.5) is usually used not only for determination of the boundary between the core at radiative equilibrium and the convective envelope, but also in place of the heat-flux equation in the convective zone. However, we may expect on the basis of simple physical considerations that rotation will tend to suppress convection. Reflections on this problem can be found in Chandrasekhar [20], who showed that rotation suppresses convection in a heated layer of fluid, and in Randers [21], who found that the motion in the convective core of a rotating gaseous mass is decelerated in the direction normal to the axis of rotation. In a study of the

/95

effect of slow rotation on convective instability of the polytropic curves of gases, Clement [22] showed that rotation suppresses at least some of the convective motions described by the lowest-order harmonics. It is possible that higher-order harmonics are not as strongly suppressed by rotation, but it is obvious in any event that the mixing length l in the convective zone may be shortened substantially by rotation. This means that the transfer of energy becomes less effective on rotation, and that a larger excess of the true lapse rate over the adiabatic lapse rate is required for transfer of a given amount of energy in a rotating star. On the other hand, Cowling [23] notes correctly that nonuniform rotation may, by causing shear, contribute to the appearance of instability and, consequently, additional heat transfer. Since no criterion that takes all of these factors into account with sufficient reliability has been found, we shall henceforth take the Schwartzschild criterion (4.5) as a condition for the transition from radiative to convective equilibrium.

5. Developed Turbulence in the Convective Envelope of the Sun

Since the Reynolds number is very large in the convective zone (on the order of 10^{20} in the least stable layers), the motion in this zone will be of the nature of developed turbulence. To study the motion of the gas in the convective envelope, we shall use a semiempirical theory of turbulence — the generalized Prandtl "mixing length" theory, which was proposed and elaborated for astrophysical applications by Wasiutinsky [24]. The basic idea of this theory is as follows: the action of turbulent Reynolds stresses τ_{ik} on the gas is assumed to resemble that of molecular viscous stresses in ordinary fluid flows; it is assumed that the Reynolds stress tensor depends linearly on the rates of deformation of the averaged motion. The coefficients of this linear relation, which form the tensor η_{ik}, have the significance of eddy viscosities. We know that in the kinetic theory of gases, the molecular viscosity coefficients μ are related to the average velocity u_T and the mean free path λ of the molecules by the formula

$$\mu = \frac{1}{3} u_T \lambda \rho.$$

In the "mixing length" theory, it is assumed that similar formulas also apply for the eddy viscosities η_{ik}, and that particle aggregates of some sort (so-called turbulent elements) assume the role of molecules, while the role of u_T is taken by the turbulent velocity in the i-th direction, and that of λ by the Prandtl "mixing length." Generally, the turbulence is anisotropic, so that the eddy viscosity is represented by a tensor. The radial direction (more precisely, the direction of the effective acceleration, but these directions coincide accurate to 10^{-5} for the sun) is the

preferred direction for convective motions in stars, since the convection is of thermal nature. The turbulent viscosity tensor in a spherical coordinate system r, ϑ, ϕ bound to the center of the star has the diagonal form /96

$$\eta_{ik} = \begin{pmatrix} \eta_{rr} & 0 & 0 \\ 0 & \eta_{\vartheta\vartheta} & 0 \\ 0 & 0 & \eta_{\varphi\varphi} \end{pmatrix}, \tag{5.1}$$

where

$$\eta_{rr} = \frac{1}{3}\overline{\rho u_r'^2}\theta = \eta, \tag{5.2}$$

while the other two tensor components are equal at

$$\eta_{\vartheta\vartheta} = \eta_{\varphi\varphi} = S\eta.$$

Here θ is the time during which a turbulence element covers the mixing length l, u_i' is the velocity of turbulent fluctuations in the i-th direction, and the parameter S is a measure of the anisotropy of the turbulent fluctuations. At S = 1, the turbulent mixing is isotropic, the case S = 0 corresponds to purely radial transport, and when S > 1, the mixing is weaker in the radial direction than along meridians and parallels. The scalar part of the eddy viscosity η is in the general case a function of r and ϑ. It must obviously vanish at the interface between the core and the envelope, where turbulence ceases. Tables of eddy viscosity coefficients calculated in accordance with the "mixing length" theory as functions of zone depth are available for the solar convective envelope [25]. The coefficient of anisotropy is usually assumed constant, although it should be treated as a function of ϑ in consideration of the effects of rotation on turbulence and the increase in effective convection with increasing ϑ. Allowance for the existing magnetic fields introduces still greater complications into study of the turbulent motions. As was shown in [20], the magnetic field tends to prevent the appearance of turbulence, increasing the stability of the motion. In addition, a magnetic field with an energy comparable to the energy of the large-scale fluctuations is capable of suppressing developed turbulence. However, the opposite effect also exists, leading to an increase in the magnetic field even in axisymmetric averaged motions owing to turbulence anisotropy [19]. In the absence of definite results on the interaction of the field and the turbulent motions, and since the energy of the average magnetic field is several orders smaller than the energy of the average turbulent fluctuations within the convective zone of the sun, we shall henceforth neglect the effects of the magnetic field on the turbulent motions. In accordance with Wasiutinsky's theory [24], we shall express the components of the turbulent Reynolds stresses in a spherical coordinate frame in the form

$$\tau_r^r = -2\eta\frac{\partial u_r}{\partial r}; \qquad \tau_\theta^\theta = -\frac{2S\eta}{r^2}\left\{\frac{\partial}{\partial\theta}(ru_\theta) + ru_r\right\};$$
$$\tau_\theta^\theta = \frac{\tau_\theta^r}{r^2} = -\frac{\eta}{r^2}\left\{\frac{\partial}{\partial r}(ru_\theta) + S\frac{\partial u_r}{\partial\theta} - 2Su_\varphi\right\};$$
$$\tau_r^\varphi = \frac{\tau_\varphi^r}{r^2\sin^2\theta} = -\frac{\eta}{r}\left\{\frac{\partial r^2\Omega}{\partial r} - 2S\Omega\right\}; \qquad (5.3)$$
$$\tau_\theta^\varphi = \frac{\tau_\varphi^\theta}{\sin^2\theta} = -\frac{S\eta}{r^2\sin^2\theta}\left\{\frac{\partial}{\partial\theta}(r\sin\theta u_\varphi) - 2r\cos\theta u_\varphi\right\} = -S\eta\frac{\partial\Omega}{\partial\theta};$$
$$\tau_\varphi^\varphi = -\frac{2S\eta}{r\sin\theta}(u_r\sin\theta + u_\theta\cos\theta),$$

where u_r, u_θ, u_φ are the velocity components in the spherical coordinate frame.

To understand the physical phenomena that occur in the interior of the convective envelope, let us derive the heat-flux and turbulent-energy equations. We shall write the heat-flux equation with consideration of the heat supply F due to radiative heat conduction and energy dissipation: /97

$$\rho\frac{de}{dt} + P\,\mathrm{div}\,V + \mathrm{div}\,F = W. \qquad (5.4)$$

Here ε is the internal energy of the gas, $W = \Pi_{ik}\frac{\partial u_i}{\partial x_k}$ is the dissipation due to molecular viscosity, and Π_{ik} is the viscous-stress tensor [26]. We shall use the subscript "0" to denote the averaged characteristics of the motion and primes to denote the turbulent fluctuations, putting

$$\rho = \rho_0 + \rho', \qquad P = P_0 + P', \qquad T = T_0 + T', \qquad (5.5)$$

and, with the definition

$$u_i^0 = \frac{\overline{\rho u_i}}{\rho_0}, \qquad (5.5')$$

we may substitute (5.5) and (5.5') into (5.4) and average, bearing in mind that the fluctuations ρ', P', and T' are so small that their products can be neglected; we obtain

$$\frac{\partial}{\partial t}[\rho_0 e_0] + \frac{\partial}{\partial x_i}[F_0^i + e_0\rho_0 u_i^0 + \overline{e'\rho_0 u_i'}] + P_0\frac{\partial u_i^0}{\partial x_i} + \overline{P'\frac{\partial u_i'}{\partial x_i}} = \overline{W}. \qquad (5.6)$$

That is to say, the effect of turbulence on the average internal energy ε is determined by the dissipation $\overline{W}$, by the work of pressure in effecting turbulent compression, and by the convective thermal-energy flux $\rho_0\overline{e'u_i'}$. Using mixing-length theory, we obtain [24]

$$\rho_0 \overline{\varepsilon' u_i} \approx c_p \eta_{ik} (\Delta \nabla T)_k;$$
$$\overline{P \operatorname{div} u'} \approx \frac{\partial}{\partial x_i} \left\{ \frac{k}{\mu m_x} \eta_{ik} (\Delta \nabla T)_k \right\} + \frac{\eta_{ik}}{T_0} g_i (\Delta \nabla T)_k. \qquad (5.7)$$

We substitute (5.7) into (5.6); then the heat-flux equation for the convective envelope assumes the form

$$\rho_0 \frac{de_0}{dt} - \frac{P_0}{\rho_0} \frac{d\rho_0}{dt} + \frac{\partial}{\partial x_i} \{F_i + J_i\} + \frac{\eta_{ik}}{T_0} g_i (\Delta \nabla T)_k = \overline{W}. \qquad (5.8)$$

Here $J_i = c_p \eta_{ik} (\Delta \nabla T)_k$ describes the convective transfer of heat by turbulent fluctuations in the i-th direction and F_i is the heat transfer by radiative heat conduction, which is much less effective in the convection zone than J_i. Thus, the turbulent fluctuations result in the appearance of an additional heat flux analogous to the flux due to ordinary heat conduction, but with a coefficient of turbulent heat conduction that is much larger than molecular and depends on the direction of transfer. The term $B = \frac{\eta_{ik}}{T_0} g_i (\Delta \nabla T)_k$ in (5.8) determines the change in internal energy due to the work of Archimedean forces on the turbulent fluctuations (g_i is the absolute value of the i-th component of the effective force of gravity). If the medium is unstably stratified, $\Delta \nabla T > 0$, $B > 0$, and this work is done at the expense of stratification potential energy and leads, as we shall see below, to an increase in the energy of the turbulent motion.

$$\overline{W} = \overline{\Pi_{ik} \frac{\partial u_i}{\partial x_k}} \approx \overline{\Pi}_{ik} \overline{\frac{\partial u_i}{\partial x_k}} + \overline{\Pi'_{ik} \frac{\partial u'_k}{\partial x_k}} = W_0 + \overline{W}_1. \qquad (5.9)$$

The first term on the right in (5.9) has the sense of the specific dissipation of averaged-motion energy under the action of molecular viscosity; the second term describes the specific dissipation of fluctuation-motion energy under the influence of viscosity. For the sun's convective envelope we shall neglect the effect of viscosity on the averaged motion, i.e., W_0. /98

A turbulent-energy balance equation can be derived from the equations of motion for the averaged characteristics and turbulent fluctuations:

$$\frac{\partial \bar{e}_\tau}{\partial t} + \frac{\partial}{\partial x_k} \left(u_k^0 \bar{e}_\tau + \frac{1}{2} \tau_{ik} - \overline{u'_i \Pi'_{ik}} + u_i^0 \tau_{ik} \right) =$$
$$= - \overline{u'_i \frac{\partial P'}{\partial x_i}} - \overline{\Pi'_{ik} \frac{\partial u'_i}{\partial x_k}} + u_i^0 \frac{\partial \tau_{ik}}{\partial x_k}; \qquad (5.10)$$

$$\frac{\partial \bar{e}_\tau}{\partial t} + \frac{\partial}{\partial x_i}\left\{\bar{e}_\tau u_i^0 + \frac{\eta_{ik}}{\rho_0}\bar{e}_\tau \frac{(\Delta\nabla T)_k}{T_0} - \overline{u_k' \Pi_{ik}'}\right\} +$$
$$+ \tau_{ik}\frac{\partial u_i^0}{\partial x_k} - \eta_{ik} g_i \frac{(\Delta\nabla T)_k}{T_0} = -\overline{W}. \qquad (5.11)$$

Here $e_\tau = {}^1/_2\ \rho u_i' u_i'$ is the turbulent energy density. Let us consider the physical meanings of all terms in (5.10) and (5.11).

We see from (5.11) that the term $B = \eta_{ik} g_i \frac{(\Delta\nabla T)_k}{T}$, which was discussed previously and describes the work of Archimedean forces on the turbulent fluctuations, appears with the minus sign, causing an increase in turbulent energy when $\Delta\nabla T > 0$. The term $A = -\tau_{ik}\frac{\partial u_i^0}{\partial x_k}$ describes the exchange of energy between the averaged and turbulent motions. Usually A > 0, i.e., the energy of the turbulent motion increases at the expense of the energy of the averaged motion. Despite the apparent paradox, motions in which A < 0 are possible in principle, i.e., turbulent-fluctuation energy can be converted to averaged-motion energy, when the turbulence is created, for example, by an influx of heat [27]. The term

$$\frac{1}{2}\tau_{iik} = \frac{1}{2}\overline{\rho u_i' u_i' u_k'} \approx \overline{e_\tau u_k'} \approx \frac{\eta_{ik}}{\rho_0}\bar{e}_\tau \frac{(\Delta\nabla T)_k}{T_0}$$

represents the diffusion of turbulent energy by fluctuation motions; $u_k^0 \bar{e}_\tau$ is related to the transfer of turbulent energy by the averaged motion, and $\overline{u_i' \Pi_{ik}'}$ to transfer by molecular-friction forces. $\overline{W} = \overline{\Pi_{ik}' \frac{\partial u_i'}{\partial x_k}}$ has the significance of the average specific dissipation of fluctuation-motion energy under the influence of viscosity:

$$\overline{W} \approx -\frac{2}{3}\mu\overline{(\operatorname{div} u')^2} + \frac{\mu}{2}\sum\left(\frac{\partial u_i'}{\partial x_j} + \frac{\partial u_j'}{\partial x_i}\right)^2.$$

If we consider a volume in a stationary state, e.g., the convective envelope of the sun, the diffusion terms make no contribution to turbulent-energy change for this volume as a whole, and we obtain

$$A + B - \overline{W} = 0,$$

Within the convective zone, therefore, turbulent energy can appear and be held in a stationary state at the expense of averaged-motion energy (term A) or at the expense of density fluctuations arising under the influence of a heat influx (term B); the expenditure of fluctuation energy is governed by the dissipation due /99

to viscosity. The ratio of turbulent energy to averaged-motion energy can be estimated approximately. According to available estimates of the turbulent velocity [25], we find this ratio for the surface layers of the convective zone:

$$\frac{\bar{e}_\tau}{E_{\text{ср}}} \approx \frac{\bar{u}'^2}{(\Omega_0 a_0)^2} \approx 10^{-2}.$$

If we assume further that the angular velocity of the rotation does not increase strongly toward the center of the star (which is consistent with existing theories), this ratio will increase rapidly with depth and will be on the order of unity in large part. Thus, we see that the turbulence energy must be made up chiefly by supply of heat to the envelope, i.e., the term B. Assuming the existence of developed turbulence in the convective envelope of the sun, and neglecting energy diffusion and the meridional circulation velocity as small compared to the rotational velocity, we can derive a developed-turbulence criterion that assumes the following form in spherical coordinates:

$$\eta \sin^2\theta \left[r^2\left(\frac{\partial\Omega}{\partial r}\right)^2 + S\left(\frac{\partial\Omega}{\partial\theta}\right)^2 + 2(1-S)r\Omega\frac{\partial\Omega}{\partial r}\right] - \eta\frac{\partial\Phi}{\partial r}\frac{(\Delta\nabla T)_r}{T} = \overline{W}. \qquad (5.12)$$

Equation (5.12), which describes the energy balance within the convective zone, or the heat-flux equation (5.8), should be used in place of condition (4.6). However, there are no reliable estimates for the turbulent dissipation $\overline{W}$ for the case of anisotropic turbulence. For nearly isotropic turbulence, Taylor [28] proposed the formula

$$\overline{W} \approx 10\nu\frac{\bar{e}_\tau}{\Lambda^2}.$$

where Λ is a length on the order of the vortex diameter, i.e., the dimension of the turbulent fluctuations, and is a rather indeterminate quantity. To close the system of equations of motion, therefore, we shall henceforth use condition (4.6).

6. Estimation of Dimensionless Parameters; The Boundary Conditions of the Problem

The internal structure of stars can be analyzed using the system of equations (2.1)-(2.7), (4.2), (4.3), and (4.6) and the boundary conditions at the center of the star, at the interface between the core and the envelope, and on the surface of the star. However, since the equation system is complex, we shall attempt to estimate the orders of the terms appearing in the equation system and simplify them as strongly as possible on the basis of observational data and certain physical hypotheses. First of all, we shall estimate the ratio of the centrifugal force

to the force of gravity, $q=\frac{\Omega^2 r}{GM_r/r^2}$. On the surface of the sun, /100
this quantity can be calculated quite accurately:

$$q_0=\frac{\Omega_0^2 a_0}{GM_0/a_0^2}\approx 10^{-5} \qquad (6.1)$$

($\Omega_0\approx 3\cdot 10^{-6}$ sec^{-1} is the angular velocity of rotation at the solar equator, $a_0\approx 7\cdot 10^{10}$ cm is the radius of the sun, $M_0\approx 2\cdot 10^{33}$ g is the mass of the sun, and G ≈ 6.668 · 10^{-8} is the gravitational constant). An approximate estimate of the ratio of the electromagnetic to the gravitational force can be made:

$$\delta\approx\frac{i\times H}{c\rho}:\frac{GM_r}{r^2}\approx q^2\frac{GH^2}{\Omega^4 r^3}\left(\frac{\bar\rho}{\rho}\right), \qquad (6.2)$$

where $\bar\rho$ is the mean density of the sun. In the surface layers of the sun, assuming H_0 to be of the order of a few gauss, $\rho_{00}\sim 4\cdot 10^{-7}$ g/cm^3, we obtain $\delta_0\sim q_0^2$, since

$$\frac{GH_0^2}{\Omega_0^2 a^2}\frac{\bar\rho}{\rho_r}\sim 1.$$

We shall henceforth assume that the ratios of the centrifugal and Lorentz forces to the gravitational force will be of approximately the same order of smallness inside the sun as on its surface. We do not yet have sufficiently reliable estimates for the meridional circulation velocity v_0 in the photosphere. Systematic study of the motion of sunspots and other identifiable objects on the surface of the sun yields different values for objects with different shapes and sizes. It appears that these observational data reflect the fact that the meridional velocity varies over the depth of the convective zone. The available data yield approximate values of $v_0\sim 10^2-10^3$ cm/sec. Near the sun's surface, we obtain the following values for the ratio of v_0 to the linear velocity of rotation:

$$\alpha_0=\frac{v_0}{\Omega_0 a}\sim 10^{-2}-10^{-3}.$$

It must be noted that this ratio will vary substantially with depth in the convective zone.

It was shown in [29] that in the zone of radiative equilibrium, the velocities of the meridional circulation are on the order of 10^{-9} cm/sec, and they will henceforth be assumed equal to zero for the core of the sun.

Using a table calculated from the "mixing length" theory [25] for the turbulence characteristics in the convective zone,

we can estimate the ratio of the turbulent-viscosity forces to the inertial term:

$$\beta = \frac{\eta/\rho}{\Omega r^2}\frac{1}{\mathrm{Re}_T}$$

(Re_T is the turbulent Reynolds number).

If we again assume that the angular velocity of the rotation has the same order of magnitude in the convective zone, then according to [25] the parameter β varies from 10^{-2} to 10^{-4}. The maximum value in the convective zone is

$$\beta_0 \approx \frac{\eta_0/\rho_0}{\Omega_0 a_0^2} \approx 10^{-3} \qquad (6.3)$$

(ρ_0 and η_0 are the maxumum values of the density and viscosity in the convective zone; $\rho_0 \sim 0.2$ g/cm^3, and $\eta_0 \sim 1.4 \cdot 10^{12}$. We see from the resulting estimates that the dimensionless parameters α and β can vary through several orders within the convective zone, and for this reason we shall henceforth make certain supplementary assumptions in regard to them. We shall neglect the electromagnetic forces, since their influence on the large-scale motion is apparently not important outside of zones of strong field concentration (e.g., sunspots). We note that the reciprocal effect of hydrodynamics on the magnetic fields is extremely important, since the magnetic Reynolds number is very large owing to the high conductivity and large linear dimensions.

We introduce dimensionless variables in accordance with the formulas

$$\begin{aligned} &x = \frac{r}{a_0}; \quad \omega = \frac{\Omega}{\Omega_0}; \quad \xi = \frac{\eta}{\eta_0}; \quad \varphi = \frac{a_0\Phi}{GM_0}; \\ &p = \frac{a_0 P}{GM\rho_0}; \quad t = \frac{k}{\mu m_x}\frac{c_0}{GM_0}T; \quad v_x = \frac{u_r}{v_0}; \\ &v_\theta = \frac{u_\theta}{v_0}; \quad f = \frac{4\pi a_0^2}{L_0}F. \end{aligned} \qquad (6.4)$$

For the convective zones, the dimensionless form of the equations of motion in the spherical coordinate frame will be /101

$$\begin{aligned} &-\frac{t}{p}\frac{\partial p}{\partial x} - \frac{\partial \varphi}{\partial x} = -q_0\omega^2 x\sin^2\vartheta + \alpha_0^2 q_0\left[v_x\frac{\partial v_x}{\partial x} + \right. \\ &\left. + \frac{v_\theta}{x}\frac{\partial v_x}{\partial \vartheta} - \frac{v_\theta^2}{x}\right] - \alpha_0 q_0\beta_0\frac{t}{p}Q_x; \end{aligned}$$

$$-\frac{t}{p}\frac{\partial p}{\partial\vartheta}-\frac{\partial\varphi}{\partial\vartheta}=-q_0\omega^2x^2\sin\vartheta\cos\vartheta+\alpha_0^2q_0\left[v_\vartheta\frac{\partial v_\vartheta}{\partial\vartheta}+xv_x\frac{\partial v_\vartheta}{\partial x}+v_xv_\vartheta\right]-$$
$$-\alpha_\vartheta q_0\beta_\vartheta\frac{t}{p}Q_\vartheta;\qquad(6.5)$$
$$\alpha_\vartheta\left[v_\vartheta\sin\vartheta\frac{\partial(\omega x)}{\partial x}+v_\vartheta\frac{\partial(\omega\sin\vartheta)}{\partial\vartheta}+v_\vartheta\omega\cos\vartheta+v_x\omega\sin\vartheta\right]=\beta_\vartheta\frac{t}{p}Q_\varphi,$$

where the Q_i are the components of the dimensionless turbulent viscosity force

$$Q_x(v_x,v_\vartheta)=\frac{2}{x^3}\frac{\partial}{\partial x}\left(\xi x^3\frac{\partial v_x}{\partial x}\right)+\frac{1}{x^3\sin\vartheta}\frac{\partial}{\partial\vartheta}\left[\xi\sin\vartheta\times\right.$$
$$\left.\times\left(\frac{\partial xv_\vartheta}{\partial x}+S\frac{\partial v_x}{\partial\vartheta}-2Sv_\vartheta\right)\right]-\frac{2\xi}{x^3}\left[\frac{1}{x}\frac{\partial(xv_\vartheta)}{\partial\vartheta}+2v_x+\operatorname{ctg}\vartheta v_\vartheta\right];$$
$$Q_\vartheta(v_x,v_\vartheta)=\frac{1}{x}\left\{\frac{1}{x^3}\frac{\partial}{\partial x}\left[x^3\xi\left(\frac{\partial xv_\vartheta}{\partial x}+S\frac{\partial v_x}{\partial\vartheta}-2Sv_\vartheta\right)\right]+\right.$$
$$\left.+\frac{2S}{x^3\sin\vartheta}\frac{\partial}{\partial\vartheta}\left[\xi\sin\vartheta\left(\frac{\partial xv_\vartheta}{\partial\vartheta}+xv_x\right)\right]-\frac{2S\xi}{x^3\sin\vartheta}(v_x\sin\vartheta+v_\vartheta\cos\vartheta)\right\};$$
$$Q_\varphi(\omega)=\frac{1}{x^3\sin\vartheta}\left\{\frac{\partial}{\partial x}\left[\xi x^3\left(\frac{\partial x^2\omega}{\partial x}-2Sx\omega\right)\right]\sin^2\vartheta+\frac{x^3}{\sin\vartheta}\frac{\partial}{\partial\vartheta}\left(\xi S\sin^3\vartheta\frac{\partial\omega}{\partial\vartheta}\right)\right\}$$

The continuity equation takes the form

$$\frac{1}{x}\frac{\partial}{\partial x}\left(\frac{p}{t}x^2v_x\right)+\frac{1}{\sin\vartheta}\frac{\partial}{\partial\vartheta}\left(\frac{p}{t}\sin\vartheta v_\vartheta\right)=0.\qquad(6.6)$$

Equation (6.6) will be satisfied automatically by introduction of the stream function ψ:

$$v_x=\frac{t}{p}\frac{1}{x^2\sin\vartheta}\frac{\partial\psi}{\partial\vartheta};\qquad v_\vartheta=-\frac{1}{x\sin\vartheta}\frac{t}{p}\frac{\partial\psi}{\partial x}.\qquad(6.6')$$

Poisson's equation is

$$\frac{\partial^2\varphi}{\partial x^2}+\frac{2}{x}\frac{\partial\varphi}{\partial x}+\frac{1-\mu^2}{x^2}\frac{\partial^2\varphi}{\partial\mu^2}-\frac{2\mu}{x^2}\frac{\partial\varphi}{\partial\mu}=\frac{\rho_0}{\bar\rho}\frac{p}{t},\qquad(6.7)$$

where ρ is the mean density of the sun, so that $\rho_0/\bar\rho\sim0{,}1$. The condition for convective equilibrium in the envelope is

$$\frac{t}{p}\frac{\partial p}{\partial x}\left(\frac{1}{t}\frac{\partial t}{\partial x}-\frac{\gamma-1}{\gamma}\frac{1}{p}\frac{\partial p}{\partial x}\right)=0.\qquad(6.8)$$

Since the meridional circulation velocities are negligibly small for a core at radiative equilibrium, the equations of motion are greatly simplified:

$$-\frac{t}{p}\frac{\partial p}{\partial x}-\frac{\partial \varphi}{\partial x}=-q_0\omega^2 x(1-\mu^2);$$
$$-\frac{t}{p}\frac{\partial p}{\partial \theta}-\frac{\partial \varphi}{\partial \theta}=-q_0\omega^2 x^2\mu\sqrt{1-\mu^2}. \qquad (6.5')$$

The third equation of motion and the continuity equation are satisfied automatically. The Poisson's equation remains unchanged and the heat- and radiant-flux equations have the dimensionless forms /102

$$\nabla f = Dp^2 t^{6.5},$$
$$\nabla t = -C\frac{p^{3-\alpha}}{t^{8.5-\alpha}}f, \qquad (6.8')$$

where C and D are constants determined from the formulas

$$D=\left(\frac{\mu m_x G}{k}\right)^{4.5}\frac{\varepsilon_0 M_0^{6.5}}{4\pi L_0 a_0^{7.5}}\left(\frac{\rho_0}{\bar{\rho}}\right)^2;$$
$$C=\frac{3L_0\varkappa_0}{4ac}\left(\frac{1}{4\pi}\right)^{3-\alpha}\left(\frac{k}{\mu m_x G}\right)^{7.5}\frac{a_0^{2\alpha+6.5}}{M^{6.5+\alpha}}\left(\frac{\rho_0}{\bar{\rho}}\right)^{2-\alpha}.$$

Thus, the system of six differential equations (6.5), (6.6), (6.7), and (6.8) determines the internal structure of the convective envelope, i.e., the functions v_x, v_θ, ω, p, t and ϕ as they depend on x and θ; the system of five differential equations (6.5'), (6.7), and (6.8') determines the motion parameters p, t, φ, f and ω in the core. Let us now turn to the formulation of the boundary conditions.

1. At the center of a star, it is natural to assume zero radiant flux and gravitational force, i.e., to assume the absence of concentrated point masses or a point radiation source at x = 0:

$$\nabla\varphi = 0; \qquad f = 0.$$

2. At the interface $x = x_\sigma$ between the core and the envelope, since we assumed uniformity of chemical composition, the boundary condition to be taken everywhere is continuity of the parameters: at $x = x_\sigma$, ϕ, $d\phi/dn$, p, and t are continuous and $v_x = v_\theta = 0$. All energy sources are assumed to be concentrated in the core; hence the additional condition

$$\int_{\text{core}} f\,d\tau = 1,$$

The interface between the core and the envelope will be determined from the condition for disturbance of radiative equilibrium in the core.

3. At the surface of a star, x_Σ, it is natural to adopt the following simplified boundary conditions: zero pressure, density, and normal velocity component; gravitational potential and its normal derivative continuous with the solution of the Laplace equation $\Delta\bar{\varphi} = 0$ regular at infinity. The surface of the star is assumed to be free of stresses, i.e., at $x = x_\Sigma$:

$$p = 0; \quad t = 0; \quad v_n = 0;$$
$$\tau_{n\tau} = 0; \quad \tau_{n\varphi} = 0; \quad \varphi = \bar{\varphi};$$
$$\partial\varphi/\partial n = \partial\bar{\varphi}/\partial n.$$

7. Possible Simplifications of the General Equation System, and Methods of Solution

Using the estimates obtained at the beginning of Sec. 6, we may assume with some confidence that the ratio of the inertial and viscous forces to the gravitational forces is small, at least of the order of smallness of q_0, and take as the zeroth approximation the hydrostatic approximation obtained from our system at $q_0 = 0$. We obtain the equations of the zeroth and first approximations in q_0 by expanding the unknown functions in serics with respect to a small parameter, e.g., /103

$$\varphi = \varphi_0(x) + q_0\varphi_1(x, \mu) + 0(q_0^2) \text{ etc.}$$

and substituting into the systems (6.5)-(6.8) and (6.5'), (6.8'). Obviously, all functions of the zeroth approximation will depend only on x. The equation system for the zeroth approximation will be written

$$\left.\begin{aligned} &\frac{d\varphi_0}{dx} + \frac{t_0}{p_0}\frac{dp_0}{dx} = 0; \\ &\frac{d^2\varphi_0}{dx^2} + \frac{2}{x}\frac{d\varphi_0}{dx} - \frac{p_0}{t_0} = 0; \\ &f_0 = -\frac{1}{C}\frac{t_0^{3.5-\alpha}}{p_0^{3-\alpha}}\frac{dt_0}{dx}, \\ &\frac{df_0}{dx} + \frac{2}{x}f_0 = Dp_0^2t_0^{3.5}; \end{aligned}\right\} \text{for the core at radiative equilibrium}$$
$$\frac{d\ln p_0}{d\ln t_0} = \frac{\gamma}{\gamma-1}. \quad \text{for the convective envelope} \qquad (7.1)$$

The interface x_0 is determined in the zeroth approximation from the condition that the lapse rate in the region of radiative equilibrium in the core becomes equal to the adiabatic lapse rate, i.e.,

$$\left(\frac{d\ln p_0}{d\ln t_0}\right) = \frac{\gamma}{\gamma-1}. \qquad (7.2)$$

The boundary conditions assume the form:

at

$$
\begin{aligned}
&x=0 \quad d\varphi_0 \qquad dx=f_0=0;\\
&x=x_0 \quad \varphi_0, \quad d\varphi_0/dx, \quad p_0 \text{ and } t_0 \text{ continuous},\\
&\qquad \int f_0 dx=1; \qquad\qquad (7.3)\\
&x=1 \quad t_0=0; \qquad p_0=Et_0^{n+1}\\
&\qquad \varphi_0=-1; \qquad d\varphi_0/dx=1.
\end{aligned}
$$

(E_0 must be determined from the theory of stellar atmospheres).

Together with the boundary conditions (7.3), Eqs. (7.1) describe the structure of nonrotating lower Main Sequence stars. These equations were first solved by Schwartzschild [1], and they have since been used in numerous studies devoted to the internal structure of stars with various opacities, energy-release laws, and chemical compositions.

The equations for the functions of first order in q_0 are obtained with the additional assumptions that α_0 and $\beta_0 \gg q_0^{4/n}$.

$$\frac{\partial \varphi_1}{\partial x}+\frac{t_0}{p_0}\frac{\partial p_1}{\partial x}+\frac{d\ln p_0}{dx}\left(t_1-\frac{t_0}{p_0}p_1\right)=\omega^2(1-\mu^2)x+\alpha_0^2 I_x-\alpha_0\beta_0\frac{t_0}{p_0}Q_x, \tag{7.4}$$

$$\frac{\partial \varphi_1}{\partial \mu}+\frac{t_0}{p_0}\frac{\partial p_1}{\partial \mu}=-\omega^2 x^2\mu+\alpha_0^2 I_\mu-\alpha_0\beta_0\frac{t_0}{p_0}Q_\theta; \tag{7.5}$$

$$\varepsilon_0=\beta_0\frac{t_0}{p_0}Q_\varepsilon.$$

Here the I_i denote the inertial terms, and α_0 and β_0 are nonvanishing only in the convective envelope. The continuity and Poisson's equations are /104

$$\frac{1}{x}\frac{\partial}{\partial x}\left(\frac{p_0}{t_0}x^2 v_x\right)-\frac{p_0}{t_0}\frac{\partial}{\partial \mu}\left[\sqrt{1-\mu^2}\,v_\theta\right]=0, \tag{7.6}$$

$$x^2\frac{\partial^2\varphi_1}{\partial x^2}+2x\frac{\partial \varphi_1}{\partial x}+\frac{\partial}{\partial \mu}\left[(1-\mu^2)\frac{\partial \varphi_1}{\partial \mu}-\left(\frac{t_0}{p_0}p_1-t_1\right)\frac{p_0}{t_0^2}x^2\right]=0. \tag{7.7}$$

Eliminating f_0 from the heat-flux equation, we obtain for the region of radiative equilibrium

$$
\begin{aligned}
&\frac{\partial}{\partial x}(x^2 f_x)-\frac{\partial}{\partial \mu}\left[(1-\mu^2)\frac{\partial t_1}{\partial \mu}\right]\frac{1}{C}\frac{t_0^{2.5-\alpha}}{p_0^{3-\alpha}}=\\
&=Dx^2 t_0^{2.5}p_0^2\left(2\frac{p_1}{p_0}+2{,}5\frac{t_1}{t_0}\right); \qquad (7.8)\\
&C\frac{p_0^{3-\alpha}}{t_0^{2.5-\alpha}}f_x+\frac{\partial t_1}{\partial x}+\left[(8{,}5-\alpha)\frac{t_1}{t_0}-(2-\alpha)\frac{p_1}{p_0}\right]\frac{dt_0}{dx}=0.
\end{aligned}
$$

The condition for convective equilibrium in the envelope is

$$\frac{\partial}{\partial x}\left[\frac{p_1}{p_0}-\frac{\gamma}{\gamma-1}\frac{t_1}{t_0}\right]=0. \tag{7.9}$$

As a result of rotation, the surface of the sun $x = x_\Sigma$ and the surface of the core $x = x_\sigma$ will deviate from spherical form:

$$x_\Sigma = 1 + q_0 x(\mu) + 0(q_0^2),$$
$$x_\sigma = x_0 + q_{01} x(\mu) + 0(q_0^2).$$

However, accurate to the first order in q_0, the boundary conditions can be taken along the surfaces $x_\Sigma = 1$ and $x_\sigma = x_0$. Indeed, let us calculate, for example, ϕ on x_σ:

$$\varphi(x_\sigma)\approx\varphi(x_0)+q_0\varphi_1(x_0,\mu)\approx\varphi(x_0)+q_0\frac{d\varphi_0}{dx}\Big|_{x_0}x_1(\mu)+q_0\varphi_1(x_0,\mu)\approx$$
$$\approx\varphi_0(x_0)+q_0\left[\frac{d\varphi_0}{dx}\Big|_{x_0}x_1(\mu)+\varphi_1(x_0,\mu)\right]+0(q_0^2).$$

Thus, the continuity condition for the function ϕ on x_σ reduces to continuity of the function ϕ_1 on x_0. Considering all of the above, we obtain the following boundary conditions for the first-approximation functions:

at

$$\begin{aligned}
&x=0 \qquad \frac{\partial\varphi_1}{\partial x}=\frac{1}{x}\frac{\partial\varphi_1}{\partial\mu}=f_x=f_\theta=0;\\
&x=x_0 \qquad t_1,\quad p_1,\quad \varphi_1,\quad \frac{\partial\varphi_1}{\partial x},\ \omega-\text{continuous},\\
&\qquad\qquad v_x=v_\theta=0;\\
&x=1; \qquad \frac{p_1}{t_1}=\frac{dp_0}{dt_0}; \qquad \varphi_1=\bar{\varphi}_1; \qquad \frac{\partial\varphi_1}{\partial x}=\frac{\partial\bar{\varphi}_1}{\partial x};\\
&\qquad\qquad \tau_x^\omega\sim x\frac{\partial\omega}{\partial x}+2\omega(1-S)=0;\ v_x=0;\\
&\qquad\qquad \tau_x^\theta\sim\frac{\partial}{\partial x}(xv_\theta)+S\frac{\partial v_x}{\partial\theta}-2Sv_\theta=0,
\end{aligned} \tag{7.10}$$

where

$$\bar{\varphi}_1(1,\mu)=\sum a_{1n}^0 P_{2n}(\mu).$$

Having determined the first-approximation functions, we determine the deviation of the star's surface from the sphere, $\bar{x}(\mu)$, from the condition /105

$$\frac{dt_0}{dx}\Big|_{x=1}x(\mu)+t_1(1,\mu)=0.$$

Similarly, we obtain the condition for $x_1(\mu)$ - the deviation of the core from spherical. Denoting the lapse-rate difference in the core by

$$\psi' \equiv \frac{1}{t}\frac{\partial t}{\partial x} - \frac{\gamma-1}{\gamma}\frac{1}{p}\frac{\partial p}{\partial x},$$

we obtain on x_σ

$$\psi'(x_*) = \psi_0'(x_0) + q_0\left[\frac{d\psi_0'}{dx}\Big|_{x_*} x_1(\mu) + \psi_1(x_0, \mu)\right] = 0,$$

from which we find

$$x_1(\mu) = -\psi_1'(x_0\,\mu)\Big/\frac{d\psi_0'}{dx}\Big|_{x_*}.$$

Let us consider how the system of equations of motion can be simplified in the convective region with additional conditions on α_0 and β_0.

1. $\beta_0 \ll 1$ ($\mathrm{Re}_T \gg 1$). The turbulent viscosity force is small on the average over the zone. In this case, irrespective of the values of the other parameters, system (7.4)-(7.7), (7.9) has a solution of the following form for the angular velocity ω and the stream function ψ:

$$\psi = \psi(x\sin\vartheta); \qquad \omega = \omega(x\sin\vartheta). \tag{7.11}$$

Difficulties are encountered here in satisfying the boundary conditions, since the equation system is found to be of lowest order as $\mathrm{Re}_T \to \infty$ (see [30]). If the boundaries of the convective envelope are stress-free

$$v_x = 0; \qquad \tau_x^\vartheta = \tau_x^\varphi = 0 \text{ at } x = x_0,\ x = 1, \tag{7.12}$$

the solution of the type (7.11) that satisfies boundary conditions (7.12) has the form

$$\psi \equiv 0; \qquad \omega = (x\sin\vartheta)^{2(S-1)} \tag{7.11'}$$

i.e., the angular velocity of rotation is a function of distance from the axis of rotation and there is no meridional circulation. However, solution (7.11) has a singularity near the axis of rotation at $S < 3/2$ as a result of an unbounded increase of $d\omega/d\vartheta$.

Thus, the solution of type (7.11) is apparently valid in the general case (as for solid boundaries when $\mathrm{Re}_T \to \infty$ [31]) only in

inviscid regions of the flow, where the velocity gradients are not large. In addition, there may be shear layers [31] in which the velocity gradients are large and, despite the large Reynolds numbers, the viscous terms in the equations of motion are significant.

2. $\beta_0/\alpha_0 \gg 1$. The turbulent-viscosity force is significant, but the meridional circulation is weak to compensate the turbulent-viscosity losses. A stationary condition will be possible with an angular-velocity distribution such that the ϕ-component of the friction force vanishes:

$$\frac{1}{x^3}\frac{\partial}{\partial x}\left\{\xi x^3\left[\frac{\partial \omega}{\partial x}+2x\omega(1-S)\right]\right\}(1-\mu^2)+\frac{\partial}{\partial \mu}\left[\xi S(1-\mu^2)^2\frac{\partial \omega}{\partial \mu}\right]=0.$$

With S = const and $\xi = \xi(x)$, putting $(\omega(x, \mu) = \omega(x)\chi(\mu),)$ we find /106

$$\frac{d/dx\left\{\xi(x)x^3\left[x\frac{d\omega}{dx}+2(1-S)\omega\right]\right\}}{S\xi x^2\omega} = -\frac{d/d\mu\left[(1-\mu^2)^2 d\chi/d\mu\right]}{\chi(1-\mu^2)} = m. \qquad (7.13)$$

Nontrivial bounded solutions for $\chi(\mu)$ exist only for $m = n(n+1)-2$ (n = 1, 2, 3, ...). In virtue of the symmetry about the equator, the general solution of (7.13) is

$$\omega(x, \mu) = \sum_1^\infty \omega_n(x)\frac{P^1_{2n+1}(\mu)}{\sqrt{1-\mu^2}}. \qquad (7.14)$$

If ξ = const, we have

$$\omega_n(x) = A_n x^{K_n^1} + B_n x^{K_n^2};$$

$$K_n^{1,2} = \frac{-5+2S \pm \sqrt{(1+2S)^2+8n(2n+3)S}}{2}.$$

The boundary conditions for ω may be as follows: if it is assumed that the turbulent fluctuations do not penetrate into the core of the star, the boundaries of the envelope should be free of stresses, i.e.,

$$\tau_x^\omega = 0 \quad \text{at} \quad \begin{matrix} x = x_0, \\ x = 1, \end{matrix}$$

then the general solution of (7.13) assumes the simple form

$$\omega(x) = \omega(1)x^{2(S-1)}.$$

If we assume that penetration of the fluctuations into the core is possible, the boundary conditions at $x = x_0$ will be continuity of

the angular velocity: $\omega_n(x)$ continuous at $x = x_0$. The condition at $x = 1$ is retained. As we noted above, $\xi(x) = \text{const}$ is a rather inappropriate value for turbulent viscosity, and the tables of [25] must be used for reality. Values for other internal-structure characteristics are obtained by substituting $\omega(x, \theta)$ into the system (7.4)-(7.9) with consideration of the boundary conditions and neglecting terms with α_0^2. After determination of v_x^0 and v_θ^0, the next approximation for ω can be found from Eq. (7.5) by substituting v_x^0 and v_θ^0, and this will be the next term in the expansion of ω in series with respect to the small parameter α/β.

Subsequent terms in the expansion can be calculated by successive approximations.

3. $(S - 1)$ is small. The resulting motion is nearly a rotation with constant angular velocity ω_0. It can be shown that in this case $\alpha \sim S - 1 \ll 1$. We eliminate the pressure and density from (7.5) and make the substitution

$$\psi = (S-1)\psi_1; \quad \omega = \omega_0 + (S-1)\omega_1;$$

we then obtain a system of two linear differential equations of sixth order for the functions ψ_1 and ω_1, with six boundary conditions on the surface and the interface between the core and the envelope.

Numerical calculation of the proposed models of the sun's internal structure will be discussed in the next article. We note for now that the introduction of anisotropic turbulence into the picture in the convective zone gives reason to assume that: 1) a steady meridional circulation will exist in the convective envelope of the model; 2) the model's angular velocity of rotation will be a function of r and θ; 3) a large-scale magnetic field /107
will appear and be held steady in the model by the hydromagnetic dynamo or the "battery" effect.

Since the present article was sent to the printer, a number of papers on the hydrodynamics of the convective zones of stars have appeared [32-39], some of them representing further developments of the present article [37, 39].

REFERENCES

1. M. Schwartzschild. Stroyeniye i evolyutsiya zvezd (The Structure and Evolution of the Stars), Russ. ed., Moscow, IL, 1961.
2. J.W. Roxburgh. On Stellar Rotation. I. The Rotation of Upper Main-Sequence Stars. Month. Not. of Royal Ast. Soc., 1964, Vol. 128, 2.

3. J.W. Roxburgh. On Stellar Rotation. II. The Rotation of Lower Main-Sequence Stars. Month. Not. of Royal Ast. Soc., 1964, Vol. 128, 3.
4. J.P. Ostriker and J.W.K. Mark. Rapidly Rotating Stars. Astrophys. J., 1968, Vol. 151, 3, Part 1.
5. J. Faulkner, J.W. Roxburgh, and P.A. Strittmatter. Uniformly Rotating Main Sequence Stars. Astrophys. J., 1968, Vol. 151, 1, Part 1.
6. J.W. Roxburgh. Steady Meridian Circulation in Rotating Magnetic Stars. Month. Not. of Royal Ast. Soc., 1961, Vol. 126, 1.
7. J.F. Monoghan. Magnetic Fields in Stellar Bodies. Month. Not. of Royal Ast. Soc., 1965, Vol. 131, 2.
8. J.Nakagawa and S.K. Trehan. An Axisymmetric Magnetic Field with Differential Rotation in a Spherical Fluid Shell. Astrophys. J., 1968, Vol. 151, 3, Part 1.
9. L. Biermann. On Meridional Circulations in Stellar Convective Zones. Electromagnetic Phenomena in Cosm. Phys., 1958, p. 548.
10. T. Sakurai. Hydromagnetical Investigation of the Solar Differential Rotation. Publ. Ast. Soc. Japan, 1966, Vol. 18, 3.
11. W.J. Cocke. On the Solar Differential Rotation and Meridional Currents. Astrophys. J., 1967, Vol. 150, 3, Part 1.
12. R. Kippenhahn. Differential Rotation in Stars with Convective Envelopes. Astrophys. J., 1963, Vol. 137, 2.
13. S.B. Pikel'ner. Osnovy kosmicheskoy elektrodinamiki (Fundamentals of Cosmic Electrodynamics). Moscow, "Nauka," 1966.
14. S.I. Braginskiy. Transfer Phenomenon in Plasma. In collection entitled: "Voprosy teorii plazmy" (Problems of Plasma Theory), No. 1, 1963.
15. S.I. Braginskiy. The Magnetohydrodynamics of the Earth's Core. Geomagnetizm i aeronomiya, 1964, Vol. 4, 5.
16. E.N. Parker. Hydromagnetic Dynamo Models. Astrophys. J., 1955, Vol. 122, 2.
17. M. Steenbeck and F. Krause. The Origin of the Magnetic Fields of Stars and Planets as a Result of Turbulent Motion of Their Matter. Magnitnaya gidrodinamika, 1967, No. 3.
18. A. Schleuter and L. Bierman. Interstellar Magnetic Fields. In collection entitled: "Problemy sovremennoy fizika" (Problems of Modern Physics), 1954, No. 2.
19. I.M. Yavorskaya. Certain Problems in the Origin and Maintenance of Cosmic Magnetic Fields. "Mekhanika zhidkosti i Gaza," 1968, No. 4.
20. S. Chandrasekhar. Hydrodynamic and Hydromagnetic Stability, Oxford, 1961.
21. G. Randers. On the Rotation of the Stars with Convective Core. Astrophys., 1942, Vol. 95, 3, 454-460.
22. M.J. Clement. The Effect of a Small Rotation on the Convective Instability of Gaseous Mass. Astrophys. J., 1965, Vol. 142, 1, 243-252.
23. T.G. Cowling. The Condition for Turbulence in a Rotating Star. Astrophys. J., 1951, Vol. 114, 2, 272-286.

24. J. Wasiutinsky. Hydrodynamics and Structure of Stars and Planets. Astrophys. Norvegica, 1946, Vol. 4.
25. N. Baker and S. Temesvary. Tables of Convective Stellar Envelope Models. New York, 1966.
26. N.Ye. Kochin, I.A. Kibel', and N.V. Roze. Teoreticheskaya gidrodinamika (Theoretical Hydrodynamics), Part II, Moscow, 1963.
27. A.S. Monin and A.M. Yaglom. Statisticheskaya gidromekhanika (Statistical Hydromechanics), Vol. I, Moscow, 1965.
28. G.I. Taylor. Statistical Theory of Turbulence. Proc. Roy. Soc., A, 1935, Vol. 151, p. 421.
29. P.A. Sweet. The Importance of Rotation in Stellar Evolution. Month. Not. of Royal Ast. Soc., 1950, Vol. 110, 6.
30. M. Van Dyke. Perturbation Methods in Fluid Mechanics. Russ. ed., Moscow, Mir, 1967.
31. K. Stewartson. On Almost Rigid Rotation. Part 2, J. Fluid Mech., 1967, Vol. 26, 1.
32. R.S. Iroshnikov. The Nature of the Sun's Differential Rotation. Astron. Zh., 1960, Vol. 46, No. 1.
33. S. Kato and G. Nakagava. The Solar Differential Rotation and Rossby-Type Waves, Solar Phys., 1969, Vol. 10, 2.
34. F.H. Busse. Differential Rotation in Stellar Convective Zone. Astrophys. J., 1970, Vol. 159, No. 2, Part 1.
35. H. Köller. Differential Rotation Caused by Anisotropic Turbulent Viscosity, Solar Phys., 1970, Vol. 13, 1.
36. B. Durney. Differential Rotation. Meridional Velocities and Pole-Equator Difference in Temperature of a Rotating Convective Spherical Shell, Astrophys. J., 1970, Vol. 163, No. 2, Part 1. /108
37. N.S. Mel'nikova and I.M. Yavorskaya. The Hydrodynamics of the Convective Envelopes of Stars. "Mekhanika zhidkosti i gaza," 1971, No. 2.
38. B. Durney and T.W. Roxburg. Inhomogeneous Convection and the Equatorial Acceleration on the Sun, Solar Phys., 1971, Vol. 16, 1.
39. B.S. Keller and I.M. Yavorskiy. The Hydrodynamics of the Convective Zone of the Sun. "Mekhanika zhidkosti i gaza," 1972, No. 5.

N75 13716

AN INVESTIGATION OF THE COSMIC RADIATION IN THE VICINITY OF THE MOON ON THE LUNA 10, 11, AND 12 ARTIFICIAL LUNAR SATELLITES

(Translation of "Issledovaniye kosmicheskoy radiatsii v okrestnostyakh Luny na ISL 'Luna-10, 11, 12.'")

N. L. Grigorov, V. G. Kurt, V. N. Lutsenko, V. L. Maduyev, N. F. Pisarenko, and I. A. Savenko

ABSTRACT

The paper reviews research on the primary cosmic radiation and solar cosmic rays from the Luna 10, 11, and 12 artificial lunar satellites. Data on the vertical distribution of cosmic rays above the moon's surface are presented, and the albedo for the primary radiation is determined. The fluxes of electrons with energies from 30 to 300 keV were registered in the solar cosmic rays. Rapid variations of the electron flux were observed. The angular distributions of 0.5-10 MeV protons moving together with the corpuscular streams responsible for Forbush decreases were investigated. With 14 illustrations and 19 source citations.

AN INVESTIGATION OF THE COSMIC RADIATION IN THE VICINITY OF THE MOON ON THE LUNA 10, 11, and 12 ARTIFICIAL LUNAR SATELLITES

/109

N.L. Grigorov, V.G. Kurt, V.N. Lutsenko,
V.L. Maduyev, N.F. Pisarenko, and I.A. Savenko

Early in 1966, preparation of experiments to investigate the radiation environment in near-moon space was begun as part of the planning for the flights of the first artificial lunar satellites (ALS). Study of the physical properties of this region of space is important both in its purely scientific aspect and in support of radiation safety on manned lunar flights.

It was necessary first of all to clarify the possible significance of the level of trapped charged particles in the vicinity of the moon. A number of experiments were designed to determine the radioactivity of the moon – both the intrinsic activity of the lunar rocks and that induced by cosmic rays. Further, the ALS was viewed as a highly convenient probe for investigation of possible traces of the earth's magnetosphere at distances around $60R_e$ (R_e is the radius of the earth). Finally, the ALS is a convenient tool for measurements of the solar cosmic radiation. Firstly, such a satellite spends much of the time outside of the earth's magnetosphere and, secondly, the presence of the moon as a body that absorbs all of the radiation incident upon it is helpful in certain cases in studying the angular distribution and manner of propagation of the solar cosmic rays.

The Artificial Lunar Satellites and the Instruments for Charged-Particle Measurements

The Luna 10 ALS was launched into a selenocentric orbit with its apocynthion at ∿1000 km and its pericynthion at 350 km on 3 April 1966. The orbit of the satellite was inclined 72° to the plane of the lunar equator. Data from the satellite's instruments were transmitted in communications episodes from 3 April through 29 May 1966. Pulses from the instrument detectors were fed to a logarithmic scaler with a capacity of up to $5 \cdot 10^8$ and were counted with a relative error no greater than 3%. The scaler circuits were interrogated once every two minutes. The pulses accumulated between communications episodes could be counted at the beginning of the next communications episode. This made it possible to determine the average counting rates of the sensors during the time between episodes.

The Luna 11 ALS was placed in selenocentric orbit on 28 August 1966. The parameters of the orbit were as follows: apocynthion 500 km, pericynthion 133 km, inclination of orbit to the plane of the lunar equator ∿10°. The instruments operated

during communications episodes held on the average once a day and lasting from 2 to 40 minutes. The detector counting rate was determined with the aid of logarithmic intensimeters, which were interrogated once every 6.75 sec. In some communications episodes the pulse counts were obtained with logarithmic scaling circuits as in the case of Luna 10. Information was acquired during the period from 28 August through 1 October 1966.

The Luna 12 ALS was placed in orbit around the moon on 22 October 1966. The apocynthion of the orbit was at 1700 km and pericynthion at 98 km; the orbit was inclined ∿16° to the plane of the lunar equator. The scientific apparatus was worked on schedules similar to those of the Luna 11. Information was obtained over the period from 22 October 1966 through 6 January 1967. /110

The instrument package for cosmic-ray studies on the Luna 10 [1] included two identical type SBT-9 end-window counters. The counters were mounted side by side on the outer surface of the satellite. The counter for registration of hard radiation was fully enclosed in brass with a thickness of ∿2.8 g·cm^{-2} while the other counter, which was mounted to register soft radiation, had a conical aperture in a similar shield. The thickness of the window (mica with a sputtered layer of gold) was ∿1.5 mg·cm^{-2}. Tnus, the first counter could register protons with energies E_p > 50 MeV, and the second (through the window) protons with energies E_p > 0.5 MeV and electrons with energies E_e > 40 keV. Both counters had a global geometry factor G_0 = 2.6 ± 0.2 cm^2, while the geometry factor of the second counter for radiation registered through the window was 0.4 cm^2·sr. Luna 10 rotated on its axis with a period of ∿3 min. Analysis of the satellite's orientation with respect to the sun indicated that the counter with the open window could not register solar x-radiation, since the sun did not enter its field. The instruments aboard Luna 11 and Luna 12 [2] consisted of gas-discharge counters with magnetic filters and a scintillation counter. The three SBT-9 gas-discharge counters were similar to those used in the instrument package on Luna 10. Collimators with cone angles of

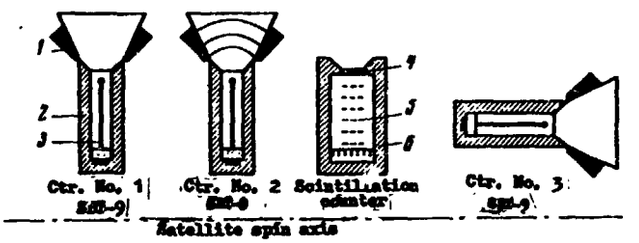

Figure 1. Placement of Sensors on Luna 11 and 12 ALS Relative to Satellite's Spin Axis. Counters Nos. 1, 2, and 3 are end-window gas-discharge counters. 1) Ferrite plates; 2) counter shielding; 3) SBT-9 counter; 4) CsI(Tl) crystal; 5) FEU-16 photomultiplier; 6) scintillation-counter shielding.

$\sim 60°$ were placed in front of the mica counter windows. The ferrite plates of the magnetic filters were mounted on the outside of the conical collimators of all counters, but these plates were magnetized on only one of the counters (No. 2). The magnetic field of this filter was such that electrons with energies below 100 keV were practically completely deflected, while the transmission of the filter did not exceed 20% at an electron energy $E_e \sim 0.6$ keV. Thus, counter No. 2 with the magnetized filter registered protons with energies above 0.5 MeV and electrons with energies $E_e \geq 0.6$ MeV. Counter No. 1 (filter unmagnetized) registered electrons with energies $E_e \geq 30$ keV and protons with energies $E_p > 0.5$ MeV. Thus, the difference between the readings of counters Nos. 1 and 2 was due to electrons with energies from 30 to 300-500 keV. Counter No. 3 was a duplicate of counter No. 1 and was oriented perpendicular to the axes of counters Nos. 1 and 2 (Fig. 1). When solar x-radiation fell directly into the counter windows, their counting rates rose above 10^3 sec^{-1}. The geometry factor of counters Nos. 1, 2, and 3 for particles registered through the window was 0.15 $cm^2 \cdot sr$. /11

The scintillation counter consisted of a CsI(Tl) crystal 1 mm thick and 12 mm in diameter with an FEU-16 photomultiplier. The crystal was mounted in a 60° collimator 10 mm high and 10 mm in diameter in the section next to the crystal. An aluminum foil 2.7 $mg \cdot cm^{-2}$ thick was secured over the CsI(Tl) crystal. The axis of the scintillation counter was parallel to that of counters Nos. 1 and 2 (Fig. 1). The electronics registered pulses corresponding to the following energy releases in the CsI(Tl) crystal: threshold I, $K_1 > 30$ keV; threshold II, $E_2 > 300$ keV; threshold III, $E_3 > 1.5$ MeV.

With consideration of absorption in the foil and the superficial dead layer of the CsI(Tl) crystal, electrons with $E_e > 60$ keV and protons with $E_p > 0.9$ MeV could be registered at the first threshold. At the second threshold, $E_e > 300$ keV and $E_p > 1.0$ MeV, and at the third 1.8 MeV $< E_p <$ 100 MeV. The corresponding thresholds for the Luna 12 instrument were $E_1 > 130$ keV, $E_2 > 1.3$ MeV, and $E_3 > 8$ MeV. The geometry factor of the scintillation counter for particles entering it through the collimator was 1.3 $cm^2 \cdot sr$, but 0.66 cm^2 for an isotropic penetrating-radiation flux.

The Luna 11 and Luna 12 satellites rotated with periods of 122 and 260 sec, respectively, around axes parallel to the axis of counter No. 3 and perpendicular to those of counters Nos. 1 and 2 and the scintillation counter.

The Absence of Lunar Radiation Belts

The September 1959 flight of Luna 2 had shown that the intensity of the penetrating radiation trapped by the moon's magnetic field equals zero within the limits of measurement error at distances of ~1000 km from the lunar surface [3]. However, the instrument on Luna 2 could not register protons with energies around 0.5 MeV, and electrons with $E_e \sim 40$ keV could be detected only from their bremsstrahlung with very low efficiency. It was therefore considered worthwhile to measure the upper limit of the flux intensity of electrons with energies $E_e \sim 40$ keV, which, according to estimates, could be held by a constant lunar magnetic field of ~10-20 γ, the possible existence of which had not been eliminated by the magnetic measurements available at that time [4].

Over a long measurement time, the instruments on Luna 10 were capable of quite reliable determination of the intensity limit of the flux of ~40 keV electrons. During much of the time from 27 April through 2 May 1966 and from 11 through 25 May 1966 (periods of low solar activity), the unshielded counter registered an average of 11.2 counts/sec [1]. Since the unshielded counter had a relative effective geometry factor for penetrating radiation amounting to 0.95 ± 0.05 of the corresponding factor for the shielded counter, whose average counting rate near the moon was 10.5 sec^{-1}, the upper-limit electron flux intensity was $N_e = 3$ $cm^{-2}sr^{-1}\cdot sec^{-1}$ for this period of the measurements.

Thus, if there is radiation that has been permanently trapped by the magnetic field of the moon at heights from 350 to 1000 km above the lunar surface, fluxes of ~40 keV electrons represent no more than 3 $cm^{-2}sr^{-1}\cdot sec^{-1}$ of this radiation. The later Explorer 35 measurements confirmed the absence of trapped radiation [the intensity of electrons with $E_e > 45$ keV and protons with $E_p > 322$ keV does not exceed 5 particles$(cm^2\cdot sec\cdot sr)^{-1}$. According to the same source, the moon's intrinsic magnetic field does not exceed 4 γ at its surface [5].

Detection of the Tail of the Magnetosphere at Distances of ~60R_e /112

In principle, extended-term measurements of charged particles and the magnetic field on artificial lunar satellites can, in virtue of the moon's rotation, answer the question as to whether the earth's magnetosphere influences the spatial intensity distribution of the soft corpuscular radiation at distances from the earth on the order of 60 R_e.

During the operating lifetime of Luna 10, the satellite passed twice through the region hypothetically occupied by the tail of the earth's magnetosphere. On both occasions — 4 and 9 April and 3 May 1966 — it registered temporary increases in the

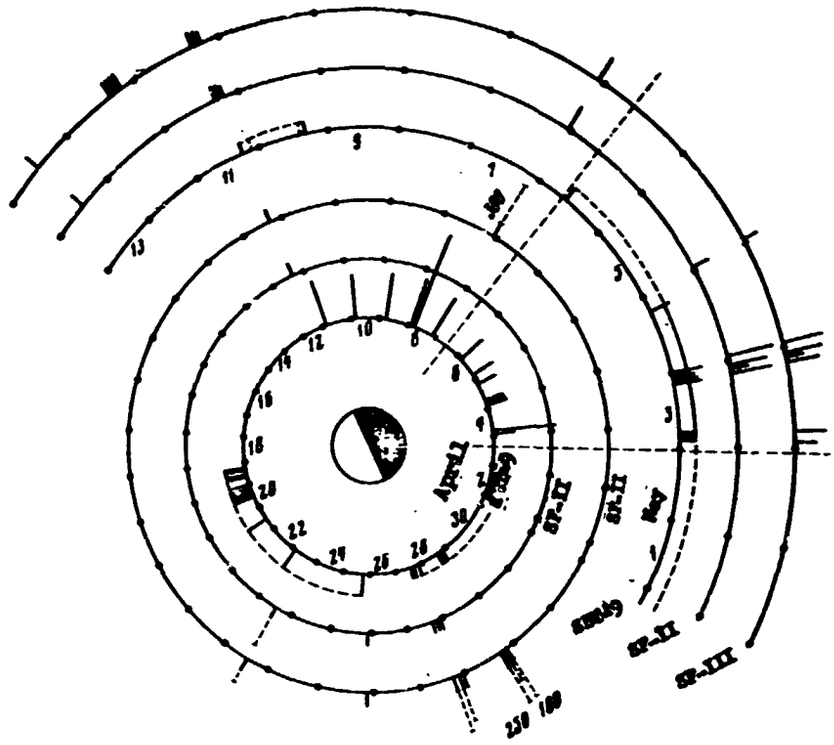

Figure 2. Readings of Luna 10 Counters in the Period from 3 April through 13 May 1966. The tick lengths are proportional to the number of counts per second; the dashed radial line indicates the possible limits of the region into which the tail of the magnetosphere extends.

soft-radiation intensity (Fig. 2). Very probably, these intensity increases were due to crossings of the tail of the earth's magnetosphere [4] and indicate that quasistationary fluxes of low-energy particles exist in the transitional region between the magnetosphere and the interplanetary magnetic field. Magnetic-field measurements made later on Explorer 33 and Explorer 35 [5] confirmed the existence of the tail of the magnetosphere out as far as the orbit of the moon. Energetic-particle fluxes were also observed when the moon crossed the terrestrial shock wave, the magnetopause, and the tail of the magnetosphere [6].

Investigation of Cosmic Rays in Near-Moon Space

The extended-time measurements made on Lunar 10, 11, and 12 over a broad range of distances from the lunar surface made it possible to investigate the moon's influence on the penetrating-radiation flux [7]. The instruments mounted on the artificial lunar satellites included shielded gas-discharge counters, which /113

registered the primary radiation. In addition, the readings of the SBT-9 end-window counters could be used to acquire information on high-energy cosmic rays in those cases in which soft radiation was absent.

The shielded-counter counting rates were measured in the "empty" space on the path from the earth to the moon during several communications episodes over three days (for each satellite).

The counting rate I(h) of an instrument registering the global cosmic-ray flux varies with height because the moon screens out part of space, preventing particles from it from striking the counter. If Ω(h) is the solid angle subtended by the moon at a point situated at a distance h from its surface, n_0 is the cosmic-ray intensity per unit solid angle, and S is the area of the counter, we have

$$I(h) = n_0 S 4\pi - n_0 S\Omega(h) = n_0 S 4\pi \left[1 - \frac{\Omega(h)}{4\pi}\right],$$

where $4\pi n_0$ is the counting rate in interplanetary space ($h \to \infty$),

$$\frac{I(h)}{I(\infty)} = 1 - \frac{\Omega(h)}{4\pi}; \qquad \Omega(h) = 2\pi\left[1 - \frac{\sqrt{1+\frac{2R_m}{h}}}{1+\frac{R_m}{h}}\right],$$

where R_m is the radius of the moon.

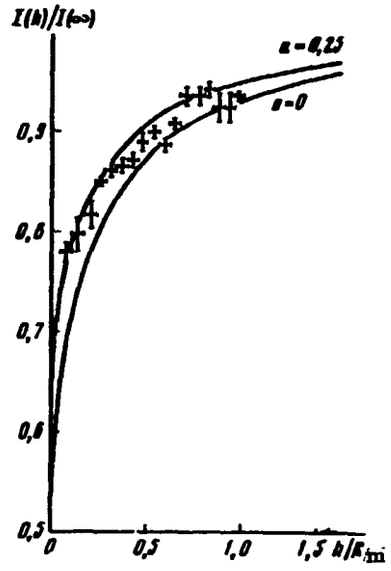

Figure 3. Curve of Shielded-Counter Counting Rate as a Function of Satellite's Height h Above the Lunar Surface (Averaged from the Luna 10, 11, and 12 Measurements).

If we assume that the lunar surface is a source of isotropic radiation of intensity αh_0 (i.e., that it is a reflecting surface subject to Lambert's law), we can show that the intensity of this radiation at height h will be proportional to the solid angle Ω(h) subtended by the moon at the instrument. Then

$$\frac{I(h)}{I(\infty)} = 1 - (1-\alpha)\frac{\Omega(h)}{4\pi}.$$

Luna 10 made measurements at distances of 350-1000 km above the lunar surface. The height range in which the vertical variation of cosmic-ray intensity was measured by Luna 11 was extended to 150-1200 km, while the Luna 12 measurements were made at heights

ranging from 100 to 1800 km. To eliminate the effects of solar modulation of the primary cosmic rays, data pertaining to periods of elevated solar activity (solar cosmic rays, Forbush decreases) were not used in the subsequent analysis. The measured results were broken up into groups corresponding to height ranges of ~100 km. The average intensity was determined within each group of measurements.

The I(h) curve obtained by averaging the measurements from all three satellites appears in Fig. 3. The same figure shows I(h) curves plotted on the assumption of zero and 25% albedos. The experimental points fall between these calculated curves. Thus, the excess radiation in the height range indicated corresponds to α between 0 and 0.25. The experimental points approach the curve with $\alpha = 0.25$ as the height h diminishes. We note that the lunar-surface albedo registered by Luna 9 was 26% [8]. This vertical variation of albedo cannot be explained either on the assumption of an isotropic albedo or with an albedo in which the secondary particles are emitted preferentially normal to the surface of the moon. /114

Protons from the Solar Flares of 28 August and 2 September 1966

Several powerful solar flares accompanied by intense charged-particle fluxes occurred during the transmitting lifetime of Luna 11. The first of these flares took place at 15h 25m Universal Time on 28 August 1966. Figure 4 shows the time variation of the Luna 11 counting rates for the first few communications episodes. The diagrams at the top indicate the satellite's position relative to the moon and the sun and, beginning with 29 August 1966, the orientation of the spin axis in the plane of the satellite's orbit. The counting rates at the three thresholds of the scintillation counter and the No. 1 (BST-9) and No. 2 (SBT-9M) end-window counters, with the unmagnetized and magnetized magnetic filters, respectively, are shown below. As we indicated, these detectors had the same orientation and scanned space in the plane perpendicular to the satellite's axis of rotation. The appropriate symbols are used to mark the times at which the sun and moon entered the fields of the sensors. The experimental points were separated by 6.75-sec intervals. Moscow Time is indicated at the bottom of the figure. The sensor counting levels corresponded to the cosmic-ray background during the first episode on 28 August 1966, 17 hours before the optical flare. The second episode, three hours after the flare, showed a counting-rate increase due to the arrival of solar protons, for the most part of high energy. Then the low-energy protons began to arrive. The proton-intensity increase was observed until 30 August 1966.

During this time, several space vehicles were within the magnetosphere of the earth, and it was possible to make simultaneous measurements of the charged-particle fluxes at several points in space. Figures 5 and 6 show the results [9] of IMP-3 earth-

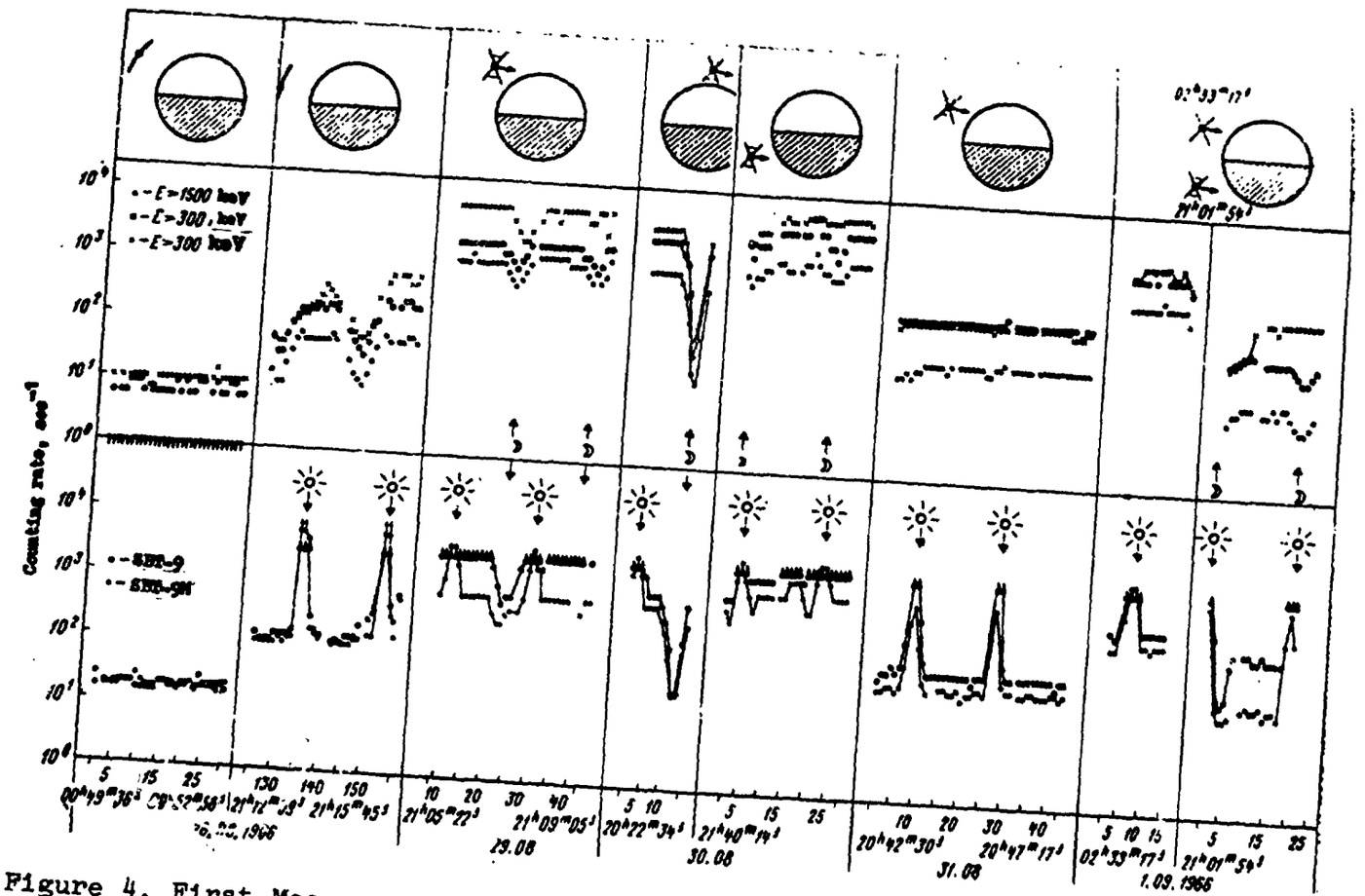

Figure 4. First Measurement Episodes on Luna 11 in the Period from 28 August Through 2 September 1966. The upper row of figures indicates the positions of the satellite on its orbit and the direction of its spin axis; the times at which the sun or moon entered the instrument fields are also noted on the figure.

REPRODUCIBILITY OF THE ORIGINAL PAGE IS POOR.

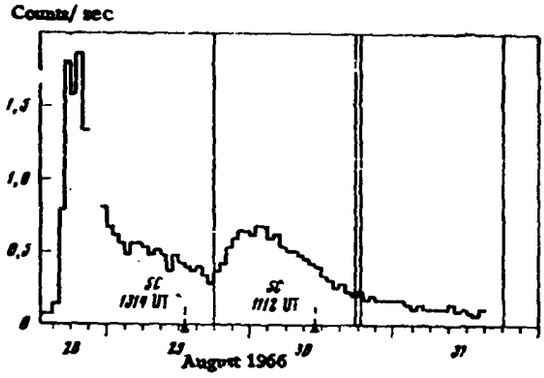

Figure 5. Ionization-Chamber Readings (Protons with E_p > 20 MeV) on IMP-3 Artificial Earth Satellite for 28-31 August 1966. The vertical lines indicate the times of our measurements.

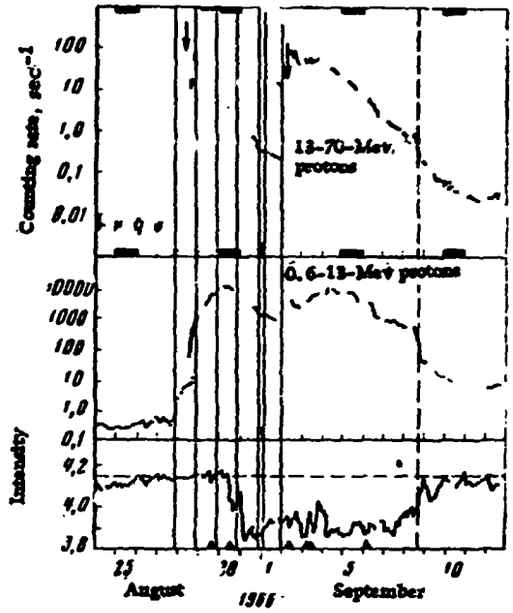

Figure 6. Flux Intensity of Protons with $E_p \sim$ 13-17 MeV and $E_p \sim$ 0.6-13 MeV, as Measured on Pioneer 7 Spaceprobe. Deep River neutron-monitor readings are indicated at the bottom (the times of our measurements are indicated by the vertical lines).

satellite measurements (protons with energy E_p > 20 MeV) and Pioneer 7 data [10] (protons with energies of 0.6-13 MeV and 13-70 MeV). However, these more extended measurements had lower time resolution. (The times of communications with Luna 11 are indicated by vertical lines in Figs. 5 and 6).

Averaged (over the episode) flux intensities of protons with E_p > 1.8 MeV and E_p > 50 MeV over the entire useful life of Luna 11 appear at the top of Fig. 7 [11]. The intensity of protons with E_p > 50 MeV increased strongly on 28 [August] and 2 September. In the latter case, it was two orders above the background value. For protons with E_p > 1.8 MeV, the intensity was more then four orders higher than the background.

Plots of the motion of active regions over the visible disk of the sun (longitude vs. time) and the coordinates of the strongest flares appear lower down on Fig. 7. Values of the K_p index, the readings from a neutron monitor (Moscow), and magnetic storms and polar-cap absorption are given at the bottom of the figure. We see that the flares of 28 August and 2 September occurred in the same active region (McMath-Hulbert 8461). A third, equally powerful flare occurred in this region on 4 September, at the /116

REPRODUCIBILITY OF THE ORIGINAL PAGE IS POOR.

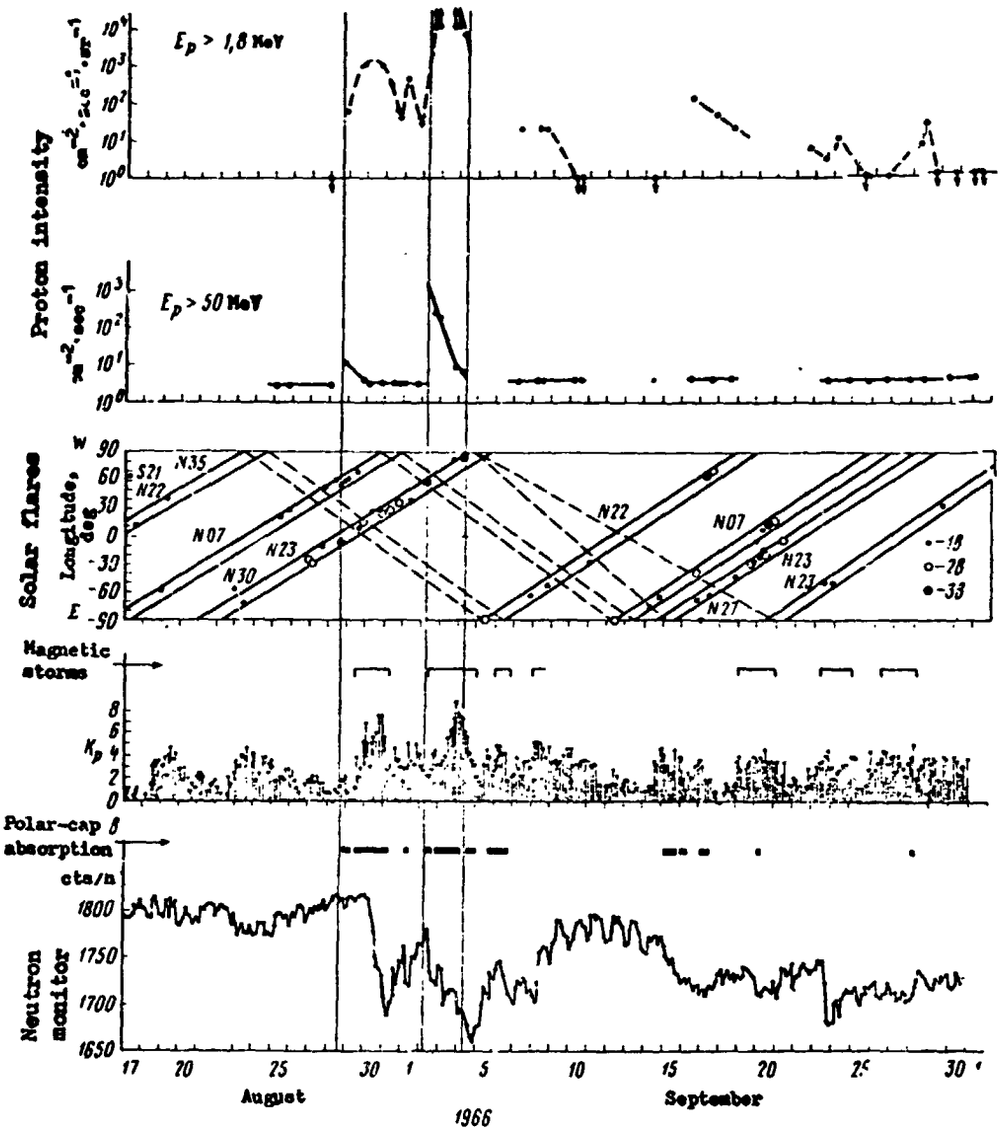

Figure 7. Flux Intensity of Protons with E_p > 1.8 MeV and E_p > 50 MeV, as Measured on Luna 11 During August-September 1966. The figure presents plots of the motion of active regions across the sun's disk, values of the K_p index (three-hour averaging), and neutron-monitor data (Moscow).

limb. The strongest fluxes were observed with the flare of 2 September, which occurred at 55° of western longitude. This is in good agreement with conceptions of proton propagation along lines of force of the interplanetary field that are bent into the shape of Archimedean spirals.

REPRODUCIBILITY OF THE ORIGINAL PAGE IS POOR.

For the second passage of the active regions across the sun's visible disk, the highest activity was registered in the period from 17 through 21 September. Although these flares were similar in strength and location to those of 28 August and 2 September, their proton efficiencies were much lower. We observed an intensity increase only for protons with $E_p > 1.8$ MeV (we should note that these increases may be attributable in part to 27-day recurrent proton fluxes). In all episodes, the intensity of protons with $E_p > 50$ MeV was near the galactic background. The neutron-monitor readings and geomagnetic data also indicate lower efficiencies for the flares of 17 and 21 September.

According to [12], the flare of 2 September was the strongest one observed during the last five years. An estimate of the integral flux of protons with energies above 30 MeV yields a figure on the order of 10^8 cm^{-2}, which corresponds to an absorbed dose of 10-20 rad behind a shield of 3 g/cm^2 [11].

Low-Energy Particles Associated with Forbush Decreases /11

Numerous observations from both ground facilities and space vehicles have shown that a Forbush decrease in cosmic-ray intensity and a geomagnetic disturbance caused by the arrival of a shock wave are observed 1-3 days after powerful solar flares. These effects are usually accompanied by a burst of protons with energies of 1-10 MeV, which are known as "high-energy storm particles" [13, 14]. These bursts often have intensities equaling those of the proton fluxes arriving directly from the flare, but they are of shorter duration (~6 hours) and have softer spectra.

Here we shall consider two cases of low-energy-proton registration on Luna 12, on 13 December 1966 and 6 January 1967; they have an apparent genetic relation to Forbush decreases caused by solar flares. /119

Figure 8 [15] shows the positions of the satellite on its lunar orbit during two measurement episodes on 13 December 1966. The satellite was turning on its axis with a period that amounted to 255.5 ± 0.5 sec on 13-16 December 1966. As we have noted, the axis of counter No. 3 was parallel to the rotation axis, while those of Nos. 1 and 2 and the scintillation counter were perpendicular to the rotation axis. The orientation of the vehicle on 13 December 1966 was determined from data on eclipsing of the sensor fields by the moon. The satellite's spin axis lay in the plane of its orbit, which practically coincided with the plane of the ecliptic, and formed an angle of about 125° with the line to the sun (Fig. 8).

Counters Nos. 1 and 2, which were set perpendicular to the rotation axis, scanned space in the plane perpendicular to the plane of the ecliptic (Fig. 8). Since the collimators of counters

Nos. 1 and 2 had a 60° aperture, the sun did not enter the counter fields.

Figure 9 shows the results of measurements for two communications episodes on 13 December. Analysis of the detector readings establishes that the registered radiation consists basically of a flux of soft protons with energies from 0.5 to 10 MeV. It is seen from Fig. 9 that the rates of counters Nos. 1 and 2 and the scintillation counter vary periodically with the period of the satellite's rotation at the beginning of the second and apparently during the first episode, while that of counter No. 3 remains almost constant. Here, as we see from Fig. 1, the field of the sensor is not eclipsed by the moon as the satellite rotates. Hence the observed modulation of the intensity indicates anisotropy of the radiation being registered. We should note that the readings of counter No. 3 and those of Nos. 1 and 2 at the times at which the axes of the latter two cross the plane of the ecliptic near the antisolar direction (these times are indicated by the vertical lines on Fig. 2) agree within the limits of measurement error. The readings of counters Nos. 1 and 2 in the plane of the ecliptic in directions near the line to the sun are three times higher than the analogous readings in the opposite direction (i.e., the observed anisotropy A ∿ 50%).

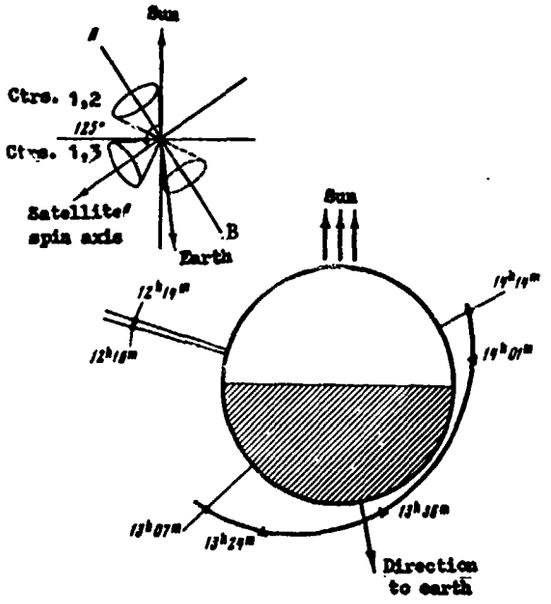

Figure 8. Position of Luna 12 on Orbit During Communications Episode of 13 December 1966, and Orientation of Detectors. Key:
13h 24m — moon begins to eclipse counters oriented perpendicular to satellite rotation axis; 13h 36m — start of eclipse of counter positioned parallel to axis of rotation; 14h 01m — emersion of counters positioned perpendicular to axis of rotation.

Figure 10 shows the angular distribution in the plane perpendicular to the plane of the ecliptic. This distribution is distinguished by the lack of symmetry about the plane of the ecliptic (line AB). The absence of central symmetry eliminates the hypothesis that the registered radiation was trapped in a magnetic inhomogeneity propagating at the velocity of the solar wind. Actually, if the spatial distribution of the radiation trapped by a magnetic inhomogeneity were steady-state, the particle fluxes in opposite directions would have been the same. Another feature of the registered flux is that the shape of the spectrum is retained

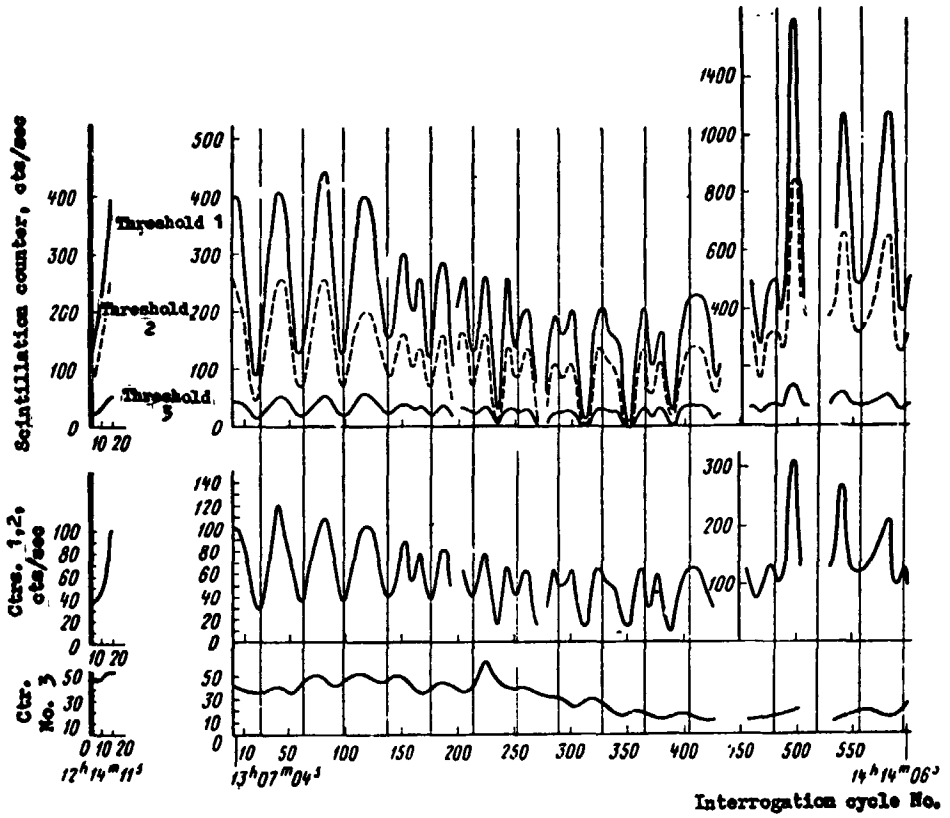

Figure 9. Counting Rates Plotted Against Time During Measurement Episodes of 13 December 1966. Counting rates in counts·sec^{-1} are plotted against the axis of ordinates and the times of the measurements (Moscow Time) against the axis of abscissas, together with the ordinal numbers of the telemetry interrogation cycles; the vertical lines indicate the times at which the detectors crossed the plane of the ecliptic in the antisolar direction.

in all directions in the plane perpendicular to the ecliptic.

Beginning at about the 150th cycle (13h 24m), the readings of the sensors (Fig. 9) oriented perpendicular to the axis of rotation begin to show the effects of eclipsing of their apertures by the moon. Then, starting with about the 400th cycle, the intensity increased within 10 minutes, with an accompanying shift of /120
the anisotropy maximum by ∿100°. The ratio between the intensities of protons in the different energy ranges did not change.

Figure 11 presents data from a neutron monitor (Deep River), measurements of protons with $E_p > 7.5$ MeV from the Pioneer 6 and Pioneer 7 satellites [16] (the relative positions of the Pioneer 6,

Pioneer 7, and Luna 12 satellites relative to the earth are indicated in the top corner of the figure), the K_p index, and certain characteristics of the flares that occurred during the period in question. These data show that the episode of 13 December 1966 was simultaneous with the small Forbush decrease that preceded the larger one. The decrease was accompanied by registration of a magnetic storm on the earth. A 12% Forbush decrease was also registered on Pioneer 7. It is reported in [16] that the Forbush decrease of 13-17 December 1966 was due to the shock waves from the flares of 9 or 10 December. The flares registered on 11 and 12 December were very weak (code I), and not a single optical flare was registered during the 10 hours before the event.

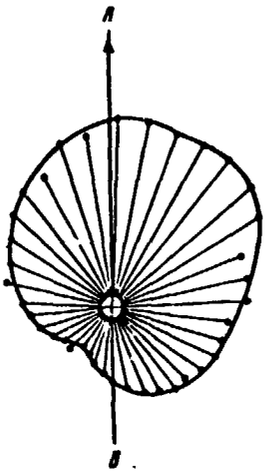

/121

Figure 10. Angular Distribution of Radiation in the Plane Perpendicular to the Plane of the Ecliptic.

Thus, the event of 13 December was characterized by:

1) the absence of any significant solar flare immediately preceding it, one in which the observed proton flux could have been generated;

2) radiation composed of a proton flux with energies from 0.5 to 10 MeV. No flux of electrons with energies above 30 keV was detected within the limits of experimental error (i.e., it did not exceed 20% of the proton flux);

3) coincidence of the proton burst with the beginning of a Forbush decrease and magnetic storm;

4) the presence of a strong flux anisotropy;

5) sharp variations of the direction of the anisotropy;

6) rapid variations of the radiation intensity (through a factor of 3 in $\sim$10 min);

7) no change in the shape of the 0.8-10-MeV proton spectrum on an increase in intensity, i.e., the absence of scatter in the arrival times of protons with different energies; this indicates that the intensity increase was due to passage of the satellite through a long-lived "corotating" particle flux;

8) the angular distribution was studied in the plane perpendicular to the ecliptic and was found to be nonsymmetrical with respect to the latter; the absence of central symmetry excludes

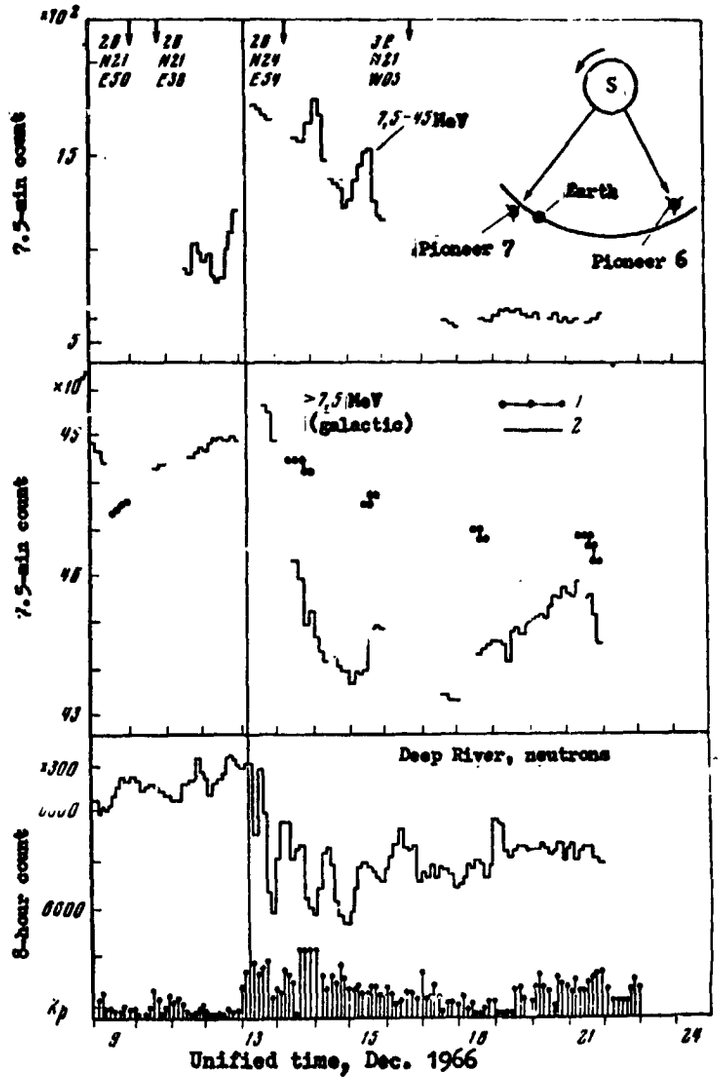

Figure 11. Results of Proton-Flux Measurements on Pioneer 6 and Pioneer 7 Space Vehicles from 9 through 22 December 1966. The figure shows the time variation of the following proton fluxes: top: with energies of 7.5-45 MeV due to Forbush decrease (according to Pioneer 7 data); middle: of galactic origin with energies $E_p > 7.5$ MeV [1) Pioneer 6 data; 2) Pioneer 7 data]. The readings of the Deep River neutron monitor and the K_p index appear at the bottom. The vertical line marks the time of the Luna 12 measurement episode.

REPRODUCIBILITY OF THE ORIGINAL PAGE IS POOR.

the trapped-radiation hypothesis;

9) the shape of the spectrum was found to be the same in all directions. We note that on the basis of the proton flux intensity, this event corresponds to the strongest of the flares studied in [14].

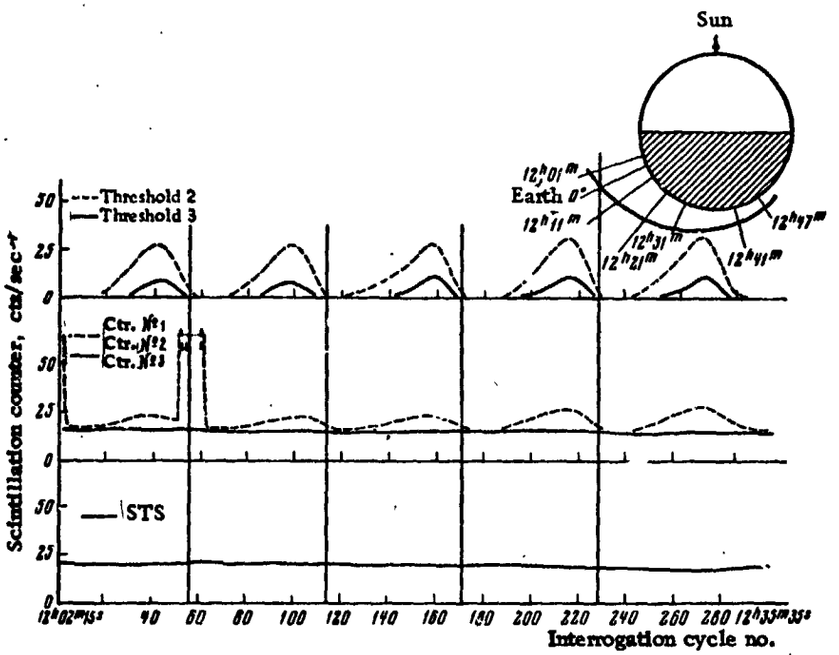

Figure 12. Detector Readings in Measurement Episode of 6 January 1967. The vertical lines mark the times at which the counters crossed the plane of the ecliptic in the antisolar direction; the diagram in the upper right corner indicates the position of the satellite on its orbit during the episode (Moscow Time).

A weaker event having much in common with the previously described event of 13 December 1966 was observed on 6 January 1967. In the measurement episodes of 5 January, the counting rates of the SBT counters were constant at 20% above the background value. The rates of the other counters corresponded to the cosmic-ray background. During the first measurement episode of 6 January, from 9h 17m through 9h 57m Moscow Time, a small ($\sim$3 particles$\cdot$cm^{-2} $\times$ sec$^{-1}\cdot$sr^{-1}) flux of protons with $E_p > 1.6$ MeV, modulated by the rotation of the satellite, was reported. The orientation of the spin axis on 6 January had changed little from the position of 13 December 1966. The anisotropy maximum shifted throughout the episode, and the angle ϕ between this maximum and the direction

REPRODUCIBILITY OF THE ORIGINAL PAGE IS POOR.

B on the plane of the satellite's orbit was closest to the satellite-sun line and varied from 40 to 90°. In the second measurement episode of 6 January, from 12h 02m to 12h 35m (Fig. 12), the intensity of protons with $E_p > 1.6$ MeV was higher by a factor of 6, and the angle ϕ was now 260°. The "off-scale" reading of the SBT counters at the beginning of the episode was due to the registration of solar x-radiation on the sunlit part of the orbit. In this episode, as on 13 December, electrons were not present in the registered radiation.

Solar and geophysical data for 5-11 January indicate that the event of 6 January was also characterized by the absence of strong solar flares during the preceding 15 hours; not a single optical flare of code I or higher was observed during the four hours before the event. As on 13 December, the event of 6 January was followed by a Forbush decrease and a geomagnetic disturbance.

The above features of the events of 13 December and 6 January can be explained by the satellite's passage through a rotating magnetized plasma, which caused the Forbush decrease and was populated by protons. The magnetic-field direction along which the protons propagate preferentially is subject to sharp variations. The protons are not trapped in this region. They either arrive directly from the sun or are accelerated within the region or on its boundaries. /12

Detection of Fluxes of Electrons with Energies $E_e > 30$ keV Associated with Solar Activity

It is known that solar flares that generate proton fluxes are accompanied by strong bursts of x-ray and radio emission. By its nature, this radiation is bremsstrahlung or synchrotron radiation of electrons with energies $E_e > 10$ keV. It is therefore reasonable to expect registration of strong electron fluxes together with the protons at the orbit of the earth. However, they had not been observed in earth-satellite measurements made beyond the magnetosphere prior to 1965. This led to the notion that the electrons lose all of their energy to radiation and remain in the neighborhood of the sun.

In 1965, the Mariner 4 spaceprobe detected radiation that was interpreted as electrons with $E_e > 45$ keV [17]. The flux intensities in the three registered cases were ~80, 58, and 5 $cm^{-2} \cdot sec^{-1} \cdot sr^{-1}$, respectively. The identification as electron radiation was based on comparisons between the readings of two different detectors: an end-window counter sensitive to electrons with $E_e > 45$ keV and protons with $E_p > 670$ keV and a semiconductor detector sensitive to protons with $E_p > 45$ MeV and insensitive to electrons. Electrons of solar origin were also detected by Anderson and Lin

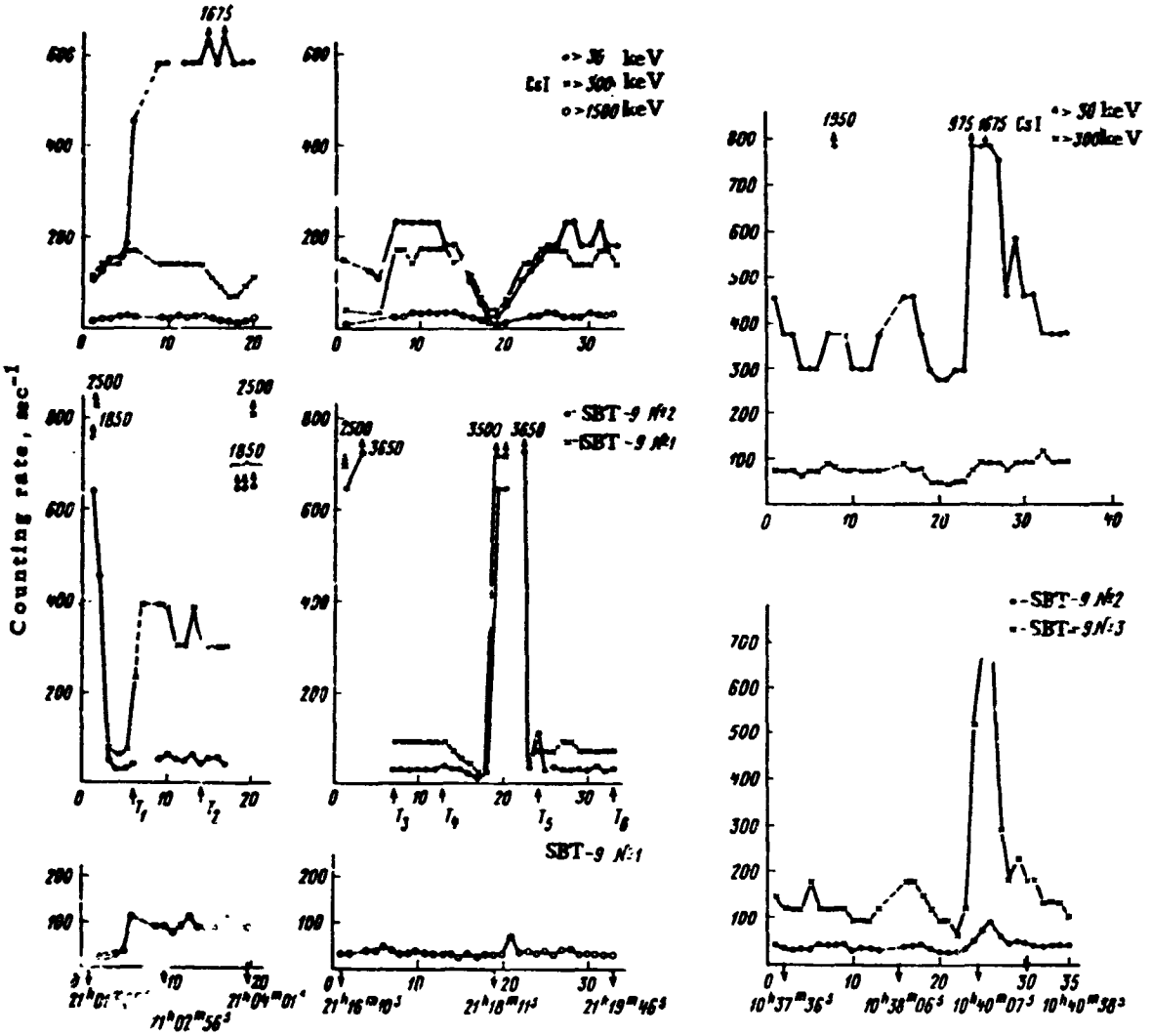

Figure 13. Examples of Sudden Increase in Electron Flux in Near-Moon Space. 21h 02m - 21h 01m, 21h 16m-21h 20m — 1 September 1966; 10h 37m - 10h 41m — 8 September 1966.

[18] in IMP-3 data obtained from a combination of an end-window counter with a scattering foil and a similar counter without the scatterer. Analysis of the readings from these detectors made it possible to estimate the electron fluxes at $E_e > 30$ keV. /124

The magnetically filtered end-window counters in the instrument packages on Luna 11 and Luna 12 were the first to provide reliable registration of electrons with energies $E_e > 30$ keV against the background of a strong low-energy-proton flux. Like the protons, the electrons were registered for a long time after the flare of 28 August (see Fig. 4).

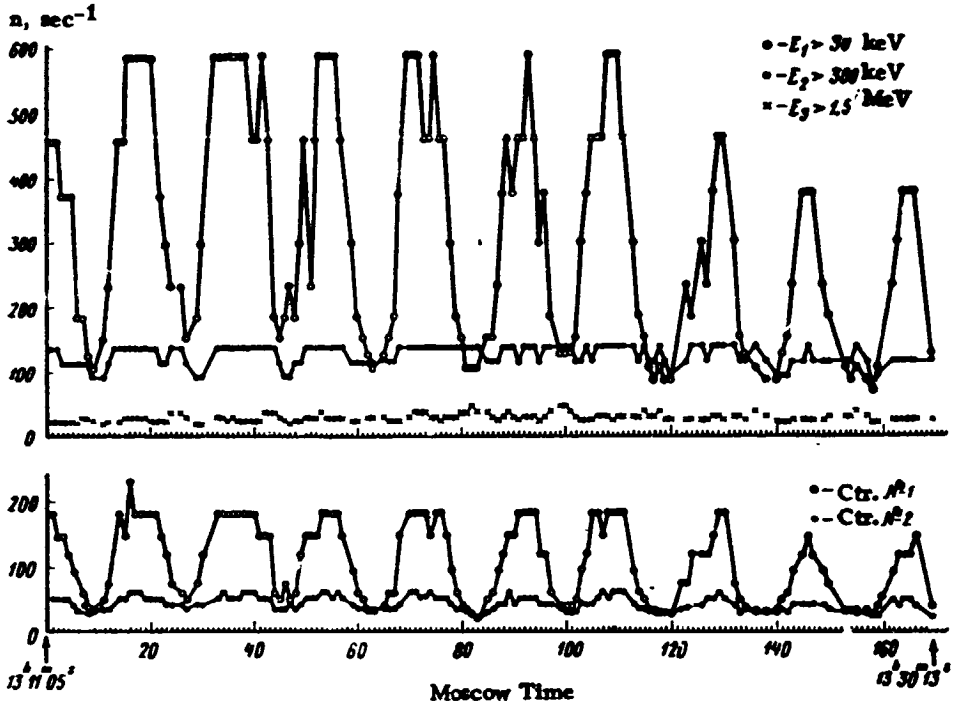

Figure 14. Communications Episode of 8 September 1966, During which a Long-Lived Flux of Electrons with E_e > > 40 keV was Registered in Near-Moon Space.

Let us consider two cases in which the electron flux greatly exceeded the proton flux [2]. The scintillation counter and counters Nos. 1, 2, and 3 registered soft radiation (protons with $E_p \sim$ 1-2 MeV) at a level several times the cosmic-ray background up to time T_1 in a episode that began at 2h 01m on 1 September (Fig. 13). The sharp increases in the counting rates of counters Nos. 1 and 2, which were repeated with a period of 122 sec (as indicated by the arrows in Fig. 13), were caused by registration of solar x-radiation. Because of its high threshold, the scintillation counter could not register this radiation. At time T_1, the Nos. 1 and 3 ЗВТ-9 counters (with unmagnetized ferrites) and scintillation counter threshold I registered a sharp increase in counting rate. Considering the time constants of the intensimeters, it can be affirmed that the intensity buildup time did not exceed 10 sec. The rate increase was obviously due to electrons with energies E_e > 30 keV. The electron flux intensity was 1700 particles/cm²·sec·sr. In a measurement episode held 16 minutes later, the electron flux intensity had dropped by a factor of 5-7. Thus, the electron burst lasted no longer than 16 min. On the right in the same figure, we have yet another example of a short-term (~25 sec) electron burst of 8 September 1966.

It should be noted that the phenomenon was observed when the Luna 11 was on the dark side of the moon and not directly exposed to the sun, so that the possibility of registration of electromagnetic radiation from the sun is excluded. A 20-minute measurement episode during which the satellite was in the shadow of the moon occurred 2.5 hours later. During these 20 minutes, the first- and second-threshold counting rates of the scintillation counter and the rates of counters Nos. 1 and 2 varied periodically and in phase, with the period of the variation coinciding with the period of rotation of Luna 11 on its axis (Fig. 14). The intensity modulation was due to partial blockage of the counter solid angles by the moon. At the maximum, the registered flux intensities of electrons with $E_e > 30$ keV were on the order of 800 $cm^{-2} \cdot sec^{-1} \cdot sr^{-1}$.

The features of the first two of the electron-resistration instances considered above to which we wish to draw attention are as follows: 1) the rapid increase in the electron flux (during 10 sec) at a nearly constant proton flux; 2) the simultaneous change in the fluxes of electrons with energies $E_e > 30$ and $E_e > 60$ keV (scintillation counter threshold I).

Two models can be proposed to explain these features:

1. A certain source, the distance to which is no greater than $5 \cdot 10^5$ km, so that the velocity scatter does not result in an arrival-time scatter exceeding 10 sec, begins to emit electrons of different energies simultaneously. The magnetosphere might be such a source.

During the episodes of 1 September, we were able to register electrons moving in the tail of the earth's magnetosphere, i.e., the sun-earth-moon angle was near 180°. In the 8 September episode, on the other hand, this angle was 90°, so that electrons propagating along lines of the geomagnetic field were unable to reach the vicinity of the moon. These sudden increases in the electron fluxes are in many respects similar to the electron bursts that Anderson observed on the sunlit side of the magnetosphere in front of the standing wave [19]. The bursts of electrons with $E_e > 45$ keV that are reported in the present paper /125
lasted no more than a few minutes, and their intensities reached $3 \cdot 10^4$ $cm^{-2} \cdot sec^{-1} \cdot sr^{-1}$. In the opinion of the authors of this paper, the electrons originated in the region of the standing shock wave and propagated away from it along lines of force of the interplanetary field. The nature of this phenomenon has not been adequately studied.

2. The electron fluxes persisted for a considerable length of time. On the other hand, the rapid buildup and decline of the flux were due to its direct localization in a certain magnetic structure in motion at the velocity of the solar wind, which

accounts for the rapid and simultaneous variations in the counting rate for electrons with $E_e > 30$ and $E_e > 60$ keV. The dimensions of the electron-localization region can be estimated at 10^4-10^5 km from its direction of motion.

CONCLUSION

Luna 10, 11, and 12 studies of corpuscular radiation substantially expanded our knowledge of the physical properties of the space ar[illegible] the moon and the solar cosmic rays, and of the influence c[illegible] the moon on the propagation of charged-particle fluxes. It has been shown that the moon has no magnetosphere and no trapped charged particles; the intrinsic radioactivity of the moon is low-level, and the radiation environment in its vicinity is determined basically by the flux of galactic and solar cosmic rays. On passage of the moon through the region of the "tail" of the earth's magnetosphere, fluxes of low-energy particles were registered, indicating the existence of this "tail" out to distances of $60R_e$. Investigation of the vertical variation of cosmic-ray intensity at the surface of the moon made it possible to determine the albedo of its surface for penetrating radiation. The intensities of the /126
proton and electron fluxes from solar flares, their angular distributions, and the effects of the moon on the fluxes of low-energy particles were measured. New data were obtained on the composition and properties of the low-energy proton fluxes accompanying Forbush decreases. Strong fluxes of >30 keV electrons associated with the flare activity of the sun were detected.

Research on near-moon space has been continued, both on Soviet ALS (Luna 14) and on American vehicles (Explorer 35).

REFERENCES

1. N.L. Grigorov, V.I. Maduyev, S.L. Mandel'shtam, N.F. Pisarenko, I.A. Savenko, and I.P. Tindo. Dokl. Akad. Nauk SSSR, 1966, Vol. 170, 3, 567.
2. N.L. Grigorov, V.N. Lutsenko, V.L. Maduyev, N.F. Pisarenko, and I.A. Savenko. Kosmicheskiye Issledovaniya, 1967, Vol. 6, 807.
3. S.N. Vernov, A.Ye. Chudakov, P.V. Vakulov, Yu.I. Logachev, and A.G. Nikolayev. Dokl. Akad. Nauk SSSR, 1960, Vol. 130, No. 3.
4. Sh.Sh. Dolginov, Ye.G. Yeroshenko, P.N. Zhudov, and N.V. Pushkov. Dokl. Akad. Nauk SSSR, 1966, Vol. 170, 574-577.
5. N.F. Ness. Space Res., IX, 678, North Holland Publ. Comp., Amsterdam, 1969.
6. N.L. Grigorov, V.L. Maduyev, N.F. Pisarenko, and I.A. Savenko. Kosmicheskiye Issledovaniya, 1966, Vol. IV, No. 6.
7. N.L. Grigorov, V.G. Kurt, V.N. Lutsenko, V.L. Maduyev, N.F. Pisarenko, and I.A. Savenko. Paper Presented at All-Union Conference on Cosmic Rays. Novosibirsk, 1967 (in preparation.)

8. S.N. Vernov, P.V. Vakulov, Ye.V. Gorchakov, Yu.I. Logachev, G.P. Lyubimov, L.G. Nikolayev, and N.V. Pereslegina. Dokl. Akad. Nauk SSSR, 1966, Vol. 169, 5, 1044-1047.
9. K.A. Anderson and R.P. Lin. Solar Phys., 1967, Vol. 1, 3.
10. C.I. Fan, M. Pick, P. Ryle, I.A. Simpson, and D.R. Smith. J. Geophys. Res., 1968, Vol. 73, 5.
11. N.L. Grigorov, V.N. Lutsenko, V.L. Maduyev, N.F. Pisarenko, and I.A. Savenko. Kosmicheskiye Issledovaniya, 1967, Vol. V, 6, 807.
12. A.J. Masley and A.D. Goedeke. Can. J. of Phys., 1968, Vol. 46, 5766.
13. D.A. Bryant, L. Cline, U.D. Desai, and F.B. McDonald. J. Geophys. Res., 1963, Vol. 68, 10, 3109.
14. K.A. McCracken, U.R. Rao, and R.P. Bukata. J. Geophys. Res., 1967, Vol. 72, 17, Part II.
15. N.L. Grigorov, V.G. Kurt, V.N. Lutsenko, V.L. Maduyev, N.F. Pisarenko, and I.A. Savenko. Kosmicheskiye Issledovaniya, 1969, Vol. VII, No. 1.
16. R.P. Bukata, K.A. McCracken, and U.R. Rao. Can. J. Phys. 1968, Vol. 46, 10.
17. I.A. Van Allen and S.M. Krimigis. J. Geophys. Res., 1965, Vol. 70, 23.
18. K.A. Anderson and R.P. Lin. Phys. Rev. Lett., 1966, Vol. 16, 24.
19. K.A. Anderson. J. Geophys. Res., 1968, Vol. 73, 7.

N75 13717

LOW-ENERGY PROTONS OF SOLAR ORIGIN AND INVESTIGATION OF THE INTERPLANETARY MEDIUM

(Translation of "Protony malykh energiy solnechnogo proiskhozhdeniya i issledovaniye mezhplanetnoy sredy.")

V. N. Lutsenko and N. F. Pisarenko

ABSTRACT

A review of experimental data on low-energy solar protons is presented. A phenomenological classification of the fluxes of these particles is suggested. Contemporary model conceptions of the propagation of low-energy proton fluxes are examined, along with information that has been obtained on the properties of the interplanetary medium from study of solar-proton fluxes. With 4 tables, 19 illustrations, and 50 source citations.

LOW-ENERGY PROTONS OF SOLAR ORIGIN AND INVESTIGATION OF THE INTERPLANETARY MEDIUM

/127

V.N. Lutsenko and N.F. Pisarenko

The study of solar cosmic rays is, among others, an important source of information on the interplanetary medium. Fluxes of charged particles accelerated at the sun during chromospheric flares come under the influence of the interplanetary magnetic fields as they propagate in interplanetary space. Thus, the various characteristics of the solar cosmic rays bear the imprint both of the physical processes taking place in the flares and of the processes in the interplanetary medium.

Historically, the study of solar cosmic rays began with the highest-energy particles (100-1000 MeV), which can be measured at the surface of the earth and in the stratosphere. A review of data pertaining to this high-energy part of the solar cosmic-ray spectrum will be found in [1-4]. Measurements within the earth's magnetosphere have yielded no substantial information on lower-energy solar cosmic rays. At the same time, protons with $E < 10$ MeV should carry most of the energy of charged particles accelerated at the sun (95-99.7% of the energy of protons with $E > 0.5$ MeV is contained in the interval of the energy spectrum from 0.5 to 10 MeV). Interest in low-energy solar cosmic rays also arises out of the fact that because of their small Larmor radii, these particles are sensitive to structural details of the interplanetary field with scales of 10^4-10^5 km. Study of the particle-flux characteristics as functions of time also yields important information on the large-scale configuration of the magnetic field, especially in the region near the sun, which is not yet accessible to direct investigation with spaceprobes.

The possibility of direct study of low-energy solar cosmic rays made its appearance comparatively recently with the launching of artificial earth satellites (AES) and spaceprobes (SP) to beyond the limits of the earth's magnetosphere. Previously, most of our information on low-energy solar rays had been obtained by indirect methods, from geophysical effects that appear in association with the incursion of the strongest solar-particle fluxes into the magnetosphere. Investigation of the x-ray and radio emission of solar flares indicated that strong fluxes of electrons with energies from 10 to 100 keV are generated in the atmosphere of the sun. Although the energy losses of these electrons to radiation are very large, we should expect at least some of them to escape into interplanetary space and, consequently, be subject to registration in the neighborhood of the earth. Indirect methods yielded rough estimates of the energies and intensities of the low-energy solar cosmic rays. But it is obvious that the possibilities of indirect methods are limited. They are capable of

registering only the strongest events and do not yield sufficiently accurate information on the composition, energy spectra, and mode of propagation of the solar cosmic rays in space.

Systematic study of the solar cosmic rays outside of the earth's magnetosphere was begun in 1963-1964. The greatest interest attaches to the experiment carried out on AES and SP (IMP-1, IMP-3), Mariner 4, Zond 3, Venus 2, Venus 4, Pioneer 6, Pioneer 7, Explorer 33, Explorer 35, Luna 11, and Luna 12. These experiments showed that near-earth space is occupied during much of the /128 time by streams of low-energy solar protons and electrons. Thus, Fan et al. [5] report that even in a year near the solar activity minimum, protons with E > 0.6 MeV exceed the background level during 40 to 80% of the time. There is an extremely wide variety of phenomena associated with low-energy solar cosmic rays.

In the present survey, we shall confine ourselves to the solar cosmic-ray proton component in the energy range from 0.5 to ∿10 MeV. These limits are quite arbitrary, and are dictated chiefly by the properties of the measurement method used.

As for low-energy electrons (E > 30 keV), there are far fewer reliable measurements outside of the magnetosphere than in the case of protons. This is due in part to the methodological difficulties that arise in registration of electrons against the background of a strong proton flux with the comparatively simple apparatus that was used [6]. Use of magnetic-analysis methods is highly promising in this respect [7].

Low-energy proton fluxes can be classified phenomenologically into three basic categories on the basis of their relation with various forms of solar activity.

1. A certain minimal background proton flux, which is observed during periods of low solar activity (for example, in the absence of active regions on the sun's visible disk). This background varies slowly with the general level of solar activity. It remains constant for about a year around the solar activity minimum.

2. Proton bursts following directly after solar flares. These bursts are characterized by a rapid intensity buildup and an exponential decrease with a time constant of ∿1 day.

3. Bursts of low-energy protons lasting from 6 hours to 2 days, for which there is no generating flare or the time interval from flare to burst exceeds 0.5 day. These bursts are due to passage through certain regions of the interplanetary magnetic field in which long-lived proton fluxes have been localized.

The analysis of experimental data to be given below (in accordance with the above classification of the fluxes) pertains

basically to 1964-1967, a period of minimal and rising solar activity. It may be found that the properties and relationships observed during these years are not altogether applicable at other times during the solar cycle.

The broad range of problems associated with the generation of cosmic rays on the sun is beyond the scope of the present review and is therefore not treated.

The Background of Low-Energy Protons

Experiments performed during 1964-1967 on spaceprobes outside of the earth's magnetosphere showed that a certain background flux of low-energy protons and alpha particles exists during periods of low solar activity and varies slowly with time. After increases associated with the passage of active regions across the sun's disk, the flux reverts to the background value, which remains practically constant for several months. In 1966, the background flux level prevailed during 20% of the time.

Figure 1 shows the differential spectrum of the background protons and alpha particles for the period around the solar activity minimum [8]. At energies $E \geq 30$ MeV/nucleon, the background spectrum merges into the familiar galactic cosmic ray spectrum. A characteristic feature of the spectrum is the "knee" in the range of 10-100 MeV/nucleon, with a large negative slope at lower energies.

Tables 1 and 2 present the results of direct measurements /129
of the intensity, spectrum, and heliocentric radial gradient of the background around the solar-activity minimum and during its increase. We note that these data are not distinguished by high accuracy and do not always agree with one another. This results from the major methodological difficulties encountered in measuring such small fluxes against the background of the much larger flux of penetrating galactic cosmic rays. Fan et al. [5] stressed that it was possible to measure the background only by virtue of the use of large-area detectors surrounded by anticoincidence shielding.

One of the fundamental questions that arise in study of the low-energy cosmic-ray background is the question as to its origin. Are these protons and helium nuclei emitted by the sun, or do they come from interstellar space like the high-energy cosmic rays? It would appear that this question could be answered by study of the effects of solar activity and solar modulation on the intensity of the background. If the background is galactic in nature, it should have intensity maxima during solar-activity minima and vice versa. If it is of solar origin, its intensity should vary like the mean level of solar activity. The measurements of Simp- /130
son's group [8] indicated that the helium-nucleus intensity rose in the period from 1964 to 1965 and fell from 1965 through 1966

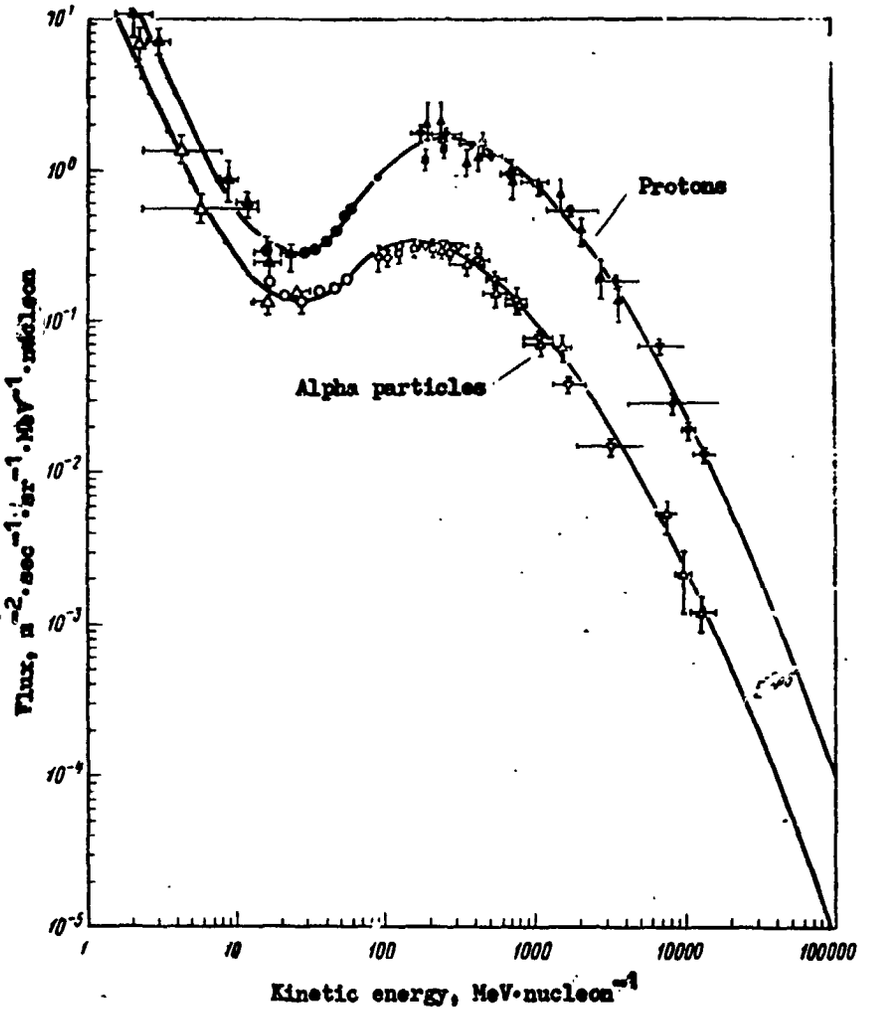

Figure 1. Differential Spectra of Background Protons and Helium Nuclei Around the 1965 Solar Activity Minimum.

in much the same way as that of high-energy galactic cosmic rays. An intensity increase was observed for protons from 1964 through 1966 (see Table 1).

Measurements of the heliocentric radial gradient (see Table 2) and the anisotropy of the background flux have a direct bearing on the origin of the background. In 1965, according to [11-13], the radial gradient of protons with E = 1-5 MeV was positive, i.e., intensity increased with distance from the sun. No direct measurements of the radial gradient were made in 1966, but the angular distribution of the flux was investigated for the first time. It was found that the background-proton flux has a nearly isotropic angular distribution. In 1966, the anisotropy maximum was nearly aligned with the direction away from the sun and its

TABLE 1. EXPERIMENTAL DATA ON THE LOW-ENERGY PROTON BACKGROUND

Time of Measurements	Space Vehicle	Instrument Used	Energy, MeV	Background Intensity, $cm^{-2} \cdot sec^{-1} \cdot sr^{-1}$	Differential Proton Spectrum, $cm^{-2} \cdot sec^{-1} \cdot sr^{-1} \cdot MeV^{-1}$	Source
Nov.-Dec. 1964	OGO-A	n-p detector telescope with anticoincidence shield	1-5	$1.3 \cdot 10^{-3}$	$17E^{-2.4}10^{-4}$	[8]
May-Nov. 1965	OGO-A	Same	1-5	$3.2 \cdot 10^{-3}$	$16E^{-2.4}10^{-4}$	[8]
Same	Gond 3	Single n-p detector	1-5	$4 \cdot 10^{-1}$	—	[9]
July 1966	Pioneer 6	n-p-detector telescope with anticoincidence shield	0.6-13	$1.7 \cdot 10^{-2}$	—	[5]
Jan.-March 1966	Pioneer 7	Same	0.6-13	$3.5 \cdot 10^{-2}$	$140E^{-2.8}10^{-4}$	[5,8]
Aug.-Dec. 1967	Venus 4	Single n-p detector	1-5	$8 \cdot 10^{-2}$	—	[10]

TABLE 2. RADIAL LOW-ENERGY-PROTON GRADIENT

Time of Measurement	Space Vehicle	Distance from Earth's Orbit, a.u.	Energy, MeV	Radial gradient, % per a.u.	Source
1965	Mariner 4	+0.56	0.5-11	570	[11]
1965	Mariner 4	+0.56	1-15	500	[12]
1965-1966	Zond 3-Venus 2	-0.13+0.27	1-5	1300	[13]
1965	Zond 3-Venus 2	-0.13+0.1	1-5	220	[13]

maximum was ~8% for E = 0.6-13 MeV (August 1966) [5] and 0.18% for E_p = 7.5=45 MeV (December 1965-November 1966) [14]. According to Rao et al. [14], this indicates that the radial gradient was negative in 1966, and that the sign change of the gradient took place somewhere in the range from 10 to 100 MeV. The aggregate of experimental data on the time variation of intensity and on the radial background gradient can be explained by assuming that the background was of galactic nature in 1954-1965 and the increase in proton flux in 1966 and the sign change of the gradient were due to solar protons that appeared as a result of the sharply increased flare activity of the sun. The helium-nucleus background was basically of galactic origin throughout the entire 1964-1966 period, since the relative content of helium nuclei in solar cosmic rays is much lower than it is in the galactic rays. We note that S.N. Vernov et al. [13] proposed a different explanation for the positive gradient of 1965. According to their hypothesis, solar protons, moving along a regular interplanetary magnetic field, accumulate in a region beyond the orbit of Mars, where the field becomes turbulent, and create a positive gradient during the solar activity minimum. In this explanation, the turbulent region must be credited with the ability to hold protons for time intervals longer than one year. /131

We should note that the question as to the nature of the low-energy proton background is of great fundamental importance. Thus, if it is assumed that the part of the spectrum in Fig. 1 below 30 MeV is of galactic nature, the spectrum can be extended beyond the limits of the solar system by applying the theory of isotropic solar modulution [15] to it. The [illegible]ulated spectrum increases so steeply with decreasing energy [illegible] requires a review of the hitherto accepted value (~1 e[illegible] cosmic-ray energy density in interplanetary spac[illegible] sociated question as to the stability of the galactic magneti[illegible]ld [12]. Apparao [16] suggested that this difficulty be eli[illegible]ated by means of an anisotropic-modulation hypothesis. On the [illegible]ther hand, there is reason to assume that the Larmor radius of the particles in this energy range is much smaller than the magnetic inhomogeneities in the

modulation region, so that these particles can reach the inner solar system unimpeded by moving along the lines of force of the interplanetary magnetic field. Another possibility is that the proton background is due at least in part to decay of solar neutrons [8].

It must be stressed in conclusion that the early experimental data now available are not sufficient for final resolution of the question as to the origin and nature of the background. This will require further research on the intensity, composition, anisotropy, radial gradient, and other characteristics over longer periods of time and in a wider interval of distances from the sun.

Proton Bursts from Solar Flares

Strongly time-dependent structures are usually superimposed on the slowly varying background of low-energy protons: bursts following directly after solar flares (after a time on the order of the time of flight from the sun) and rapid flux variations associated with passage of the SP through quasistationary fluxes localized in magnetic regions. Under this heading, we shall examine events of the first type. Flare bursts of low-energy protons are, at the moment, the most thoroughly studied phenomenon for the low-energy solar cosmic rays, since the effects are large and easily registered by comparatively simple apparatus.

Some information on low-energy flare protons has been obtained by indirect methods: from measurements of the absorption of cosmic radio noise in the polar caps [17, 18] and in experiments on the scattering of radio waves in the ionosphere [19]. These measurements have been made continuously over several years, and this accounts for their value.

Direct observations of solar-flare protons in the energy range from 0.2 to 10 MeV were begun in 1960 with the rocket experiments of Ogilvie et al. [20] over Fort Churchill. The first measurements of low-energy protons beyond the magnetosphere were carried out by Bryant et al. [21] on the Explorer 12 satellite in 1961. A stream of protons with E > 3 MeV from one flare of 28 September 1961 was observed in these experiments; the flux reached 10^3 $cm^{-2} \cdot sec^{-1} \cdot sr^{-1}$. Considerable flux anisotropy was observed during the intensity rise. A review of several pre-1966 studies of low-energy solar-flare protons will be found in the book by L.I. Dorman and L.I. Miroshnichenko [3]. Among these, those of greatest interest are the extended-term measurements made on Zond 3, Venus 2 and 3 [9], Mariner 2 [22], and Mariner 4 [11] in 1964-1965. For the first time, the solar cosmic rays were studied simultaneously from several SP at distances in the millions of kilometers. /132

In 1966-1967, improved instruments carried on a number of spaceprobes made it possible to acquire a large amount of new

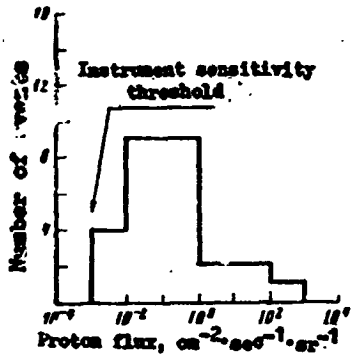

Figure 2. Intensity Distribution of Flare Bursts of Protons with E = 7.5-45 MeV.

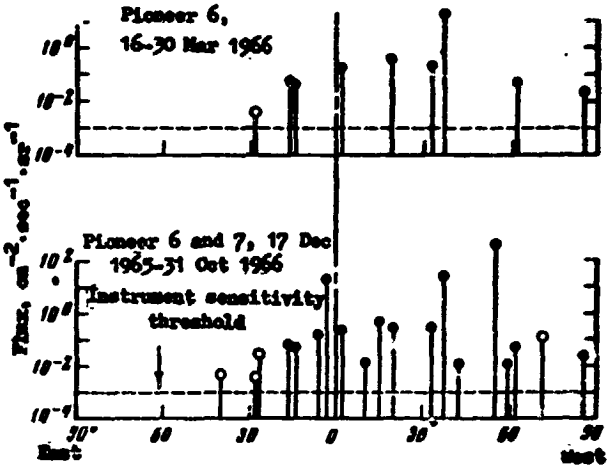

Figure 3. Maximum Fluxes of Protons with E = 7.5-45 MeV and the Longitudes of the Corresponding Flares According to Pioneer 6 and 7 Data.

information on the frequency of occurrence, spectra, and angular and spatial distributions of protons from solar flares. These measurements, along with investigation of the interplanetary magnetic field and plasma, led to the appearance of qualitatively new model conceptions of the generation and propagation of solar cosmic rays.

According to McCracken et al. [23], 80% of code 3 and 2B flares during the period of rising solar activity in 1966 generated fluxes of protons in the range from 7.5 to 45 MeV. Figure 2 shows the intensity distribution of the flare bursts for 39 investigated events. The smallest flux registered by the instruments in this study was 10^{-3} $cm^{-2} \cdot sec^{-1} \cdot sr^{-1}$. The number of events increases as their intensity diminishes. It appears that a further increase in the sensitivity of the instruments would make it possible to register a larger number of even weaker events. These data can be regarded as indicating that no unusual conditions are required for generation of low-energy protons: it can evidently occur in the majority of flares.

Figure 3 [28] illustrates the well-known predominance of effects from flares on the western part of the sun's disk. Most of the registered events are due to western flares. Figure 3 also shows that the strongest proton fluxes are observed when the flare occurs in the longitude range from 0 to 50°W.

TABLE 3

Energy, MeV	Time of Flight [5], min	Rise Time [5], min	Calculated Time of Flight, min
0.6-13	152-215	70-300	600-270
13-70	35-119	20-48	25-60

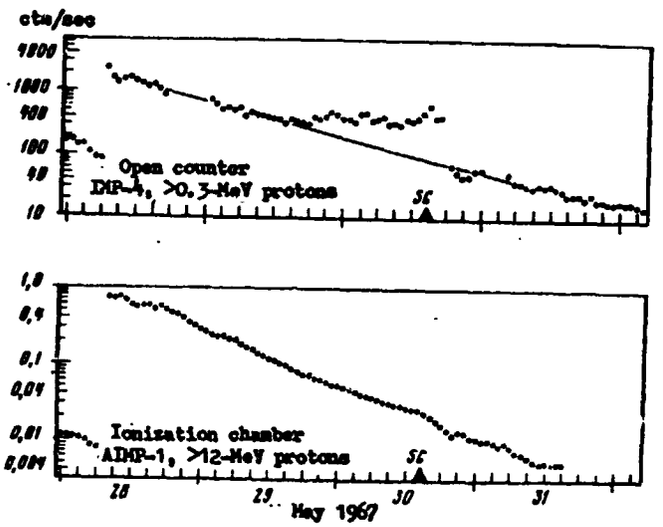

Figure 4. Intensity-vs.-Time Curve of Protons from Flare of 28 May 1967.

Examples of the time variation of proton intensity for certain flares appear in Figs. 4 and 5. In the simplest cases, the time interval between the maximum of the solar radio and x-ray burst and the appearance of the first protons is of the same order as the time of flight from the sun to the spacecraft. Then the intensity increases rapidly to its maximum. The rise time is determined both by the time for which protons are emitted from the source and by the dispersion of the arrival times, which is governed by the limited width of the registered proton-velocity range. We note that selection of the electromagnetic-radiation burst as a time origin is somewhat arbitrary. Table 3 gives the characteristic arrival and buildup times for proton fluxes that have been observed for the energy ranges 0.6-13 MeV and 13-70 MeV [5]. It also gives theoretical times of flight along lines of force of the interplanetary field from the outer corona to the observation point. Considering the great width of the energy ranges, the existing uncertainty as to the time of emission, and the occasional inaccuracies in identification of the flare, the agreement between the experimental and calculated times must be considered good. /133

The decrease in the flux is usually slower than the increase. For large solitary flares and $E_p \sim 10$ MeV, the exponential law $I(t) = J_0 e^{-t/\tau_0}$ with $\tau_0 = 0.5$-1.5 day is followed closely. Thus, for

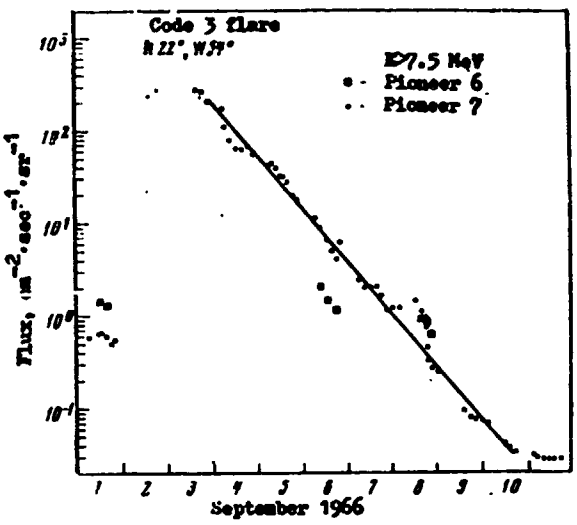

Figure 5. Intensity-vs.-Time Curve of Protons with E > 7.5 MeV from Flare of 2 September 1966.

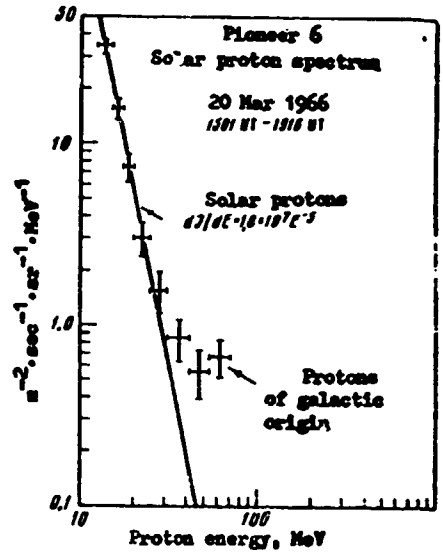

Figure 6. Differential Spectrum of Protons from Flare of 20 March 1966 According to Pioneer 6 Data.

the event of 2 September 1966 (see Fig. 5), an exponential decrease is observed through $9.2\tau_0$ (τ_0 was equal to 18.1 hours). The intensity decrease is sometimes more complex in nature for lower energies. /134

The intensity rise has been observed to be very slow for certain flares (~10 hours) [23]. In these cases, identification of the corresponding flare was difficult, and the flares themselves had a tendency to be located on the eastern part of the solar disk. Irregular intensity variations are often superimposed on the time curve of the burst.

Reliable data on the flare-proton spectrum are available only for $E_p \geq 3$ MeV. According to McCracken et al. [23], the integral spectrum has a power-law form in the 7.5-45 MeV range: $I(E \geq E_0) \sim E^{-\gamma}$ with the exponent γ = 3-4. According to Fan et al. [5], the differential specrrum also follows a power law with γ = 5 in the 3-30-MeV range (Fig. 6).

It has been known since the measurements of Bryant et al. [21] on the Explorer 12 satellite in 1961 that the flux of low-energy protons is substantially anisotropic in the initial phase of a flare. The first systematic investigation of the angular distributions of the flux in the plane of the ecliptic were made on the Pioneer 6 and 7 spaceprobes. Proton intensities were measured in

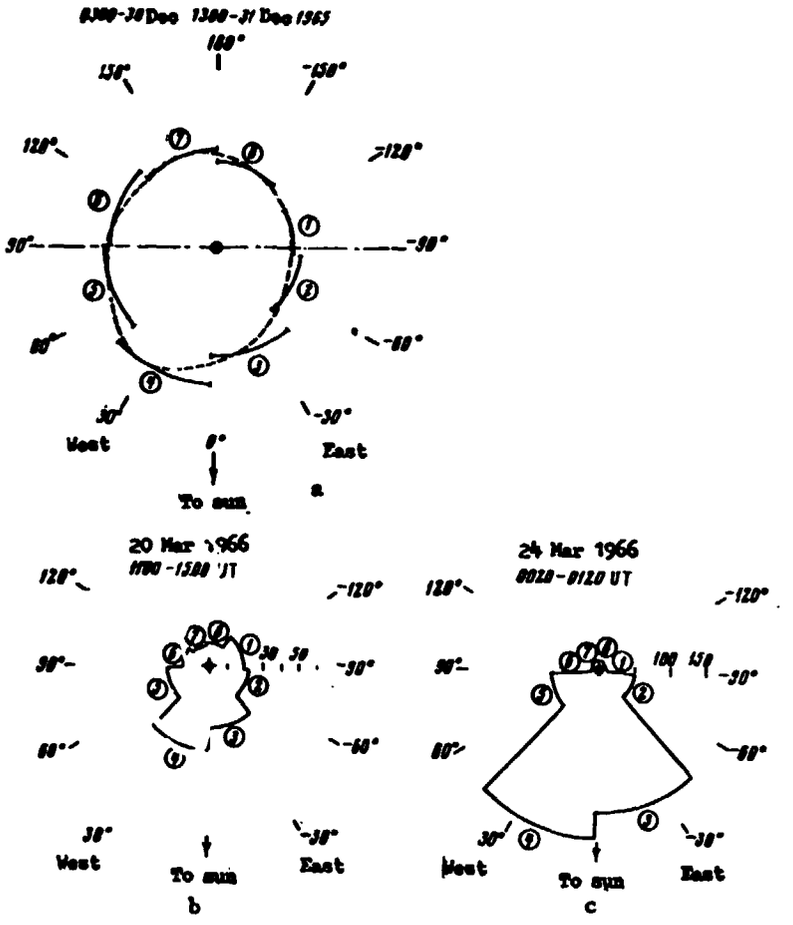

Figure 7. Angular Distributions of Proton Intensity in the Plane of the Ecliptic with Averaging of Data over 34 Hours (a), 4 Hours (b), and 1 Hour (c) (Pioneer 6). 1-8) Sector numbers.

four [23] or eight [5, 24] angle sectors whose positions were fixed relative to the line to the sun. Figure 7 presents the corresponding angular-distribution diagrams obtained by averaging the data over several hours [5, 24]. The diagrams of Fig. 8 indicate the time variation of the angular distributions. It is seen that the flux is strongly anisotropic and that the direction of the maximum changes rapidly (by up to 90° in ten minutes). It follows from the diagram with 10-minute averaging that the flux is concentrated in a narrow angle range at any given point in time, and that the comparatively broad angular distributions in Fig. 7 are obtained as a result of time averaging of the rapid directional variations. Simultaneous measurements of the interplanetary magnetic field have shown that there is a strong correlation between the direction of the angular-distribution maximum and that of the

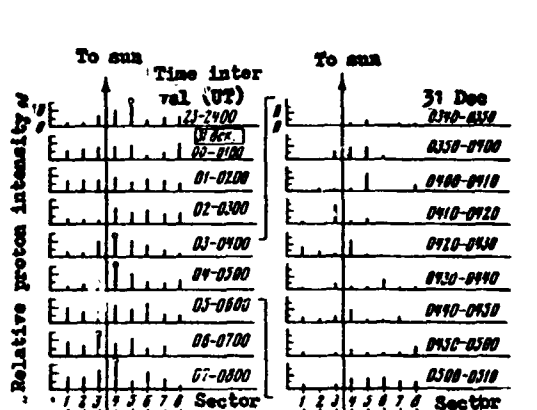

Figure 8. Time Variation of Angular Distributions. Left: hourly averages; right: ten-minute averages.

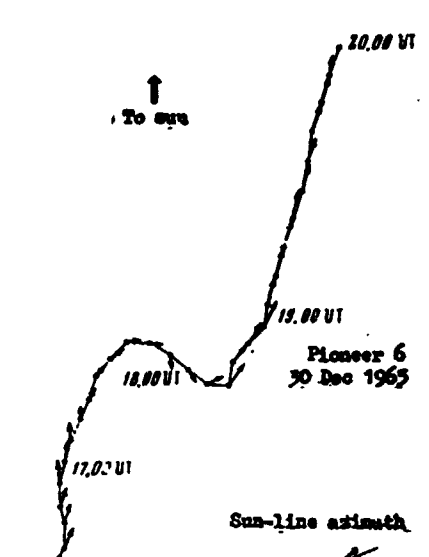

Figure 9. Projections of Magnetic Field and Anisotropy of Protons with E = 7.5-45 MeV.

magnetic field [25, 26]. The correlation persists even on a strong deviation of the field direction from the average, or, in other words, the protons propagate preferentially along lines of force. This is nicely illustrated by Fig. 9, which shows the projections of the magnetic field and the proton anisotropy onto the plane of the ecliptic in successive time intervals [25]. Thus, the anisotropy fluctuations are due to the bending and crossing of the interplanetary-field tubes of force in which the protons propagate. According to Pioneer 6 and 7 measurements, these tubes have typical diameters of (0.5-4) $\cdot 10^6$ km. /136

The manner in which the anisotropy varies is also illustrated by Fig. 10, which shows the time variation of intensity in quadrants oriented toward the sun and in the antisolar direction. For certain events, a strong anisotropy was observed for 48 hours.

A so-called equilibrium anisotropy of 5-10% is usually established during the stage of declining intensity, with the maximum on the sun-spacecraft line irrespective of the magnetic-field direction [23].

Let us now consider the spatial distribution of the low-energy proton flux from a solar flare. The most direct method of studying the spatial distribution and, in particular, the distribution in the heliocentric-longitude direction, consists in simultaneous

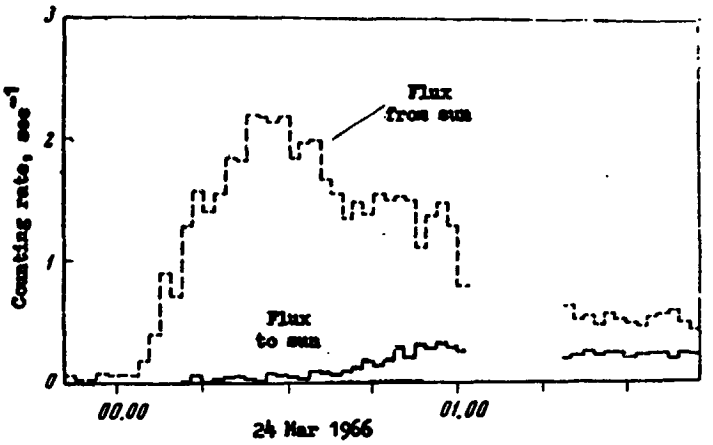

Figure 10. Time Variation of Intensity of 7.5-45-MeV Protons in Quadrants Oriented Toward the Sun and in the Antisolar Direction for the Event of 24 March 1966.

measurements made from two or more spaceprobes separated from one another by large distances. Figure 11 shows the results of simultaneous measurements of protons with E = 7.5-45 MeV on the Pioneer 6 and 7 spaceprobes [23]. The sketch at the top of the figure indicates the relative positions of the spaceprobes and the sun. An active sunspot group had crossed the western limb of the sun (for Pioneer 7) on 27 September 1966, and a flare in this group was apparently responsible for the flare burst observed on Pioneer 7 on 27 September. At the same time, this flare occurred 35° west of the central solar meridian for Pioneer 6 and, consequently, this vehicle was positioned more favorably for registration of solar protons than Pioneer 7. The flux registered on Pioneer 6 on 30 September could have been generated in this flare (the beginning of the flare was not registered owing to loss of communication). With this interpretation of the measurements,

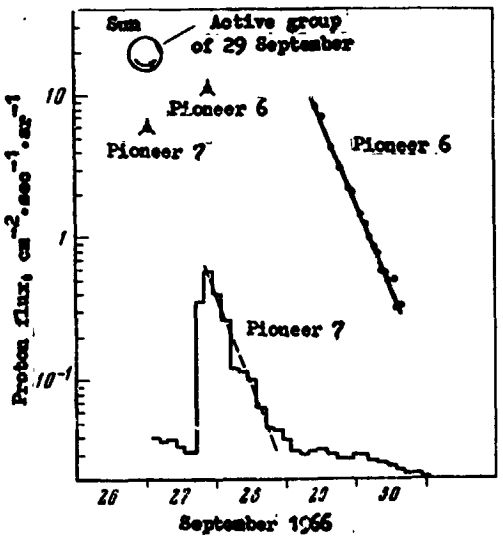

/137

Figure 11. Simultaneous Measurements of 7.5-45-MeV Proton Intensities from the Flare of 29 September 1966, as Made Aboard Pioneer 6 and 7. The relative positions of the spacecraft and the active sunspot group on 29 September 1966 are indicated at the top.

an azimuthal flux gradient of more than two orders of magnitude must have existed for a long time at 60° of heliocentric longitude. We draw attention to the distinctly exponential character of the proton-intensity decrease [23]. A burst of protons with E > 1 MeV that was registered on the 228th day of 1965 on IMP-3 from a flare at longitude 75° W with respect to IMP-3 may serve as an example of a large azimuthal gradient for lower-energy protons. At the same time, Mariner 4, which was situated 40° to the east of IMP-3, detected no increase at all [27]. The azimuthal gradient becomes steeper at higher energies. Thus, Fan et al. [5] observed a discrete burst of protons with E = 13-70 MeV about 70 minutes after a flare at longitude 90° W. Statistical analysis of the flux intensity as a function of flare longitude yields an indirect estimate of the azimuthal gradient (see, for example, Fig. 3).

Experimental data on the low-energy proton fluxes beyond the earth's magnetosphere are available for specific flares in [28-31].

Proton Bursts Associated with Transits Through Spatially Localized Fluxes

In the preceding section, we discussed bursts of low-energy protons that are registered directly after solar flares. Bursts of another type, characterized either by the absence of a generating flare or by a lapse of 1-3 days, i.e., a time much longer than the time of flight, between the flare and the arrival of the particles, constitutes a no less common phenomenon. As a rule, the appearance of these protons is accompanied by a Forbush decrease in the intensity of the galactic cosmic radiation, and sometimes by a geomagnetic storm of sudden onset.

Another important property of these bursts that is detected in direct earth satellite and spaceprobe measurements is the absence of scatter of the arrival times for different energy ranges. The time curves of intensity are almost the same for protons with energies from 0.5 to 10 MeV. This permits the conclusion that we are dealing with quasistationary particle fluxes localized in certain regions of disturbed solar plasma. Here the time variation of the registered flux is due to passage of the spaceprobe through such a region as the latter moves with the velocity of the solar wind. The duration of the burst may range from a few hours to two days. The magnetic field carried by such a region containing a particle flux modulates the intensity of the galactic cosmic rays (Forbush decrease), while the flux of disturbed plasma itself gives rise to the geomagnetic disturbances when it encounters the earth's magnetosphere.

Bursts of this type can be divided into two groups in accordance with their modes of propagation and their duration.

1. Bursts associated with shock waves propagating from strong /138 solar flares. Following Bryant et al. [21], who were the first to

investigate this phenomenon with satellites, the particles responsible for bursts of this kind were at one time often called "energetic storm particles" (ESP). The ESP burst was observed 1-3 days after a flare. ESP fluxes are often of higher intensity than the bursts of low-energy protons that follow directly after the flare, but have softer spectra [32]. Rao et al. [32] investigated 7 cases of ESP registered by instruments on Pioneer 6 and 7. These instruments could measure the intensity of protons with energies from 7.5 to 45 MeV with a time resolution of 7.5 min in 4 quadrants centered near the plane of the ecliptic.

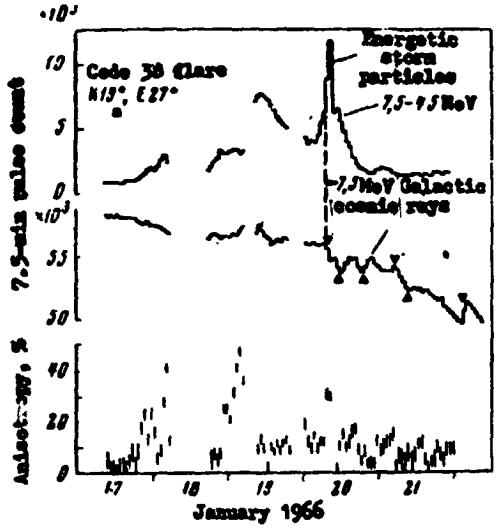

Figure 12. Time Variation of Counting Rate for Protons with E = 7.5-45 MeV and E > 7.5 MeV (Galactic Cosmic Rays) During the Period from 17 to 21 January 1966.

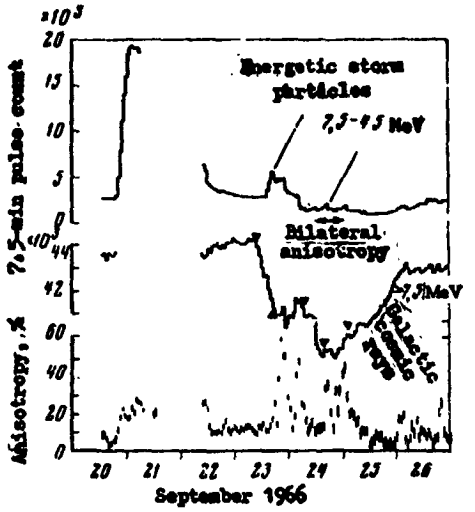

Figure 13. Time Variation of Counting Rate for Protons with E = 7.5-45 MeV and E > 7.5 MeV (Galactic Cosmic Rays), During the Period from 20 to 26 September 1966.

The time variation of proton intensity is illustrated in Figs. 12 and 13. Bursts of this type are of relatively short duration (~6 hours), and the rise and fall times are of the same order, unlike those of flare bursts. Highly interesting data were obtained in this study on the anisotropy of the ESP. The degree of the anisotropy increases rapidly at first and reaches a maximum (up to 60%) that is simultaneous with the particle-intensity maximum. The anisotropy then decreases and steadies at the 5-10% level observed before the burst. The authors of [32] call this the "equilibrium" anisotropy. It is important to note that the direction of the "equilibrium" anisotropy (the direction of maxiuum particle flux) coincides for much of the time with the sun-spaceprobe line. The anisotropy direction during a burst differs from the equilibrium direction and is subject to sudden changes.

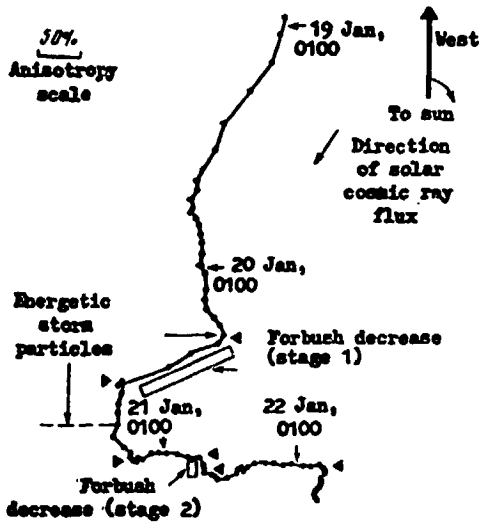

Figure 14. Variation of Anisotropy Amplitude and Azimuth for Protons with E = 7.5-45 MeV for the Period from 19 to 22 January 1966.

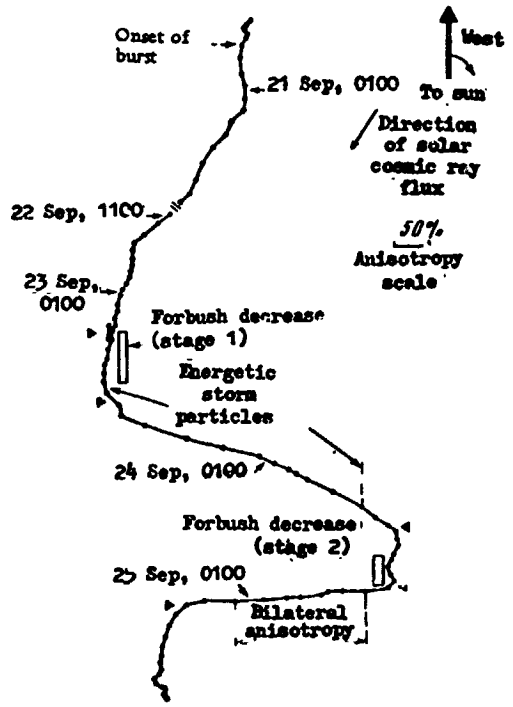

Figure 15. Variation of Anisotropy Amplitude and Azimuth for Protons with E = 7.5-45 MeV for the Period from 21 to 25 September 1966.

Figures 14 and 15 present diagrams similar to Fig. 9, showing the manner in which the magnitude and direction of the anisotropy vary. The only physically preferred direction for protons is that of the interplanetary magnetic field, and the presence of strong anisotropy indicates that the protons propagate for the most part along the field. At times of the "equilibrium" anisotropy, this relation between the directions of the anisotropy and the magnetic field breaks down. The triangles in Figs. 12, 13, 14 and 15 mark corresponding times. It is easily seen that the times of sharp variation in the anisotropy direction correspond to the characteristic points on the curve of the cosmic-ray variations. Rao et al. [32] report that the Forbush decrease accompanying the ESP often has two steps. In certain cases, a bilateral anisotropy has been observed after the minimum of the Forbush decrease has been reached (see Fig. 13), with two oppositely directed maxima in the angular distribution.

N.L. Grigorov et al. [33] obtained important data on ESP for the events of 13 December 1966 and 7 January 1967 from Luna 12 artificial lunar satellite measurements. The instruments on Luna 12 had higher time (6.75 sec) and angle (60°) resolution than those

on Pioneer 6 and 7 and could measure electrons with E > 50 keV and protons from 0.5 to 10 MeV (in several energy ranges).

In contrast to [32], the angular distribution of the radiation was studied in a plane perpendicular to the plane of the ecliptic and forming a 55° angle with the sun line. Figure 16 shows the measured results for a segment of the translunar orbit on which the detector fields had not yet been blocked by the moon. The maximum flux of protons with E > 4.5 MeV was ∿2000 cm^{-2} sec^{-1} sr^{-1}. The results of Bukata et al. [34] for the period from 9 through 22 December 1966 are cited in Fig. 11 of the article by Grigorov et al. (see the present collection, p. 166); the vertical line marks the previously mentioned time of the Luna 12 measurements. It is shown in [34] that the burst is due in this case to the shock wave arriving from one of the 2B flares that occurred on 9 and 10 December on the eastern part of the sun's disk. The basic conclusions to be drawn from the Luna 12 measurements are as follows:

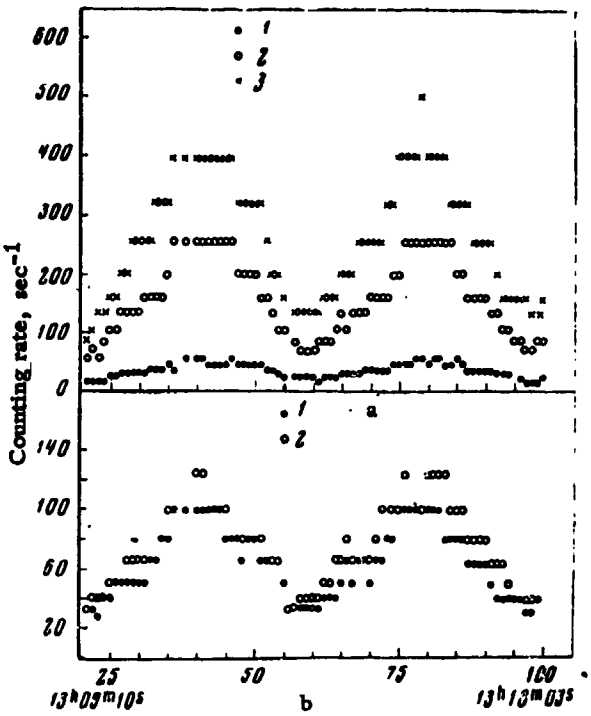

Figure 16. Counting-Rate Modulation of Luna 12 Artificial Lunar Satellite Sensors Due to Anisotropy of Proton Flux and Rotation of the Vehicle. a) Counting rates for three thresholds of scintillation counter with CsI crystal; 1) E > 8 MeV; 2) E > 1.6 MeV; 3) E > 0.15 MeV; b) counting rates of end-window gas-discharge counters: 1) SBT-9M with deflecting magnet; 2) SBT-9 without magnet. /140

1) the radiation (ESP) consists basically of protons with E = = 0.5-10 MeV;

2) the flux is strongly anisotropic (A ∿ 60%);

3) rapid variations of the intensity (through a factor of three in 10 min) and direction (through ∿100° in 10 min) of the anisotropy are observed;

4) the proton spectrum does not change during the intensity increase and is the same in all directions;

5) the angular distribution has a single maximum, whence it

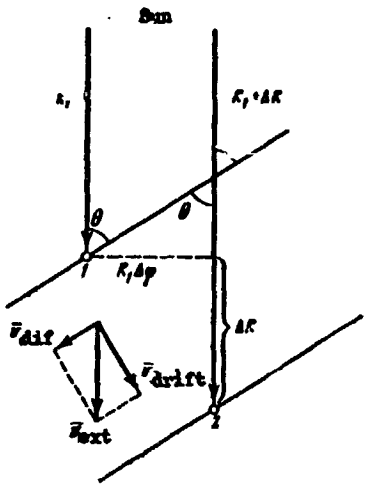

Figure 17. Registration of Long-Lived Flux Rotating Together with the Sun on Two Widely Separated Spaceprobes (1 and 2).

follows that the radiation has not been captured in a magnetic trap.

2. The second group of bursts associated with transiting of long-lived particle streams propagating along spirally bent lines of force of the interplanetary field from certain flares or active regions on the sun.

The most characteristic feature of these bursts, which distinguishes them from bursts of the first group, is the "rotation" effect that results from the long lifetimes of such streams. Simultaneous measurements made at two points in interplanetary space show a time shift Δt of the effect that is related to the velocity v_p of the solar wind, the inclination angle θ of the lines of force, and the distances ΔR and $\Delta\phi$ (see Fig. 17) between the measurement points as follows:

$$\Delta t = \frac{\Delta R + R\Delta\varphi\cot\theta}{v_p}. \qquad (1)$$

If the velocity v_p can be assumed constant, we have

$$\tan\theta = \frac{R\Omega}{v_p} \quad \text{and} \quad \Delta t = \frac{\Delta R}{v_p} + \frac{\Delta\varphi}{\Omega}. \qquad (2)$$

Here Ω is the angular velocity of the sun's rotation ($\sim$13° per day) and R is distance from the sun.

The event of 8 July 1966, which is discussed in the papers of Lin et al. [35] and Svestka [36], is a good example of such a "rotating" stream. A 2B flare with the heliographic coordinates 36°N, 48°W began at 0023 (Unversal Time) on 7 July 1966 and reached a maximum at 0036. The region of the flare was somewhat to the east and north of the beginning of the magnetic-field line of force that passed through the earth. Particle-flux measurements were made simultaneously on 3 earth satellites: Explorer 33, IMP-3, and OGO-3, the first two of which were outside of the earth's magnetosphere. /141

The first particles (electrons with E > 45 keV) were registered at 0058 $\pm$ 2. Low-energy (4-34-MeV) protons appeared at 0135. The exponential intensity decrease typical for flare bursts was observed after the counting rate had reached its maximum (Fig.

C-3

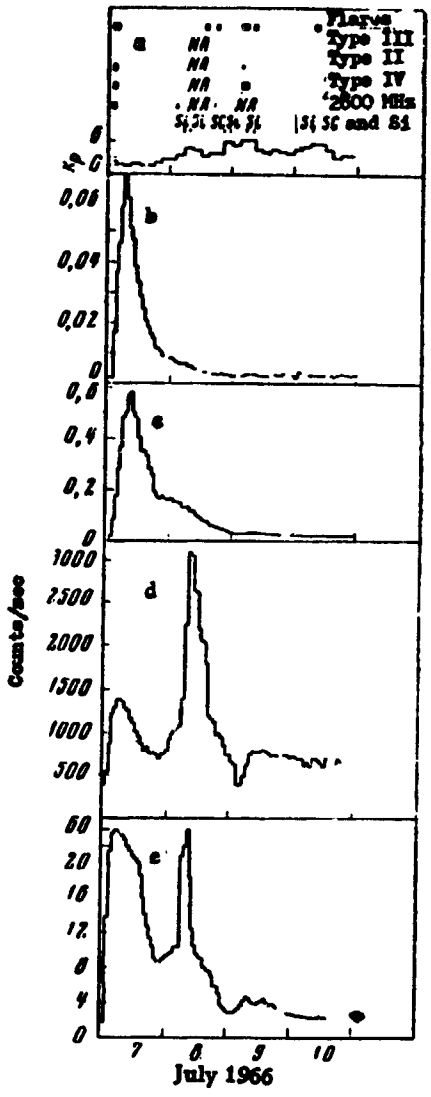

Figure 18. Time Variation of Proton Intensity for the Period from 7-10 July 1966 (IMP-3 and Explorer 33). a) Types of flares; b) $E_p \geq 20$ MeV, IMP-3; c) $E_p \geq 15$ MeV, Explorer 33; d) $E_p \geq 0.3$ MeV, $E_e > 22$ keV, Explorer 33; e) $E_e \geq 45$ keV, Explorer 33.

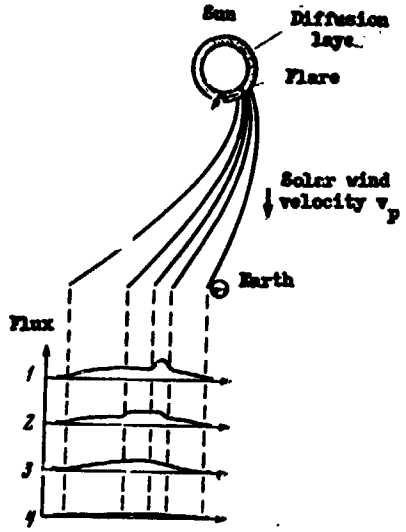

Fig. 19. Structure of Long-Lived Stream of 7 July 1966. 1) $E_e \geq 45$ keV; 2) $E_p \geq 0.5$ MeV; 3) E_p = 4-20 MeV; 4) $E_p \geq 20$ MeV.

18). An increase in the flux of protons with E > 0.5 MeV and electrons with E > 45 keV began at 1900 on 7 July. At the same time, the intensity of protons with E > > 20 MeV continued to fall. The increase in the flux of low-energy particl against the "tail" of the flare burst as a background continued for about 30 hours. Lin et al. [35] report the characteristic structure of the stream: a narrow strong "core," consisting basically of protons with E > > 0.5 MeV and electrons with E > > 45 keV, and a broad "halo," in which higher-energy (3-20 MeV) protons were also present. The authors noted that this structure rotated together with the sun and that the origin of the corresponding lines of force of the interplanetary magnetic field was in the vicinity of the flare. Figure 19 shows the schematic structure of the stream and the spatial intensity variations for particles in

various energy ranges.

We note that the Forbush decrease and the sudden-onset geomagnetic disturbance due to the shock wave from the 7 July flare were observed after passage of the "halo" and "core," and were obviously not directly related to these particle fluxes.

Svestka [36] proposes a somewhat different interpretation for the event of 8 July 1966. Noting that the 8 July flux increase coincided with the crossing of a boundary between sectors of the interplanetary magnetic field, the author suggests that low-energy solar protons and electrons were accumulated and held at the eastern part of the boundary.

"Rotating" streams are often found to be so long-lived that they are observed on several rotations of the sun as recurrent events with a period of 27 days. Here the intensity of the bursts varies over a broad range. As in the case of ESP, bursts of this type are accompanied by modulation effects of the Forbush-decrease type and sometimes by geomagnetic disturbances of sudden onset. Several of these sequences of recurrent events were observed in 1965-1967; some of them could be followed through nine rotations of the sun [5, 27]. Some of the recurrent bursts coincided with magnetic-sector boundaries. McCracken et al. [37] associate these recurrent events with M regions on the sun and point to their proximity to the 1964-1965 sector boundaries. It is also observed in this study that the magnetic field increased by a factor of 4 in the initial phase of the Forbush decrease, returning later to its original value. Since such a change in the field should be expected on crossing the front of a shock wave, the authors propose a model according to which a quasistationary shock wave rotating with the sun exists at the boundary between regions with different solar-wind velocities. A good argument in favor of this model is found in the observation of a single shock-wave front from two spaceprobes with the times of registration of the front shifted by 88 hours as compared to a theoretical time of (89 $\pm$ 2) hours [32].

Recurrent proton streams are characterized by comparatively low intensity ($\lesssim$20 $cm^{-2} \cdot sec^{-1} \cdot sr^{-1}$ at E > 1 MeV) and steeply declining spectra. For this reason, recurrent bursts are not always registered, especially with apparatus having a high energy threshold. Thus, McCracken et al., who registered many ESP bursts, did not observe any with E = 7.5-45 MeV that coincided with "rotating" Forbush decreases. However, such bursts were observed with equipment having thresholds of 0.5-0.6 MeV [5, 27]. /142

Certain Model Representations of the Propagation of Low-Energy Solar Protons /143

There is at the present time no model that explains the entire aggregate of phenomena associated with low-energy solar protons because the information available thus far has been inadequate.

However, certain general conclusions pertaining to the proton-propagation mechanism can be drawn even from the presently available experimental data. Although it cannot be claimed that the model representations to be examined below are sufficiently strongly supported, they can be used as helpful working hypotheses.

The basic factor determining the manner of propagation of the solar protons is the interplanetary magnetic field. The structure of the interplanetary field during periods around a solar activity minimum have been studied by direct spaceprobe measurements [38]. It is a well-known fact that extraction of the frozen magnetic field by the radial stream of solar plasma and the rotation of the sun confer the form of Archimedean spirals on the lines of force near the plane of the ecliptic. A whole spectrum of magnetic-field irregularities associated with the inconstant velocity of the solar wind and other manifestations of solar activity is superimposed on this organized structure.

In accordance with this structure of the interplanetary magnetic field, the motion of a charged particle can be resolved into a spiral motion along the mean direction of the lines of force and scattering on magnetic inhomogeneities.

Let us first consider the features of the motion in a regular field. The intensity of the magnetic field drops off rapidly with increasing distance from the sun. For example, the radial component varies as R^{-2}. This circumstance should result in strong collimation of the particles. In fact, it follows from conservation of magnetic moment (first adiabatic invariant) that $B/\sin^2\alpha = \text{const}$, where α is the angle between the particle velocity and the magnetic field (the pitch angle). Therefore $\sin^2\alpha$ decreases by a factor of $\sim 10^4$ on removal from the sun to the orbit of the earth, and $\alpha \ll 1°$. The high degree of flux anisotropy, with the maximum directed along the lines of force, that is characteristic for solar low-energy protons is quite consistent with the above argument.

The lines of force of the interplanetary field can be represented as simple Archimedean spirals only in the mean. We now have convincing proofs of the existence of individual sharply defined filamentary tubes of force at whose boundaries the magnetic field and plasma characteristics undergo abrupt changes [39]. The transverse dimensions of the filaments range from $0.5 \cdot 10^5$ to $4 \cdot 10^6$ km. The filamentary structure is also manifested in the time variation of proton intensity, with the boundary between filaments having a thickness on the order of the proton Larmor radius. The individual filaments can bend in curious fashion, forming loops (see Fig. 9). On passage through such loops, the field direction changes simultaneously with the direction of the anisotropy. This close relation of the particles to magnetic tubes of force makes it possible to "trace" the lines of force by observation of the solar protons and to acquire information on the magnetic-field structure far from the observation point. For

example, the hypothesis has been advanced that the lines of force of one sector of the interplanetary field merge smoothly somewhere beyond the orbit of the earth with oppositely directed lines of force of the adjacent sector. In this case, we might expect the recurrent streams to have oppositely directed "twins" in the neighboring sector. Since such "twins" have not yet been observed, the hypothesis of smooth joining of the force lines appears improbable [38]. The filamentary structure of the interplanetary-field lines /144 of force is responsible for short-period fluctuations of the flux of low-energy protons.

Motion of protons along lines of force of the average field also readily explains such properties of the streams as their time of arrival after flares, their high anisotropy and the direction of the anisotropy, t e large longitudinal gradient of the flux, the stronger effect from western flares, etc. However, the anisotropy seldom approaches 100% despite the strong collimation. It is only 30-50% even during the buildup and maximum of a burst. This indicates that there is a certain mechanism that tends to render the flux isotropic. Scattering of particles on magnetic inhomogeneities is such a mechanism. A particle is most efficiently scattered on inhomogeneities with dimension l of the order of the Larmor radius ρ_L. When $l \ll \rho_L$, the scattering angle is small, and when $l \gg \rho_L$ the particle moves around the inhomogeneity, following lines of force.

The isotropic-diffusion model [3] is the simplest model that describes the propagation of particles in the presence of strong scattering. It is assumed in this model that the inhomogeneities are distributed spherically symmetrically in space and that the particle flux is isotropized quite rapidly. In addition, the distance from the source to the observation point must be considerably greater than the free path Λ for description of the time variation of the total proton flux. Sometimes this model gives a fair description of the time variation of the intensity of flare protons with energies above 100 MeV. However, the isotropic-diffusion model does not agree with experiment for the low-energy protons. McCracken et al. [23] showed that in 1966, the free path to large-angle scattering was often $\sim$1 a.u. for 7.5-45-MeV protons, i.e., one of the basic conditions for applicability of this model was not satisfied. Nor does this model account for the strong anisotropy during a burst. Other experimental data [5, 40] also indicate that scattering in the space between 0.3 and 1.0 a.u. is not a significant factor for low-energy protons. At the same time, description of the later stage of the burst (the intensity decrease) requires consideration of scattering on magnetic inhomogeneities beyond the earth's orbit. Scattering results in the appearance of an isotropic component of the flux and a gradual decrease in the anisotropy. Study of the isotropic component or the part of the flux directed toward the sun yields the most direct information on solar-proton diffusion. In the paper of McCracken cited above, the free path obtained in precisely this way was $\Lambda \sim 1$ a.u.,

while application of the isotropic-diffusion theory to the total flux in the initial stage of the burst yielded values of $\Lambda \sim 0.05$ a.u.

The anisotropic-diffusion model, in which the diffusion coefficient D is a tensor, gives a better approximation of reality. The value of this coefficient $D_\parallel$ along the magnetic field is considerably larger than the value $D_\perp$ in the perpendicular direction. For practical purposes, diffusion is one-dimensional along lines of force.

The exponential intensity decrease that is characteristic for flare bursts is obtained in diffusion models by introducing particle leakage out of the diffusion region. Not only interplanetary space, but also the solar corona, which contains disordered magnetic fields (see below), can be treated as such regions.

The magnitude and direction of the "equilibrium" anisotropy observed at the later stages of bursts can be obtained within the framework of these models [23]. Diffusion equilibrium is established some time after the beginning of the burst, when the solar protons have propagated to several astronomical units. It is manifested in constancy of the ratio of the proton fluxes from and to the sun. Since the radial proton density gradient is directed toward the sun, the proton flux due to diffusion is directed along /145 lines of force away from the sun. The motion of the magnetic field frozen into the solar wind causes the protons to drift [41] at a velocity

$$v_{\text{drift}} = \frac{(r_p \times B) \times B}{B^2}. \qquad (3)$$

The absolute magnitude of $v_{drift} = v_p \sin\theta$, where v_p is the velocity of the solar wind and θ is the angle of the Archimedean spiral.

The resultant velocity v_{ext} produces the observed anisotropy. Experiment has shown that v_{ext} is directed nearly radially outward from the sun, so that

$$v_{\text{dif}} = \frac{v_{\text{drift}}}{\operatorname{tg}\theta} = v_p \cos\theta. \qquad (4)$$

$$v_{\text{ext}} = \sqrt{v_{\text{drift}}^2 + v_{\text{dif}}^2} \approx v_p. \qquad (5)$$

At diffusion equilibrium, therefore, the solar protons are swept out of the solar system at the velocity of the solar wind.

According to [41] and [42], the magnitude of the anisotrcpy is

$$A = (3+\gamma)\frac{v_p}{v}, \qquad (6)$$

where γ is the exponent in the differential proton energy spectrum and v is the velocity of the protons. For 7.5-45-MeV protons, relation (6) gives A = 5.9% at v_p = 400 km/sec, in good agreement with experiment (5-10%).

Returning to our examination of nonequilibrium fluxes (the initial phase of the burst), we note that the intensity of protons registered at a given point in space depends on the population density in the neighborhood of the sun on the line of force passing through this point. Thus, the interplanetary-field lines of force project the proton source to a distance R $\sim$ 1 a.u.

We noted above that strong proton anisotropy has been observed in a number of cases for many hours after the beginning of a burst (up to 48 hours). This indicates prolonged emission of particles by the sun, due either to continuous generation or to some type of particle storage in the corona and the upper chromosphere. The mechanism that supports the second possibility might be diffusion in the nonregular fields of the solar atmosphere, with subsequent leakage of protons into tubes of force of the interplanetary field. The corresponding model, which was proposed by Reid [43] and developed by Axford [44], explains the high anisotropy of the proton flux, the exponential intensity decrease, and cases of observation of flare bursts from flares quite far from the base of the line of force drawn from the point of measurement. Unfortunately, calculations were made only for the 130-600-MeV protons for which experimental data were available at the time. According to Fan et al. [5], explanation of the arrival times of the first flare protons requires, in addition to diffusion, introduction of direct propagation of protons from the point of the flare along the lines of force of the fields in the chromosphere and corona to the beginning of the corresponding line of force of the regular magnetic field. This paper presents the following picture of proton propagation from powerful solar flares. The flare generates protons and gives rise to a blast wave. The radially expanding blast wave pulls the magnetic field out of the flare region, promoting rapid propagation of protons in the lower corona. This is followed by leakage of protons into tubes of force of the interplanetary field. The result is formation of characteristic propagation cones.

The protons propagate along the interplanetary lines of force /146 almost without scattering to distances up to 1 a.u., and diffusion in the lower corona supports the stream for many hours. At distances beyond 1 a.u., scattering becomes important, and a flux directed toward the sun appears and increases some time after the beginning of the burst. The anisotropy and azimuthal (longitudinal)

gradients of the flux decrease.

The structure of long-lived, quasi-stationary streams of low-energy protons was examined in the papers of Lin et al. [45] and Anderson [46]. The basic features of the model that they proposed are the same as those of Fan's model. According to Lin et al., the time variation of intensity observed when a spaceprobe crosses the stream represents the projection of the three-dimensional profile of the solar source by the interplanetary lines of force. The injection profile can be explained as resulting from the geometry of the magnetic fields in the region of the flare. Particles generated during the flare are divided into two types: those that move out rapidly from the flare region and those that are stored for a long time in its vicinity. Most of the high-energy particles "escape," while low-energy particles are for the most part retained. The "escaping" particles diffuse in a certain layer of the solar corona in all directions from the generation region and move away along lines of force of the interplanetary field, forming a component that decreases exponentially with time (the Reid-Axford model). The more energetic among the "stored" particles are distributed over a larger longitude range than those with lower energies. Leakage of these particles into interplanetary space results in formation of the "halo" of the long-lived stream. The "core" is formed by lines of force of the interplanetary field connecting directly to the region of particle generation.

TABLE 4*

$\frac{h}{r_\odot}$	Hydrogen concentration, at/cm^3	Half-range time	
		$E = 0{,}5$ MeV, $v = 10^9$ cm/sec	$E = 10$ MeV, $v = 4{,}3 \cdot 10^9$ cm/sec
0,01	10^9	150 sec	3000 sec
0,03	$1{,}6 \cdot 10^8$	1000 sec	$2 \cdot 10^4$ sec $\approx$ 6 h
0,2	$4 \cdot 10^7$	4000 sec $\approx$ 1 h	$9 \cdot 10^5$ sec $\approx$ 10 days
1,0	$1{,}8 \cdot 10^6$	$8 \cdot 10^4 \approx$ 1 day	$1{,}7 \cdot 10^6$ sec $\approx$ 1 month

*Commas indicate decimal points.

There is as yet no definite answer to the question as to whether the long-lived streams owe their existence to pulsewise generation with subsequent storage or to continuous generation. However, an upper limit can be indicated for the storage time. During storage, the particles should lose some of their energy in the gas of the sun's atmosphere. The ranges of 0.5- and 10-MeV protons in fully ionized hydrogen are $5 \cdot 10^{-4}$ and $5 \cdot 10^{-2}$ g/cm^2, respectively.

Table 4 presents estimates of the times required for protons to cover half of their range at various heights above the sun's surface.

The height $h = 0{,}01\ r_\odot$ corresponds to the thermosphere. The radio sources accompanying the flare (high-energy electrons) lie in the height range from $0{,}2\ r_\odot$ to several $r_\odot$ (the solar corona) [47], so that we may assume that the storage region is in this height range.

Table 4 shows that the energy losses during one day of storage are not significant for protons with E = 10 MeV. On the other hand, storage of 0.5-MeV protons for the same amount of time requires "pumping." Otherwise a knee would appear in the spectrum in the 0.5-1-MeV energy range. Measurements of the spectra in the 3-15-MeV range [5, 45] failed to detect such a knee. Systematic measurement of the spectra at lower energies would be highly important for clarification of questions related to the possible energy losses in the corona and to the nature of the long-lived streams. /147

Several hypotheses have been suggested to explain the nature of the ESP. It was assumed in the earliest one (Bryant et al. [21]) that the protons are trapped in the flare region by a magnetized plasma cloud, which is responsible for the geomagnetic disturbance and the Forbush decrease, and are conveyed by this cloud to the vicinity of the earth. Study of the ESP anisotropy has shown that these particles are not trapped.

Several authors (Rao et al. [32, 48]) have assumed the existence of continuous particle acceleration at the front of the shock wave arriving from the flare. However, there is insufficient justification for this assumption, and other authors do not concur with it [5]. For example, it is difficult in this model to explain the strong proton anisotropy and the fact that in many cases the arrival of the shock wave is accompanied by a decrease in proton intensity rather than a burst [49]. It is more natural to assume that the ESP represent a variety of long-lived streams originating from the flare region [46]. The role of the shock wave may be reduced merely to magnetic connection of the observation point with this region [50].

Investigation of low-energy solar protons began only three or four years ago. However, even the first data acquired have revealed a broad range of phenomena of importance for understanding of the processes taking place on the sun and in interplanetary space.

REFERENCES

1. T. Obayashi, Space Sci. Rev., 1964, Vol. 3, 79.
2. J.G. Roederer. Space Sci. Rev., 1964, Vol. 3, 487.
3. L.I. Dorman and L.I. Miroshnichenko. Solnechnyye kosmicheskiye luchi (Solar Cosmic Rays), Moscow, "Nauka," 1968.
4. C.E. Fichtel. Proceedings of the 10th International Cosmic Ray Conference. Calgary, Canada, 1967, p. 194.
5. C.Y. Fan, M. Pick, K.R.Pyle, J.A. Simpson, and D.R. Smith. J. Geophys. Res., 1968, Vol. 73, 1555.
6. J.A. Van Allen and S.M. Krimigis. J. Geophys. Res., 1965, Vol. 70, 5737; K.A. Anderson, H.K. Harris, and R.J. Paoli. J. Geophys. Res., 1965, Vol. 70, 1939.
7. N.L. Grigorov, V.N. Lutsenko, V.L. Maduyev, N.F. Pisarenko, and I.A. Savenko. Kosmicheskiye issledovaniya, 1967, Vol. 5, 891.
8. C.Y. Fan, G.G. Gloeckler, and J.A. Simpson. Can. J. of Phys., 1968, Vol. 46, 548.
9. S.N. Vernov, A.Ye. Chudakov, P.V. Vakulov, Yu.I. Logachev, G.P. Lyubimov, A.G. Nikolayev, and N.V. Pereslegina. Dokl. Akad. Nauk SSSR, 1966, Vol. 171, 847.
10. S.N. Vernov, A.Ye. Chudakov, P.V. Vakulov, Ye.V. Gorchakov, N.N. Kantor, et al. Trudy V Vses. zimney shkoly po kosmofizike (Trans. Fifth All-Union Winter School on Space Physics), Apatity, 1968, p. 5.
11. S.M. Krimigis and J.A. Van Allen. Phys. Rev. Lett., 1966, Vol. 16, 419.
12. J.J. O'Gallagher and J.A. Simpson. Astrophys. J., 1967, Vol. 147, 819.
13. S.N. Vernov, A.Ye. Chudakov, P.V. Vakulov, Yu.I. Logachev, G.P. Lyubimov, and N.V. Pereslegina. Dokl. Akad. Nauk SSSR, 1966, Vol. 171, 583.
14. U.R. Rao, K.G. McCracken and W.C. Bartley. J. Geophys. Res., 1967, Vol. 72, 4343.
15. G. Gloeckler and J.R. Jokipü. Phys. Rev. Lett., 1966, Vol. 17, 203.
16. M.V.K. Apparao, Preprint, 1967.
17. D.K. Bailey. J. Geophys. Res., 1957, Vol. 62, 431.
18. G.C. Reid and C. Collins. J. Atm. and Terr. Phys., 1959, Vol. 14, 63; H. Leinbach and G.C. Reid. Phys. Rev. Lett., 1959, Vol. 2, 60.
19. A.S. Besprozvannaya. In collection entitled: "Issledovaniye ionosfery" (Investigation of the Ionosphere), Izd-vo Akad. Nauk SSSR, 1961, No. 6, 58; J.B. Gregory. J. Geophys. Res., 1963, Vol. 68, 3097.
20. K.W. Ogilvie, D.A. Bryant, and L.R. Davis. J. Geophys. Res., 1962, Vol. 67, 929. /148
21. D.A. Bryant, T.L. Cline, U.D. Desai, and F.B. McDonald. J. Geophys. Res., 1962, Vol. 67, 4983.
22. J.A. Van Allen, L.A. Frank, and D. Venhatesan. Trans. Am. Geoph. Un., 1964, Vol. 45, 80.
23. K.G. McCracken, U.R. Rao, and R.P. Bukata. J. Geophys. Res., 1967, Vol. 72, 4293.

24. C.Y. Fan, I.E. Lamport, J.A. Simpson, and D.R. Smith. J. Geophys. Res., 1966, Vol. 71, 3289.
25. K.G. McCracken and N.F. Ness. J. Geophys. Res., 1966, Vol. 71, 3315.
26. K.G. McCracken, U.R. Rao, and N.F. Ness. J. Geophys. Res., 1968, Vol. 73, 4159.
27. J.J. O'Gallagher and J.A. Simpson. Phys. Rev. Lett., 1966, Vol. 16, 1212.
28. D.A. Bryant, T.L. Cline, U.D. Desai, and F.B. McDonald. Astroph. J., 1965, Vol. 141, 478.
29. S.W. Kahler, K.A. Anderson, and J.H. Primbsch. Trans. Am. Geoph. Un., 1967, Vol. 48, 178.
30. C.O. Bostrom, J.W. Kohl, and D.J. Williams. Trans. Am. Geoph. Un., 1968, Vol. 49, 274.
31. S.T. Lindgren. Sol. Phys., 1968, Vol. 5, 382.
32. U.R. Rao, K.G. McCracken, and R.P. Bukata. J. Geophys. Res., 1966, Vol. 72, 4325.
33. N.L. Grigorov, V.G. Kurt, V.N. Lutsenko, V.L. Maduyev, N.F. Pisarenko, and I.A. Savenko. Kosmicheskiye Issledovaniya, 1967, Vol. 7, 137.
34. R.P. Bukata, K.G. McCracken, and U.R. Rao. Can. J. Phys., 1968, Vol. 46, 994.
35. R.P. Lin, S.W. Kahler, and E.C. Roelof. Sol. Phys., 1968, Vol. 4, 338.
36. Z. Svestka. Sol. Phys., 1968, Vol. 4, 361.
37. K.G. McCracken, U.R. Rao, and R.P. Bukata. Phys. Rev. Lett., 1966, Vol. 17, 928.
38. J.M. Wilcox. Sp. Sci. Rev., 1968, Vol. 8, 258.
39. I.B. Strong, J.R. Asbridge, S.J. Bame, and A.J. Hundhausen. Trans. Am. Geoph. Un., 1967, Vol. 48, 191.
40. S.M. Krimigis and J.A. Van Allen. J. Geophys. Res., 1967, Vol. 72, 4471.
41. H.S. Ahluwalia and A.J. Dessler. Planet. Sp. Sci., 1962, Vol. 9, 195.
42. A.H. Compton and I.A. Getting. Phys. Rev., 1935, Vol. 47, 817.
43. G.C. Reid. J. Geophys. Res., 1964, Vol. 69, 2659.
44. W.I. Axford. Planet. Sp. Sci., 1965, Vol. 13, 1301.
45. R.P. Lin, S.W. Kahler, and E.C. Roelof. Sol. Phys., 1968, Vol. 4, 338.
46. K.A. Anderson. Sol. Phys., 1969, Vol. 6, 111.
47. V.V. Zheleznyakov. Radioizlucheniye Solntsa i Planet (The Radio Emission of Sun and Planets), Moscow, "Nauka," 1964.
48. E.N. Parker. Phys. Rev. Lett., 1965, Vol. 14, 55.
49. J.A. Van Allen and N.F. Ness. J. Geophys. Res., 1967, Vol. 72, 935.
50. S.W. Kahler. Trans. Am. Geoph. Un., 1968, Vol. 49, 274.

N75 13718

THERMAL INSTABILITY AND ENERGY RELATIONS IN THE CONVECTIVE ENVELOPES OF SLOWLY ROTATING STARS

(Translation of "O termicneskoy neustoychivosti i energeticheskikh sootnosheniyakh v konvektivnykh obolochkakh medlenno vrashchayushchikhsya zvezd.")

I. M. Yavorskaya

ABSTRACT

The nonstationary convection that arises due to thermal instability in the envelopes of lower Main Sequence stars (and the sun in particular) is investigated. The convection that arises in the envelopes as a result of thermal instability is of nonstationary turbulent nature. The paper derives various energy relations that should be satisfied in these envelopes. It is shown that construction of a consistent model of the zones of turbulent convection in the stars requires the use, along with the Reynolds equations, not of a barotropicity condition, but the complete heat-flux equation with consideration of the terms that appear because of turbulence. Expressions for these additional terms in terms of averaged characteristics of the motion and eddy viscosity coefficients are derived on the basis of the Prandtl-Wasiutinsky theory. Asymptotic representations are obtained for the heat-flux equation for the convective envelopes of lower Main Sequence stars.
With 1 table and 22 source citations.

THERMAL INSTABILITY AND ENERGY RELATIONS IN THE CONVECTIVE ENVELOPES OF SLOWLY ROTATING STARS

I.M. Yavorskaya

§ 1. The most interesting feature in the structure of lower Main Sequence stars and of the sun in particular is the structure of their convective envelopes, since the processes taking place here determine, in large part, the phenomena observed on the surface of the sun and in its chromosphere and corona. It is known [1] that stars of this type consist of a core at radiative equilibrium, in which nuclear reactions take place and enormous amounts of energy are released for subsequent transfer to the periphery by radiation, and an envelope, in which the conditions of radiative equilibrium are violated. The true temperature gradient is superadiabatic in the envelope, and the region becomes thermally unstable. Schwartzschild's criterion states that for disturbance of thermal equilibrium, the true temperature gradient ∇T of the medium must be larger in absolute magnitude than the adiabatic gradient $\nabla_a T$ [1]

$$\Delta\nabla T = -\nabla T - (-\nabla_a T) > 0^1. \tag{1.1}$$

Convection arises when this condition is satisfied in an ideal fluid, becoming the basic mechanism of heat transfer in this zone. However, if the actual properties of the medium are taken into account (viscosity, thermal conductivity), it is found that the gradient difference must exceed a quite definite value for convection to appear.

Analysis of convective instability by the method of small perturbations for a layer of incompressible fluid or a compressible gas in the Boussinesq approximation has shown that the dimensionless Rayleigh number [2] can serve as a parameter characterizing the onset of convection:

$$\mathrm{Ra} = \frac{d^4 g \beta \nabla T}{\nu \chi}, \tag{1.2}$$

where d is the layer thickness, g is the effective acceleration, β, ν, and χ are the coefficients of thermal expansion, viscosity, and thermal diffusivity of the medium. For an ideal gas, $\beta = T^{-1}$, and ∇T must be replaced by $\Delta\nabla T$ for the compressible medium. Convection begins when $\mathrm{Ra} \geq \mathrm{Ra}_c$, where Ra_c is the critical value of

---

[1]The gradients in (1.1) are written with the minus sign because they are always negative in stars in the spherical coordinate system (r, ν, ϕ) bound to the center of the star.

the Rayleigh number, which depends on the boundary conditions [2]. At $Ra = Ra_c$, convection is of stationary cellular nature; when $Ra > Ra_c$, the amplitudes of the convective motions increase exponentially with time in linear approximation, nonlinear effects come to predominate, and the establishment of nonlinear stationary convection subsequently becomes a possibility. The thermal instability of a compressible gas has been most thoroughly studied in the linear approximation for thin layers (layer thickness d << any height scale), when the Boussinesq approximation is valid. Convection takes place in stars under conditions that differ strongly from those cited above, and the classical results of Rayleigh and Schwartzschild are little suited for their study. It is necessary to consider the rotation of the stars and the effects of their magnetic fields [2]; density stratification in the convective regions prohibits the use of the Boussinesq approximation [3] (thus, density varies through six orders in the convective envelope of the sun). The convective layers of stars border on thermally stable layers, and the penetration of convective disturbances into these layers must be taken into account to obtain the correct physical picture [4]. Moreover, the conduction in stars is strongly nonlinear and distinctly turbulent in nature. Let us see how these factors can be taken into account in study of the motions in the convective zones of stars. /150

Chandrasekhar studied the suppression of convective motions by rotation in a viscous thermally conductive fluid in the Boussinesq approximation and found that the onset of convection is delayed if the angular velocity Ω of the rotation and the acceleration of gravity g are parallel and is not delayed if Ω and g are perpendicular. The critical value of the Rayleigh number depends on the dimensionless Taylor and Prandtl numbers Tr and Pr:

$$\mathrm{Tr} = \frac{4\Omega^2}{\nu^2} d^4, \qquad \mathrm{Pr} = \frac{\nu}{\chi}.$$

In the case of strong rotation, when $\mathrm{Tr} \to \infty$, Ra_c does not depend on the form of the boundary conditions (the influence of the boundary conditions is confined to a very thin Ekman layer [5]):

$$\mathrm{Ra_c} \approx 8.69\,\mathrm{Tr}^{3/4} \text{ as } \mathrm{Tr} \to \infty. \tag{1.3}$$

Consideration of the sphericity of the convective layer yielded the following condition for the onset of axisymmetric convection at large Taylor numbers:

$$\mathrm{Ra_c} \approx 20.7\,\mathrm{Tr}^{3/4}. \tag{1.4}$$

But Roberts showed that the onset of convection for spheres is associated with asymmetrical motions at arbitrary Tr and Pr [6].

Another important result obtained by Chandrasekhar is that convection can arise as an oscillatory instability in a rotating fluid at $Pr < \sqrt{3/5}$. But for comparatively slow rotation $Tr \leq Tr^*(Pr)$,[2] convection is of stationary cellular character even at small Pr.

It should be noted that on rotation, the effects of solid and free boundaries on the onset of convection are reversed [7]. In the absence of rotation, the presence of solid boundaries delays the onset of convection, and it begins at larger Ra_c than in the case of free boundaries. As a result of the dual role of viscosity (which acts not only as an energy-dissipation mechanism, but also as a mode for releasing it), the presence of solid boundaries accelerates the onset of convection when rotation is present.

All of the foregoing results pertained to the condition for onset of convection with rotation. But once convection has begun, how does rotation modify the convective motions? We find that the dimensions of the convective cells decrease on rotation. For Rayleigh convection, for example, the dimensionless wave number b, which characterizes the horizontal dimension of the cell, has the following asymptotic behavior at high rotational velocities:

$$b_{min} = (1/2\,\pi^2\,Tr)^{1/6} = 1.305\,Tr^{1/6} (Tr \to \infty). \qquad (1.5)$$

The results of (1.3)-(1.5) are applicable to layers of a viscous heat-conducting compressible fluid in the Boussinesq approximation, i.e., when the density variations are due basically to temperature and are so small that they need be considered only in the mass forces acting on small perturbations; otherwise the fluid is assumed to be incompressible.

Investigation of the convection-initiating condition in a compressible but ideal fluid ($\nu = \chi = 0$) in rotation at a constant angular velocity Ω led Randers [8] to the following modification of the Schwartzschild criterion for the radial displacements: /151

$$g\frac{\Delta\nabla T}{T} > 4\Omega^2 \sin^2\theta. \qquad (1.6)$$

However, Cowling [9] showed that Eq. (1.6) is valid only if we assume that the perturbed motions are axisymmetric. In the general case, on the other hand, the right-hand side of (1.6) depends not only on Ω, but also on the horizontal wave number k, and tends to zero as $k \to \infty$. That is, without consideration of viscosity and thermal conductivity, the Schwartzschild criterion (1.1) does not change on rotation; the effect of rotation is to stabilize certain perturbations that were unstable in the absence

[2] Tr^* is a certain characteristic value of the Taylor number that depends on the Prandtl number Pr.

of rotation. In a study of the instability of polytropic spherical configurations in slow rotation, Clement [10] found that rotation suppresses some of the convective motions that are described by lower-order spherical harmonics. This means that the mixing length l in the convective zone may be reduced substantially by rotation, and that the convective energy transport H becomes less effective, since

$$H \sim l^2 c_p \rho \left(\frac{g}{T}\right)^{1/2} (\Delta \nabla T)^{3/2},$$

where ρ is the density and c_p is the heat capacity at constant pressure. Although the criterion (1.1) remains unchanged, the difference between the true and adiabatic gradients $\Delta\nabla T$ may be larger for rotating configurations for transfer of the same amount of heat H. Another study of convective instability in stratified layers of ideal gas with consideration of rotation was made by Lebovitz [11]. He showed that while the condition $\Delta\nabla T > 0$ results, in the absence of rotation, in simultaneous instability of disturbances with any horizontal wave number, rotation with $\Delta\nabla T > 0$ stabilizes all long-wave perturbations with $k < k_\omega$.

Since an energy-dissipation mechanism (e.g., viscosity) always operates in any real medium, it suppresses short-wavelength disturbances with horizontal wave numbers $k > k_\nu$. We may therefore conclude that in an unstably stratified medium with consideration of rotation and dissipation, convective instability may be manifested in the form of perturbations in a limited range of wave numbers $k_\omega < k < k_\nu$, and may not occur at all when $k_\omega = k_\nu$.

Since all of the above results pertain to small-amplitude convective motions, quantitative estimates can hardly be applied directly to the convective zones of stars. However, the qualitative picture should remain unchanged. We may therefore draw the following conclusions, which are valid for convective motions in general:

1) rotation delays the onset of convection, i.e., other conditions being equal, larger heat fluxes are required to initiate convective motions;

2) if convection begins notwithstanding, the primary effect of rotation is to suppress the largest-scale and axisymmetric convective motions; this evidently reduces the convective transfer of heat for given values of $\Delta\nabla T$ as compared to convection without rotation;

3) rotation has a suppressive effect on convective motions basically in regions where $\Omega \| q$, i.e., in the polar regions of the stars, since the local Taylor number $\mathrm{Ta} = 4d^4\Omega^2 \cos^2\vartheta/\nu^2$ is largest there;

4) in zones with substantial density variations, the convective motions contain a whole hierarchy of scales proportional to the local height scale. Obviously, the largest-scale motions (which have dimensions on the order of the depth of the zone) are generated near the bottom of the convective zone and are most strongly affected by rotation. Depending on the angular velocity of the rotation, they may either be suppressed or be manifested in the form of nonaxisymmetric and perhaps nonstationary motions; /152

5) If the angular velocity is not constant $\Omega = \Omega(r, \theta)$, the presence of shear stresses may be a source of dynamic instability [9], and the resulting motions may, like convective disturbances, transfer thermal energy even in the case of stable temperature stratification $\Delta\nabla T < 0$.

§2. Nonlinear effects acquire increasing importance with increasing Rayleigh number, and the convection assumes a chaotic turbulent character when Ra = 500 000 >> Ra_c. The transition from stationary Benard cellular convection (at Ra ~ Ra_c) to disordered turbulent convection takes place via a series of stationary or quasistationary conditions [12] in which each successive condition is less ordered than the one preceding it. In this case, the onset of convection is no longer determined by Ra, but instead by the degree of the instability (turbulization) of the convective flows. As a result of the strong variation of density and temperature, the Rayleigh numbers of the convective regions of stars are not constant, but vary through several orders of magnitude over the depth of the zone. The thermal diffusivity in (1.12) is determined by the radiation of the medium and can be represented in the following form everywhere except in the layers at the very surfaces of the stars [1]:

$$\chi = -\frac{4}{3}\frac{acT^3}{\varkappa\rho^2 c_p}, \qquad (2.1)$$

where a is the Stefan-Boltzmann constant, κ is the absorption index, and c is the velocity of light. For the viscosity in layers with fully ionized matter, we may take [13]

$$\nu = \frac{2.2}{\Lambda/10}\frac{T^{5/2}}{\rho}\cdot 10^{-16}, \qquad (2.2)$$

where Λ is the Coulomb logarithm. Ra can be estimated for various solar convective zone depths from (2.1) and (2.2). We find that in the least stable layers, the Rayleigh number reaches values on the order of 10^{20} (under astrophysical conditions, the layer thickness d is replaced by the so-called mixing length l). Lower Main Sequence stars, of which the sun is one, are characterized by comparatively weak rotation. The dimensionless parameter q, which

represents the ratio of the centrifugal and Coriolis forces to the force of gravity, is small for such stars. Thus, for the surface of the sun

$$q = \frac{\Omega_\odot^2 a_\odot^3}{GM} \sim 10^{-5}. \qquad (2.3)$$

where $a_\odot$ is the radius of the sun, M is its mass, and G is the gravitational constant.

Thus the stabilizing effect of rotation on convective motions in such stars will be insignificant, and the convection, characterized by Rayleigh numbers of the order of 10^{20}, should be distinctly turbulent. The thermal diffusivity χ, which is determined by radiation, is much larger than ν, so that the Prandtl number is much smaller than unity for these zones. Thus, the Sun has a very small Prandtl number, $\sim 10^{-9}$. However, Ra · Pr is of the order of 10^3, i.e., the convective heat flux is a significant factor in the structure of the zone [15].

There is no satisfactory theory of turbulent convection even in the Boussinesq approximation. The only theory that makes it possible, if very roughly, to calculate turbulent convective envelopes in stars is the so-called mixing-length theory [14]. To apply it, the depth (below the surface of the photosphere) at which the upper boundary of the convective zone is situated is determined first, since it is known that the upper layers of the photosphere are stable with respect to convection. Convective instability begins at an approximate optical depth $\tau = 0.71$–1.0 (depending on the metal content of the photosphere), which corresponds to a geometric depth of 27–250 km. Convective instability arises at this depth as a result of the sharp increase in opacity with increasing temperature and, consequently, increasing depth. This causes a sharp increase in the radiative temperature gradient, and the instability condition $\nabla T \geqslant \nabla_r T$ begins to hold at some depth. It is assumed that the equals sign defines the upper boundary of the zone and the corresponding values of the temperature T, density ρ, and pressure T. This is followed by a calculation based on the simplest conceptions of convection as consisting of ascending and descending convective elements of the medium. Four different temperature gradients are distinguished: $\nabla_r T$, the radiative temperature gradient (which forms at radiative equilibrium); $\nabla_a T$, the adiabatic gradient; ∇T, the mean temperature-stratification gradient, and $\nabla' T$, the temperature gradient of the buoyant convective element, which differs from the adiabatic gradient as a result of radiative heat transfer with the surrounding medium. Below we present the energy relations that are satisfied for the motion of convective elements over the mixing length l. /153

1. The average kinetic energy of a moving element is proportional to the work of the Archimedean force on the mixing length:

$$v^2 = \tilde{\nu} g l^2 \frac{\nabla' T - \nabla T}{T} Q, \qquad (2.4)$$

where v is the average velocity of the convective element, g is the acceleration of gravity, $\tilde{\nu}$ is a parameter that takes viscous drag into account, and finally, $Q = 1 - \frac{T}{\mu}\frac{\partial \mu}{\partial T}$ is a coefficient that takes account of the temperature variations of the average molecular weight of the medium.

2. The sum of the convective and radiative heat fluxes is constant and equal to the radiation flux at the boundary:

$$\alpha \rho c_p v l (\nabla' T - \nabla T) - \frac{16}{3}\frac{\sigma T^3}{\varkappa \rho}\nabla T = \sigma T_{\text{eff}}^4, \qquad (2.5)$$

where T_{eff} is the effective temperature, $\sigma = ac/4$, and α is the correlation coefficient between velocity and temperature.

3. The difference between $\nabla' T$ and $\nabla_e T$ results from radiation of the convective element. For this reason, the average thermal energy deficiency in the convective cell, which is proportional to $\nabla' T - \nabla_e T$ and appears as a result of radiation, should be equal to the energy radiated by the element during its lifetime. From this,

$$\frac{\nabla T - \nabla' T}{\nabla' T - \nabla_e T} = f\frac{\rho^2 c_p \varkappa v l}{\sigma T^3}, \qquad (2.6)$$

where f is a parameter that takes account of the radiative losses of the moving element and depends on the model used for it.

Equations (2.4)-(2.6) can be used to determine ∇T, $\nabla' T$, and v in terms of T, P, l and the parameters $\tilde{\nu}$, α, and β. The stratification of the zone is then found by integrating the equations

$$\frac{dT}{dz} = -\nabla T \qquad \frac{dP}{dz} = g\rho$$

(where the depth z is measured from the level of the star's photosphere). The turbulent viscosity coefficient is determined from the relation $\eta = \overline{\rho v l}$. /154

Although the theory considered above may appear quite crude, it makes it possible to obtain useful and qualitatively correct

results concerning the structure of the convective zone [15]. The basic hypotheses adopted in this theory were: 1) replacement of the quadratic terms by vortical terms with turbulent transport coefficients proportional to $\rho v l$, and 2) substitution of $1/l$ for the derivatives in the turbulent-convection equations. The latter reduces the quantitative value of the results considerably. Yet another serious uncertainty is inherent in the choice of l. Various definitions have been proposed for the "mixing length" l: proportionality to the local pressure-height scale h_p [14, 16], proportionality to the local density-height scale h_ρ, the distance to the nearest zone boundary z [15], and a few combined definitions [17] of the type

$$l = \begin{cases} z & z \leqslant {}^1/_2 h_\rho, \\ {}^1/_2 h_\rho & \text{for } z > {}^1/_2 h_\rho,\ z_0 - z > {}^1/_2 h_\rho, \\ z - z_0 & z - z_0 \leqslant {}^1/_2 h_\rho, \end{cases}$$

where z_0 is the depth of the convective zone. There are as yet no sufficiently convincing physical arguments in favor of any definition of l. In addition, it must be remembered that the turbulent transport coefficients may be different for the different processes — momentum transport and heat transfer. And whereas the characteristic mixing length for momentum exchange will be proportional to the pressure-height scale, heat exchange will be more likely to take place over distances proportional to the entropy (S) height scale, because $\nabla S \sim \Delta \nabla T$. It should also be noted that the parameters α, $\tilde{\nu}$, and f that appear in Eqs. (2.4)-(2.6) are not defined explicitly enough [14, 18].

This semiempirical theory of turbulent convection does not take account of the effects of rotation on the convection characteristics of the zone. At small values of the parameter q, rotation will evidently have a weak influence on the average stratification of the convective envelope and on its depth. Rotation should have its basic effects on the turbulent transport coefficients, which should, in this case, be functions not only of r, but also of ϑ.

Since the convection-rotation interaction is determined by the Taylor number, it may be assumed that the dependence of η on ϑ will be expressed through the dependence on Tr:

$$\eta(r, \vartheta) = \eta[r, \mathrm{Tr}(r, \vartheta)];$$

in stratified zones, the Taylor number $\mathrm{Tr} = 4\Omega^2 d^4 \cos^2 \vartheta / \nu^2$ is itself a function of r and ϑ.

For slowly rotating configurations, it is logical to assume, as an approximation, that η depends linearly on Tr, and, using the

conclusions of §1, we may write

$$\eta(r, \vartheta) = \eta(r, \pi/2)[1 - \delta(r)\cos^2\vartheta], \qquad (2.7)$$

where $\delta(r)$ is a certain function of radius: $|\delta(r)| \ll 1$ but $|\delta(r)| > 0$. Unfortunately, there are no theoretical or experimental facts that permit more accurate determination of the function $\delta(r)$.

§3. The major difficulties that arise in calculation of turbulent-convection zones resulted at first in the use of hydrostatic models to study the structure of stellar convective envelopes [1]. The polytropic relation between P and ρ was usually used instead of the heat flux equation. /155

Thus, this relation was taken in the form $P = C\rho^n$ and $n = \gamma$ in the pioneering works of Schwartzschild [1] (γ is the ratio of heat capacities). This means that the true temperature gradient is exactly equal to the adiabatic gradient:

$$\Delta\nabla T \equiv -\nabla T + \frac{\gamma - 1}{\gamma}\frac{T}{P}\nabla P = 0. \qquad (3.1)$$

Use of Eq. (3.1) for the sun was justified by the fact that the ratio $\Delta\nabla T/\nabla T$ is small, on the order of 10^{-6}.

The spherically symmetrical model described by the hydrostatic equation, the Schwartzschild condition (3.1), and the equation of state

$$P = \frac{k}{\mu m_H}\rho T \qquad (3.2)$$

(μ is the average molecular weight expressed in units of the proton mass, m_H is the mass of the proton, and k is Boltzmann's constant), with the appropriate boundary conditions [1], gives a good description of the average temperature and density distributions in the convective envelopes of lower Main Sequence stars and of the sun in particular.

However, the phenomena of solar granulation, stellar differential rotation, the high temperature of the chromosphere and of the corona in particular, and many others cannot be explained without consideration of the physical processes that take place in the convective envelope, without understanding of its fine structure. The hydrostatic model is found to be inadequate for these purposes, and it becomes necessary to study hydrodynamic flows in the envelopes [19] with consideration of the energy-transfer mechanism, rotation, turbulence, and sometimes electromagnetic fields. The equation of motion in the convective zone has the form

$$\frac{dv}{dt} = -\frac{1}{\rho}\nabla P - \nabla\mathcal{G} + \frac{1}{\rho c}(j \times H) + \frac{1}{\rho}\nabla\mathcal{P} + \frac{1}{\rho}\nabla\mathcal{T}, \tag{3.3}$$

where $V(u^1, u^2, u^3)$ is the velocity of the averaged motion, $\mathcal{G}$ is the gravitational potential, $1/c\,(j \times H)$ is the electromagnetic Lorentz force, $\mathcal{P}$ is the viscous-stress tensor, and $\mathcal{T}$ is the turbulent Reynolds stress tenscr. The continuity and Poisson's equations are written in the usual form:

$$\frac{d\rho}{dt} + \rho \operatorname{div} V = 0, \tag{3.4}$$

$$\Delta\mathcal{G} = -4\pi\rho. \tag{3.5}$$

Various terms in Eqs. (3.3)-(3.5) can be neglected, depending on the specific problem. The heat flux equation, in whose derivation it is necessary to consider turbulent convection, radiative heat transfer, and the release of Joule heat, assumes the form

$$\rho\frac{d\varepsilon}{dt} + \frac{\partial}{\partial x^i}[F^i + \overline{\varepsilon'\rho u'^i}] + P\frac{\partial u^i}{\partial x^i} + \overline{(P+P')\frac{\partial u'^i}{\partial x^i}} = \overline{\Phi} + \overline{\frac{\nu_m}{4\pi}(\operatorname{rot} H)^2}. \tag{3.6}$$

where ε is the averaged internal energy, F^i is the i-th component of the average radiation flux, u', P', and ε' are the fluctuation components of velocity, pressure, and internal energy, the terms on the right of (3.6) are governed by viscous and Joule heat dissipation, and ν_m is the magnetic viscosity. Thus, the effect of turbulence in the heat flux equation will be expressed by the term $\overline{\varepsilon'\rho u'^i}$, which describes the transfer of internal energy by turbulent fluctuations, by the work $\overline{(P+P')\frac{\partial u'^i}{\partial x^i}}$ of the pressure forces for turbulent compression of the medium, and by the corresponding increase in viscous and Joule heat dissipation on the turbulent fluctuations. /156

The equation system (3.3)-(3.6) must be supplemented by the Maxwell electromagnetic equations. It appears that electromagnetic forces in the convective envelope are quite small for stars of the sun's type and have no substantial influence on the hydrodynamic currents. We shall therefore henceforth omit the electromagnetic terms in (3.3) and (3.6). Allowance for the turbulent nature of the motion in the convective zones has led to the appearance of a number of new unknowns in the equations of motion and the heat flux equation: $\tau^{ij} = -\overline{\rho u'^i u'^i}$, the turbulent Reynolds stresses; $\overline{\rho' u'^i}$ and $\overline{T' u'^i}$, the correlations of the velocity, density, and temperature fluctuations, etc.

These new unknowns have appeared as a result of averaging of the Navier-Stokes equation, and their appearance is a direct consequence of the nonlinearity of the fluid-mechanics equations. To close the system (3.3)-(3.6), it is necessary either to supply additional equations for these unknowns or to attempt to express them in terms of the averaged quantities and their derivatives. These supplementary relations are either purely empirical ones from experimental data or are derived from qualitative considerations of a physical nature. One of the best known of these semiempirical theories that relate the additional unknowns with the averaged variables is the Prandtl momentum-transfer theory (see, for example, [20]). Prandtl introduced the notion of the "mixing length" l – the distance travelled by a "turbulent element" before it is mixed and exchanges momentum with other elements. This concept is to some extent analogous to the molecular free path in the kinetic theory of gases. The mixing-length concept is used to define the eddy viscosity η, which is analogous to the molecular viscosity ν and establishes a linear relation between the turbulent stresses and the rate of deformation. Prandtl developed his theory for plane-parallel motion, in which there is only one velocity component along the x axis: $u = u(z)$. Working from the same premises, Wasiutinsky [19] generalized the Prandtl theory to three-dimensional motions in stars. Using physically lucid arguments and the definition of the mixing length, Wasiutinsky obtained a linear expression for the turbulent-stress tensor in terms of the deformation rates. In tensor form, this relation can be written as follows in spherical coordinates:

$$\tau_{ik} = -\eta_i^i(\nabla_i u_k + g_{kk}\Gamma_{i\alpha}^k u^\alpha) - \\ -\eta_k^k\left(\nabla_k u_i + g_{ii}\Gamma_{k\alpha}^i u^\alpha + g_{kk}g_{ii}\delta_k^i\frac{\partial g^{kk}}{\partial x^\alpha}u^\alpha\right)^* \qquad (3.7)$$

(summation only over α), where i, k, and α assume the values r, θ, φ, ∇_j are the covariant derivatives, $\Gamma_{j\beta}^n$ are Christoffel symbols, g_{ji} and g^{ji} are the fundamental metric tensors, δ_j^n is the unit tensor, and η_j^i is the eddy viscosity tensor, which is of diagonal form in spherical coordinates bound to the center of the star.

The eddy viscosities are defined as

$$\eta_i^i = \overline{\rho\theta u'^i u_i'} \qquad (3.8)$$ /157

where θ is the time during which a turbulent element covers the "mixing length." The linear relation (3.7) between the tensor τ_{ik}

*Here and below, the inferior and superior indices pertain to the covariant and contravariant components of the vectors and tensors.

and the deformation rates was obtained later by Elsasser [21] by rigorous derivation from the Boltzmann equation under the following assumptions:

1) the mixing length l is much smaller than the characteristic linear dimension of the problem;

2) the mixing time θ does not depend on the velocity of the turbulent element;

3) the tensor η_j^i is of diagonal form in spherical coordinates;

4) the tensor η_i^i does not depend on the coordinates or, if it does depend on r,

$$\left|\frac{\partial \ln \eta_r^r}{\partial r}\right| < \left|\frac{\partial \ln u_r}{\partial r}\right| \text{ and } \left|\frac{\partial \ln \eta_i^i}{\partial r}\right| < \frac{2}{r} \quad (i = \vartheta, \varphi).$$

Using the mixing-length concept and the eddy viscosities, Eq. (3.6) can be transformed by expressing the pulsation time correlations in terms of the averaged characteristics of the motion:

$$\rho \frac{de}{dt} - \frac{P}{\rho}\frac{d\rho}{dt} + \nabla_i [F^i + c_p \eta^{ik} \Delta\nabla_k T] - \frac{\eta^{ik}}{T\rho}\frac{\partial P}{\partial x^i}\Delta\nabla_k T = \overline{\Phi}, \tag{3.9}$$

where

$$\Delta\nabla_k T = -\frac{\partial T}{\partial x^k} + \left(\frac{dT}{dP}\right)_s \frac{\partial P}{\partial x^k}.$$

A term describing the energy dissipation as a result of viscosity on turbulent fluctuations appears on the right side of (3.9). Unfortunately, there are as yet no reliable estimates of $\overline{\Phi}$ [19] for free turbulent convection in an unstably stratified medium. Taylor's estimates are available for isotropic turbulence:

$$\overline{\Phi} \sim \nu E_T / \lambda^2, \tag{3.10}$$

(E_T is the turbulent energy density, λ is a length on the order of the turbulent-vortex diameter, and ν is the kinematic viscosity).

Wasiutinsky's theory made it possible to use fewer additional unknowns and to reduce them to three diagonal components of the turbulent-friction tensor. Leaving the influence of rotation on the friction coefficients out of account, we may assume further that the directions ϑ and ϕ of the spherical coordinate system are equivalent and the direction r is singular for turbulent fluctuations:

$$\eta_r^r = \eta; \qquad \eta_\vartheta^\vartheta = \eta_\varphi^\varphi = \eta_s. \tag{3.11}$$

In fact, the Archimedean force, which is the cause of turbulent convection, is directed along the vector of r. The coefficient S is known as the coefficient of anisotropy and is a measure of the degree of anisotropy of the turbulent fluctuations. At S = 1, the turbulent mixing is isotropic; when S > 1 mixing is weaker in the radial direction than along meridians and parallels; when S < 1 exchange of momentum is stronger in the radial direction. The scalar part of the viscosity η should in the general case, be a function only of r (since we neglect rotation). The coefficient of anisotropy can evidently be assumed constant.

Consideration of slow rotation results in a relation of the type (2.7) for η as a function of r and ϑ. In addition, rotation may cause a nondiagonal component $\eta_{\vartheta}^{\varphi}$ to appear in the tensor η owing to distortion of the principal axes of the turbulent-friction tensor [22]. /158

In the generally accepted semiempirical theories of turbulence [20], the eddy viscosity or the mixing length l, in terms of which it is expressed, is found directly from experiment or from hypotheses, which are then confirmed by experiment. Unfortunately, this is impossible when we are concerned with turbulent convection in stars.

§4. The equations of motion for the averaged characteristics (2.5) and the corresponding equations for the turbulent fluctuations can be used to derive a turbulent-energy balance equation and an energy equation for the averaged motion by applying Wasiutinsky's semiempirical theory.

$$\frac{\partial E_\tau}{\partial t} + \nabla_i \left(u^i E_\tau + \eta^{ik} \frac{E_\tau}{\rho} \frac{\Delta \nabla_k T}{T} \right) - A - B + \overline{\Phi} = 0, \tag{4.1}$$

$$\frac{\partial E}{\partial t} + \nabla_i (u^i E + \tau_k^i u^k) = \rho u^i g_i - u^i \nabla_i P - A. \tag{4.2}$$

Here $E_T = {}^1/_2 \overline{\rho u'^i u'_i}$ is the turbulent energy density, E is the kinetic-energy density of the averaged motion, the term $\eta^{ik} \frac{E_\tau}{\rho} \times \frac{\Delta \nabla_k T}{T}$ represents the diffusion of turbulent energy by the fluctuation motion, and $u^i E_T$ the diffusion by the averaged motion. The term $A = -\tau_i^k \nabla_k u^i$ describes the exchange of energy between the averaged and fluctuation motions. Usually $A > 0$, i.e., the turbulent-motion energy increases at the expense of the averaged-motion energy, although it is possible for $A < 0$ in specific regions. The term $B = \eta^{ik} g_i \frac{\Delta \nabla_k T}{T}$ represents the work of Archimedean forces on the turbulent fluctuations; in the case of an unstably stratified medium, $\Delta \nabla T > 0$, this work is performed at the expense of stratification potential energy and leads, as we see from (4.1), to an increase in turbulence energy.

The heat flux equation (3.9) can be written as follows:

$$P\frac{\partial}{\partial t}\ln\frac{T^{\gamma/\gamma-1}}{P}-c_p\rho u^i\Delta\nabla_i T+\nabla_i\left[F^i+c_p\eta^{ik}\Delta\nabla_k T\right]+B=\overline{\Phi}. \qquad (4.3)$$

If we consider a steady-state situation and apply Eqs. (4.1), (4.2), and (4.3) to a closed volume of gas τ on whose boundaries Σ_1 and Σ_2 there is no turbulent-energy influx and no stresses are applied, for example, to the convective envelope of the star, we obtain the condition

$$A_\tau+B_\tau=\overline{\Phi}_\tau, \qquad (4.1')$$

$$A_\tau=-\int_\tau u^i\nabla_i P\,d\tau, \qquad (4.2')$$

$$-\int_\tau u^i\nabla_i P\,d\tau+F_n|_{\Sigma_2}-F_n|_{\Sigma_1}+B_\tau=\overline{\Phi}_\tau \qquad (4.3')$$

or

$$F_n|_{\Sigma_2}=F_n|_{\Sigma_1}$$

for maintenance of stationary motion and developed turbulence in this volume. The last relation, (4.3'), indicates that the thermal regime of the volume is stationary and that there are no heat sources in it. Eq. (4.1') indicates that to maintain developed turbulence in the volume τ in the stationary state, it is necessary to supply an energy equal to $\overline{\Phi}$ to the fluctuation motion, and that this input can be obtained at the expense of the averaged-motion energy A and the work B of the Archimedean forces. Equations (3.3)-(3.5) and (4.3) can be used to study the hydrodynamics of stellar convective envelopes if the angular momentum of the envelope, the boundary conditions, zone depth, and turbulent-viscosity tensor are assigned. The zone depth and turbulent transport coefficients must first be determined from auxiliary considerations, e.g., as in §2. /159

Here, depending on what connotation we place on the coefficients η^i_k, there are various possible approaches to study of the convective-zone hydrodynamics. The eddy viscosity can be defined as the effective viscosity that arises as a result of all small-scale convective motions after separating convective flows on the largest scale, of the order of the zone depth, and the problem of the interaction between laminar convection and rotation in a medium with an effective eddy viscosity η can be solved. Here it is found that the effective Rayleigh number is above critical:

$$\mathrm{Ra}_e=\frac{\beta g d^4\Delta\nabla T}{T\eta^2}>\mathrm{Ra}_e.$$

This formulation of the problem is justified by the fact that rotation has the strongest influence on the large-scale flows. The influence of rotation on convective modes of small scales can be taken into account by assuming a relation between η and the Taylor number, e.g., in the form of (2.7). With (4.1), the heat flux equation becomes

$$-\frac{\gamma}{\gamma-1}pV\frac{\Delta\nabla T}{T}+\operatorname{div}(F+H)=\overline{\Phi}. \qquad (4.4)$$

Here H is the heat flux due to the effective thermal conductivity and Φ is the dissipation due to the effective viscosity. The value of the radiation flux F at the boundary must be assigned.

If the effective viscosity η is defined as the total viscosity from the convective modes of all scales, the problem is one of investigating the meridional currents that arise in the stellar envelopes under the influence of slow rotation due to the anisotropy of the transport coefficients. In this case, the effective Rayleigh number is smaller than the critical value Ra_c. The general problem of turbulent convection in stratified envelopes of slowly rotating stars can be separated in this way into two successive problems, of which the first is a problem of turbulent convection in a stratified medium and is solved by the mixing-length method (§2), while the second is one of the meridional currents that arise on rotation in a medium with an anisotropic effective viscosity. For this separation to be made rigorously, it is necessary that the scale of the convective motions (i.e., the mixing length) be much smaller than the scale of the meridional circulation, i.e., the zone depth d [21]. The calculations of [16] indicate that this condition is satisfied for the sun everywhere except the lower boundary of the zone, where $l \approx 0.8 \cdot 10^{10}$ cm, with a total zone depth $d \approx 2 \cdot 10^{10}$ cm.

For lower Main Sequence stars, the factors causing the structure of the star to deviate from hydrostatic are small; thus, the ratio of centrifugal force to the force of gravity at the equator on the surface of the sun is $q \approx 10^{-5}$ and the ratio ΔVT/VT is, on the average, of the order of 10^{-5}-10^{-6}. Hydrostatic equilibrium, together with the adiabaticity condition, can therefore be regarded as the zeroth approximation in study of the envelope structures, and the deviations due to rotation and heat flux can be treated as small perturbations of the same order that are superimposed on the basic spherically symmetrical state. Introducing /160 the dimensionless variables[3]

[3]Here M is the mass, a_0 is the radius, and Ω_0 the surface angular velocity of the star, and η_0, F_0, and ρ_0 are the characteristic values of these parameters in the convective envelopes.

$$\tau = \frac{t}{\Omega_0}, \quad \xi = \frac{\eta}{\eta_0}, \quad f = \frac{F}{F_0}, \quad x = \frac{r}{a_0},$$
$$R = \frac{\rho}{\rho_0}, \quad p = \frac{a_1 P}{GM\rho_0}, \quad v = \frac{V}{a_0\Omega_0}, \quad t = \frac{k}{\mu m_H}\frac{a_0 T}{GM},$$

We may write the equations in dimensionless form and then expand with respect to the small parameter q. The nature of the meridional circulation that appears will be determined by the effective Reynolds number

$$\mathrm{Re}_\tau = \Omega_0 a^2/(\eta_0/\rho_0).$$

In dimensionless form, the heat-flux equation becomes

$$p\frac{\partial}{\partial\tau}\left(\ln\frac{t}{p^{\gamma-1/\gamma}}\right) - \frac{p}{t}v_x\Delta\nabla_x t - \frac{p}{t}\frac{v_\theta}{x}\Delta\nabla_\theta t + \frac{1}{\mathrm{Nu}-1}\frac{1}{\mathrm{Re}_\tau}\frac{\gamma-1}{\gamma}\times$$
$$\times\left[\frac{1}{x^2}\frac{\partial(x^2F_x)}{\partial x} + \frac{1}{x\sin\theta}\frac{\partial(\sin\theta F_\theta)}{\partial\theta}\right] + \frac{1}{\mathrm{Re}_\tau}\left[\frac{1}{x^2}\frac{\partial}{\partial x}(\xi x^2\Delta\nabla_x t) + \right.$$
$$\left. + \frac{S\xi}{x^2\sin\theta}\frac{\partial}{\partial\theta}(\sin\theta\Delta\nabla_\theta t)\right] - \frac{\gamma-1}{\gamma}\frac{1}{\mathrm{Re}_\tau}\times \qquad (4.5)$$
$$\times\left[\xi\frac{\partial p}{\partial x}\frac{1}{R}\frac{\Delta\nabla_x t}{t} + \frac{S\xi}{R}\frac{\partial p}{\partial\theta}\frac{\Delta\nabla_\theta t}{x^2 t}\right] = \overline{\Phi}.$$

where Nu is the dimensionless Nusselt number, which determines the ratio of the total heat flux to the heat flux in the absence of convection. The total resulting flux will obviously be determined by the condition at the lower boundary at the convective zone, and will be equal to the radiation flux from the core of the star, which carries the energy released there as a result of nuclear reactions to the surface. Convection is still very weak near the boundary with the core, since the temperature fluctuations and convection velocity are small there, i.e., radiation is the main transfer mechanism, and Nu is near unity. However, the calculations of [16] (see table) indicate that η increases sharply near the boundaries and convection becomes the chief mechanism of energy transfer. The thermal boundary layer, whose structure is determined by the radiation, is very thin. To simplify calculation of hydrodynamic currents in the convective zones, therefore, we can neglect the radiation flux, assigning the convective heat flux or, more precisely, $\Delta\nabla T$, on a slightly modified boundary and putting $\mathrm{Nu} = \infty$ in Eq. (4.5).

We obtain the heat-flux approximation for the first approximation with respect to q by using the expansion of the function with respect to the parameter q:

$$p(r, \theta) = p_0(r) + qp_1(r, \theta) + \ldots,$$

and, retaining first-order terms,

$$-\frac{p_0}{t_0}\left(v_x\Delta\nabla_x t_1+\frac{v_\theta}{x}\Delta\nabla_\theta t_1\right)+\frac{1}{\mathrm{Re}_\tau}\left[\frac{1}{x^2}\frac{\partial}{\partial x}(\xi x^3\Delta\nabla_x t_1)+\right.$$
$$\left.+\frac{S\xi}{x^3\sin\theta}\frac{\partial}{\partial\theta}(\sin\theta\Delta\nabla_\theta t_1)\right]-\frac{\gamma-1}{\gamma}\frac{1}{\mathrm{Re}_\tau}\left[\xi\frac{\partial p_0}{\partial x}\frac{1}{R_0}\frac{\Delta\nabla_x t_1}{t_0}\right]=\overline{\Phi}. \qquad (4.6)$$

Without consideration of the effects of rotation and convection, the turbulent dissipation $\overline{\Phi}$ is obviously a function only of x, and it can be determined accurate to a constant by using the Taylor formula (3.10), the value of ν from (2.2), and the values obtained from mixing-length theory for E and λ [16]. The undetermined constant can be determined by applying the turbulent-energy balance equation to the entire convective volume.

CHARACTERISTICS OF THE SUN'S CONVECTIVE ENVELOPE (from [16]) /161

Depth D, cm	Density ρ, g/cm^3	Mixing length l, cm	Eddy viscosity η, g/cm·sec	Turbulent fluctuation velocity, cm/sec	cm^2/sec
3.4 (6)	4.0 (−7)	2.3 (7)	7.3 (4)	2.4 (4)	1.8 (11)
1.3 (7)	4.6 (−7)	3.3 (7)	1.1 (6)	2.2 (5)	2.4 (12)
3.7 (7)	8.3 (−7)	4.5 (7)	1.9 (6)	1.5 (5)	2.3 (12)
1.5 (8)	7.2 (−6)	8.3 (7)	1.5 (7)	7.6 (4)	2.1 (12)
3.6 (8)	6.2 (−5)	1.5 (8)	1.3 (8)	4.2 (4)	2.1 (12)
1.0 (9)	8.2 (−4)	4.5 (8)	2.6 (9)	2.2 (4)	3.1 (12)
3.3 (9)	8.3 (−3)	1.6 (9)	4.9 (10)	1.1 (4)	5.5 (12)
1.1 (10)	7.6 (−2)	5.5 (9)	7.5 (11)	5.4 (3)	9.8 (12)
1.8 (10)	1.8 (−1)	7.8 (9)	1.4 (12)	2.9 (3)	7.7 (12)
1.9 (10)	2.1 (−1)	8.1 (9)	1.1 (12)	2.0 (3)	5.2 (12)

Remarks: Mixing length l = 1.5× pressure-height scale. D is depth from the upper boundary of the photosphere. The convective zone ranges from D = 2.7×10^6 cm to D = $1.9 \cdot 10^{10}$ cm. The characteristic of the number is indicated in the parentheses.

Equations (4.5) and (4.6) define the function $\Delta\nabla t(x,\theta)$, i.e., the deviation of the true temperature gradient from adiabatic in various convective-shell layers. It is interesting to estimate the deviation from barotropy $\nabla\rho\times\nabla P=0$ that may result from rotation of stars. In the case of thermally stable stratification $\Delta\nabla T<0$, the deviation from barotropy may result in the appearance of a baroclinic instability owing to the release of gravitational energy. It can be assumed that the absence of barotropy will have an even stronger effect on the character of the motions in the case of thermally unstable stratification.

Let us consider the form taken by (4.6) for the cases of small and large Reynolds numbers. For $Re_t >> 1$, the influence of eddy viscosity in the zone is insignificant, and the heat flux equation reduces, as we should expect, to the adiabaticity condition for the motion:

$$\frac{d}{dt}\left(\frac{p}{\rho^{\gamma}}\right) = 0.$$

In the other extreme case, when the viscous forces are large (and Re_t is small), Eq. (4.6) assumes the form

$$\frac{\partial^2 z}{\partial x^2} + \frac{1}{x}\frac{\partial z}{\partial x}\left(2 + \frac{d\ln\xi}{d\ln x} + \frac{d\ln t_0}{d\ln x} - \frac{\gamma}{\gamma-1}\frac{x}{R_0 t_0}\frac{dp_0}{dx}\right) + \\ + \frac{S}{x^2\sin\vartheta}\frac{\partial}{\partial\vartheta}\left(\sin\vartheta\,\frac{\partial z}{\partial\vartheta}\right) = \frac{\overline{\Phi}(x)}{\xi t_0}. \qquad (4.7)$$

Here Φ, ξ, and the zeroth-approximation functions p_0, R_0, and t_0 depend only on x and z denotes

$$z = \frac{\gamma-1}{\gamma}\frac{p_1}{p_0} - \frac{t_1}{t_0}.$$

The general solution of (4.7) can be written with separation of variables in the form

$$z = \sum_{n=0}^{\infty}\left(C_{1n}Z_{1n} + C_{2n}Z_{2n}\right)P_{2n}(\mu) + Z_{00}(x). \qquad (4.8)$$

where $\mu = \cos\vartheta$, $Z_{1n}(x)$ and $Z_{2n}(x)$ are solutions of the ordinary differential equation /162

$$\frac{d^2Z}{dx^2} + \frac{dZ}{dx}\frac{1}{x}\left(2 + \frac{d\ln\xi}{d\ln x} + \frac{d\ln t_0}{d\ln x} - \frac{\gamma}{\gamma-1}\frac{x}{R_0 t_0}\frac{dp_0}{dx}\right) - \frac{2ZSn(2n+1)}{x^2} = 0.$$

$P_{2n}(\mu)$ are Legendre polynomials, C_{1n} and C_{2n} are arbitrary constants determined from the boundary conditions, and Z_{00} is a particular solution of the inhomogeneous equation (4.7) and depends only on x. For the convective envelopes of slowly rotating stars, it can be assumed with good accuracy that the boundary conditions for x are independent of ϑ. Then $\Delta\nabla t_1 = t_0\nabla z$ will be a function only of x, and the motion remains barotropic in this approximation.

The next approximation of (4.6) can be found on expansion in series with respect to the small Re_t. In this case, the heat flux equation will be an inhomogeneous linear equation whose right-hand side is a function of x and ϑ and is defined in terms of the functions of

the preceding approximation:

$$\frac{1}{x^3}\frac{\partial}{\partial x}(\xi x^2 \Delta\nabla_x t_2) - \frac{\gamma-1}{\gamma}\xi\frac{dp_0}{dx}\frac{1}{R_0}\frac{\Delta\nabla_x t_2}{t_0} + \frac{\xi S}{x^2\sin\theta}\frac{\partial(\sin\theta\Delta\nabla_\theta t_2)}{\partial\theta} =$$
$$= \frac{p_0}{t_0}\left(v_x\Delta\nabla_x t_1 + \frac{v_\theta}{x}\Delta\nabla_\theta t_1\right),$$

i.e., $\Delta\nabla t_2$ will be a function of x and θ.

In the general case, in which the hypotheses $Re_t << 1$ and $Re_t >> 1$ are not justified, the general form of the heat flux equation (4.3) should be used to close the system of fluid-dynamics equations (3.3)-(3.5), which describes the meridional circulation in slowly rotating convective envelopes.

We have analyzed the state of thermal instability of the medium in stellar convective envelopes for lower Main Sequence stars. It has been shown that results obtained in hydrodynamics on convective instability in rotating media cannot be applied directly to the convective envelopes, since the medium is strongly stratified in this case (density varies through 5-6 orders) and the Rayleigh numbers range up to 10^{20}, which is characteristic of a strongly turbulized convection situation. In the absence of a satisfactory theory of turbulent convection (even in the Boussinesq approximation and without considering rotation), it is suggested that the problem of meridional flows in the convective envelopes of slowly rotating stars be solved in two steps. First, an extremely primitive theory - mixing-length theory - is used to calculate the characteristics of the turbulent fluctuations in a plane convective layer without consideration of rotation, and the eddy viscosity is found as a function of depth in the convective zone. This coefficient is then used to find the turbulent Reynolds stresses (in the form proposed by Wasiutinsky) in the fluid-dynamics equations that describe the meridional flows that arise in convective envelopes as a result of the combined action of rotation and eddy-viscosity anisotropy. Instead of the barotropy condition, it is proposed that the complete heat flux equation be used with consideration of heat transfer by turbulent fluctuations. This will make it possible to take account of the redistribution of the temperature-gradient difference $\Delta\nabla T$ due to the meridional circulation that arises.

REFERENCES

/163

1. M. Schwartzschild, The Structure and Evolution of the Stars (Russ. ed.), Moscow, IL, 1961.
2. S. Chandrasekhar. Hydrodynamic and Hydromagnetic Stability. Oxford, 1961.
3. G.W. Simon and N.O. Weiss. Supergranules and the Hydrogen Convective Zone, Zeit. für Astrophys., 1968, Vol. 69, 6, 435-450.

4. G. Veronis. Penetrative Convection. Astrophys. J., 1963, Vol. 137, 2, 641-663.
5. P.P. Niiler and F.E. Bisshopp. Onset of Convection in a Rapidly Rotating Fluid Sphere, J. Fl. Mech., 1965, Vol. 23, 3, 459-469.
6. P.H. Roberts. On the Thermal Instability of a Rotating Fluid Sphere Containing Heat Sources, Phil. Trans. Roy. Soc., 1968, Vol. A263, 1136.
7. G. Veronis. Cellular Convection with Finite Amplitude in a Rotating Fluid, J. Fl. Mech., 1959, Vol. 5, 3, 401-435.
8. G. Randers. On the Rotation of the Stars with Convective Core, Astrophys. J., 1942, Vol. 95, 3, 454-460.
9. T.G. Cowling. The Condition for Turbulence in Rotating Stars. Astrophys. J., 1951, Vol. 114, 1, 272-281.
10. M.G. Clement. The Effect of a Small Rotation on the Convective Instability of a Gaseous Mass, Astrophys. J., 1965, Vol. 142, No. 1, 243-252.
11. N.R. Lebovitz. The Principle of Exchange of Stabilities, II. The Onset of Convection in the Presence of Rotation, Astrophys. J., 1967, Vol. 150, 1, Part 1, 203-212.
12. W.V. Malkus. Discrete Transitions in Turbulent Convection, Proc. Roy. Soc., 1954, Vol. A225, 1161, 185-195.
13. S.I. Braginskiy. Transfer Phenomena in Plasma. In collection entitled: "Voprosy teorii plazmy" (Problems of Plasma Theory), No. 1, Moscow, Atomizdat, 1963.
14. E. Böhm-Vitense. Hydrogen-Convection Zone in Stars with Various Effective Temperatures and Luminosities. Zeit. für Astrophys., 1958, Vol. 46, 2, 108-143.
15. E.A. Spiegel and K.H. Bohm. The Solar Atmospheric Convection Zone, IAU Symposium, No. 28, 1967.
16. N. Baker and S. Temesvary. The Tables of Convective Stellar Envelope Models, New York, 1966.
17. S. Muzuno and M. Nishida. On the Structure of the Outer Solar Convection Zone, Publ. Ast. Soc. Japan, 1969, Vol. 21, 2.
18. K.H. Böhm and E. Stückl. The Lower Thermal Boundary Layer of the Solar Convection Zone, Zeit. für Astrophys., 1967, Vol. 66, 487-495.
19. J. Wasiutinsky. Studies in the Hydrodynamics and Structure of Stars and Planets, Astrophys. Norvegica, 1946, Vol. 4.
20. A.S. Monin and A.M. Yaglom. Statisticheskaya gidromekhanika (Statistical Fluid Mechanics), Vol. 1, Moscow, "Nauka," 1965.
21. K. Elsasser. Anisotropic Friction. Zeit. für Astrophys., 1966, Vol. 63, 2, 65-78.
22. R.S. Iroshnikov. The Nature of the Differential Rotation of the Sun, Astron. Zh., 1969, Vol. 46, No. 1.

N75 13719

CALCULATION OF THE SHAPE OF THE BOUNDARY OF THE MAGNETOSPHERE

(Translation of "O raschete formy granitsy magnitosfery.")

S. A. Mart'yanov

ABSTRACT

The possibilities of calculating the shape and dimensions of the magnetopause are discussed. Initial equations are proposed. A review of existing methods is given. With 2 illustrations and 26 source citations.

CALCULATION OF THE SHAPE OF THE BOUNDARY OF THE MAGNETOSPHERE

S.A. Mart'yanov

Knowledge of the position and shape of the boundary of the magnetosphere (the magnetopause) is important in calculation of the magnetic field within the magnetosphere. According to present-day conceptions, one of the chief causes of the deviation of this field from the dipole model is the magnetic field of currents flowing along the magnetopause. The problem of calculating the shape and dimensions of the magnetosphere's boundary is now stated in the following form.

A stationary uniform flux of collisionless quasineutral plasma with a frozen magnetic field flows past a point magnetic dipole. There are two surfaces of discontinuity — the shock wave and the magnetopause. The main attribute of the shock wave is a nonzero plasma flux across the surface of discontinuity with a simultaneous plasma-density jump, while the basic attribute of the magnetopause consists of abrupt changes in the magnetic-field components tangential to the surface of discontinuity (as we know, the normal magnetic-field component is always continuous).

Let us assume that the motion of the plasma is described by a certain closed equation system that interrelates the various macroscopic quantities describing the plasma. It is then possible in principle to solve the flow problem stated above with consideration of the conditions at the surfaces of discontinuity and, consequently, to find the shape of the magnetopause.

Several such equation systems are now known. The simplest among them are the system of magnetohydrodynamic equations and the system of quasihydrodynamic equations derived in [1] (see also [2]). Strictly speaking, the magnetohydrodynamic equations (in our case with infinite conductivity) are not valid, since the plasma is collisionless. However, the following arguments can be cited in support of the magnetohydrodynamic approach. In a rarefied plasma, the interaction of waves developed due to various types of instabilities may be manifested in the form of effective collisions between plasma particles. Theoretical data obtained in [3] agree satisfactorily in many respects with experimental data. The results of [1, 2] also provide some justification for the approach considered.

Finally, Yu.L. Klimontovich and V.P. Silin [26] showed that when $T_e \gg T_i$ a collisionless plasma can be described in a certain range of characteristic frequencies by the equations of single-fluid hydrodynamics with infinite conductivity ($T_{i,e}$ are the ion and electron temperatures, respectively).

The other possibility rests on a system of quasihydrodynamics equations. Unlike those of magnetohydrodynamics, the equations of quasihydrodynamics enable us to take account of pressure anisotropies present in the plasma. To close this equation system, it is necessary to neglect the third moments along the magnetic field in the electron velocity distribution function. If all quantities vary little in the direction of the magnetic field, this simplification is acceptable [1].

Let the magnetic moment M of the dipole be parallel (anti- /165
parallel) to the homogeneous magnetic field at infinity, B_0, and perpendicular to the stream velocity U, and let the flow in the equatorial plane (i.e., in the plane passing through the center of the dipole and perpendicular to M) be considered two-dimensional. It is then possible to solve the two-dimensional problem of supersonic flow past a "plane magnetic dipole" in a magnetic field perpendicular to the plane of the flow.[1]

We should note that the difference between the two approaches under consideration does not consist entirely in the fact that the pressure is a scalar quantity in one case and a tensor in the other. That is to say, the equations [1, 2]

$$\frac{d}{dt}\left(\frac{p_\perp}{\rho B}\right)=0, \qquad \frac{d}{dt}\left(\frac{p_\parallel B^2}{\rho^3}\right)=0$$

must be used as equations of state in the latter case. Here $p_\perp$ and $p_\parallel$ are the pressure-tensor components perpendicular and parallel to the magnetic field, respectively, B is the absolute value of the magnetic field, and ρ is the density of the plasma.

In the magnetohydrodynamic equation system, it appears to be most reasonable to use the equation of state of the ideal gas and to treat the motion along the streamlines as adiabatic with an effective exponent γ taken in accordance with experimental data.

In fact, no calculations have as yet been made, even in a formulation as limited as that described above. All previous calculations (except for two, of which we shall speak later) fit into the following scheme:

There is no matter within the magnetosphere, and the approximate formula $p = p_0 + p_d \cdot \cos^2\chi$, where p_0 and p_d are constants and χ is the angle between the surface normal and the plasma velocity

---

[1] A two-dimensional problem of this kind with recourse to the quasihydrodynamics equations was apparently first stated in [4]. However, that study contained a number of substantive errors. See below for a critique of [4] and a discussion of the possibilities for such formulation of the problem.

U, is used for the mass pressure on the outer side of the magnetosphere's boundary. The external magnetic field is left out of account. Thus, the magnetopause is automatically treated as a tangential discontinuity.

Within the magnetosphere, the magnetic field B satisfies the equation system curl B = 0, div B = 0 and has a dipole singularity at a point which we shall take as the coordinate origin, and the condition $p = B_t^2/8\pi$ (B_t is the component of vector B tangential to the boundary of the magnetosphere) is satisfied on the boundary of the magnetosphere. The problem is widely known in this formulation as the Chapman-Ferraro problem.

The term p_0 in the formula for the pressure takes account of the presence of a homogeneous and isotropic background, while the term $p_d \cos^2\chi$ admits of two interpretations.

On the one hand, the pressure has this form if there is a homogeneous monovelocity flux of noninteracting particles incident on the surface and subject to elastic reflection from it. Chapman and Ferraro endorsed precisely this model interpretation in their original paper.

On the other hand, the semiempirical Newton-Lees formula of ordinary gas dynamics gives an approximate description of the motion of a gas on the surface of a blunt body in supersonic flow [5] and takes the form $p = p_d \cdot \cos^2\chi$. Since we do not consider the magnetic field in the stream, it appears reasonable to use this formula.

1. The Three-Dimensional Case

/166

Use of the formula $p = p_0 + p_d \cdot \cos^2\chi$ (with the condtiion $B_0 = 0$) makes it possible to find the boundary of the magnetosphere without at the same time solving the complex problem of solar-wind flow around it. But even then only numerical solution of the problem is possible in the three-dimensional case.

One of the approaches to solution of this problem was elaborated in a series of Beard's papers. The paper by Mead and Beard [6] must be recognized as the fundamental work setting forth the method and results obtained from its application.

The idea of the method is as follows. We have on the surface of the magnetosphere

$$p_d \cdot \cos^2\chi = B_t^2/8\pi \quad (p_0 = 0), \text{ or: } |n \times B_t| \sim n \cdot s. \qquad (1.1)$$

Here n is the unit vector normal to the surface, s is the unit vector parallel to the plasma velocity at the particular point on the surface, and B_t is the magnetic field (tangential to

the surface). Let $r = \underline{R}(\theta, \varphi)$ be the equation of the unknown surface in spherical coordinates (the polar axis is parallel to the dipole axis, with the origin at the center of the dipole). The components of the vector n can be expressed in accordance with the familiar formulas of differential geometry in terms of the partial derivatives $\partial\underline{R}/\partial\theta$ and $\partial\underline{R}/\partial\varphi$.

Substituting their values into (1.1), we obtain a first-order partial differential equation with $R(\theta, \phi)$ as the unknown function if B_t is regarded as known.[2] However, B_t depends on the shape of the surface and the current distribution on it. Successive approximations are of assistance here.

Thus, we consider two points separated by an infinitesimal distance and situated on opposite sides of the magnetopause. At the point on the interior side, let $B_t = B_d + B_p + B_c$, where B_d is the dipole magnetic field, B_p is the magnetic field of the currents flowing on the plane tangent to the magnetopause at the point under consideration, which have the same density as the currents flowing in the neighborhood of that point, and B_c is the magnetic field due to the curvature of the surface. Since it is assumed that there is no field in the exterior region, we have $B_d - B_p + B_c = 0$ at the point on the outside of the surface. Actually, the components of B_d and B_c are continuous, and the field of the currents flowing along the plane changes sign from one side of the plane to the other.

Thus, $B_t = 2(B_{dt} + B_{ct})$. Assuming $B_{ct} \approx 0$, we find that the magnetic field on the inside of the surface is equal in first approximation to twice the dipole magnetic field component tangential to the surface, i.e., a known quantity. Substituting this value into (1.1) and solving the above partial differential equation, we find the unknown surface in first approximation and integrate over it with the Biot-Savart formula to find B_c in the second approximation:

$$B_c(r) = \int \frac{j \times r'}{|r'|^3} ds.$$

---

[2]Confining ourselves to the first approximation, we may assume $B_t \approx 2B_{dt}$ (see below) or $B_t \approx fB_{dt}$, where f is a constant. On the other hand, it is obvious that $\partial R/\partial\phi = 0$ in the plane of the noon-midnight meridian at arbitrary angles α between U and M. In the present approximation, therefore, the equation of the curve on which the magnetopause cuts the plane of the noon-midnight meridian is determined by solution of an ordinary differential equation. Calculations using such an equation were carried out by Spreiter and Briggs [7].

Here ds is a surface element, r' is its radius vector (with respect to the surface point under consideration, while j is calculated from the familiar formula for surface-current density (see /167 [8])); $j = \frac{1}{4\pi} n \times B_i \simeq \frac{1}{2\pi} n \times (B_d + B_c)$, so that in the first approximation $j = \frac{1}{2\pi} n \times B_{dt}$.

This process can obviously be continued; the authors of [6] carried the calculations to the fourth approximation and established that the difference between the first and fourth approximations is small.

As a check, they also calculated the magnetic field at a distance double that from the center of the dipole to the vertex of the magnetopause. It was fould to be less than 1% of the dipole field, and in most cases less than 0.1%.

Calculations were made for the case of mutually perpendicular U and M. In this case, the surface of the magnetosphere has two planes of symmetry. Substantial use was made of this in the calculation.[3]

The approximate formula $B_t \simeq 2B_{dt}$ obtained by the authors can also be used in other calculation methods suitable for arbitrary orientations of M and U (this formula is obviously inapplicable in the neighborhood of the "neutral points," i.e., the points at which B = 0).

Another method of solving the present problem was proposed by Midgley and Davis [10] and consists in the following. As we know, the magnetic-field vector B can always be represented in the form B = curl A, where A is a vector potential. For the magnetic field created by currents with density j flowing along a certain surface S:

$$A(r) \sim \int_S \frac{j(r_1)\,dS}{|r_1 - r|}$$

Let us expand the vector potential of the surface-current field in series in spherical functions and then make use of the fact that B = 0 outside of the magnetosphere. This does not imply that we must put all of the coefficients in the expansion of the total vector potential equal to zero, since the vector potential is defined accurate to the spatial gradient of an arbitrary function as a term. Only certain linear combinations of the coefficients in the expansion must be equated to zero. To

[3]The method is extended to the case of arbitrary α in [9].

find them, the authors of [10] used the fact that a scalar magnetic-field potential exists in the exterior region of the space, where there are no currents (so that $\boldsymbol{B} = \nabla\psi$), and the coefficients of the expansion of this potential in spherical functions must vanish, since $B = 0$ (we assume $\psi = 0$ at ∞). However, the relation between the coefficients in the expansions of both potentials can be found in general form (and this was done).

Further, the current density j was replaced by a function f(x, y) (z axis antiparallel to U), which is constant along the vector lines j and equal to the total current flowing between the line under consideration and the line passing through the vertex. Introduction of this function evidently simplifies the calculations to some degree, but the two-dimensional integral equations to which the derived conditions for the coefficients of the expansion reduce are solved in approximation by assigning a function f of special form with free parameters (these authors used several dozen). Here the question as to selection of the function with the most suitable form remains open. The calculations are considerably less accurate than in the later paper [11]. However, the latter dealt with the much simpler problem of a magnetic dipole immersed in a homogeneous rarefied plasma at rest, i.e., with $p_d = 0$ and only $p = p_0 \neq 0$.

A third method is proposed by Slutz and Winkelman [12]. The plasma pressure on the boundary was calculated by the formula $p = p_0 + p_d\cos^2\chi$. Within the magnetosphere, $\boldsymbol{B} = \nabla\psi$, $\Delta\psi = 0$ everywhere except at the origin, at which ψ has a singularity of the form $\psi \sim 1/r^3$. Working from Green's second identity, it can be shown that in this case /168

$$\psi_t = \frac{M\sin\lambda}{4\pi r^3} + \frac{1}{4\pi}\int_S \psi_s\, d\Omega_{st}.$$

This formula indicates that the magnetic-field potential ψ_t at an arbitrary point t is composed of two parts. The first part is governed by the magnetic-dipole field (in spherical coordinates with the polar axis parallel to the dipole axis; λ is latitude and r is the distance from the center of the dipole to the point t). The second part is the contribution of the magnetic field of the currents flowing on the boundary S of the magnetosphere; ψ_s is the magnetic-field potential at a point infinitesimally close to the boundary of the magnetosphere (at the boundary itself, there is no potential because curl $\boldsymbol{B} \sim j \neq 0$; $d\Omega_{st}$ is the solid angle subtended by the magnetosphere-surface element at point t).

Considering a point t infinitesimally close to the surface of the magnetosphere in this equation, we obtain an equation in which only the values of ψ_s on the boundary of the magnetosphere

appear:

$$\psi_s = \frac{M \sin \lambda}{4\pi r^2} + \frac{1}{4\pi}\int \psi_s \, d\Omega. \tag{1.2}$$

Further, the condition $p = B^2/8\pi$ on the boundary of the magnetosphere yields

$$p_0 + p_d \cos^2 \chi = \frac{1}{8\pi}(\nabla \psi_s)^2. \tag{1.3}$$

The fundamental scheme of the solution was as follows. A surface representing the boundary of the magnetosphere in the first approximation was assigned. The integral equation (1.2), which is linear in ψ_s, was solved numerically for this surface. Both sides of Eq. (1.3) were calculated from the assigned surface and the function ψ_s found for it. This is possible because $B_n = 0$ on the boundary of the magnetosphere and, consequently, $\nabla\psi$ can always be calculated if ψ is known only on this surface. The surface and potential were determined by expanding in a spherical-harmonic series. More than 10 nonzero terms were used in each series (only the case of mutually perpendicular M and U was treated). Since the expansion in spherical harmonics cannot produce the inflection of the surface at the neutral point (B = 0), an additional shape change of the surface was applied in each plane passing through the straight line $\lambda = 0$, $\phi = 0$, which is parallel to U. In its last stage, the problem reduces to minimization of the difference between the left-hand and right-hand sides of Eq. (1.3) by a modified method of least squares.

Finally, Blum proposed yet another method in [13]. Inside the magnetosphere, $\boldsymbol{B} = -\nabla\Omega =$ curl A, and on its boundary

$$\frac{B^2}{8\pi} = p_d \cos^2 \chi, \tag{1.4}$$

$$\frac{\partial \Omega}{\partial n} = 0. \tag{1.5}$$

Here $\partial/\partial n$ denotes the derivative along the surface normal, and it is understood that Eq. (1.5) is written for points infinitesimally close to the magnetopause on the magnetosphere side.

Let the angle α between M and U be equal to 0 or π. Then Eqs. (1.4) and (1.5) can be rewritten in the respective forms

$$G(r, \theta) \equiv \Omega(r, \theta) \pm \sqrt{8\pi p_d} \cdot r \cdot \sin\theta - K = 0, \tag{1.4'}$$

$$F(r, \theta) \equiv r \cdot \sin\theta \cdot A(r, \theta) - C = 0. \tag{1.5'}$$

Here A is the magnitude of the vector potential (taken with the proper sign), C and K are constants, and the sign in front of the radical in (1.4') is determined by the angle α chosen (0 or π). The polar axis is parallel to M; r, θ, and ϕ are spherical coordinates, and the angle ϕ is absent owing to the axial symmetry of the problem. /169

Equations (1.4') and (1.5') define a family of surfaces with different functions Ω and A, which are determined from the equations $\Delta\Omega = 0$. $\Delta A = 0$. The surface belonging to both families must obviously be the magnetopause. The functions Ω and A are approximated by the first N terms of the expansions in Legendre polynomials:

$$\Omega = \frac{M}{r^2}\cos\theta - \sum_{n=1}^{N}(n+1)A_n r^n P_n(\cos\theta),$$

$$A = \frac{M}{r^2}\sin\theta + \sum_{n=1}^{N} A_n r^n P_n^1(\cos\theta).$$

Here P_n and P_n^1 are, respectively, the Legendre polynomials and associated Legendre polynomials of the first kind. Substituting these expressions into (1.4') and (1.5') and assigning N values of the angle $\theta = \theta_j (j = 1,2, \ldots, N)$, at which these equations are satisfied simultaneously, and also, for example, A_n (normalization condition), we obtain a system of 2N transcendental equations with 2N unknowns $r(\theta_j), A_1, \ldots, A_{n-1}, K$ [$C = 0$, since $F(0) = 0$]. Here the question as to the optimum choice of N and $\theta = \theta_j$ remains open (Blum [13] chose N = 6).

Finally, Blum proposed in [14] an interpolation equation for the surface of the magnetosphere for arbitrary angles α, which was such that it yielded the known results for the cases $\alpha = 0, \pi/2, \pi$.

2. The Two-Dimensional Case

It is natural to attempt an analysis of the two-dimensional problem in order to advance further. Here it is possible to consider a flow in the plane of the equator and a flow in the plane of the noon-midnight meridian.

Let us first examine the former possibility. In this case, the magnetic field B(x, y) is perpendicular to the flow plane (x, y). The stationary magnetohydrodynamic equations for an infinitely conductive fluid take the form

$$\rho(v, \nabla)v = -\nabla\left(p + \frac{B^2}{8\pi}\right), \qquad (2.1)$$

$$\operatorname{div}\rho v = 0, \qquad (2.2)$$

$$\mathrm{rot}(v \times B) = 0 \qquad (2.3)$$

(the equation div B = 0 becomes an identity). Here ρ, p, B, v, B are, respectively, the density, the pressure, the absolute magnitude of the magnetic field, the velocity, and the magnetic field.

Equations (2.2) and (2.3) permit introduction of the stream function ψ and the potential ϕ:

$$\rho v = \{\psi_y, -\psi_x\}, \qquad (2.2')$$

$$v \times B = \{\varphi_x, \varphi_y\}. \qquad (2.3')$$

From here on, letter subscripts will signify differentiation with respect to the corresponding variables. Let the velocity v have the components u and q, i.e., $v \equiv \{u, q\}$; we then have from (2.2') and (2.3')

$$\rho\{u, q\} = \{\psi_y, -\psi_x\}, \quad B\{q, -u\} = \{\varphi_x, \varphi_y\},$$

whence $\varphi = \varphi(\psi)$, $\rho_\psi = -B/\rho$, i.e., the ratio B/ρ is constant along any streamline.

Let the flow scheme be similar to that shown in Fig. 1. The region with index 0 is a region of homogeneous flow with constant parameters. Regions 0 and 1 are separated by a shock wave and regions 1 and 2 by a tangential discontinuity. /170

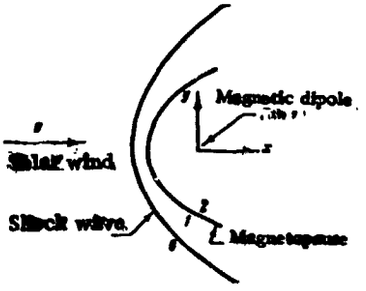

Figure 1. Diagram of Supersonic Flow Past Magnetic Dipole in Plane of Equator.

The equations agree with the gas-dynamic equations in the regions of continuity if the effective pressure $p_{ef} = p + B^2/8\pi$ is introduced. They also agree on the shock wave if we also introduce an effective internal energy per unit mass $\varepsilon_{ef} = \varepsilon + B^2/8\pi\rho$ [8]. It is interesting to note that since $B/\rho = -\phi_\psi(\psi)$ is continuous on the shock wave [8], while $B/\rho = \text{const}$ in region 0, we have $B/\rho = \text{const} = B_0/\rho_0$ for all of region 1; here and below, the subscripts 0, 1, and 2 will be used to indicate the region to which the quantities under consideration pertain.

Thus, the problem of the flow past the magnetosphere is mathematically equivalent in the present formulation to the problem of a homogeneous supersonic ideal-gas flow past a blunt solid body with the shape of the magnetosphere (both the equations and the boundary conditions are the same). Here the role of the velocity of sound is taken by

$$c_{ef} = \sqrt{\left(\frac{\partial p_{ef}}{\partial \rho}\right)_S} = \sqrt{\left(\frac{\partial p}{\partial \rho}\right)_S + \frac{B_0^2}{4\pi\rho_0^2}\rho} =$$
$$= \sqrt{c^2 + \frac{B_0^2}{4\pi\rho_0^2}\rho}\,.$$

Here c is the velocity of sound and S is the entropy.

Many studies have now been devoted to numerical methods of solving two-dimensional blunt-body flow problems (those of Belotserkovskiy, Telenin, and others).

Thus, the following scheme can be proposed for numerical solution of the problem stated. We assign the boundary of the magnetosphere. We solve the problem of supersonic gas flow past a blunt solid body with the same boundary by one of the known methods. We find the distribution of effective pressure along the boundary of the body and, consequently, along the outer surface of the magnetopause. We then solve the problem of a gas flow with the equation of state $p_{ef} = \tilde{F}_2(S)\rho^\gamma + \tilde{Q}_2(S)\rho^2$ (assuming that S = const along a streamline, i.e., $\tilde{F}_2(S) = (1/\gamma)F_2(\psi)$, $\tilde{Q}_2(S) = {}^1/_2 Q_2(\psi)$) inside the region of the assigned boundary. Thus, we obtain the distribution of effective pressure on the inside of the magnetopause. Generally speaking, we find that $p_{ef1} \neq p_{ef2}$, while equality should prevail for the boundary sought. We therefore adjust the shape of the boundary, repeat the calculation, and so forth until $p_{ef1} = p_{ef2}$ with the desired accuracy. It is natural to take the surface obtained in the approximation in which $p_{ef} \sim \cos^2\chi$ on the boundary as the initial boundary of the magnetosphere.

The following difficulty arises in solution of this problem. /171 While the flow past the magnetosphere is uniquely defined for the assigned shape of its boundary (this is postulated and is confirmed by computational practice in all calculations of supersonic ideal-gas flows past blunt bodies), the flow inside the magnetosphere is by no means uniquely determined by the boundary condition $p_{ef1} = p_{ef2}$.

In fact, substituting (2.2') and $B/\rho = -\varphi_\psi$ into (2.1)-(2.2) and assuming $p \sim \rho^\gamma$, we obtain

$$\left(\psi_y \frac{\partial}{\partial x} - \psi_x \frac{\partial}{\partial y}\right)\left\{\frac{\psi_y}{\rho}, -\frac{\psi_x}{\mu}\right\} = -[F(\psi)\rho^{(\gamma-1)} + Q(\psi)\rho]\nabla\rho. \qquad (2.4)$$

The sense of the functions $F(\psi)$ and $Q(\psi)$ is clear from the relation

$$p = \frac{1}{\gamma}F(\psi)\rho^\gamma; \qquad \frac{B^2}{8\pi} = \frac{1}{2}Q(\psi)\rho^2.$$

The functions are uniquely defined in region 1. Namely, $Q(\psi) = \text{const} = B_0^2/4\pi\rho_0^2$, and $F(\psi)$ is uniquely determined from the slope of the shock wave at each point and by the parameters in region 0; however, the shape of the shock wave is uniquely defined by the parameters of the homogeneous flow and by the shape of the body in the flow (with the above reservation).

This is not the case with the flow inside the magnetosphere. If, without loss of generality, we regard the curve $\psi(x, y) = 0$ as the streamline passing through the vertex, i.e., also through the boundary of the magnetosphere in the particular case, the solution of system (2.4) inside the magnetosphere must satisfy only the condition

$$\frac{2}{\gamma} F_2(0)\rho_2^\gamma + Q_2(0)\rho_2^2 = \frac{2}{\gamma} F_1(0)\rho_1^\gamma + \frac{B_0^2}{4\pi\rho_0^2}\rho_1^2$$

on the boundary of the magnetosphere. Otherwise the functions $F_2(\psi)$ and $Q_2(\psi)$ are arbitrary. This property corresponds to our freedom in distributing the entropy S along the streamlines (since we have $S = S(\psi)$). The form of these functions depends on the initial conditions that prevailed before the flow became stationary. In particular, if the flow was initially nonvortical, it will remain nonvortical (the Thomson theorem, which is applicable because the problem has been reduced to a purely gasdynamic problem).[4]

It is interesting to note that of all the forms of potential flows, only those for which $F_2(\psi) = \text{const}$ and $Q_2(\psi) = \text{const}$ suit us.

In fact, let the flow be potential, i.e., let curl v = 0 in region 2. Then

$$\operatorname{rot} \boldsymbol{v} \times \boldsymbol{v} \equiv -\nabla\frac{v^2}{2} + (\boldsymbol{v}, \nabla)\boldsymbol{v} = 0,$$

where v is the absolute value of the velocity. Thus, we can rewrite Eq. (2.1) on the assumption that $p_{ef} = (1/\gamma)F\rho^\gamma + {}^1/_2 Q\rho^2$ in the form

$$\rho\nabla\frac{v^2}{2} = -\nabla\left(\frac{1}{\gamma}F\rho^\gamma + \frac{1}{2}Q\rho^2\right). \qquad (2.1')$$

Projecting this equation onto the streamline and integrating along the latter, we obtain

---

[4]This holds if the time elapsed since establishment of the steady state is not yet too long, since otherwise even a very small effective viscosity may make itself felt.

$$\frac{v^2}{2}+\frac{F(\psi)}{(\gamma-1)}\rho^{(\gamma-1)}+Q(\psi)\rho=G(\psi). \qquad (2.1'')$$

Eliminating v^2 from (2.1') and (2.1"), we find that $\frac{1}{\gamma(\gamma-1)}\rho^{\gamma}F_{\psi}+\frac{1}{2}\rho^2Q_{\psi}=G_{\psi}$ wherever $\nabla\psi\neq 0$. The equalities $F_{\psi}(0)=Q_{\psi}(0)=G_{\psi}(0)=0$ appear improbable except when $F_{\psi}\equiv Q_{\psi}\equiv G_{\psi}\equiv 0$. Another possibility, the case $\rho=\rho(\psi)$, must be eliminated, since then ρ = const along the boundary of the magnetosphere and, consequently, p_{ef2} = const, which cannot be, since v varies from 0 at the vertex to U at infinity along the outer boundary of the magnetosphere and, consequently, p_{ef1} = $= p_{ef2}$ also varies. /172

Thus, if the flow inside the magnetosphere is potential, we have $F_2(\psi)=F_2(0), Q_2(\psi)=Q_2(0), G_2(\psi)=G_2(0)$, and v and ρ are related by (2.1").

The relations $F_2(\psi)$, $Q_2(\psi)$, and $G_2(\psi)$ can, in principle, be determined from experimental data. Indeed, let there be a satellite whose trajectory lies in the equatorial plane, with the apogee outside the magnetosphere and the perigee in the upper layers of the ionosphere. Let the distributions of ρ, B, p, and ρv_n, where v_n is the plasma-velocity component perpendicular to the trajectory of the satellite (and lying in the equatorial plane) be measured along some revolution in orbit. Integrating along the trajectory from the boundary of the magnetosphere in the direction toward the earth to an arbitrary point s, we obtain

$$\psi(s)=\int_{\bullet}^{\bullet}\rho v_n ds,$$

where ds is an element of length along the trajectory (see [15]). We then find $F(\psi)$ and $Q(\psi)$ from the formulas $p=(1/\gamma)F(\psi)\rho^{\gamma}$, $B^2/8\pi = \frac{1}{2}Q(\psi)\rho^2$. The function $G(\psi)$ can be found from (2.6) if we also measure the distribution v(s) and determine γ from data on several orbital revolutions (it is obvious that, in principle, data from a single ascent or descent are sufficient to find all of the quantities).

In conclusion, let us dwell briefly on the difficulties of the present formulation of the problem from the standpoint of application to the real pattern of flow past a three-dimensional magnetic dipole in the equatorial plane, apart from neglect of the inclination of the dipole axis to the plane of the ecliptic, and the difficulties noted in the introductory remark as being common to all of the flow problems considered here.

When we write the equations of motion in the form (2.1)-(2.3), it will make sense to leave only the term with $\nabla B^2/8\pi$ only if it is

large by comparison with the discarded term $\frac{1}{4\pi}(B,\nabla)B$, i.e., if $\left|\nabla\frac{B^2}{2}\right| \gg |(B,\nabla)B|$. This is clearly not the case for empty space.

Indeed, in this case curl B = 0, and, consequently, curl $B\times B \equiv$ $\equiv -\nabla\frac{B^2}{2}+(B,\nabla)B=0$, i.e., these terms are even equal to one another. In particular, this is also true for the field of the magnetic dipole, from which the field in the magnetosphere does not, as we know, differ too strongly (except for regions near the boundary and in the tail).

It is not now clear to what degree this affects the reasonableness of the problem statement considered above.

As we noted at the outset, this problem was originally formulated in the quasihydrodynamic frame of reference by N.V. Samokhin in the paper [4], which, however, contains a number of errors that substantially discredit the results obtained in it.

In the case under consideration, the system of quasihydrodynamic differential equations agrees formally with the system of magnetohydrodynamic equations, the only difference being that the transverse component $\bar{P}_\perp$ takes over the role of the pressure. But the conditions on the discontinuities, and on the shock wave in particular, are different. One free parameter appears in the conditions on the shock wave (since $\bar{P}_\perp$ and $\bar{p}_\parallel$ appear now in place of the pressure p), and a value must somehow be chosen for it. But even if it is chosen such that the position of the shock wave coincides with that calculated in the magnetohydrodynamic approach, there still remains a randomness similar to that discussed above as affecting the choice of the functions $F(\psi)$ and $Q(\psi)$ in the region of the magnetosphere. /173

Samokhin ignores these facts and proceeds as though the flow pattern were uniquely determined by the parameters in the undisturbed region and by the dipole singularity of the magnetic field in the magnetosphere. In addition, it is quite doubtful that solutions with surfaces of discontinuity could be obtained by using only the quasihydrodynamic differential-equation system without the relations on the discontinuities.

Let us turn to the next possibility, i.e., treatment of the flow in the plane of the noon-midnight meridian as a two-dimensional flow. Here there have been a number of studies in which substantial advances were made as compared to the three-dimensional case.

V.N. Zhigulev and Ye.A. Romishevskiy [16] (and also Hurley [17]) assigned the pressure on the boundary in the form $p = p_d\cos^2\chi$. Within the magnetosphere, curl B = 0 and div B = 0 everywhere except at the coordinate origin, in which the magnetic dipole was

situated. Using the conformal-mapping method known in the hydrodynamics and electrostatics of two-dimensional fields, the authors obtained formulas for the boundary (and for the magnetic field inside the magnetosphere), in analytic form. Since the answer was obtained in the form of a series, we present it here in closed form.

Let the complex potential F(z) of the magnetic field have a dipole singularity at the origin:

$$F(z)|_{|z|\ll 1} \simeq \frac{2M}{z} e^{i\alpha},$$

i.e., the angle between the direction of the solar wind and the axis of the magnetic dipole equals α, while the magnetic moment of a unit length of the field source equals M. Let $\alpha > 0$, and let the point coordinates be x and y, with the x axis coinciding with the direction of the solar wind. Then the equation of the boundary in parametric form is

$$\frac{y(\varphi)}{0.5\,(2\pi M)^{1/2}\,(2\pi p_\infty)^{-1/4}} = \tilde{y}(\varphi) =$$

$$= \begin{cases} \cos\varphi + 1 - \dfrac{2\alpha}{\pi} & \text{for } 0 \leqslant \varphi \leqslant \pi; \\ -\cos\varphi - 1 - \dfrac{2\alpha}{\pi} & \text{for } \pi \leqslant \varphi \leqslant 2\pi - \alpha; \\ -\cos\varphi + 3 - \dfrac{2\alpha}{\pi} & \text{for } 2\pi - \alpha \leqslant \varphi \leqslant 2\pi, \end{cases}$$

$$\tilde{x}(\varphi) = -\frac{2}{\pi}\{\ln[1 - \cos(\varphi + \alpha)] - \ln|\sin\varphi| +$$

$$+ \cos 2\varphi + \cos\varphi \cdot \ln\left|\tan\frac{\varphi}{2}\right|\}.$$

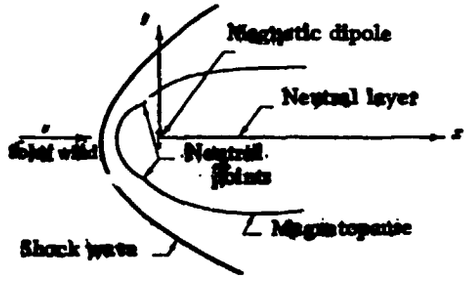

Figure 2. Diagram of Supersonic Flow Past Magnetic Dipole in the Plane of the Noon-Midnight Meridian with Consideration of the Neutral Layer of the Tail ($\alpha = \pi/2$).

Atkinson and Unti [18] solved the problem for the case $\alpha = \pi/2$ in the same formulation and by the same method as Zhigulev and Romishevskiy, from whom they varied in assuming the presence of a neutral layer of infinitesimal thickness in the equatorial plane on the night side (Fig. 2) in an attempt to approximate the real structure of the tail [19]. In the last step, the problem was solved numerically for various values of the magnetic flux C in the tail. The calculations indicated that:

1) the position of the vertex of the magnetosphere is not very sensitive to the value of C; /174

2) sensitivity is slightly higher at the neutral points, but still low;

3) the position of the inner margin of the neutral layer (the outer margin is at infinity) depends strongly on C.

The authors offer the opinion that the results of solution of this two-dimensional problem permit inferences, even quantitative ones, as to the results of solution of the three-dimensional problem. For example, the section through the magnetosphere in the plane of the noon-midnight meridian differs little in the three-dimensional problem from that in the two-dimensional problem, even to the positions of the neutral points. This is, we might add, despite the fact that the magnetic field of the two-dimensional dipole $\sim 1/r^2$, while that of the three-dimensional dipole $\sim 1/r^3$.

A different approach is developed in the papers of Yu.S. Sigov [20, 21]. While the same conditions as in the studies set forth above are used inside the magnetosphere, a noninteracting-particle model is used outside the magnetosphere, with mirror reflection of the particles from the latter's boundary. The author assumes the presence of a homogeneous and isotropic background that creates a pressure p_0 = const on the boundary and an ensemble of fast particles whose distribution "in the neighborhood of the magnetosphere is such that their pressure on the boundary S can be written as the pressure of an ensemble of particles defined on a certain cylindrical surface C_0 of radius r_1 centered at some fixed point (for example, at the coordinate origin), and each fast particle moves at a velocity v toward the center, undergoing mirror reflection from S" [21]. In the general case, the velocity v is not fixed, and there are distribution functions $f_{i,\,e}(v, \varphi, r_1)$ for the ions and electrons. Here ϕ and r_1 are the polar coordinates of a point on the circumference of C_0.

Conformal mapping is again used in this study, and numerical calculations are made in the last step. True, it was assumed in the calculations that $f_i = f_e = n_1 \cdot F(\varphi)\delta(v - V)$, where δ is the Dirac delta function. Here the function $F(\phi)$ is tkaen in the form $F(\phi) = \frac{1-\lambda\cos\varphi}{1+\lambda}$, where λ is a parameter, and $0 \leqslant \lambda \leqslant 1$. In particular, this form of $F(\phi)$ implies that the angle $\alpha = \pi/2$.

The author showed that other interpretations of the results are possible. For example, it may be assumed that the fast-particle source is a surface near the surface of the shock wave.

Thus, the pressure distribution along the outer boundary of the magnetosphere is assigned in all of the above studies, even in

two-dimensional problems, in a form that permits separation of the solution of the problem of flow past the magnetosphere from calculation of the shape of its boundary. The presence of plasma inside the magnetosphere is also neglected.

Let us now write an equation system for solution of the two-dimensional problem in the framework of magnetohydrodynamics. We have (using the same notation as above)

$$\rho(v, \nabla)v = -\nabla p + \frac{1}{4\pi}\operatorname{rot} B \times B, \tag{2.5}$$

$$\operatorname{div}\rho v = 0, \tag{2.6}$$ /175

$$\operatorname{rot}(v \times B) = 0, \tag{2.7}$$

$$\operatorname{div} B = 0. \tag{2.8}$$

Let us assume that B lies in the flow plane (x, y). From Eqs. (2.6) and (2.8)

$$\rho v = \{\psi_y, -\psi_x\}, \qquad B = \{\theta_y, -\theta_x\}. \tag{2.9}$$

We have further from (2.7) $v \times B = \nabla\varphi = \{0, 0, \partial\varphi/\partial z\} = \{0, 0, \text{const}\}$, i.e., a constant in the continuity region. In the case under consideration, the electric field-strength vector $E = -(1/c)v \times B$ is perpendicular to the flow plane and therefore tangent to a surface of discontinuity of either type. But, as we know, the electric-field components tangential to a surface of discontinuity are always continuous. As a result, $v \times B = U \times B_0$ through the space in which there is matter. From this we also obtain from (2.9)

$$\rho v \times B = k(\psi_x\theta_y - \psi_y\theta_x) = U \times B_0,$$

i.e.,

$$\psi_x\theta_y - \psi_y\theta_x = a\cdot\rho. \tag{2.10}$$

Here k is the unit vector along the z axis and the constant $a = \pm |U \times L_0|$.

From (2.9):

$$\operatorname{rot} v = \left\{0, 0, -\left(\frac{\psi_x}{\rho}\right)_x - \left(\frac{\psi_z}{\rho}\right)_y\right\},$$

from which

$$\rho \operatorname{rot} v \times v = -\left[\left(\frac{\psi_z}{\rho}\right)_x + \left(\frac{\psi_y}{\rho}\right)_y\right]\nabla\psi. \tag{2.11}$$

Similarly,

$$\operatorname{rot} \boldsymbol{B} \times \boldsymbol{B} = -\Delta\theta \cdot \nabla\theta. \tag{2.12}$$

Using the identity $(v, \nabla)v \equiv \nabla v^2/2 + \operatorname{curl} v \times v$, substituting (2.11)-(2.12) into (2.5), and remembering that $p = f(\psi)\rho^\gamma$ together with (2.10), we finally obtain

$$\psi_x \nabla\left(\frac{\psi_x}{\rho}\right) + \psi_y \cdot \nabla\left(\frac{\psi_y}{\rho}\right) = \left(\frac{\Delta\psi}{\rho} + \nabla\psi \cdot \nabla\frac{1}{\rho}\right)\nabla\psi - \tag{2.13}$$
$$- \nabla\left[f(\psi)\rho^\gamma\right] - \frac{1}{4\pi}\Delta\theta \cdot \nabla\theta,$$

$$\psi_x\theta_y - \psi_y\theta_x = a \cdot \rho. \tag{2.14}$$

If we disregard the fact that the function $f(\psi)$ is unknown, we have obtained a system of three equations with three unknown functions: $\rho(x, y)$, $\psi(x, y)$, and $\theta(x, y)$. To them we must add the conditions at the discontinuities — the shock wave and the magnetopause. As for the choice of the function $f(\psi)$, we may repeat here the arguments regarding selection of the function $F(\psi)$ that were given above in connection with the problem of flow in the equatorial plane.

The magnetic field, i.e., the function $\theta(x, y)$, can, if desired, be excluded from this equation system. This is done by scalar multiplication of both sides of (2.13) by the vector $\{-\psi_y, \psi_x\}$ and application of Eq. (2.14). We then obtain

$$\Delta\theta = P. \tag{2.15}$$

Substituting (2.15) into (2.13), we obtain /176

$$\nabla\theta = \{Q, R\}. \tag{2.16}$$

Here P, Q, and R are functions that depend on ρ and ψ and their derivatives with respect to the coordinates but do not depend on the function θ and its derivatives. From (2.15) and (2.16),

$$\frac{\partial Q}{\partial x} + \frac{\partial R}{\partial y} = P, \qquad \frac{\partial Q}{\partial y} = \frac{\partial R}{\partial x},$$

i.e., we obtain a system of two equations with two unknown functions ψ and ρ. Using (2.16), θ can also be eliminated easily from the boundary conditions and from the conditions on the discontinuities.

As compared with the case of equatorial-plane flow, however, we may make the following remark here. Let $U \times B_0 \neq 0$. If the boundary of the magnetosphere is regarded as a tangential discontinuity, B tends to infinity over the entire boundary of the magnetosphere in virtue of the condition $v \times B = U \times B_0$, since

$v \| B$ on it. This can be avoided if we assume that the magnetospheric boundary separates a region occupied by plasma with a frozen magnetic field from a region occupied only by the magnetic field and is not a tangential discontinuity.

Let us first consider the auxiliary problem of the flow of a supersonic plasma stream described by the magnetohydrodynamic equations with infinite conductivity and without viscosity past a solid dielectric (without magnetic susceptibility). At infinity, we should have $\rho \to \rho_0, p \to p_0, v \to U, B \to B_0$, and on the contour of the body $v_n = 0$, where v_n is the plasma-velocity component normal to the contour. We make the natural assumption that these conditions uniquely define the flow pattern. In the absence of a frozen field ($B_0 = 0$), this assumption is, as we have noted, generally accepted, and it has been confirmed by computational practice.

Then the fundamental scheme of the solution to our problem will take the following form in the light of the above. First we determine the velocity and density fields $v(x, y)$ and $\rho(x, y)$ of the plasma. We then find the magnetic field $B(x, y)$ over the entire flow region from the known velocity and density fields. The magnetic field component B_n normal to the boundary of the body is determined from the plasma velocity along the boundary by the formula $B_n = |B_0 \times U| / v$. Assuming that there are no extraneous currents in the dielectric, we conclude that the tangential magnetic-field component is absent near the boundary inside the body, while the normal component is known.

It is easily seen that the problem of determining the magnetic field inside the body then reduces to a Neumann problem and has a unique solution.

We now consider a second auxiliary problem. Let there be a certain region with currents flowing along its boundary, a magnetic dipole within it (at the coordinate origin), and no field on the outside. On the inside, the field is described by a function $\theta(x, y)$ such that $B = \{\theta_y, -\theta_x\}$, $\Delta\theta = 0$ over the entire region, except for the origin. It can be assumed without loss of generality that the boundary of the region coincides with the curve $\theta(x, y) = 0$.

Let $r = R(\phi)$ be the equation of the boundary in polar coordinates. Then we have on the inside $\theta = -\frac{2M}{r}\sin(\varphi - \alpha) - \chi(r, \varphi), \Delta\chi = 0$ and the function χ has no singularities, while $\chi = \frac{2M}{R(\varphi)}\sin(\varphi - \alpha)$ on the boundary. Here M and α are the parameters of the dipole. Thus, the problem has been reduced to a Dirichlet problem and has a unique solution.

Let us now return to the first problem and place a magnetic dipole inside the region and extraneous currents on the boundary such that their magnetic field and the dipole field cancel one another in the external region. There will obviously be no change in the flow pattern, and the magnetic field in the dielectric will be a superposition of three fields: from the magnetic dipole, from the extraneous currents in the dielectric along its boundary, and from the currents flowing in the plasma. Here, according to the above proof, the magnetic field inside the dielectric will be determined uniquely for the flow pattern found, and its determination will reduce to solution of the familiar Neumann and Dirichlet problems for a singly-connected region. The equality

$$p_1 + \frac{B_1^2}{8\pi} = p_2 + \frac{B_2^2}{8\pi}$$

will be satisfied on the boundary of an isotropic dielectric in virtue of the momentum-flux continuity condition.

Here the subscripts 1 and 2 refer to the plasma and the body, respectively. By varying the shape of the body, we can arrive at a situation such that $p_2 = 0$ over its entire boundary. Now, removing the body, we obtain the solution of the problem of finding the boundary shape of the magnetosphere for the flow pattern described. In the resulting solution, we no longer have $B \to \infty$ over the entire boundary, but only at the vertex (and at the convergence point of the stream). However, it may be hoped that the flow pattern will change only slightly and the field at the vertex will remain finite when consideration is given to a finite but large conductivity.

Unless we posit the absence of plasma in the cavity, the solution becomes nonunique. Here the version with an immobile plasma in the cavity must be rejected, since in this case the magnetic field tends to infinity over the entire region occupied by the immobile plasma.

We note also that in the case of equatorial flow there is no solution with a plasma-free region, since the magnetic field is constant in such a region.

3. On the Nature of the Magnetopause

In all of the cases considered above, the magnetosphere was treated as a tangential discontinuity (if the condition $p \sim \cos^2\chi$ is treated in the hydrodynamic sense). At the same time, the magnetohydrodynamic equations admit of interpretation of the magnetopause as a rotational discontinuity characterized in the general case by a mass flux across the surface of discontinuity, the presence of a magnetic-field component B_n normal to it, and continuity of the density and the absolute value of the magnetic field [8].

According to [22], the plasma velocity near the magnetopause is directed tangentially to it, a point in favor of its treatment as a tangential discontinuity.

The papers [23] were devoted to the variations of the magnetic field during passage across the magnetopause. It was found that, as a rule, there is no normal magnetic-field component, although this component is sometimes nonzero during magnetic storms.

Finally, in a study devoted specifically to the problem in question [24], analysis of magnetic-measurement data did not indicate the existence of rotational discontinuities in spite of the favorable (according to Petschek) circumstances — high geomagnetic activity with a rather strong radial (with respect to the sun) interplanetary-field component.

CONCLUSIONS

A review of papers devoted to theoretical calculation of the magnetosphere's boundary in the three-dimensional case indicates that, despite the use of a number of assumptions that simplify solution of the problem (absence of the interplanetary field, absence of matter in the magnetosphere, a simple formula for the pressure on the boundary of the magnetosphere, specific statement of the relative orientation of the dipole moment and the solar-wind direction, and various others), it has not been possible to complete the calculations correctly (in the mathematical sense). In each of the methods considered, additional simplifying assumptions (such as unjustified selection of the number of free parameters, the form of the approximating functions, etc.) were introduced in the process of integrating the equations used. From this standpoint, Beard's method would appear more correct than the others (and it does, incidentally, "pass tests" rather well as compared with the exact solution of Zhigulev and Romishevskiy). /178

It appears that numerical solution with acceptable accuracy within the magnetohydrodynamic framework is possible at the present time only for the two-dimensional problems.

Solution of the problem within the framework of magnetohydrodynamics would make it possible to estimate the influence of the interplanetary magnetic field and the presence of plasma in the magnetosphere[5] on its boundary. It would hardly make sense to use the quasihydrodynamic equations at the present time, since we do not know an additional condition that would make possible unique calculation of the parameters on one side of the shock wave from their known values on the other side. It apparently makes sense to regard the boundary of the magnetosphere as a tangential or rotational discontinuity.

[5]The only solution with consideration of the presence of plasma in the magnetosphere was carried out in [25], but without consideration of the solar wind.

We note also that solution of the problem in the magnetohydrodynamics framework would make possible simultaneous determination of the magnetic field within the magnetosphere.

The author is deeply grateful to A.I. Yershkovich for his sustained interest in the work and numerous helpful discussions.

REFERENCES

1. G.Chu, M. Goldberger, and F. Low. In collection entitled: "Problemy sovremennoy fiziki" (Problems of Modern Physics), No. 7, IL, 1957, 139.
2. T.F. Volkov. In collection entitled: "Voprosy teorii plazmy" (Problems of Plasma Theory), No. 4, Moscow, Gosatomizdat, 1964, 3.
3. J. Spreiter and A. Alksne. Planet. and Space Sci., 1968, Vol. 16, 8, 971.
4. M.V. Samokhin. In collection entitled: "Magnitnaya gidrodinamika" (Magnetohydrodynamics), 1966, No. 4, 19.
5. J. Giraud. Basic Problems of Hypersonic Flow Theory, Moscow, "Mir," 1965, 108.
6. G. Mead and D. Beard. J. Geophys. Res., 1964, Vol. 68, 7, 1169.
7. J. Spreiter and B. Briggs. J. Geophys. Res., 1962, Vol. 67, 1, 37.
8. L.D. Landau and Ye.M. Lifshits. Elektrodinamika sploshnykh sred (Electrodynamics of Continuous Media), Moscow, Fizmatgiz, 1959, Vol. 153, 295, 284.
9. W.P. Olson. J. Geophys. Res., 1969, Vol. 74, No. 24, 5742.
10. J. Midgley and L. Davis. J. Geophys. Res., 1963, Vol. 68, 18, 5111.
11. J. Midgley and L. Davis. J. Geophys. Res., 1962, Vol. 67, 2, 499.
12. R. Slutz and J. Winkelman. J. Geophys. Res., 1964, Vol. 69, 23, 4933.
13. R. Blum. Phys. Fluids, 1965, Vol. 8, 9, 1708; 1967, Vol. 10, 5, 1122.
14. R. Blum. J. Geophys. Res., 1968, Vol. 73, 7, 2411.
15. M.A. Lavrent'yev and B.V. Shabat. Metody teorii funktsiy kompleksnogo peremennogo (Methods of the Theory of Functions of a Complex Variable), Moscow, Fizmatgiz, 1958, 222.
16. V.N. Zhigulev and Ye.A. Romishevskiy. Dokl. Akad. Nauk SSSR, 1959, Vol. 127, 5, 1001.
17. J. Hurley. Phys. Fluids, 1961, Vol. 4, 7.
18. T. Unti and J. Atkinson. J. Geophys. Res., 1968, Vol. 73, 23, 7319.
19. R.F. Ness. J. Geophys. Res., 1965, Vol. 70, 2989.
20. Yu.S. Sigov. Space Res., 1966, Vol. VII, 1, 550.
21. Yu.S. Sigov. Kosmicheskiye Issledovaniya, 1969, Vol. 7, No. 5, 731.
22. J.W. Freeman. J. Geophys. Res., 1968, Vol. 73, 13, 4151; J.F. Freeman, J.C.S. Warren and J.J. Maguire. J. Geophys. Res.,

1968, Vol. 73, 17, 5719; Space Sci. Rev., 1969, Vol. 10, 262.
23. B.U.O. Sonnerup and L.J. Cahill. J. Geophys. Res., 1967, Vol. 72, No. 1, 171; 1968, Vol. 73, No. 5, 1757.
24. W.D. Cummings and P.J. Coleman. J. Geophys. Res., 1968, Vol. 73, 17, 5699.
25. Vo Khong An' and B.A. Tverskoy. Geomagnetizm i Aeronomiya, 1969, Vol. 9, No. 4, 599.
26. V.L. Ginzburg and A.A. Rukhadze. Waves in Magnetoactive Plasma, In series "Sovr. problemy fiziki" (Contemporary Problems of Physics), Moscow, "Nauka," 1970, 47.

N75 13720

TRANSPORT OF CHARGED PARTICLES IN THE EARTH'S MAGNETOSPHERE

(Translation of "O perenose zaryazhennykh chastits v magnitosfere zemli.")

V. P. Shalimov

ABSTRACT

A review of recent data on and conceptions of processes in which high-energy particles are transported across magnetic shells in the earth's magnetosphere is presented. The processes discussed include adiabatic processes (with conservation of all three adiabatic invariants of charged-particle motion in the magnetic field), diffusion processes (with violation of only the third or third and second invariants), and the so-called fast nonadiabatic processes, which appear to result from the action of strong electric fields. Convection of the magnetospheric plasma is not considered. With 140 source citations.

TRANSPORT OF CHARGED PARTICLES IN THE EARTH'S MAGNETOSPHERE

V.P. Shalimov

At the end of the 1960's, progress in the study of outer space had led to the emergence of a new composite branch of geophysics — the physics of the magnetosphere. A number of review papers have been devoted to research in this field (see, for example, [1] and its bibliography), but even the most recent of these reviews [1] does not adequately reflect such very recent results as the concept of magnetospheric substorms that has been developed, apart from journal articles, in the monograph [2], or Frank's discovery of a solar-wind proton fraction with energies from 5 to 50 keV that correlates distinctly with geomagnetic disturbances [3], a discovery that, in combination with registration of such protons in the transitional region, the tail of the magnetosphere, and the region of the "ring current," enables us to speak of injection of these particles into the magnetosphere as the cause of many geophysical phenomena [4, 5].

The purpose of the present study is to present a comprehensive review of the phenomena of charged-particle transport in the earth's magnetosphere in the context of present-day achievements and problems in magnetospheric physics.[1]

1. Adiabatic Transport of Charged Particles in the Earth's Magnetosphere

It is known (see, for example, [6]) that the motion of charged particles in the geomagnetic field can be considered by two methods. The first is due to Störmer; it consists essentially in finding the first integrals of the motion and zones that are allowed and forbidden to particles in space, with subsequent numerical integration of the trajectories. This method is convenient for magnetic fields that exhibit symmetry (for example, the dipole fields); in the real geomagnetic field, on the other hand, the particle trajectories are investigated numerically from the very outset. But when a particle describes a very large number of loops, the calculations become difficult even when modern computers are used. This approach is therefore used only in study of cosmic rays (for the present state of the problem, see, for example, [7]).

The second method is the (Alfven) perturbation method, which considers the motion of particles in a magnetic field with small inhomogeneities. It has come into extensive use in space-physics problems, and its development has led to an adiabatic (drift)

[1]The review will deal basically with work published no later than 1969.

theory of charged-particle motion [6, 8].

In the drift approximation, each charged particle has three motions in the geomagnetic field: Larmor rotation, oscillations along magnetic lines of force between mirror points, and an azimuthal drift around the earth (owing to magnetic-field inhomogeneities and the curvature of the lines of force).[2] In the case of slow spatial and temporal variation of the field, a certain constant (accurate to first-order terms) quantity — the adiabatic invariant — corresponds to each type of motion. For the Larmor rotation, given small space and time variations of the magnetic field during a revolution, the "orbital magnetic flux" is conserved (in the nonrelativistic case, the first adiabatic invariant would be the magnetic moment of the particle). The second "longitudinal" invariant is preserved for oscillations between reflection points in the case of insignificant field variations during a period. On the other hand, if the magnetic-field variations are small during a revolution of the particle around the earth, the magnetic flux across the surface along which the guiding center of the particle drifts will be the third adiabatic invariant. /180

The conservation equations of the three invariants describe the relation between the velocity (momentum) and pitch angle of the particle and the parameter of the invariant shell along which its guiding center drifts at various points in time. This equation system can be used to describe not only the stationary distribution pattern of the trapped radiation in the earth's magnetosphere, but also the processes of adiabatic charged-particle transport in the slowly varying geomagnetic field.

The effects of these processes during magnetic storms were first discussed in [9, 10]. Particle-flux intensity decreased with decreasing geomagnetic-field intensity in the main phase and increased with its increase in the recovery phase of the storm. This effect was interpreted as reversible betatron particle acceleration. The problem was developed further in [11-13]. The time variations of the electron and proton fluxes in the outer radiation belt and their correlation with geomagnetic-field variations have been under study by numerous investigators right up to the present time (see, for example, the reviews [14, 15]). Particularly detailed data have been obtained on the behavior of particles during the storm of 17-18 April 1965 [12, 16-21], when both adiabatic and nonadiabatic effects were observed.

Particle transport has been examined theoretically in various models of the geomagnetic field with conservation of the invariants [9, 12, 13, 22-25]. It was shown in [13] that the

[2]A corresponding additional drift arises in the presence of an electric field (or other forces of nonmagnetic origin). In the earth's magnetosphere, electric fields have a strong influence on the motion of particles with energies $\leq$1-10 keV.

reversible betatron acceleration can be regarded in the drift approximation as the result of simultaneous operation of two betatrons – a gyrobetatron and a drift betatron. Their electric eddy fields act along the Larmor circle and along the drift trajectory around the earth, respectively. This description is equivalent to conventional calculations using adiabatic invariants (see, for example, [12]), but since each betatron pertains to a characteristic type of motion, this separation is physically natural and casts light on the relation between particle acceleration and the varying magnetic field. We note that the gyrobetatron produces 40% of the total acceleration, and the drift betatron 60%, i.e., the latter is 1.5 times stronger; in addition, the betatrons may act in opposition to one another (depending on the model of the magnetic-field disturbance). Attention should be drawn to the fact that, according to [13], oscillation along lines of force in the geomagnetic field does not introduce an additional acceleration during adiabatic disturbances. This can be understood if it is remembered (see [6], Sec. 2.3.7) that when a particle is reflected from a moving magnetic mirror, it experiences betatron acceleration inside of the mirror and, consequently, the Fermi acceleration will be the only manifest effect of the gyrobetatron in the case under consideration.

The variation of the particle angular distribution and energy was studied in [22] for a given variation of the magnetic-shell parameter L and conservation of the first two adiabatic invariants (see also [23], Sec. 4). These results can also be applied to adiabatic transfer if the variation of L is obtained from conservation of the third invariant.[3] In [24], elementary models of the geomagnetic field during a storm were used to examine the behavior of trapped particles for which all three invariants are conserved. An axisymmetric geomagnetic-field model suitable for description of the disturbances in the main and recovery phases of geomagnetic storms was proposed in [25], which also examined the adiabatic transport of particles during the recovery phase. It was shown that this process may be effective for particle filling of the trapped-radiation belt if, of course, the adiabaticity conditions are violated with injection of fresh particles into the earth's magnetosphere during the storm. In addition, such irreversible effects as loss of charged particles, for example, by spillage into the upper layers of the atmosphere, may also be important (see [24]). /181

Adiabatic effects interest investigators not only because they make a substantial contribution to the dynamics of the

[3]We should note that adiabatic displacements are reversible, i.e., the original particle distribution is recovered when the initial magnetic field is recovered. In the case of axial symmetry of the magnetic field and the disturbance, reversibility follows directly from conservation of the generalized angular momentum (see [23], §4).

trapped radiation, but also because it is often difficult without knowledge of their action in the real geometry of the geomagnetic field to identify the nonadiabatic effects associated with violation of the invariants. Several examples illustrating the above are given in [26]. Thus, when the usual (B, L) McIlwain coordinate system was used to process the experimental data, Explorer 12 measurements of charged-particle fluxes for 24-27 September and 4-10 October 1961 showed "diffusion waves" — diffusion of particles toward the earth across L shells.[4] However, consideration of the symmetrical ring current and the currents flowing along the surface of the magnetosphere (for certain models) introduced such large corrections into the B, L coordinates that the particle adiabatic transport effects came to predominate in these measurements and the manifestation of radial diffusion was reduced to practically nothing. Another example in which nonadiabatic effects were distinguished against an adiabatic background is given in [21].

2. Diffusion of High-Energy Charged Particles in the Outer Radiation Belt

Kellogg [33] was the first to suggest the idea that charged particles are transported across magnetic lines of force under the action of disturbances that violate the third (flux) adiabatic invariant (with conservation of the first two). This transport is accompanied by betatron acceleration of the particles.[5] Radial diffusion under the action of large-scale geomagnetic disturbances arising as a result of a change in the solar-wind pressure on the boundary of the magnetosphere has attracted most of the attention (see [35-38, 23, 39-42]). The marginal case of small-amplitude electromagnetic disturbances has also been examined [43], and effects of time-dependent large-scale potential electric fields[6] [45-46] and the appearance of field fluctuations of ionospheric origin [47] have been studied. Immediately following [ ], the changes in particle energy and pitch-angle distribution [illegible] violation of the third invariant (without specific statement of the transport mechanism) were calculated in [48], whose authors also compare the results with the experimental particle distribution in the outer radiation belt. Particle diffusion in the coordinates α, β (α, β are the Euler potentials, see, for example, [8]) was considered in [49] (see also [34]).

---

[4]Similar "diffusion waves" were also observed by the authors of [27-32]. For a theoretical analysis, see §13, 14 in [23].

[5]See [34] for an up-to-date survey of papers on radial diffusion with violation of the third invariant.

[6]It is suggested in the review [45] that such fields may be associated with magnetic bays; an electric field due to convection in the magnetosphere is analyzed in [46].

In most of these papers, particle diffusion was described by the one-dimensional Fokker-Planck equation, whose coefficients - /182
the mean and root-mean-square radial particle displacements - were determined in accordance with the proposed model of the disturbance.[7]

When the geomagnetic field was considered to be closing into the magnetospheric plasma, it became possible to find a general relation among these coefficients and reduce the Fokker-Planck equation to a diffusion equation [51, 52]. A similar relation was also obtained in the case of arbitrary stochastic electromagnetic disturbances [53, 54].

In [39-42], particle diffusion in the dipole field under the action of electromagnetic impulses was studied with numerical models without expanding the field in series and with no frozen-field hypothesis (the electric-field component parallel to the magnetic field was not compensated). A somewhat different dependence of the coefficients in the Fokker-Planck equation on the coordinates was obtained. It should be noted that, although the frozen-field approximation is widely used in papers on charged-particle transport, it is a hypothesis that must be approached quite cautiously, since conditions such that the electric-field component parallel to the magnetic field is nonzero may exist in the magnetosphere (see, for example, [6], Chap. 5, and [34]).

Comparison of the results of diffusion theory with experimental data gives results that are both encouraging and discouraging. Initially, the development of the theory of particle transport under the action of sudden impulses[8] (see [36-38, 23]) yielded rapid progress, and the agreement with experiment was so good (see also [48]) that the basic mechanism of formation of the radiation belts could be regarded as established [22]. But even in [38], the diffusion coefficients obtained theoretically for protons were found to be somewhat smaller than those needed to explain the observed intensity distribution in the outer belt. Note is also taken in [21] of the need to increase the diffusion coefficients over the theoretically calculated values to account for nonadiabatic transport of 100-1700-keV protons during the recovery phase of a magnetic storm.

The method proposed in [56] for comparing the predictions of diffusion theory with experiment brought out substantial disagreements in the L profiles of proton flux intensity with a magnetic

---

[7]Concerning allowance for losses in the Fokker-Planck equation, see, for example, in [23, 37, 38]. Diffusion of particles with arbitrary pitch angles was considered in [50].

[8]Concerning sudden impulses, see [55].

moment exceeding the assigned value.[9] Application of this method to the calculations of [39] confirmed the conclusion of [56] to the effect that diffusion under the influence of sudden impulses is apparently not the principal mechanism forming the outer proton belt. Nonstationary solutions of the Fokker-Planck equation also lead to a similar conclusion [40, 41]. The times for diffusion from the boundary of the magnetosphere to shells L ≈ 4-6 are found to be 1-2 orders larger than those determined from the data of [27, 32]. Even though the experimental material is not adequate for categorical conclusions of any kind, it can be assumed (see [42]) that the role of diffusion under the influence of sudden impulses has been clearly overestimated, at least for protons with energies below 500-1000 keV.

Concerning outer-zone electrons, we again have examples both of agreement (see [23]) and of contradiction between theory and experiment. The empirical radial diffusion coefficients calculated in [57] for energies of 50-100 keV on L = 4-7 were found to be more than an order larger than those expected theoretically.[10]

The theory of charged-particle transport in the real geomagnetic field is greatly complicated by the need to consider particle interactions with various types of waves in the magnetosphere, which result in pitch-angle diffusion. A list of possible processes of this kind is given in [59]. For a detailed survey on pitch-angle electron diffusion, the reader is referred to [60], which also contains a bibliography on resonant interaction of waves and particles in the earth's magnetosphere. Here we wish to draw attention only to the relation between pitch-angle diffusion and radial diffusion. /183

Not only the third, but also the second and first adiabatic invariants may be violated as a result of resonant interactions.

If the disturbance has a period near that of the drifting motion of the particles around the earth, violation of the third flux invariant results, as was shown in [61], in nonconservation of the longitudinal invariant with the same degree of accuracy, i.e., even if the electric field has a small amplitude, it becomes impossible in this case to separate the oscillatory and azimuthal drifting motions.[11] The longitudinal invariant is also violated

[9]The good agreement of the results of [23, 36-38, 48] with measurements for protons with energies above 100 keV is obtained automatically as a result of use of the Davis energy spectrum, which does not permit detection of deviations of the L profile of intensity from exponential.

[10]Concerning electron transport coefficients for L < 5, see also [58].

[11]If the electric field perpendicular to the magnetic field is so large as to cause a considerable shift of the particle from the original line of force during one oscillation between mirrors, the inseparability of the oscillatory and drifting motions becomes obvious (see [8]).

under the influence of disturbances with periods near the period of particle oscillations between mirrors (ion-acoustic waves, MHD fluctuations, see [42] and [60]); disturbances resonant with the particle gyrofrequency also violate the first adiabatic invariant.

The diffusion of the particles becomes anisotropic as a result of nonconservation of the longitudinal invariant; for the most part, the transport takes place, as before, across magnetic lines of force, but there is also a shift of the reflection points that is substantial for particles reflected at high latitudes. The latter should, according to [61], be manifested in a change in the energy spectrum of the trapped radiation along the magnetic lines of force, but observed particle distributions in the belts do not confirm this effect. This may be because the bulk of the belt particles have a pitch-angle distribution with a maximum of 90°, and diffusion remains practically one-dimensional near the plane of the geomagnetic equator, since the reflection points are shifted only slightly at low latitudes.

A general analysis of anisotropic diffusion and its consequences[12] is given in [62], where the conclusion is that diffusion under the influence of slow disturbances with periods near the azimuthal-drift period of the particles is not the dominant process. However, other types of disturbances may be more effective (see [60]). Pitch-angle diffusion may result in "effective mixing" of particles along magnetic lines of force and equalization of their energies.

Thus, it is more likely that the observed charged-particle distribution in the outer radiation belt results from a combination of two different diffusion processes — one with a constant magnetic moment and another with constant energy.

The simultaneous operation of these processes has been observed experimentally [63-66] (see also [59]), and such a "bimodal" diffusion in a dipole field was modelled numerically in [67-69].

A lucid physical picture of the emergence of radial diffusion as a result of pitch-angle scatter of the particles in the geomagnetic field is drawn in [70, 71]. As a result of splitting of magnetic shells (due to the absence of axial symmetry of the field [72, 70]), particles with different pitch angles that begin their azimuthal drift from the same line of force will have /184
different drift trajectories. In a complete revolution around the earth, each particle will return to the same line of force if its pitch angle has not changed during this time. Otherwise the particle will experience a radial displacement whose direction will depend on local time and the sign of the pitch-angle change.

[12]The diffusion coefficients are also discussed in [34, 50] as they depend on the latitude of the particle-reflection points.

The features of the trapped-particle distribution in the geomagnetic field (pitch-angle and spatial distribution, nonuniformity of drift velocity around the earth, etc.) are such that in the range beyond the intensity maximum for particles of a given energy, these particles are diffused away from the earth. The coefficients of this diffusion, which takes place in first approximation with conservation of particle energy, were examined in [73, 74] and found to be small. In addition, pitch-angle scatter carries belt particles into the loss cone. Being, on the whole, more of a loss mechanism than a mechanism pumping particles into the belt, this effect cannot therefore make a large contribution to the formation of the earth's radiation belts, although it will doubtless have a certain influence on the particle energy spectrum. It appears that this diffusion away from the earth (with energy conservation) is combined in the geomagnetic field with a diffusion toward the earth that increases particle energy (with conservation of at least the first adiabatic invariant), with the former mechanism more noticeable during magnetically quiet periods and the latter more conspicuous during disturbances (see [63-66, 59]. It is noted in [59] that when these transport mechanisms act successively, it becomes possible for certain electrons to be subject to recurrent acceleration, and this may contribute to the formation of the high-energy electronic component of the radiation belts.

3. Rapid Nonadiabatic Transport of Charged Particles

The preceding section was devoted to comparatively slow diffusion processes of charged-particle transport in the magnetosphere of the earth. However, rapid nonadiabatic effects are frequently observed. As a rule, they are associated with magnetic storms (see, for example, [11, 16-20, 75, 76] and the reviews [14, 15]) and with magnetospheric substorms ([2], Chap. 9).

If they are repeated, sudden onsets of magnetic storms may, as one of the types of large-scale disturbances, cause diffusion (see §2). Here we shall discuss the possibility of rapid transport (and/or acceleration) of particles under the action of single impulses.

In spite of the inadequacy and sometimes uncertain quality of the experimental material, some observations can be treated as manifestations of this effect (for example, [75]). At least or of several cases of registration of a rapid (during 1-2 min) increase in the fluxes of protons with energies above 100 keV and 20-100-keV electrons that were cited in [77] was associated with a sudden storm onset. According to [76], an increase in the fluxes of electrons with energies above 300 keV on L = 5 began no later than 2.5 hours after the sudden onset of the magnetic storm of 5-11 February 1965. The lag time increased with increasing energy (to 0.5 day for 1.0 MeV) for higher-energy electrons on the same shell. Prolonged nonadiabatic electron transport from L = 5 to L = 4 at an approximately constant velocity of $1.5R_E$/day (irrespective of particle energy) was observed immediately after the sudden

onset of the storm. Under quieter conditions, the diffusion velocity is much lower[13] (0.12-0.02 R_E/day on L = 4 [28, 30] with proportionality to L^{8-9}).

Thus, a single pulse of finite amplitude (such as the sudden onset of a storm) may, in addition to nonadiabatic particle transport directly during the pulse, result in a substantial increase /185
in the diffusion rate during the period that follows. Calculations of the first of these effects with the Chapman-Ferraro model were made in [79]. In addition, this effect appears as a constituent part in all studies of diffusion in the case of small disturbances (see §2). There has recently been a revival of interest in this problem, both from the methodological standpoint [80, 81] and in connection with the possible geophysical consequences [82].[14] As for the increase in the velocity of diffusion, this effect is most probably due to the appearance (or strengthening) of large-scale electric fields of magnetospheric or perhaps ionospheric origin during the initial phase of the magnetic storm.

We should note, however, that substantial departures from the above scheme of high-energy-electron behavior at the beginning of a magnetic storm have also been observed. Thus, the first rise in the electron fluxes during the storm of 18 April 1965 was not registered until 12 hours had elapsed after the sudden onset [18]. A decrease in the intensity at the electron-belt maximum immediately after the sudden onset of a storm is reported in [87]. The cause of these effects is apparently to be sought in features of the storm's development.

The magnetic-field intensity decreases in the outer radiation belt during the main phase of the storm as a result of development of the "ring current," and effects of adiabatic transport of trapped particles away from the earth are observed (see §1). Against the background of this comparatively slow process, the electron-flux intensities at all energies above 150 keV show a sharp decrease that is approximately proportional to $L^{13\pm2}$ and increases with increasing particle energy [15]. This phenomenon (see in [87-90, 17]) is probably due to sweeping of many of the magnetic lines of force into the tail of the magnetosphere both by

[13]It is reported in [15] that "rapid diffusion" of electrons at a velocity differing by more than an order of magnitude from the quiet velocity often occurs after sudden onset (see [78]).

[14]Frank's discovery [83, 84] of particles with energies <50 keV, which make the basic contribution to the "ring current," poses the question as to the possibility of their transport into the magnetosphere (from shells with L ≈ 7-8 during quiet periods to L ≈ ≈ 3-5 during a storm) during the initial [84] or perhaps the main [84] phase of the storm. In addition, particle transport as a result of single application of a large-scale impulse of large amplitude may be substantial at the beginning of a magnetospheric substorm [86].

an earthward motion of the neutral layer of the tail and as a result of an increase in the "ring current."

However, the intensity of electrons with energies above 40 keV does not always decrease during this period [30]. In addition, asymmetry of the magnetic-field disturbance during the main phase [91-95] results from injection of "fresh" particles in the evening sector of the magnetosphere [84, 4]. Their transport toward the earth requires an electric field directed toward the west on the night side of the magnetosphere. Since the increase of the "ring current" is closely related to the development of polar magnetic substorms [96-104] (with the maximum of the DP variation leading the maximum of the main phase of the storm), it is possible that electric fields arising during magnetospheric substorms are the basic factor in particle injection into the trapping zone.

In [105, 106], followed closely by [101, 102], the principal role in particle transport is reserved for an electric field accompaning convective motion of the plasma from the tail of the magnetosphere toward the earth; charged-particle transport during the main phase of a storm with conservation of the first two adiabatic invariants under the action of a westward electric field operating at high latitudes was examined in [85]; it was shown in [86] that the required electric field can be created in the initial phase of a magnetospheric substorm. The effects of various types of instabilities were also studied (Chap. 10 of [2]). However, it is possible that charge-separation fields may prove to be the most important factor; they may arise in the so-called Alfven layer (see [107, 108]) and as a result of magnetospheric penetration of solar-wind protons with energies around 10 keV, whose azimuthal drift enters resonance with the rotation of the earth [109].

In the recovery phase of the storm, there is an increase in /186
trapped-particle intensity (see, for example, [14, 15]) that can be explained in part by adiabatic [25] and slow nonadiabatic [21] transport of particles toward the earth. The effects of the rapid nonadiabatic process are exemplified by a sharp increase in the intensity of 150-1200-keV electrons [15, 30, 110] at the beginning of the recovery phase. This may be due to the return of magnetic lines of force that were previously swept into the tail. However, an important peculiarity that has not yet been satisfactorily explained was reported in [110]: the fluxes of electrons with energies above 280 keV increase first of all on the inner L shells ($L \approx 2$-4), and then diffusion both toward the earth and away from it is observed.

Let us now examine certain transport effects observed during magnetospheric substorms. The substorm concept, which is a relatively new one (see [2, 111]), regards auroral and polar magnetic substorms and other disturbances of similar nature in the polar ionosphere, as well as disturbances of the magnetic field and of the charged-particle fluxes in the zone of trapped and unstable

radiation and in the tail of the magnetosphere as manifestations of a single process.

The characteristic features of substorm development in the ionosphere (see [2]) – a sudden onset on the midnight side of the auroral oval near its low-latitude boundary and subsequent propagation of the disturbance in all directions (but more rapidly toward the pole than toward the equator and more rapidly eastward than westward) – argue that some sort of local explosive process takes place inside the magnetosphere where the magnetic lines of force are still closed near the plane of the midnight meridian with subsequent asymmetrical propagation of the disturbance toward the earth, into the tail, and onto the morning and evening sides. The same picture also emerges from correlation measurements of the magnetic field and the fluxes of trapped and spilled particles in the tail of the magnetosphere [112-115], at low altitudes [115-122], and on a synchronous orbit [93, 123-127]. The sudden increase in the flux intensities of both trapped and spilled particles at low altitudes appears first near local midnight on magnetic shells corresponding to the low-latitude boundary of the auroral oval (at which point the development of a negative bay is registered on ground-station magnetic records for this sector of the auroral zone). An abrupt increase in magnetic-field intensity from the low evening values is observed simultaneously on an ATS orbit and at low-latitude ground stations near the midnight meridian. On the ATS, the increase in the particle fluxes at all energies is also observed first at around midnight, with a subsequent azimuthal drift of electrons toward the morning side and of protons toward the evening side. "Islands" of particles in the tail of the magnetosphere appear after registration of the corresponding spillage in the atmosphere and magnetic bays on high-latitude ground stations.

Such space-time localization of the process, and the quasi-periodic nature of the substorms, are difficult to explain either in partial-ring-current models[15] [128] or by recourse to cross-connection of magnetic lines of force in the tail of the magnetosphere [105, 106, 130-132]. The possible roles of instabilities on the outer boundary of the capture zone [133, 134] and in the tail of the magnetosphere [135] have also been studied. For a discussion of these hypotheses see Chap. 10 of [2]. A possible relation of substorms to oscillations of the geomagnetic tail is noted in [136].

Conceptions of substorms as relaxation processes caused by tensions in the tail of the magnetosphere are developed in [137]. According to [138], the causes of substorms are related to the

[15]The decrease in the geomagnetic-field intensity in the evening sector of the magnetosphere can be explained by a partial ring current (low-latitude negative magnetic bays are observed on the earth in this sector) [129].

internal structure of the magnetosphere itself, to the morning-evening asymmetry of the magnetic-field and plasma-layer configurations on the night side. The local change in this configuration – a considerable shortening of the magnetic lines of force[16] accompanied by plasma convection – is adequate to explain the observed particle acceleration even without invoking field-annihilation mechanisms. /187

It is possible that the rotation of the earth, combined with viscous friction as the magnetic lines of force are swept into the tail, is an important factor in creating conditions for the appearance of this process. In addition, the position of the plasma (and neutral) layers of the tail varies continuously as a result of the noncoincidence of the magnetic axis with the axis of the earth's rotation, and this may influence the development of instability in this layer.[17]

An attempt is made in [86] to link the initial explosive phase of the magnetospheric substorm with the formation (perhaps as a result of development of instability) of a region of increased resistance on the margin of the tail current layer closest to the earth near the plane of the midnight meridian. The disturbance of the magnetic field due to the spreading of currents around this region is modelled with the aid of an additional growing dipole whose magnetic moment is parallel to the moment of the terrestrial dipole. The induced electric field supports transport and acceleration of charged particles in a significant volume of the low-latitude magnetosphere.

Because of the complexity of the problem and the inadequacy of the experimental data, theoretical investigation of magnetospheric substorms has not yet advanced beyond hypothetical description of the possible processes and the development of numerical estimates. Additional facts must be accumulated to form a basis for a choice among the existing models or the creation of new ones. The electric fields during substorms and the causes of their appearance remain unknown, and the relation of magnetospheric substorms to magnetospheric penetration of protons with energies below 50 keV, which are so important in the formation of the "ring current," remains unclear [4, 5]. But even today it appears certain that magnetospheric substorms make the main contribution to the dynamics of the earth's radiation belts.

---

[16]The importance of betatron and Fermi acceleration in collapse of magnetic lines of force on the night side of the magnetosphere was stressed in [131], which closely followed the ideas advanced in [139].

[17]In this case, the characteristic features of the substorms should exhibit diurnal and seasonal peculiarities. The corresponding analysis has not yet been carried out.

We have briefly discussed the characteristic features of certain processes of charged-particle transport in the earth's magnetosphere (we have not considered convective motions of the plasma; for a survey of this problem see, for example, in [140]). We have noted that these processes vary in importance, and are understood with varying degrees of clarity. At the present stage, it is natural that adiabatic and diffusion processes are more easily understood, but they do not appear to be the principal ones in the dynamics of the magnetosphere. At the moment, rapid nonadiabatic particle transport during magnetic storms and magnetospheric substorms have been studied least of all. The development of research in this direction is one of the basic problems of magnetospheric physics at this time.

In conclusion, I take this opportunity to thank A.I. Yershkovich for a discussion of the problems touched upon in this review.

REFERENCES

1. A.I. Ershkovich, G.A. Skuridin, and V.P. Shalimov. Space Sci. Rev., Vol. 10, 262, 1969 (see this collection, pp. 1-34).
2. S.I. Akasofu. Polyarnyye i magnitosfernyy subburi (Polar and Magnetospheric Substorms), Moscow, "Mir," 1971.
3. L.A. Frank. On the Presence of Low-Energy Protons ($5 \leq E \leq 50$ keV) in the Interplanetary Medium. U. of Iowa Res. Rep. 69-24 May 1969, see also J. Geophys. Res., 1970, Vol. 75, 707.
4. L.A. Frank. J. Geophys. Res., 1970, Vol. 75, 1263. /188
5. L.A. Frank. In: "Particles and Fields in the Magnetosphere." Reinhold Publ Corp., New York, 1969, 320.
6. H. Alfven and C.-G. Faelthammar. Cosmical Electrodynamics (Russ. ed.), Moscow, "Mir," 1967.
7. A.J. Dragt. Rev. Geophys., 1965, Vol. 3, 255.
8. T. Northrop. Adiabatic Motion of Charged Particles (Russ. ed.), Moscow, Atomizdat, 1967.
9. A.J. Dessler and R. Karplus. J. Geophys. Res., 1961, Vol. 66, 2289.
10. C.Y. Fan, P. Meyer, and J.A. Simpson. J. Geophys. Res., 1961, Vol. 66, 2607.
11. C.E. McIlwain. Processes Acting Upon Outer Zone Electrons. I. Adiabatic Perturbations. Paper Presented at Interunion Symposium on Solar-Terrestrial Physics, Belgrade, Sept. 1966.
12. C.E. McIlwain. J. Geophys. Res., 1966, Vol. 71, 3623.
13. R.W. Fillius and C.E. McIlwain. J. Geophys. Res., 1967, Vol. 72, 4011.
14. J.A. Van Allen. Rev. Geophys., 1969, Vol. 7, 233.
15. S.N. Vernov, E.V. Gorchakov, S.N. Kuznetsov, Yu.I. Logachev, E.N. Sosnovets, and V.G. Stolpovsky. Rev. Geophys., 1969, Vol. 7, 257.
16. L.R. Davis and J.M. Williamson. In: "Radiation Trapped in the Earth's Magnetic Fields," D. Reidel Publ. Co., Dordrecht, Holland, 1966, 215.

17. D.J. Williams. J. Geophys. Res., 1967, Vol. 72, 1644.
18. L.J. Lanzerotti, C.S. Roberts, and W.L. Brown. J. Geophys. Res., 1967, Vol. 72, 5893.
19. W.L. Brown, L.J. Cahill, L.R. Davis, C.E. McIlwain, and C.S. Roberts. J. Gelphys. Res., 1968, Vol. 73, 153.
20. L.J. Lanzerotti. J. Geophys. Res., 1968, Vol. 73, 438.
21. F. Sörass. Comparison of Post-Storm Non-Adiabatic Recovery of Trapped Protons with Radial Diffusion, Goddard Space Flight Center, X-612-69-241, June 1969.
22. Yu.S. Krymov and B.A. Tverskoy. Geomagnetizm i Aeronomiya, 1964, Vol. 4, 397.
23. B.A. Tverskoy. Dinamika radiatsionnykh poyasov Zemli (Dynamics of the Earth's Radiation Belts), Moscow, "Nauka," 1968.
24. V.P. Shabanskiy. Geomagnetizm i Aeronomiya, 1966, Vol. 6, 479.
25. V.D. Pletnev and V.P. Shalimov. Kosmicheskiye Issledovaniya, 1970, Vol. 8, 251.
26. L.D. Kavanagh. J. Geophys. Res., 1968, Vol. 73, 185.
27. L.A. Frank, J.A. Van Allen, and H.K. Hills. J. Geophys. Res., 1964, Vol. 69, 2171.
28. L.A. Frank. J. Geophys. Res., 1965, Vol. 70, 3533.
29. S.N. Vernov, I.A. Savenko, M.V. Tel'tsov, and P.I. Shavrin. Geomagnetizm i Aeronomiya, 1966, Vol. 7, 377.
30. J.D. Craven. J. Geophys. Res., 1966, Vol. 71, 5643.
31. I.B. McDiarmid and J.R. Barrows. Can. J. Phys., 1966, Vol. 44, 1361.
32. S.N. Vernov, S.N. Kuznetsov, Yu.I. Logatsev, G.B. Lopatina, Ye.N.Sosnovets, and V.G. Stolpovskiy. Geomagnetizm i Aeronomiya, 1968, Vol. 8, 401 (see also: Space Res., 1968, Vol. 8, 120).
33. P.J. K[illegible] Nature, 1959, Vol. 183, 1295.
34. C.G. Fälthammar. In "Earth's Particles and Fields," Reinhold Publ. Co., New York, 1968, 157.
35. E.N. Parker. J. Geophys. Res., 1960, Vol. 65, 3117.
36. L. Davis and D.B.Chang. J. Geophys. Res., 1962, Vol. 67, 2169.
37. B.A. Tverskoy. Geomagnetizm i aeronomiya, 1964, Vol. 4, 436.
38. M.P. Nakada and G.D. Mead. J. Geophys. Res., 1965, Vol. 70, 4777.
39. A.I. Yershkovich, G.A. Skuridin, L.S. Chesalin, and V.P. Shalimov. Kosmicheskiye Issledovaniya, 1967, Vol. 5, 792 (see also: J. Atmos. Terr. Phys.,1967, Vol. 29, 459).
40. L.S. Chesalin, A.I. Ershkovich, and G.A. Skuridin. Space Res., 1968, Vol. 8, 164.
41. A.I. Yershkovich and L.S. Chesalin. Trudy V. Vsesoyuznoy yezhegodnoy zimney shkoly po kosmofizike (Trans. Fifth All-Union Annual Winter School on Space Physics), Apatity, 21 March-5 April 1968, 231.
42. L.S. Chesalin. Dissertation for the Degree of Candidate of Physicomathematical Sciences, Moscow, Institute of Space Research, Acad. Sci. USSR, 1969.
43. J.W. Dungey. Space Sci. Rev., 1965, Vol. 4, 199.
44. C.G. Fälthammar. J. Geophys. Res., 1965, Vol. 70, 2503.

45. J.W. Dungey. In: "Radiation Trapped in the Earth's Magnetic Fields," 1966, p. 389.
46. T.J. Birmingham. J. Geophys. Res., 1969, Vol. 74, 2169.
47. J.B. Cladis. J. Geophys. Res., 1966, Vol. 71, 5019.
48. M.P. Nakada, J.W. Dungey, and W.N. Hess. J. Geophys. Res., 1965, Vol. 70, 3529 (see also: Space Res., 1965, Vol. 5, 399).
49. T.J. Birmingham, T.G. Northrop, and C.G. Fälthammar. Phys. Fluids, 1967, Vol. 10, 2389.
50. B.J. Conrath. J. Geophys. Res., 1967, Vol. 72, 6069.
51. C.G. Fälthammar. J. Geophys. Res., 1966, Vol. 71, 1487.
52. C.G. Fälthammar. In: "Radiation Trapped in the Earth's Magnetic Fields," 1966, p. 398.
53. P.A. Sturrock. Phys. Rev., 1966, Vol. 141, 186.
54. D.E. Hall and P.A. Sturrock. Phys. Fluids, 1967, Vol. 10, 2620.
55. A. Nishida and L.J. Cahill. J. Geophys. Res., 1964, Vol. 69, 2243.
56. A.I. Yershkovich and V.P. Shalimov. Kosmicheskiye Issledovaniya, 1966, Vol. 4, 788. /189
57. L.D. Kavanagh. J. Geophys. Res., 1968, Vol. 73, 2959.
58. L.L. Newkirk and M. Walt. J. Geophys. Res., 1968, Vol. 73, 7231.
59. J.G. Roederer. In: "Earth's Particles and Fields," 1968, p. 143.
60. C.S. Roberts. Rev. Geophys., 1968, Vol. 7, 305.
61. G. Haerendel. J. Geophys. Res., 1966, Vol. 71, 1857.
62. G. Haerendel. In: "Earth's Particles and Fields," 1968, p. 171.
63. F.R. Paolini, G.C. Theodoridis, and S. Frankental. J. Geophys. Res., 1967, Vol. 72, 4590.
64. F.R. Paolini, G.C. Theodoridis, and S. Frankental. Ann. Geophys., 1968. Vol. 24, 129.
65. F.R. Paolini, G.C. Theodoridis, and S. Frankental. In: "Earth's Particles and Fields," 1968, p. 23.
66. S.M. Krimigis. In: "Earth's Particles and Fields," 1968, p. 59.
67. G.C. Theodoridis. Ann. Geophys., 1968, Vol. 24, 999.
68. G.C. Theodoridis, F.R. Paolini, and S. Frankental. Ann. Geophys., 1968, Vol. 24, 1015.
69. G.C. Theodoridis, F.R. Paolini, and S. Frankental. J. Geophys. Res., 1969, Vol. 74, 1238.
70. J.G. Roederer. J. Geophys. Res., 1967, Vol. 72, 981.
71. J.G. Roederer. In: "Earth's Particles and Fields," 1968, p. 193.
72. E.C. Stone. J. Geophys. Res., 1963, Vol. 68, 4157.
73. J.G. Roederer and M. Schulz. J. Geophys. Res., 1969, Vol. 74, 4117.
74. C.G. Fälthammar and M. Walt. J. Geophys. Res., 1969, Vol. 74, 4184.
75. R.A. Hoffman, L.R. Davis, and J.M. Williamson. J. Geophys. Res., 1962, Vol. 67, 5001.
76. L.J. Lanzerotti. Ann. Geophys., 1968, Vol. 24, 847.
77. A. Konradi. J. Geophys. Res., 1968, Vol. 73, 3449.
78. S.N. Vernov, S.N. Kuznetsov, Yu.I. Logachev, G.B. Lopatina, Ye.N. Sosnovets, and V.G. Stolpovskiy. Trudy V Vsesoyuznoy

yezhegodnoy zimney shkoly po kosmofizike (Trans. Fifth All-Union Annual Winter School on Space Physics), Apatity, 21 March-5 April 1968.
79. L.R. Henrich. J. Geophys. Res., 1963, Vol. 68, 1295.
80. L.D. Kavanagh. J. Geophys. Res., 1967, Vol. 72, 6120.
81. T.J. Birmingham and F.C. Jones. J. Geophys. Res., 1968, Vol. 73, 5505.
82. V.P. Shalimov. Dissertation for the Degree of Candidate of Physicomathematical Sciences. Moscow, Institute of Space Research, Acad. Sci. USSR, 1971.
83. L.A. Frank. J. Geophys. Res., 1967, Vol. 72, 1905.
84. L.A. Frank. J. Geophys. Res., 1967, Vol. 72, 3753.
85. V.P. Shalimov. Kosmicheskiye Issledovaniya, 1968, Vol. 6, 941.
86. V.P. Shalimov. Kosmicheskiye Issledovaniya, 1971, Vol. 9, 141.
87. S.N. Kuznetsov, E.N. Sosnovets, and V.G. Stolpovskiy. In Collection entitled: "Issledovaniya kosmicheskogo prostranstva" (Investigation of Cosmic Space), "Nauka," 1965, p. 420.
88. N.F. Ness and D.J. Williams. J. Geophys. Res., 1966, Vol. 71, 322.
89. D.J. Williams and N.F. Ness. J. Geophys. Res., 1966, Vol. 71, 5117.
90. S.N. Kuznetsov. Izv. Akad. Nauk SSSR, Seriya Fiz., 1966, Vol. 30, 1827.
91. S.I. Akasofu and S. Chapman. Planet. Space Sci., 1964, Vol. 12, 607.
92. L.J. Cahill. J. Geophys. Res., 1966, Vol. 71, 4505.
93. W.D. Cummings and P.J. Coleman. Radio Sci., 1968, Vol. 3, 758(I), 762(II).
94. R.A. Langel and J.C. Cain. Ann. Geophys., 1968, Vol. 24, 857.
95. S.I. Akasofu and C.I. Meng. Planet. Space Sci., 1969, Vol. 17, 707.
96. S.I. Akasofu and S. Chapman. J. Geophys. Res., 1963, Vol. 68, 125, 3155.
97. G.I. Korobkova. "Problemy Arktiki i Antarktiki", No. 18, 78, 1964.
98. S.I. Akasofu and S. Yoshida. J. Geophys. Res., 1966, Vol. 71, 231.
99. T.N. Davis and M. Sugiura. J. Geophys., 1966, Vol. 71, 785.
100. T.N. Davis and R. Parthasarathy. J. Geophys. Res., 1967, Vol. 72, 5825.
101. S.I. Belyakova, S.A. Zaytseva, and M.I. Pudovkin. Geomagnetizm i Aeronomiya, 1968, Vol. 8, 712.
102. S.A. Zaytseva, M.I. Pudovkin, and O.I. Shumilov. Geomagnetizm i Aeronomiya, 1968, Vol. 8, 905.
103. G.I. Ol' and A.I. Ol'. In collection entitled "Solnechno-zemnaya fizika" (Solar-Terrestrial Physics), No. 1, Moscow, 1969.
104. M.W. Haurwitz. J. Geophys. Res., 1969, Vol. 74, 2348.
105. W.I. Axford. Space Sci. Rev., 1967, Vol. 7, 149.
106. J.H. Piddington. J. Atmosph. Terr. Phys., 1967, Vol. 29, 87.
107. M.A. Schield, J.W. Freeman, and A.J. Dessler. J. Geophys. Res., 1969, Vol. 74, 247.

108. M.A. Schield. The Auroral Oval and Alfven Layer. U. of Iowa Res. Rep., November 1968.
109. A.V. Gurevich and V.P. Shcherbakov. Geomagnetizm i Aeronomiya, 1970, Vol. 10, 791.
110. D.J. Williams, J.F. Arens, and L.J. Lanzerotti. J. Geophys. Res., 1963, Vol. 73, 5673.
111. E. Selzer. Ann. Geophys., 1968, Vol. 24, 607.
112. J.P. Heppner, M. Sugiura, T.L. Skillman, B.G. Ledley, and M. Campbell. J. Geophys. Res., 1967, Vol. 72, 5417.
113. P. Rothwell and V. Wallington. Planet. Space Sci., 1968, Vol. 16, 1441.
114. T.P.Armstrong and S.M. Krimigis. J. Geophys. Res., 1968, Vol. 73, 143.
115. E.W. Hones, S. Singer, and C.S.R. Rao. J.Geophys. Res., 1968, Vol. 73, 7339.
116. A. Konradi. J. Geophys. Res., 1967, Vol. 72, 3829.
117. D. Jelly and N. Brice. J. Geophys. Res., 1967, Vol. 72, 5919. /190
118. F.V. Corotini, R.L. McPherron, and G.K. Parks. J. Geophys. Res., 1968, Vol. 73, 1715.
119. W.C. Lin, I.B. McDiarmid, and J.R. Barrows. Can. J. Phys., 1968, Vol. 46, 80.
120. C.S.R. Rao. J. Geophys. Res., 1969, Vol. 74, 794.
121. I.B. McDiarmid and J.R. Barrows. J. Geophys. Res., 1969, Vol. 74, 1749.
122. W. Bernstein, G.I. Inouye, N.L. Sanders, and R.L. Wax. J. Geophys. Res., 1969, Vol. 74, 3601.
123. W.D. Cummings, J.N. Barfield, and P.J. Coleman. J. Geophys. Res., 1968, Vol. 73, 6687.
124. T.W. Lezniak, R.L. Arnlody, G.K. Parks, and J.R. Winckler. Radio Sci., 1968, Vol. 3, 710(I), 715(II).
125. G.K. Parks and J.R. Winckler. J. Geophys. Res., 1968, Vol. 73, 5786.
126. K.A. Pfirtzer and J.R. Winckler. J. Geophys. Res., 1969, Vol. 74, 5005.
127. R.L. Arnoldy and K.W. Chan. J. Geophys. Res., 1969, Vol. 74, 5019.
128. W.D. Cummings. J. Geophys. Res., 1966, Vol. 71, 4495.
129. O.A. Troshichev and Ya.I. Fel'dshteyn. Kosmicheskiye Issledovaniya, 1969, Vol. 7, 309.
130. G. Atkinson. J. Geophys. Res., 1966, Vol. 71, 5157.
131. G. Atkinson. J. Geophys. Res., 1967, Vol. 72, 1491.
132. W.I. Axford. In: "Aurora and Airglow," Reinhold Publ. Co., New York, 1967, p. 499.
133. D.W. Swift. J. Geophys. Res., 1965, Vol. 70, 3061.
134. D.W. Swift. Planet. Space Sci., 1967, Vol. 15, 1225.
135. B. Coppi, G. Laval, and R. Pellat. International Center for Theoretical Phys. Publ., 1965.
136. A.I. Yershkovich. Kosmicheskiye Issledovaniya, 1969, Vol. 7, 944.
137. G.L. Siscoe and W.D. Cummings. Planet. Space Sci., 1969, Vol. 17, 1795.

138. J.R. Winckler. The Origin of Energetic Electrons in the Earth's Environments. Paper Presented at the Seminar on the Problems of Interplanetary Space Physics, Leningrad, 4-7 June 1969.
139. J.W. Dungey. Phys. Rev. Letters, 1961, Vol. 6, 47.
140. W.I. Axford. Rev. Geophys., 1968, Vol. 7, 421.

N75 13721

VIBRATIONS OF THE EARTH'S MAGNETIC TAIL

(Translation of "Kolebaniya magnitnogo khvosta zemli.")

A. I. Yershkovich and A. A. Nusinov

ABSTRACT

The natural-vibration period of the tail (regarded as bundle of magnetic line-of-force strings) and the characteristic time of recurrence of magnetospheric substorms are of the same order, suggesting the possibility of a relation between these phenomena. A model of the tail in the form of a plasma cylinder whose free boundary is immersed in the interplanetary plasma is examined. The nature of the natural oscillations of the tail excited by variations of the solar-wind pressure (for example, on the appearance of geoeffective 5-50-keV protons) is studied in this model. These vibrations have a total energy of $\sim 10^{22}$ erg, which is sufficient to generate magnetospheric substorms. With 18 source citations.

VIBRATIONS OF THE EARTH'S MAGNETIC TAIL*

/191

A.I. Yershkovich and A.A. Nusinov

The characteristic time of recurrence of magnetospheric substorms is of the order of 1-3 hours [1-3]. The frequency of the auroras and their intergral luminous flux are subject to a similar periodicity [4]. It is possible that there may be a relation between these phenomena and natural vibrations of the geomagnetic tail with a period of the same order of magnitude. In the simplified model of [5], the tail was regarded as a bundle of magnetic line-of-force strings along which Alfven waves propagate. The vibrations are excited by a blow against the lateral surface of the tail that results from a change in solar-wind velocity. This problem is analogous to the problem of excitation of a string of length l secured at its ends[1] by a blow from a flat rigid hammer of width l at velocity $\bar{v}_\perp$. In the coordinate frame whose z axis is parallel to the undisturbed magnetic field B, the solution of the vibration equation

$$\frac{\partial^2 y}{\partial t^2} = V_A^2 \frac{\partial^2 y}{\partial z^2} \tag{1}$$

has in this case the form [7]

$$y(z,t) = \frac{4v_\perp l}{\pi^2 V_A} \sum_{n=1}^{\infty} \frac{1}{n^2} \sin^2 \frac{n\pi}{2} \sin \frac{n\pi z}{l} \sin \frac{n\pi V_A t}{l}, \tag{2}$$

where $V_A = \frac{B}{\sqrt{4\pi\rho}}$ is the Alfven velocity and ρ is the plasma density. The magnetic-field disturbance b is determined from the equation of the magnetic line of force: $dz/B = dy/b$. Since the series (2) converges rapidly, we can confine ourselves to the first harmonic, obtaining as a result

$$b(z,t) = \frac{4v_\perp B}{\pi V_A} \cos \frac{\pi z}{l} \sin \frac{\pi V_A t}{l} = b_0 \cos \frac{\pi z}{l} \sin \frac{\pi V_A t}{l}. \tag{3}$$

Averaging over time and integrating over z, we find the total energy of the tail vibrations [5]:

---

*Paper prepared in 1969.

[1]The tail length l can be understood as the distance to a large-scale field inhomogeneity, e.g., to the neutral point in Dungey's model [6], which arises on the appearance of a southward component of the interplanetary magnetic field.

$$W = \frac{b_0^2}{16\pi}\pi a^2 l = \frac{v_\perp^2}{\pi^2 V_A^4} B^2 \pi a^2 l, \qquad (4)$$

where a is the radius of the tail. As an estimate, we shall take $l \approx 200\ R_E$ (R_E is the radius of the earth, $6.4 \cdot 10^8$ cm), $a \approx 25R_E$, average field in the tail $B \approx 10\ \gamma$, and an average particle concentration $\sim 0.1\ \text{cm}^{-3}$ (cf. [8]). Then the Alfven velocity $V_A \approx 10^8$ cm/sec and the period of the natural vibrations (the fundamental tone) $\tau_0 = 2l/V_A \approx 3 \cdot 10^3$ sec. The blow against the lateral surface of the tail may be due, for example, to protons with energies of ~5-50 keV, which were detected in the solar wind by Frank [9]. The average velocity of these protons corresponds approximately to the approximately one-day lag time between flares on the sun and phenomena on the earth: $v \sim 2000$ km/sec. The aberration due to the orbital motion of the earth (the aberration angle α is about 0.1 rad [10]) gives rise to an impact velocity $v_\perp \approx \alpha V \sim 200$ km/sec normal to the lateral surface of the tail. /192

In this case, the vibration amplitude $b_0 = \frac{4\pi v_\perp B}{\pi V_A} \sim 2.5\gamma$ and the energy of the tail's vibrations $\sim 10^{22}$ erg, which is comparable with the energy of a substorm. The maximum slope of a line of force to the z axis is $b_0/B \sim 0.2$. The results of direct measurements of the magnetic field in the tail (see, for example, [11, 12]) can apparently be interpreted as a manifestation of natural vibrations with values of b_0/B of the same order.

For more detailed study of the mechanism by which the natural vibrations of the tail are excited on a change in solar-wind parameters, and the nature of the vibrations themselves, let us consider a model of the tail in the form of a plasma cylinder whose free boundary is immersed in the interplanetary plasma. We shall assume that the plasma is homogeneous, ideally conductive, and incompressible, and that the frozen magnetic field B is homogeneous and parallel to the axis z of the cylinder. We shall regard the lines of force at the ends of the cylinder $z = 0$, $z = l$ as frozen into superconductive planes perpendicular to the z axis. In this case, the linearized system of magnetohydrodynamic equations for small perturbations takes the form

$$\begin{aligned} &\rho \frac{\partial \boldsymbol{v}}{\partial t} = -\nabla\Phi + \frac{1}{4\pi}(\boldsymbol{B}\nabla)\boldsymbol{b}, \\ &\operatorname{div}\boldsymbol{v} = 0, \\ &\frac{\partial \boldsymbol{b}}{\partial t} = \operatorname{rot}[\boldsymbol{v}, \boldsymbol{B}], \end{aligned} \qquad (5)$$

where v is the velocity of displacement of an elementary plasma

volume from its equilibrium position and $\Phi = \delta\left(p + \frac{B^2}{8\pi}\right)$ is the total-pressure (gaskinetic and magnetic) perturbation. We introduce the displacement vector ξ of the elementary plasma volume, so that $v = \partial\xi/\partial t$; system (5) can then be written

$$\rho \frac{\partial^2 \xi}{\partial t^2} = -\nabla\Phi + \frac{1}{4\pi}(B\nabla)(B\nabla)\xi,$$
$$\operatorname{div}\xi = 0, \qquad (6)$$
$$b = (B\nabla)\xi.$$

We shall seek all perturbed quantities in the form of superpositions of standing cylindrical waves, i.e., products of the form

$$\xi(r)(\zeta_1 \cos kz + \zeta_2 \sin kz)(\zeta_3 \cos m\varphi + \zeta_4 \sin m\varphi)\cos \omega t,$$

where r, ϕ, and z are cylindrical coordinates and the ζ_i are constants. We obtain from the first equation of (6)

$$\xi = \frac{\frac{1}{\rho}\nabla\Phi}{\omega^2 - k^2 V_A^2}. \qquad (7)$$

Substituting ξ into the second equation of (6) (incompressibility condition), we obtain the Laplace equation $\Delta\Phi = 0$ for Φ, from which, considering the boundedness of the solution as $r \to \infty$ and $r \to 0$ and the boundary condition $\xi_r = \xi_\varphi = 0$ at $z = 0, l$, we obtain the perturbation potential Φ on the inside and outside of the cylinder in the form /193

$$\Phi_i(r, t) = \sum_{\substack{n=1 \\ m=0}}^{\infty} C_{nm} I_m(kr) \sin kz \cos m\varphi \cos \omega t,$$
$$\Phi_e(r, t) = \sum_{\substack{n=1 \\ m=0}}^{\infty} A_{nm} K_m(kr) \sin kz \cos m\varphi \cos \omega t, \qquad (8)$$

where $k = n\pi/l$, I_m and K_m are modified Bessel functions of order m, C_{nm} and A_{nm} are constants that depend on the boundary conditions, and the subscripts i and e pertain to the interior and exterior plasma. The plasma parameters (density and magnetic field) change stepwise at the surface of the cylinder, i.e., we have a tangential-discontinuity-type boundary condition on the free surface. In virtue of the equality of the total pressures on either side of the tangential discontinuity (in both the equilibrium and perturbed states), we obtain

$$\Phi_i(a) = \Phi_e(a). \qquad (9)$$

The existence condition of the boundary requires continuity of the radial displacement component ξ_r on passage across the discontinuity:

$$\xi_{re}(a) = \xi_{ri}(a). \tag{10}$$

Substituting the potential values of (8) into the boundary conditions (9) and (10) and applying (7), we obtain a homogeneous algebraic equation system for the coefficients A_{nm} and C_{nm}:

$$\begin{aligned} &A_{nm}K_m(ka) - C_{nm}I_m(ka) = 0, \\ &\frac{A_{nm}}{\rho_e}\frac{K'_m(ka)}{\omega^2 - k^2V_{Ae}^2} - \frac{C_{nm}}{\rho_i}\frac{I'_m(ka)}{\omega^2 - k^2V_{Ai}^2} = 0. \end{aligned} \tag{11}$$

A dispersion equation for the natural frequencies follows from the existence condition for nontrivial solutions of system (11):

$$\omega^2 = \omega_{nm}^2 = \frac{k^2}{4\pi}\frac{B_i^2 - B_e^2\dfrac{I'_m(ka)K_m(ka)}{I_m(ka)K'_m(ka)}}{\rho_i - \rho_e\dfrac{I'_m(ka)K_m(ka)}{I_m(ka)K'_m(ka)}}. \tag{12}$$

Recognizing that the average plasma concentration in the tail ($\sim$0.1 cm^{-3}) is much lower than the concentration in the solar wind ($\sim$5 cm^{-3}, cf. [13]), we can let $\rho_i \to 0$ in the dispersion equation (12), so that it assumes the form

$$\omega^2 = \frac{k^2}{4\pi}\left(\frac{B_e^2}{\rho_e} - \frac{B_i^2}{\rho_e}\frac{I_m(ka)K'(ka)}{I'_m(ka)K(ka)}\right). \tag{13}$$

This dispersion equation actually describes the natural vibrations of a cylinder with a "vacuum" (i.e., particle-free) magnetic field surrounded by the interplanetary plasma, and the problem of finding the perturbations inside of the earth's magnetic tail reduces to investigation of perturbations in a vacuum magnetic field (which is equivalent to investigating the vibrations of a plasma cylinder with a subsequent unit transition $\rho_i \to 0$). Since curl $b_i = 0$, in this case, we shall seek the b_i in the form /194

$$b_i = \nabla\psi(r, t). \tag{14}$$

The condition div $b_i = 0$ leads to a Laplace equation for $\psi(r, t)$. Considering that the lines of force are frozen in at the ends (i.e., $b_{zi} = 0$ at $z = 0, l$) and recognizing that the solution

is bounded as r → 0, we obtain

$$\psi(r,t)=\sum_{\substack{n=1\\m=0}}^{\infty} D_{nm} I_m(kr)\cos kz\cos m\varphi\cos\omega t, \tag{15}$$

where D_{nm} is a coefficient that depends on the boundary conditions. In the case at hand, the boundary conditions are similar to those for a fully skinned pinch [14]. Here the potential Φ_i in (9) must by replaced by $\frac{B_i b_i}{4\pi}$ (the change in the magnetic pressure), and the boundary condition (10) then corresponds to a perturbed magnetic field tangential to the perturbed boundary:

$$n\cdot b_i(a)=n(B_i\nabla)\xi_e(a), \tag{16}$$

where n is the unit vector of the normal to the unperturbed boundary. Substitution of $\Phi_e(r,t)$ and $\psi(r,t)$ into (9) and (16) yields a system of algebraic equations for the unknown constants A_{nm} and D_{nm}:

$$\begin{aligned} &A_{nm}K_m(ka)+D_{nm}\frac{B_i}{4\pi}kI_m(ka)=0,\\ &A_{nm}\frac{B_i}{\rho_e}\frac{kK'_m(ka)}{\omega^2-k^2V_{Ae}^2}-D_{nm}I'_m(ka)=0, \end{aligned} \tag{17}$$

from whose solvability condition the dispersion equation (13) follows, as we should expect. We take the following estimates: concentration of exterior plasma ∿5 cm^{-3}, $B_e \approx 5\ \gamma$, concentration inside the tail ∿0.1 cm^{-3} as before, and $B_i \approx 10\ \gamma$. We consider also that $r/l < a/l \ll 1$; then $I'_m/I_m \approx m/kr$; $K'_m/K_m \approx -m/kr$ for $m \neq 0$ and $I'_0/I_0 \approx kr/2$; $\frac{K'_0}{K_0} \approx -\frac{1}{kr\ln\frac{1}{kr}}$. From the dispersion equation (13) we obtain the natural-vibration frequency

$$\left.\begin{aligned} \omega &= \frac{B_i}{a\sqrt{4\pi\rho_e}}\sqrt{\frac{2}{\ln\frac{l}{\pi a}}} && \text{at } m=0,\\ \omega &= \frac{\pi}{l\sqrt{4\pi\rho_e}}\sqrt{B_i^2+B_e^2} && \text{for } m\neq 0. \end{aligned}\right\} \tag{18}$$

Thus, the period of the natural vibrations τ_0 ∿ 2 hours at m = 0 and τ ∿ 6 hours when m ≠ 0.

Both the period of the vibrations and their total energy are close to the values characteristic for a magnetospheric substorm, indicating a possible relationship between these phenomena. If

some nonlinear mechanism (which will not, however, be considered here) disturbs the steady-state vibration process, this energy may be released, at least in part, during a characteristic time $\sim l/V_a$, supplying energy at a rate of $\sim 10^{18}$ erg/sec, which is close to the amount observed during a substorm.[2]

The amplitude of the magnetic-field perturbations at the earth can be estimated by equating the energy flux $(b^2/8\pi)\pi a^2 V_A$ in the tail to the energy flux at the earth (see [5, 7]). Since the Alfven velocity $V_A \sim 10^9$ cm/sec near the earth, and the polar caps have /195 an area of $\sim 3 \cdot 10^{17}$ cm^2, the amplitude of the periodic magnetic-field vibrations at the earth is ~ 20 γ. This figure agrees with spectral energy density measurements for long-period ($\gtrsim 10^3$ sec) vibrations at the surface of the earth [15]. The electric field in the tail

$$E = -\frac{1}{c} v \times B \qquad \text{at} \quad \frac{v}{V_A} = \frac{b}{B} \sim 0.1 \qquad \text{is about} \quad \sim 10^{-5}\ \text{V/cm}.$$

Fields of this magnitude have been observed in the tail of the magnetosphere [16]. Extending them into the ionosphere along equipotential lines of force, we obtain $E \sim 10^{-3}$ V/cm, in agreement with the measurements of [17]. An estimate from the drift velocities of auroral forms leads to the same values [18]. It is natural to link the changes in drift direction during a magnetospheric substorm [18] to natural vibrations of the tail. The hydromagnetic fluctuations that have been considered give rise to ordered particle motion.

We know that the average kinetic-energy density of particles in hydromagnetic waves is of the order of the average energy density of the magnetic perturbation. Here the average particle energy (at least on the periphery of the tail) is ~ 1 keV. Obviously, the energy of the thermal motion cannot be substantially smaller than this value (ordered-motion energy can be transformed into thermal energy, e.g., by the development of a two-stream-type instability). Thus, the natural-vibration mechanism may be responsible for heating of the tail plasma to ~ 1 keV. According to [8], this is the temperature of the plasma in the tail.

The rotation of the earth may give rise to forced vibrations of the tail [5]: $b(z,t) = b_1 \cos\frac{2\pi z}{V_A \tau} \sin\frac{2\pi t}{\tau}$, where τ = 24 hours. Estimates [5] indicate that the amplitude of the vibrations appearing as a result of the inclination of the geomagnetic axis to the axis of

[2]The reverse effect, resonant buildup of tail vibrations by magnetospheric substorms, is also obviously possible in principle.

rotation is $b_1 \sim 1.5$ γ, which gives a vibration energy $W \sim 3 \cdot 10^{24}$ ergs. Here the expenditure of the earth's rotational energy is much smaller than the tidal expenditure and does not result in any appreciable deceleration of the earth.

We note in conclusion that the magnetic energy stored in the tail, $\frac{B^2}{8\pi}\pi a^2 l \sim 10^{23}$ erg, is sufficient to cause a magnetic storm of several hundred gammas. Obviously, the tail should disappear temporarily after such a storm (if it is the source of the latter's energy).

REFERENCES

1. G.K. Parks, T.W. Lezniak, and J.R. Winckler. Trans. Amer. Geophys. Union, 1968, Vol. 49, 228.
2. B. Hultqvist. Rev. Geophys., 1969, Vol. 7, 129.
3. S.I. Akasofu. Space Research, 1968, Vol. VIII, 213.
4. V.N. Samsonov and N.S. Zaretskiy. Space-Time Distribution of the Auroras. Paper at Thirteenth General Assembly of the International Union of Geodesy and Geophysics. Berkeley, 1963.
5. A.I. Yershkovich. Kosmicheskiye Issledovaniya, 1969, Vol. 7, 944.
6. J.W. Dungey, Phys. Rev. Lett, 1961, Vol. 6, 47.
7. A.N. Tikhonov and A.A. Samarskiy. Uravneniya matematicheskoy fiziki (The Equations of Mathematical Physics), Moscow, GTTI, 1953.
8. Physics of the Earth in Space. A Program of Research, 1968-1975, Nat. Acad. of Science, Nat. Res. Council, 1968.
9. L.A. Frank. Further Comments Concerning Low-Energy Charged-Particle Distributions within the Earth Magnetosphere and its Environments. Preprint Univ. of Iowa, 1969, 69-42.
10. F. Mariani and N.F. Ness. J. Geophys. Res., 1969, Vol. 74, 5633.
11. V.L. Patel. Space Res., 1966, Vol. VI, 758.
12. K.W. Behannon and N.F. Ness. Physics of the Magnetosphere. D. Reidel Publ. Co., Holland, 1969, p. 409.
13. R. Lust. In collection entitled: "Solar-Terrestrial Physics" (Russ. ed.), Moscow, "Mir," 1968, p. 13.
14. B.B. Kadomtsev. In collection entitled "Voprosy teorii plazmy" (Problems of Plasma Theory), Vol. [illegible] Moscow, Atomizdat, 1963, pp. 134-136.
15. T.J. Herron. J. Geophys. Res. [illegible], 1759.
16. J.A. Van Allen and N.F. Ness. J. Geophys. Res., 1969, Vol. 74, 71.
17. E.M. Wescott, J.D. Stolarik, and J.P. Heppner. J. Geophys. Res., 1969, Vol. 74, 3479.
18. G.V. Starkov, Ya.P. Fel'dshteyn, and N.F. Shevnina. Motions of Auroral Forms During the Development of an Auroral Substorm. Trans. Polar Geophysics Institute of the Polar Branch, Academy of Sciences of the USSR (in preparation).

N75 13722

SHORT-RANGE REPULSIVE FORCES BETWEEN ATOMS AND MOLECULES OF ATMOSPHERIC GASES

(Translation of "Korotkodeystvuyushchiye sily ottalkivaniya mezhdu atomami i molekulami atmosfernykh gazov.")

A. P. Kalinin, V. B. Leonas, and A. V. Sermyagin

ABSTRACT

The results of experimental determination of the paired interaction potential of atoms and molecules composing the atmospheres of the earth and the planets are described. Three tables, 1 illustration, and 9 source citations.

274

SHORT-RANGE REPULSIVE FORCES BETWEEN ATOMS AND MOLECULES OF ATMOSPHERIC GASES

A.P. Kalinin, V.B.Leonas, and A.V. Sermyagin

1. Investigation of short-range repulsive forces is of interest both for the physics of atomic collisions and for description of various macroscopic phenomena in which these collisions are a dominant factor. Thus, data on the interaction potentials are of interest for the problem of energy exchange between translational and vibrational degrees of freedom of molecules and can be used to improve the methods and, consequently, the results of quantum-mechanical calculations of the energies, in analysis of hot-atom chemical data, etc.

Among the numerous practical applications, we should note the problem of determining the kinetic properties of gases at temperature above 1000°K, when all direct methods for measurement of these properties become difficult or even impossible.

The present paper describes the results of determination of the paired-interaction potentials of the atoms and molecules composing the atmosphere of the earth and the planets. Specifically, the following systems were studied: NO-NO, NO-N_2, NO-O_2, CO-CO, CO-NO, CO-N_2, CO-O_2, CO_2-CO_2, CO_2-O, CO_2-O_2, CO_2-CO, CO_2-N_2, CH_4-CH_4, CH_4-N, and NH_3-NH_3. Elastic scattering offers the most convenient experimental method of determining the intermolecular-interaction potentials. To overcome the well-known difficulties of constructing a universal particle source for beams of electron-volt energy, Amdur [1] proposed a modification of the method that uses the scattering of fast particles (energies $\sim$1 keV) at very small angles ($\sim 10^{-3}$ rad).

2. An apparatus for investigation of small-angle elastic scattering was described in detail in [2, 3], and we shall therefore dwell briefly only on certain improvements made to it.

A neutral beam of practically arbitrary atoms, molecules, and radicals is formed by charge exchange in an ion beam passed through an analyzing magnet and separation of the neutrals from the mixed beam in a planar separating capacitor. The beams were ribbon-shaped, and their energy could be varied from 600 to 4000 eV. They were registered with a secondary electron multiplier (SEM), and their intensities were sufficient for measurement of the total and differential scattering cross sections (through angles up to 10°).

Neutral beams in a predetermined electron state (ground or metastable) were created by selecting the charge-exchange partners. The geometry of the setup was such that particles deflected through angles larger than 10^{-3} rad during charge exchange would not enter

the collimated neutral beam; this provided for selection of particles that exchange charge with a small energy defect.

An electromagnetic valve admitted the gas to be investigated into the scattering chamber. Use of a constant-flow valve made it possible to reduce the relative error of the scattering-cross-section measurements to ±1% and made it easier to work with scattering gases that "poison" the heated filament of the ionization manometer (for example, hydrocarbons).

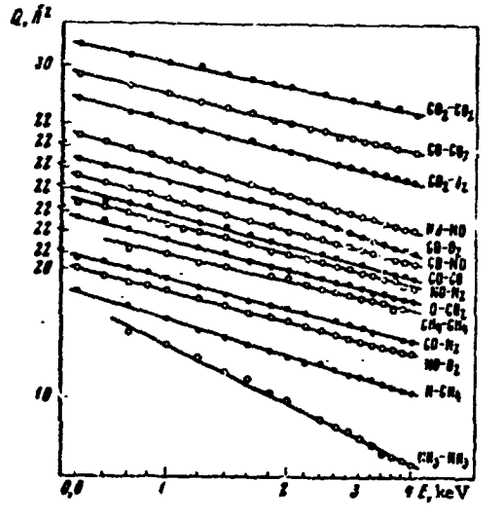

Effective Total Scattering Cross Sections $\bar{Q}$ as Functions of Energy E.

3. When fast neutral beams are elastically scattered, the quantity to be measured is the integral scattering cross section Q(E) as a function of beam energy. The integral cross section is related to the attenuation ΔI of the initial intensity I_0 of a beam that has traveled a distance Δl in a target with density n by the relation /197

$$Q(E) \simeq \frac{\Delta I}{I_0 n \Delta l}. \qquad (1)$$

The figure shows experimental curves of cross section vs. energy for the systems studied.

As was shown in [4], the measured cross section Q(E) can be represented in the classical approximation in the form

$$Q(E) = 2\pi \int_0^{\pi} \sigma(\theta)\,[1 - f_0(\theta)] \sin\theta d\theta = 2\pi \int_0^{\infty} b\,[1 - f_0(\theta(b))]\,db. \qquad (2)$$

In this expression, σ(θ) is the differential scattering cross section, b is the impact parameter, and $f_0(\theta)$ is an instrumental function that characterizes the efficiency for registration of particles scattered at an angle θ. The function $f_0(\theta)$, which is determined by the geometry of the apparatus and by the characteristics of the beam, was calculated for the conditions of the present experiment in [4]. The interaction potentials of the systems listed above are anisotropic, since the interaction forces depend on orientation. In this case, expression (2) assumes the form

$$Q(E) = \frac{1}{8\pi} \int_0^{\infty} db \iint_{(\varphi)} d^2\varphi_i \iint_{(\chi)} b(\theta, E, \varphi_i, \chi_i)\,[1 - f_0(\theta(b))]\,d^2\cos\chi_i, \qquad (3)$$

where ϕ_i and χ_i are the angles describing the relative orientation of axisymmetric molecules relative to the plane perpendicular to the relative-velocity vector of the colliding particles.

To take account of nonsphericity in the present study, we chose a noncentral-field model in the form of the sum of contributions from force centers situated at the points occupied by the atoms of the molecule and assumed to be identical.

TABLE 1. POTENTIAL PARAMETERS OF SYSTEMS INVESTIGATED /198

System	α, A^{-1}	A, keV	$\bar{\alpha}$, A^{-1}	$\bar{A}$, keV	System	α, A^{-1}	A, keV	$\bar{\alpha}$, A^{-1}	$\bar{A}$, keV
NO—NO	3.40	0.326	3.26	2.158	CO_2—CO	3.81	0.897	3.55	19.22
CO—CO	3.60	0.653	3.47	4.742	CO_2—O_2	3.81	0.490	3.33	8.720
CO—NO	3.63	0.570	3.49	4.283	CO_2—N_2	4.03	1.170	3.78	30.00
CO—N_2	3.79	0.896	3.66	7.059	CO_2—O	4.03	1.00	3.89	10.00
NO—N_2	3.78	0.735	3.64	5.780	NH_3—NH_3 *			2.65	0.120
CO—O_2	3.27	0.408	3.15	2.701	N—CH_4 *			3.92	2.290
NO—O_2	3.94	0.844	3.78	7.622	CH_4—CH_4 *			4.45	24.000
CO_2—CO_2	3.96	1.090	3.43	44.900					

The parameters $\bar{A}$ and $\bar{\alpha}$ correspond to a molecular force-field model in the form of a point repulsion center; they were calculated with a statistical error of 3%.

We see from expression (3) that to calculate Q(E) it is necessary to find the deflection angle $\theta(b, \varphi_i, \chi_i, E)$ for a given b. In the small-angle approximation ($\theta \approx V/E \ll 1$), which is satisfied in the experiment described, the deflection angle $\theta = \Delta p/p$ [5], where Δp is the transverse and p the longitudinal momentum, which is determined by the relative velocity. Thus, to find $\theta(b, \varphi_i, \chi_i, E)$ it is necessary to calculate $\Delta p(b, \varphi_i, \chi_i, E)$. For this purpose, the interacting molecules are projected onto the plane normal to the relative-velocity vector; then the distances between the projections of the atoms onto this plane are found to equal the impact parameters for scattering of the atoms of the impinging molecule by each atom of the target molecule. These distances can be related to r_e, the equilibrium interatomic distance in the molecule, and with the impact parameter, which corresponds to the motion with respect to the centers of gravity of the incident molecules. The vector sum of the momenta acquired by atoms of the incident molecule on interaction with atoms of the target molecule can be used to determine the deflection angle for a given relative orientation of the interacting particles.

For the systems studied, the additive potential is characterized by the interatomic repulsion, which was assumed to depend exponentially on the interatomic distance: ($V = A \exp(-\alpha r)$).

Expression (3) was calculated by a Monte Carlo method using an electronic computer (a BESM-4). The parameters A and α were so chosen that the calculated Q(E) relation would coincide with the measured one. The statistical error in calculating the integral (3) was 1%, with a number of trajectories on the order of 10^4. Table 1 gives values of the parameters A and α for the systems investigated.

For a selected orientation of the interacting molecules, the interaction potential $V(r, r_e) = \sum_{i,j} V(r_{ij})$, where r is the distance beteween the centers of gravity of the molecules and r_{ij} is the distance between atom i of the beam molecule and atom j of the target molecule. For practical application, it is necessary to have the spherically symmetrical potential averaged over all orientations:

$$V(r, r_e) = \frac{1}{(4\pi)^2} \int_{(\varphi)} \int_{(\chi)} V(r, r_e) \sin \chi_i d\chi_i d\varphi_j. \qquad (4)$$

It was found that the averaged intermolecular potential is described accurately in the interaction-energy range 0.1-10 eV by the exponential relation /199

$$V = \bar{A} \exp(-\bar{\alpha} r). \qquad (5)$$

The parameters $\bar{A}$ and $\bar{\alpha}$ are also given in Table 1.

4. Until recently, it had not been possible to analyze applicability of the empirical combination rule $V_{ij} = \sqrt{V_{ii} \cdot V_{jj}}$ for polyatomic molecules. The data of Table 1 for the averaged parameters $\bar{A}$ and $\bar{\alpha}$ provide a good opportunity to run this check. On the whole, it can be stated that, except for the $CO-O_2$ system, the values of the interaction potential energies obtained by combination agree closely with the energies obtained for the parameters found from direct measurements. In most cases, however, the parameters $\bar{A}$ and $\bar{\alpha}$ found by combination do not agree with those found from measurements. For the NO-CO system, for example, the parameters obtained by combination are $\bar{A}$ = 3200 eV, $\bar{\alpha}$ = 3.37, while direct measurement yields $\bar{A}$ = 4283 eV, $\bar{\alpha}$ = 3.49; the interaction-energy values for distances of 2.9 and 1.5 Å are 0.137 and 3.85 eV respectively (combination) and 0.123 and 4.00 eV (direct measurement).

Thus, a simple rule of combination can be used to estimate the interaction energies of complex molecular systems, but caution must be exercised in using the combination parameters for calculation of collision cross sections.

5. There are practically no reliable data that might be used for comparison for the systems studied in the present paper. Walker

et al. interpreted their measurements of diffusion in flames [6] in terms of the interaction potentials for the NO_2-CO_2 and O_2-CO_2 systems. The potential parameters do not agree with the data of the present study in the overlapping range of intermolecular distances.

Mason and Yun [7] used a semiempirical method to determine the V(r) in the overlapping range of approach distances for the N-NO, NO-O_2, and NO-N_2 systems. Comparison shows that the theoretical values are approximately double the experimental values (the ratio of the approach distances for the same V equals $\sim$0.9). The difference is apparently due both to the crudeness of the semiempirical method itself and to its application to molecules. Recent thermal conductivity measurements in the range to 1500°K are available for the CO-CO system [8], but it is convenient to make the comparison in terms of the collision integrals. The value of the reduced collision integral $\bar{\Omega}^{(2,2)}$ calculated from the data of [8] agrees at 1000°K with that found in the present study.

6. The transfer coefficients are usually calculated with the so-called reduced collision integrals ($\bar{\Omega}^{(l,s)}$). Strictly speaking, the collision integrals should be found for the resulting anisotropic potential, but the complexity of the calculations justifies the determination of $\bar{\Omega}^{(l,s)}$ for the averaged potential $\bar{V} = \bar{A}\exp(-\alpha r)$.

The reduced collision integrals are related to the parameters $\bar{A}$ and $\bar{\alpha}$ in Table 1 by the relation given in the literature [9]

$$\bar{\Omega}^{(l,s)} = \frac{8\beta^{-\bar{\alpha}^{-2}} I_{(l,s)}}{(s+1)!\left[1-\frac{1}{2}\frac{1+(-1)^l}{1+l}\right]},$$

where $\beta = \ln(\bar{A}/kT)$, and the $I_{(l,s)}$ are tabulated in [9].

The calculated values of $\bar{\Omega}^{(1,1)}$, $\bar{\Omega}^{(2,2)}$ are given in Tables 2 and 3 and can be used directly to calculate the coefficients of diffusion, viscosity, heat conduction (translational), etc. in the atmospheres of the earth and planets, both at the high temperatures corresponding to conditions behind the shock wave and for the undisturbed atmosphere. /201

7. The results of the present study indicate that small-angle scattering of fast beams is a highly efficient method for investigation of atom-molecule interactions in the electron-volt energy range.

The large number of easily accessible systems and the possibility of wide variation of the collision parameters render this method suitable for study of the interaction of complex polyatomic systems.

TABLE 2. REDUCED COLLISION INTEGRALS $\overline{\Omega}^{(1,1)}$[Å^2] FOR THE SYSTEMS STUDIED

T°, K	NO—NO	CO—CO	CO—NO	CO—N_2	NO—N_2	CO—O_2	NO—O_2	CO_2—CO_2	CO_2—CO	CO_2—O_2	CO_2—N_2	CO_2—O	NH_3—NH_3	N—CH_4	CH_4—CH_4
1000	8,53	8,83	8,56	8,56	8,31	9,59	8,13	13,37	10,89	10,78	10,30	8,05	6,27	5,94	6,95
3000	6,72	7,07	6,82	6,92	6,69	7,56	6,58	11,13	8,94	8,70	8,57	6,52	4,51	4,73	5,78
5000	5,93	6,30	6,09	6,19	6,00	6,72	5,89	10,21	8,11	7,84	7,80	5,87	3,97	4,21	5,28
7000	5,42	5,83	5,63	5,76	5,56	6,18	5,49	9,58	7,58	7,28	7,30	5,48	3,19	3,89	4,96
9000	5,09	5,50	5,315	5,43	5,23	5,79	5,18	9,12	7,18	6,90	6,97	5,18	2,90	3,49	4,73
11000	4,84	5,23	5,05	5,17	5,00	5,48	4,93	8,79	6,90	6,58	6,67	4,96	2,67	3,31	4,54

TABLE 3. REDUCED COLLISION INTEGRALS $\overline{\Omega}^{(2,2)}$[Å^2] FOR THE SYSTEMS STUDIED

T°, K	NO—NO	CO—CO	CO—NO	CO—N_2	NO—N_2	CO—O_2	NO—O_2	CO_2—CO_2	CO_2—CO	CO_2—O_2	CO_2—N_2	CO_2—O	NH_3—NH_3	N—CH_4	CH_4—CH_4
1000	9,98	10,23	9,93	9,96	9,64	11,17	9,39	15,17	12,42	12,36	11,76	9,28	7,76	7,02	8,21
3000	7,93	8,28	8,01	8,05	7,83	8,92	7,67	12,77	10,30	10,14	9,82	7,62	5,58	5,53	6,84
5000	7,06	7,44	7,19	7,27	7,05	7,97	6,92	11,71	9,40	9,17	9,00	6,89	4,69	4,97	6,24
7000	6,51	6,91	6,67	6,77	6,56	7,36	6,45	11,04	8,82	8,55	8,46	6,44	4,15	4,59	5,86
9000	6,12	6,53	6,30	6,44	6,20	6,93	6,12	10,57	8,40	8,11	8,07	6,12	3,69	4,32	5,58
11000	5,81	6,23	6,01	6,13	5,93	6,59	5,85	10,19	8,07	7,77	7,77	5,85	3,40	4,10	5,37

In conclusion, the authors thank Yu.M. Belyayev and N.V. Kamyshov for their help in the work.

REFERENCES

1. Amdur, J. and E. Jordan. In collection entitled "Molecular Beam Research" (Russ. ed.), Chap. 2, Moscow, "Mir," 1969.
2. A.B. Kamnev, V.B. Leonas, and V.T. Popov. Pribory i Tekhn. Eksperim., 1966, No. 2, 182.
3. Yu.N. Belyayev, V.B. Leonas, and A.V. Sermyagin. Collected Topics (VI. C.P.E.A.C.).
4. A.P. Kalinin, V.B. Leonas, and A.V. Sermyagin. Vestnik MGU, Seriya Fiz., 1971, No. 3, 245.
5. L.D. Landau and Ye.M. Lifshits. Mekhanika (Mechanics), Moscow, 1958.
6. R.E. Walker, L. Monchik, A.A. Westenberg, and S. Favin. Plan. Space Sci., 1961, Vol. 4, 221.
7. K.S. Yun and E.A. Mason. Phys. Fluids, 1962, Vol. 5, 380.
8. S.C. Saxena and G.P. Gupta. Thermophysics. I. T. Bevaus ed., 1970,
9. L. Monch[illegible]s. Fluids, 1964, Vol. 4, 695.

N75 13723

APPARATUS FOR CALIBRATION OF ON-BOARD INSTRUMENTS AND LABORATORY MODELLING OF RAREFIED PLASMA FLOWS PAST MODELS

(Translation of "Ustanovka dlya kalibrovki bortovykh priborov i laboratornogo modelirovaniya obtekaniya modeley razrezhennoy plazmoy.")

Ye. N. Yevlanov, V. B. Leonas, and S. V. Umanskiy

ABSTRACT

Problems of laboratory simulation of artificial earth satellite flight conditions in the ionosphere are examined, and a setup capable of reproducing the basic parameters of ion flows (with energies of 5-10 eV, energy-spectrum width ~2.5 eV, and an intensity of $2 \cdot 10^{-8}$ A/cm^{-2}) past measurement instruments and satellite models is described. Possibilities for further improvement of the apparatus are discussed. With 2 tables, 5 illustrations, and 5 source citations.

APPARATUS FOR CALIBRATION OF ON-BOARD INSTPUMENTS AND LABORATORY MODELLING OF RAREFIED PLASMA FLOWS PAST MODELS

Ye.N. Yevlanov, V.B. Leonas, and S.V. Umanskiy

Satellite investigations of the ionosphere necessitated the development of apparatus for simulation of the characteristic conditions of outer space and, in particular, systems for laboratory modelling of the motion of artificial earth satellites (AES) in the ionospheric plasma.

TABLE 1. BASIC PARAMETERS OF THE IONOSPHERE*

Height, km	300	500	1000	2000	3000
Average neutral-particle concentration n_0, cm^{-3}	9.8·10⁸	5.4·10⁷	2.9·10⁶	1.1·10⁶	1.0·10⁵
Average charged-particle concentration n_e, cm^{-3}	6.2·10⁵	1.4·10⁵	4.3·10⁴	1.3·10⁴	1.1·10⁴
Average electron temperature T_e, °K	1000	1500	2000	2500	2700
Thermal velocity of electron, $V_{T_e} = \sqrt{\frac{kT_e}{m_e}}$	1.2·10⁷	1.5·10⁷	1.8·10⁷	1.9·10⁷	2.0·10⁷
Thermal velocity of ion, $V_{T_i} = \sqrt{\frac{kT_i}{m_i}}$	6.4·10⁴	8.6·10⁴	1.4·10⁵	2.7·10⁵	3·7·10⁵
Average molecular weight	20,2	16,7	9,2	2,9	2,0
Principal ion component	O⁺	O⁺	He⁺	He⁺	H⁺
Satellite velocity V_{sa}, cm/sec	7.7·10⁵	7.6·10⁵	7.4·10⁵	6.9·10⁵	6.5·10⁵
Magnetic field H_0(g)	0,44	0.37	0.32	0.23	0.15
Average frequency of electron-ion collisions ν_{ei}, sec^{-1}	780	220	36	24	14
Electron-ion free path λ_{ei}, cm	2.5·10⁴	1.1·10⁵	7,8·10⁵	1,3·10⁶	2,3·10⁶

*Commas indicate decimal points.

The present paper describes apparatus designed both for laboratory calibration of on-board instruments used to study the upper ionosphere and for study of rarefied ionized-gas flows past scaled-down AES models.

Naturally, the parameters of the laboratory plasma must make a close approach to those encountered in the upper layers of the ionosphere; Table 1 presents a brief summary of ionospheric data. Ion-current densities per 1 cm^2 of satellite surface at $v_{sa} \approx 8 \cdot 10^5$ cm/sec are given in Table 2 [1].

It may be concluded from examination of Tables 1 and 2 that a device for calibration of on-board instruments must meet the following requirements.

TABLE 2. CURRENTS PICKED OFF 1 cm^2 OF DETECTOR SURFACE AREA ON A SATELLITE (A/cm^2)*

H, km	Component	
	O^+	$O^+ + NO^+$
200	$2.4 \cdot 10^{-8}$	$1.6 \cdot 10^{-8}$
250	$4.8 \cdot 10^{10-8}$	$4 \cdot 10^{-10}$
300	$4 \cdot 10^{-8}$	$2.4 \cdot 10^{-10}$
400	$1.6 \cdot 10^{-8}$	—

*Commas indicate decimal points.

The neutral-gas pressure must be quite low, $p_c \approx 1 \cdot 10^{-7}$ Torr in order to simulate the vacuum conditions of the upper ionosphere (Table 1) and prevent undesirable charge exchange and scattering of ions on the residual gas.

A monoenergetic ion beam /203 with energies of 5-10 eV and a current density $\sim 2 \cdot 10^{-8}$ A/cm must be formed. (The energy of the ions incident on the surface of the satellite is determined basically by the latter's velocity and, for example, is 4.3 eV for oxygen (O^+) ions with an energy-spectrum width of ~ 2 eV.) Provision for monitoring the ion composition of the stream would be desirable. The stream cross section must be quite large ($D_{beam} \approx 5\text{-}10\ D_{model}$).

The ion stream must be neutralized for laboratory simulation of flows past AES models, and the parameters of the resulting plasma must correspond to the dimensionless modelling scale coefficients [2].

Description of Apparatus

An apparatus for simulation of rarefied-plasma flows and calibration of on-board instruments used to measure the parameters of the upper ionosphere was built with consideration of the requirements set forth in the introduction.

A diagram of the apparatus appears in Fig. 1. Its external appearance is shown in Fig. 2. It incorporates an ultrahard-vacuum chamber with a sorption-type evacuating system, an ion source with neutralizer to form the stream of rarefied plasma, and diagnostic equipment for the plasma stream.

The vacuum system of the unit must meet special requirements. The pressure of the neutral gas in the working space must be so low as to minimize charge exchange and scattering of beam ions on the residual gas, since the formation of charge-exchange ions may strongly distort the results of measurements both of flows past reduced AES models and in the course of calibrating on-board instruments. The evacuating units must have high capacity to maintain the low pressures, considering the rather high gas loads on the vacuum system when strong ion beams are produced (energies of 5-10 eV).

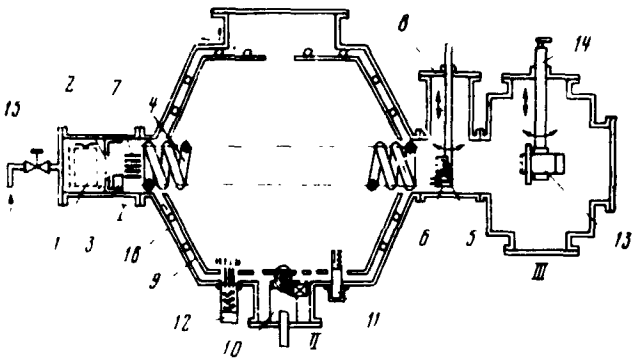

Figure 1. Diagram of Apparatus. 1) Ion source; 2) diaphragm; 3) neutralizer; 4) solenoid; 5) Faraday cylinder; 6) ion flux direction sensor; 7) condenser; 8, 14) rotary fixtures; 9) liquid-nitrogen-cooled copper surface (azotite); 10) titanium vaporizer; 11) manometer; 12) mass spectrometer; 13) instruments to be calibrated; 15) gas-admission valve; 16) chamber housing.

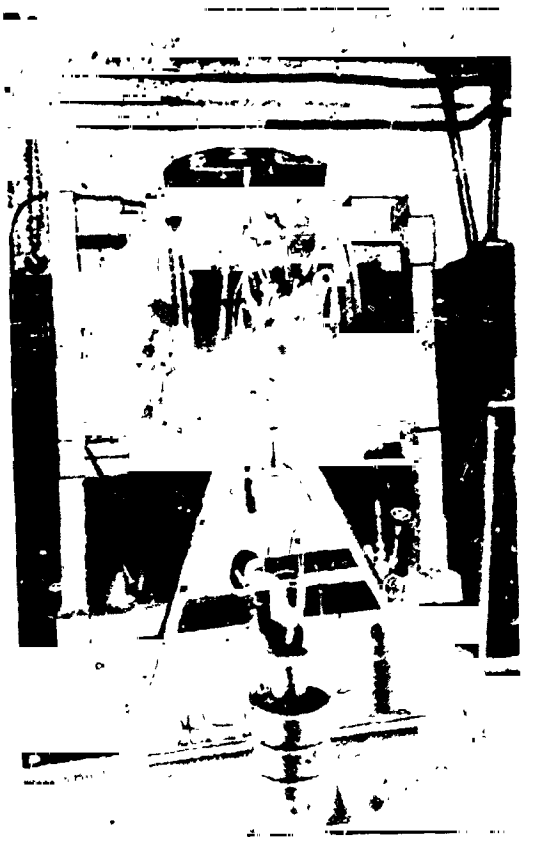

Figure 2. External Appearance of Apparatus.

Organic substances (oils) that form films on the detecting elements of the diagnostic instrumentation may not be present in vapor form in the residual gas, i.e., the vacuum systems must be oilless. The so-called azotite evacuation system, which is formed by a titanium film vaporized onto a surface that can be cooled to the temperature of liquid nitrogen (the azotite) conforms best to the above requirements. This type of evacuation was used in the present unit.

The vacuum system of the apparatus is not heatable; the packings are of rubber. The chamber used in the installation is a stainless-steel cylinder 1 m in diameter and 0.64 m long. It accommodates a cylindrical copper liner (azotite), cooled to the temperature of liquid nitrogen. An electron-beam titanium vaporizer with a capacity of 0.1 g/min is installed in an extension on the bottom of the chamber. Titanium is vaporized onto the entire inner surface of the liner. /205

The end flanges of the unit carry the ion source and instruments for diagnosis of the plasma stream. It is not desirable to place on-board instruments in the main chamber space for calibration because of the presence of the continuously vaporized titanium. Deposition of titanium results in the formation of

electrically conductive coatings on the walls, current leadins, insulators, etc. Screening of the instruments lowers the evacuation rate substantially owing to the reduced effective evacuating area. On-board instruments to be calibrated are secured on a rotary fixture that permits study of their angular characteristics. Diagnostic apparatus for determination of the principal characteristics of the beam are mounted in the adapter pipe (Fig. 1) coupling the working space to the main chamber. The Faraday cylinder is mounted on a plotter for determination of the ion-current density. The divergence of the ion beam is analyzed with a closely collimated channel electron multiplier (CEM) with an entrance-aperture diameter of 1 mm and a gain of $\sim 10^6$. The collimator was a tube 40 mm long and 1 mm in diameter. The divergence is measured accurate to 10 minutes.

The channel multiplier is also used as a detector in measurements of the energy and mass composition of the ion beam. It is proposed that electron concentrations and temperatures be measured with probes mounted on the same plotter.

The neutral-gas pressure in the device is measured with types LM-2 and MI-2 open metallic manometers. A quadrupole mass spectrometer is used for gas analysis.

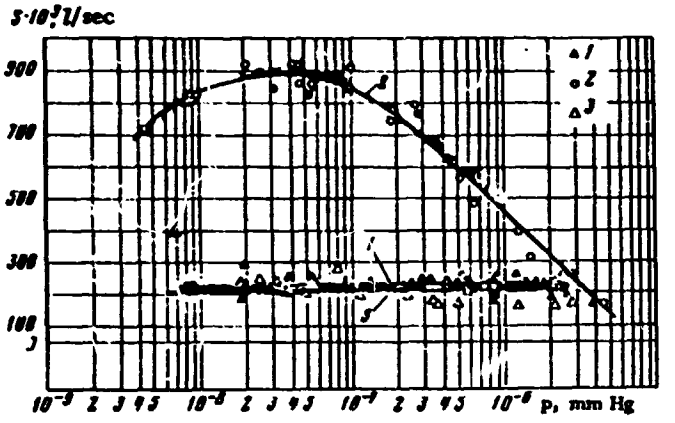

Figure 3. Rate of Neutral-Gas Evacuation as a Function of Pressure. 1) N_2; 2) H_2; 3) CO_2.

A hard-vacuum VA-2-3 pumping unit fitted with a reliable nitrogen trap is used for preliminary evacuation of gas from the unit. When in operation, this unit evacuates the space between the chamber and the azotite. The walls of the azotite are unbroken on the diffusion-pump side, and this sharply reduces migration of oil vapor from the pump into the working space of the apparatus. These precautionary measures result in a practically oilless vacuum in the unit.

The gas evacuation rate S is determined in units of this type by the surface area F of the titanium-coated azotite (liner), provided that the metal is vaporized rapidly enough. $S = \gamma \frac{V_t}{4} F$; V_t is the average thermal velocity of the neutral-gas molecules, and γ is the sticking probability. The latter depends on the nature of the gas; for N_2 and H_2, for example, $\gamma \approx 1$, and is small for inert gases. A diffusion pump is used for evacuation of inert gases. The measured evacuation rates are plotted against pressure in Fig. 3 and amount to $S = 800 \cdot 10^3$ l/sec for H_2 and $S = 200 \cdot 10^3$ l/sec for N_2 at a pressure of $1 \cdot 10^{-5}$ Torr.

When the VA-2-3 diffusion unit is used alone, the maximum vacuum in the apparatus is $1 \cdot 10^{-7}$ Torr. Cooling of the azotites with liquid nitrogen gives $1 \cdot 10^{-7}$ Torr. Thirty minutes after vaporization of titanium, the chamber pressure is $2 \cdot 10^{-8}$ Torr. The vacuum limit after several hours of operation is $1 \cdot 10^{-9}$ Torr (with titanium vaporization). Mass spectrograms of the residual gas in the chamber indicate the total absence of oil vapor (residual gas composed of CO_2, H_2, and CH_4).

The limiting current that can be obtained from the ion source can be estimated from the vacuum capabilities of the system. Let us assume that the working pressure in the chamber is $1 \cdot 10^{-7}$ Torr so as to exclude charge exchange and scattering of beam ions on the neutral gas. The working gas is nitrogen N_2. Full simulation of upper-ionosphere conditions would require that oxygen (O^+ ion) also be used in the working gas, but oxygen can be replaced by any gas of similar mass for flow-problem and calibration work, since O^+ and, for example, N_1^+ are registered identically. /206

The maximum neutral-gas (N_2) flux that we can admit into the chamber at a pressure of 10^{-7} Torr is

$$q_{max} = S p_k.$$

where S is the evacuation rate in l/sec and p_k is the operating pressure in the chamber. For N_2, the evacuation rate $S = 200 \cdot 10^3$ l/sec. Consequently, $q_{max} = 6 \cdot 10^7$ sec^{-1}. The pressure in the neutral-gas stream will be somewhat higher, but at a distance of 1 meter (location of the instruments to be calibrated), it is 10^{-7} Torr. If we assume a sticking probability $\gamma \approx 10^{-4}$ (for a source with electron-impact ionization), the maximum current that can be taken off the ion source is $I_{max} \approx 10^{-5}$ A. At a beam diameter of 6 cm, the current density $I_{max} \approx 3 \cdot 10^{-7}$ A/cm^2 (at a height of 500 km above the surface of the earth, the O^+-ion current density $I_{O^+} = 2 \cdot 10^{-8}$ A/cm^2).

A rarefied-plasma stream with the necessary parameters is formed by a source with electron-impact ionization, with the space

charge of the ion beam compensated by electrons generated by special neutralizers. The choice of an ion source of this type was dictated by the need to obtain a beam of low-energy ions (5-10 eV) with a rather narrow energy spectrum (Δw = 2 eV) and a large beam cross section (diameter 8 cm). Sources of other types do not meet these requirements [3].

The source consists of a cathode unit that forms a flat electron beam, an ionization space formed by two grids, and an accelerating grid. The gas is ionized in the equipotential space by a transverse electron beam, thus ensuring rather small scatter of the ion energies.

The Pierce system [4] is used to produce a flat electron beam that defines the ionization space sharply (which is essential if a monoenergetic ion beam is to result). The flat straight-channel cathode is of yttrium oxide applied to a tantalum base. The cathode is 10 cm long, 1.5 mm wide, and operates at 1400°C. The cathode unit delivers an emission current of 30 mA; the broadening of the electron beam due to the space-charge effect on the ionization length (10 cm) is 10 mm. /207

The ionization-space and accelerating grids are made of copper with a 0.05 × 0.05 mm mesh and 85% transparency.

A positive potential corresponding to the ion energy (5-10 V) is applied to the ionization-space grids; the accelerating grid is at chamber potential. The ions formed in the ionization space (the energy of the ionizing electrons is adjusted to the maximum ion current and is usually 50-200 eV) leave it with thermal velocities, and are then accelerated to the chamber by the grid and move in the equipotential space of the chamber. The gas stream supplied into ionization space is shaped by a set of passages to ensure optimum directivity (passage length 20 mm, diameter 0.3 mm, total number 200).

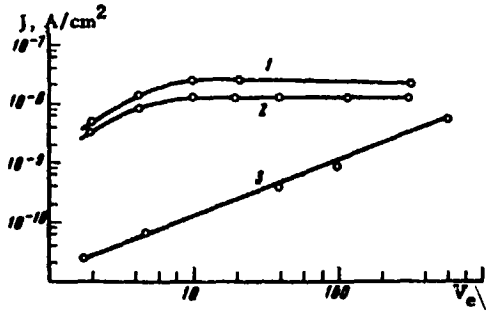

Figure 4. Ion Current as a Function of Ion Energy (Nitrogen Working Gas). 1,2) 15 cm from source; 1) I_e = 10 mA; 2) I_e = 5 mA; 3) 150 cm from source, I_e = = 5 mA.

Acquisition of strong ion beams with 5-10-V energies presents certain difficulties. Consideration of the space charge created by the ions lowers the current that can be taken from the source (3/2 law). For 10-eV ions and a distance of 1 cm between the extracting electrode and the plasma boundary, $I_{max} \approx 3.3 \cdot 10^{-7}$ A/cm², which is quite adequate for flow modelling and calibration. Ion beams diverge strongly at such low

energies owing to Coulomb repulsion and as a result of the defocusing action of the initial thermal velocities and the effects of the grid meshes. The strength of the beam drops off accordingly. For the N_2 ion, for example (initial ion-current density $5 \cdot 10^{-8}$ A/cm^2, energy 10 eV, ion-beam diameter 6 cm), beam intensity drops off by a factor of 2500 on a length of 150 cm, and the diameter of the beam increases by a factor of 50. Figure 4 shows an experimental plot of ion current against accelerating voltage. The intensity of the ion flux was measured both near the source (15 cm) and at a distance of 150 cm, and the working gas was nitrogen N_2. The figure shows that in the former case the intensity of the ion beam reaches saturation even at an extracting voltage of 5 V, i.e., the ion current is not limited by the space-charge effect. For the 150-cm source distance, the ion current increases with accelerating voltage and becomes equal to the current for the 15-cm distance at U = 300 V.

The divergence of the ion beam due to Coulomb repulsion can be reduced substantially by compensating the ion-beam space charge with electrons generated by a special source.

The ion source described above delivers ion beams with ion energies from 5 eV with intensities of $2 \cdot 10^{-8}$ A/cm^2 and higher.

The energies of the beam ions were determined by two methods: the decelerating-potential method and the time-of-flight method using a base of known length. The decelerating-potential method is well known; it has disadvantages in the possibility of error due to changes in the grid potentials when an adsorbed layer forms on them, the contact potential difference, and sagging of the elec-/208 trostatic field in the meshes of the grids [5]. The time-of-flight method is free of these shortcomings. This method is universal in that it can be used to determine the velocity distribution function of the ions and its moments, density, velocity, and energy.

Successful application of this method requires a fast electrical shutter to interrupt the ion flow and an ion detector with a small time constant. The ion-beam shutter must not distort the characteristics of the ion beam being studied (distribution function, energy, mass composition, etc). In our case, a condenser is used as a shutter. It consists of fifty series-connected planar capacitors placed one above the other (distance between plates 3 mm, plate length 10 cm, width 15 mm).

The stacked construction of the condenser makes it possible to reduce its bulk substantially and to eliminate the influence of its stray electric field on the motion of the ions at 90% transmission. This condenser has a short time of flight for an ion moving at a velocity of $8 \cdot 10^5$ cm/sec (10^{-6} sec), a factor of importance in analysis to determine the monoenergetic property of the ion beam. In practice, the velocity distributions of the ions were measured as follows: a continuous voltage ($\sim$ 20 V) was applied

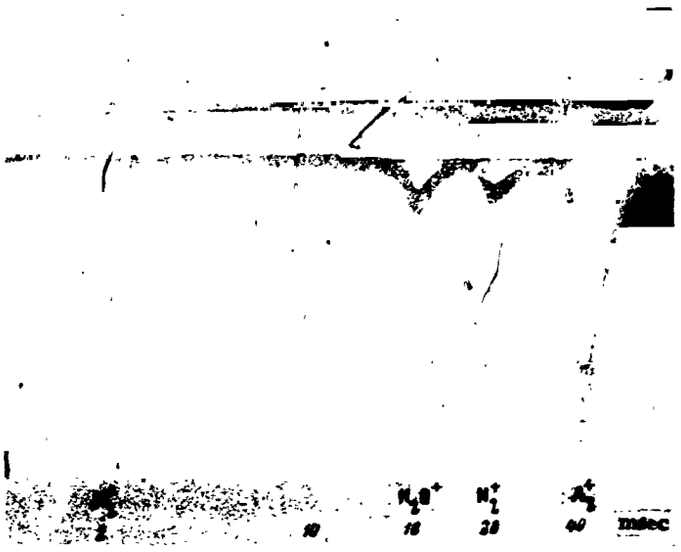

Figure 5. Measurement of Ion Velocity in Beam and Composition of Beam. The upper scan indicates the shutter opening time; the lower scan is the time-of-flight distribution of the ions (flight base 150 cm, ion energy 20 V).

to the condenser plates to deflect the ion beam; at time t = 0, the voltage was removed from the condenser and the ion beam struck the collector. The ion-deflecting voltage was again applied to the condenser at a time $t \approx \tau$. In this case, the collector ion current will be described by the formula

$$I(t) = I_0 \int_{t-\tau}^{t} \varphi(t)\, dt;$$

where I_0 is the steady-state beam current, τ is the shutter open time, and t is the observing time. If we take $\tau \ll t$, we have $I(t) = I_0 \phi(t)\tau$. Thus, we obtain the time-of-flight distribution function of the ions at once, and since t = L/v, we also have the ion velocity distribution. For monoenergetic beams, this method can also be used to determine the mass composition of the beam. /209

A typical oscillogram of the ion current onto the collector in time-of-flight measurements appears in Fig. 5. It is easily determined from the oscillogram that the ion beam consists of ions of hydrogen H_2^+, argon Ar^+, Ar^{+1}, and nitrogen N_2^+ (the original gas mixture). The energy-spectrum width for argon ions Ar^+ is 2.5 eV.

CONCLUSION

An apparatus was built for study of rarefied plasma flows past earth-satellite models and calibration of on-board instruments for measurement of the structural parameters of the upper ionosphere. The vacuum system of the apparatus has a high evacuation rate and can maintain low pressures (10^{-7} Torr) under its operating conditions. The ion flux (with energies from 5 to 10 eV and 2.5 eV monochromaticity at a flux intensity of $2 \cdot 10^{-8}$ A/cm^2) is quite adequate for calibration of on-board instruments. The energy of the beam can be raised to 300 eV. The necessary diagnostic apparatus has been built and tested.

REFERENCES

1. COSPAR International Reference Atmosphere. Acad. Press., Amsterdam, 1965.
2. W. Clayden and C. Hurdle. Rarefied Gas Dynamics, London, Acad. Press, 1967, p. 1717.
3. M.D. Gabovich. Usp. Fiz. Nauk, 1965, Vol. 56, No. 2, 215.
4. J. Pierce. Theory and Design of Electron Beams (Russ. ed.), "Sov. Radio," 1955. S. Stephanokis and Willard H. Bennet. Rev. Sci. Instr., 1968, Vol. 39, No. 11, 1714-1720.

☆ U.S. GOVERNMENT PRINTING OFFICE: 1974—635-045 / 38

Translated for the National Aeronautics and Space Administration by Scripta Technica, Inc., NASw-2484.